TECHNISCHE UNIVERSITÄT MÜNCHEN
Fakultät für Chemie

Chromophore-based Coordination Polymers (CPs) as Materials for Optical Applications

Sebastian Josef Weishäupl

Vollständiger Abdruck der von der Fakultät für Chemie der Technischen Universität München zur Erlangung des Grades eines

Doktors der Naturwissenschaften (Dr. rer. nat)

Genehmigten Dissertation.

Vorsitzender: Prof. Dr. Jürgen Hauer

Prüfer der Dissertation: 1. Prof. Dr. Dr. h.c. Roland A. Fischer
2. Prof. Dr. Tom Nilges

Die Dissertation wurde am 12.07.2022 bei der Technischen Universität München eingereicht und durch die Fakultät für Chemie am 27.07.2022 angenommen.

Die vorliegende Arbeit wurde am Lehrstuhl für Anorganische und Metallorganische Chemie der Technischen Universität München im Zeitraum von Januar 2019 bis Mai 2022 erstellt.

“My mama always said life was like a box of chocolates.

You never know what you’re gonna get”

- Forrest Gump

Danksagung

Zuallererst möchte ich mich bei **Herrn Prof. Dr. Roland Fischer** bedanken, dass er mir die Möglichkeit gegeben hat, an meinem Forschungsthema, dass mich bereits seit meiner Masterarbeit fasziniert hat, weiter zu arbeiten, sowie für den guten wissenschaftlichen Diskurs den wir in den letzten knapp 4 Jahren hatten. Darüber hinaus werde ich unsere zahlreichen Lehrstuhls-Abende nie vergessen, an denen wir mehrere Partien „Wattn“ als Partner gespielt und auch (zu meist) gewonnen haben.

Ich danke auch **Prof. Jürgen Hauer** für die Übernahme des Amtes des Vorsitzenden, sowie **Prof. Tom Nilges**, dass er sich dazu bereit erklärt hat, trotz seiner zeitintensiven Funktion als Dekan, die Zweit-Prüfung zu übernehmen.

Ein besonderer Dank gilt ebenfalls meinem Betreuer **Dr. Alexander Pöthig**, der mich die letzten Jahre durch meine ganzen wissenschaftlichen Höhen und Tiefen hindurch begleitet hat. Danke, dass deine Tür für mich immer offen war und du mir in jederlei Hinsicht nicht nur ein guter Betreuer, sondern auch ein guter Freund warst.

Als nächstes möchte ich dem akademischen Mittelbau unseres Lehrstuhls danken, **Dr. Christian Gemel**, **Dr. Julien Warnan**, **Dr. Markus Drees**, **Dr. Gabrielle Raudaschl-Sieber**, **Dr. Mirza Cokoja**, **Dr. Gregor Kieslich** und **Dr. Dominik Halter**, die nicht nur unseren großen Lehrstuhl durch ihr tatkräftiges Engagement am Laufen halten, sondern auch in unseren Seminaren ihren wissenschaftlichen Input geben.

Das am Laufen halten unseres Lehrstuhls wäre allerdings auch nicht möglich, ohne die Hilfsbereitschaft unseres AMC-Sekretariats, **Martin Schellerer** und **Dr. Dana Weiß**, die bei administrativen Fragestellungen stets zur Stelle waren, als auch ohne unsere Technikerinnen, **Maria Matthews** und **Rodica Dumitrescu**.

Danken möchte ich auch **Jürgen Kudermann**, **Ulrike Ammari**, **Burghard Cordes** und **Christian Jandl,** die mir bei meinen unzähligen Messungen geholfen haben.

I want to thank also **Yang Cui** and **Erling Thyrhaug** from the group of **Prof. Jürgen Hauer**, for the fruitful discussions and measurements sessions that led to three joint publications. I hope that our work is the kick-off for a good long-term cooperation between our groups.

Ich möchte mich auch bedanken bei …

… meinen Forschungspraktikanten, sowie Bachelor und Masteranden, **Tim Kipfer**, **Simon Deger**, **Florian Zahn**, **Philipp Güllich**, **Johannes Voigtland**, **Wenyi Zeng** und **Shinjoo Park**, deren Werdegang ich im Rahmen meiner Doktorarbeit als Betreuer mitbegleiten durfte.

… meiner Neufahrn-Gang, den **Schmid(t)s**, den **Daigers**, den **Austeggers**, den **Burschmidts**, den **Hemmlys**, den **Keildeckers**, sowie den **Heydewitters,** weil sie in den letzten Jahren zu meinen besten Freunden geworden sind, wodurch diese Zeit zur besten meines Lebens wurde.

… **Dave**, der mich damals bei meiner Masterarbeit unter seine Fittiche genommen hat und mir geholfen hat, ein besserer Chemiker zu werden.

… dem ganzen **AMC-Lehrstuhl**, für die nette Arbeitsatmosphäre die ich seit meiner Masterarbeit erleben durfte.

Schließlich möchte ich mich bei meiner Familie bedanken, nämlich bei …

… meinem **Papa** und meiner **Mama**, die mich zu dem Menschen erzogen haben, der ich heute bin. Ohne eurer moralischen, seelischen bis hin zur finanziellen Hilfe, wäre ich jetzt nicht an der Stelle, an der ich heute bin. Alles was ich erreicht habt, habe ich zu großen Teilen euch zu verdanken.

… meinem **Bruder**, der, seit ich auf der Welt bin, immer für mich da ist. Ohne deiner Hilfe hätte ich es nicht einmal aufs Gymnasium geschafft, geschweige denn dann mein Studium mit anschließender Promotion. Du bist der beste große Bruder, den man sich nur wünschen kann. Du warst und bist immer mein großes Vorbild.

… meinen Schwiegereltern **Peter** und **Sabine**, weil sie mir das größte Geschenk beschert haben, dass ich je in meinem Leben bekommen werde.

Zu guter Letzt möchte ich mich bei meiner Frau **Patricia** bedanken, dass sie es mittlerweile acht Jahre mit mir aushält. Ich kann gar nicht in Worte fassen, was für ein Glück ich habe, dass du ein Teil meines Lebens bist. Ich bin jeden Tag aufs Neue froh, dass ich mich damals dazu entschlossen habe, Chemie an der TUM zu studieren, weil ich dadurch dir, der Liebe meines Lebens, begegnet bin.

Zusammenfassung

Nichtlineare optische Effekte wie die Multiphotonenabsorption, die Summenfrequenzerzeugung und die Frequenzverdopplung sind in der modernen Forschung von großem Interesse, da sie für optoelektronische Geräte von großem Nutzen sind. Die meisten der in diesem Forschungsbereich verwendeten Materialien sind Chromophore, die jedoch durch ihre thermische Instabilität sowie ihr unkontrolliertes Aggregationsverhalten in hochkonzentrierten Lösungen eingeschränkt sind. Eine prominente Materialklasse, die sich als vielversprechende Alternative zur Verhinderung dieser Probleme anbietet, sind chemisch hochgradig anpassungsfähige Koordinationspolymere basierend auf Chromophoren (CPs). Zudem können durch den Einbau von Chromophoren als Linker die photophysikalischen Eigenschaften der Materialien aufgrund der Einschränkung der strahlungsfreieren Abregungswege verbessert werden.

Die vorliegende Arbeit ist in drei Teile gegliedert: Der erste und zweite Teil befasst sich mit den Verstärkungseffekten der Multiphotonenabsorption von Push/Pull-Chromophoren, die durch den Einbau in Koordinationspolymere erzeugt werden. Der dritte Teil dieser Arbeit untersucht neuartige perylenbasierte CPs für die photokatalytische Singulett-Sauerstofferzeugung.

In der ersten Studie wurde ein neues dipolares Push/Pull-Chromophor, Dipropyl-9-(4-nitrophenyl)-carbazol-3,6-dicarboxylat (H_2CbzNO_2), synthetisiert und anschließend strukturell und photophysikalisch durch Röntgeneinkristallbeugung, UV/Vis- und Photolumineszenz (PL)-Spektroskopie vollständig charakterisiert. Dabei zeigte sich im Absorptionsspektrum des Chromophors eine rotverschobene TICT-Bande (Twisted Intramolecular Charge Transfer) mit zunehmender Lösungsmittelpolarität. Darüber hinaus wurde der Festkörper des Materials in Pulverform mit Hilfe der PL-Spektroskopie hinsichtlich seiner Photolumineszenzeigenschaften untersucht. Dabei wurde eine Festkörperemission bei 520 nm festgestellt, die auf die Bildung von Excimeren zurückzuführen ist.

In der zweiten Studie wurden drei neue, stark MPA-aktive Koordinationspolymere $Zn_2(sbcd)(DMAc)_2(H_2O)_{1.5}$, $Sr(fbcd)(DMAc)_{0.25}(H_2O)_{3.5}$ und $Ba(fbcd)(DMAc)_{2.5}(H_2O)_{1.5}$ synthetisiert, die auf zwei carbazolhaltigen Linkermolekülen basieren: ein bereits literaturbekannter Linker 9,9'-Stilben-bis-carbazol-3,6-dicarbonsäure (H_4sbcd), sowie einen neuen Linker 2,7-Fluoren-9,9'-dimethyl-bis-carbazol-3,6-dicarbonsäure (H_4fbcd). Die Einkristallstrukturanalyse der CPs zeigte, dass das Zink-basierte Koordinationspolymer als 2D-CP in *sql*-Netzwerktopologie kristallisiert, während die isostrukturellen Barium- und Strontium-haltigen 2D-CPs in einer 4,8-verbundenen Netzwerktopologie kristallisieren. Die Z-Scan-Analyse der synthetisierten Materialien zeigt große Zwei-Photonen-Querschnitte von 2100 bis 33300 GM, was eine Verbesserung um bis zu drei Größenordnungen im Vergleich

zu den solvatisierten Linkermolekülen darstellt. Behält man das Molekül H_4fbcd als Linker bei, wählt zugleich aber andere Metallionen für die sekundäre Baueinheit (SBU), so zeigt das Strontium basierende CP einen dreifach höheren Zwei-Photonen-Querschnitt als das Barium basierende Material. Dieses Verhalten könnte dabei auf den geringeren intermolekularen Carbazol-Carbazol-Abstand (3,39 Å bis 3,65 Å) im Strontiumgerüst zurückzuführen sein, da die Carbazoleinheiten den Charge-Transfer bestimmen, was wiederum zu höheren Zwei-Photonen-Querschnitten führt.

Der dritte Teil dieser Arbeit befasst sich mit der Synthese und Charakterisierung eines neuartigen 2D-Koordinationspolymers auf der Basis eines Perylendiimids (PDI) $Zn(tpdb)(DMF)_3$, das in einer solvothermischen Synthese von Zinknitrat in DMF mit dem in der Literatur bekannten 1,6,7,12-Tetrachlorperylendiimid-N,N'-di-benzoesäure (H_2tpbd) erhalten wurde. Die Einkristallanalyse, sowohl des Linkers, als auch des Koordinationspolymers, zeigt eine starke Aggregation der dicht gepackten Chromophore, die auf den starken π-Stacking-Effekt der PDI-Einheiten zurückgeführt werden kann. Anschließend wurden die photophysikalischen Eigenschaften untersucht und diskutiert, einschließlich der unterschiedlichen Verschiebungen der Absorptions- und Emissionsbanden in den jeweiligen Spektren. Schließlich wurden die synthetisierten Materialien in der Photosensibilisierung von Triplett-Sauerstoff zu Singulett-Sauerstoff unter Verwendung von 1,3-Diphenylisobenzofuran (DBPF) als Trapping-Agent getestet. Dabei zeigen sowohl das CP als auch das freie Linkermolekül eine effiziente Photosensibilisierungsaktivität, was zeigt, dass die Peryleneigenschaften nach dem Einbau in Koordinationspolymere erhalten bleiben.

Abstract

Non-linear optical effects such as multiphoton absorption, sum frequency generation and second harmonic generation are of high interest in modern research as they are highly applicable for optoelectronic devices. However, most of the commonly materials used in this research field are chromophores, which are limited by their thermal stability, as well as their uncontrolled aggregation behaviour in highly concentrated solutions. A prominent material class, which represents themselves as a promising alternative to overcome those problems, are chromophore-based coordination polymers (CPs), since they are highly chemically tuneable and by incorporating chromophores as linkers, the photophysical properties can be enhanced due to the restriction of radiationless energy decay pathways.

This thesis presented is divided into three parts: The first and second part deals with enhancement effects of multiphoton absorption of push/pull chromophores through the incorporation in coordination polymers. The thrid part of this thesis is investigating novel perylene-based CPs for photocatalytic singlet oxygen generation.

In the first study, a novel dipolar push/pull chromophore dipropyl-9-(4-nitrophenyl)-carbazole-3,6-dicarboxylate (H_2CbzNO_2) was synthesized and subsequently structural and photophysical fully characterized using single-crystal X-ray diffraction, UV/Vis and photoluminescence (PL) spectroscopy. Thereby, the absorption spectrum of the chromophore revealed a red-shifting twisted intramolecular charge transfer (TICT) band with increasing solvent polarity. Furthermore, the solid-state powder of the material was investigated towards its photoluminescence properties by means of PL spectroscopy, revealing a solid-state emission located at 520 nm, which can be attributed to excimer formation.

In the second study, three novel highly MPA active coordination polymers $Zn_2(sbcd)(DMAc)_2(H_2O)_{1.5}$, $Sr(fbcd)(DMAc)_{0.25}(H_2O)_{3.5}$ and $Ba(fbcd)(DMAc)_{2.5}(H_2O)_{1.5}$ were synthesized, derived from two carbazole containing linker molecules: a previously reported 9,9'-stilbene-bis-carbazole-3,6-dicarboxylic acid (H_4sbcd) and a new linker 2,7-fluorene-9,9'-dimethyl-bis-carbazole-3,6-dicarboxylic acid (H_4fbcd). Single-crystal structure analysis of the CPs showed, that the zinc-based coordination polymer is crystallizing as 2D-CP with *sql* network topology, whereas the isostructural barium and strontium containing 2D-CPs are crystallizing in a 4,8-connecting network topology. Z-scan analysis of the synthesized materials shows large two-photon cross sections of 2100 to 33300 GM, which is an enhancement of up to three orders of magnitude compared to the solvated linker molecules. When retaining the molecule H_4fbcd as a linker but selecting different metal ions for the secondary building unit, the strontium-based CP shows a threefold higher two-photon cross section than the barium derived material. This behaviour may originate from the smaller intermolecular carbazole-carbazole distance (3.39 Å to 3.65 Å) in the strontium framework, as

the carbazoles units are determining the charge-transfer character, which in turn renders higher two-photon cross sections.

The third part of this thesis deals with the synthesis and characterization of a novel peryelene-diimide (PDI)-based 2D-coordination polymer Zn(tpdb)$(DMF)_3$ obtained from a solvothermal synthesis of zinc nitrate in DMF with the literature known 1,6,7,12-tetrachloroperylenediimide-*N,N'*-di-benzoic acid (H_2tpbd). Single-crystal analysis of both linker and coordination polymer reveals a strong aggregation of tightly packed chromophores which can be attributed to the strong π-stacking effect of PDIs. Subsequently, the photophyiscal properties are examined and discussed, including the different shifts of absorption and emission bands in the respective spectra. Finally, the synthesized materials are tested in photosensitization of triplet oxygen to singlet oxygen using 1,3-diphenylisobenzofurane (DBPF) as trapping agent. Thereby, both the CP and the free linker molecule show an efficient photosensitizing activity, showing that the perylene properties can be retained after incorporation in coordination polymers.

Table of Contents

1 Introduction

Optics is the field of physics, which deals with the interaction of light and matter i.a. diffraction, absorption and scattering. These interactions provide us with visual feedback about our world.[1] Thereby, the matter consists of an assembly of atoms, which are mostly positively charged and surrounded by the negatively charged electrons. As a consequence, the induced light primarily interacts with the valence electrons of the valence shell leading to electronic polarization of the matter induced by the incident light.[2]

However, the subgroup optics as a part of physics can be divided into two subfields: the linear and nonlinear optics. The linear optics describes the absorption and emission of linearly behaving light. For example, if one photon is absorbed, then one photon is being reemitted. In contrast, the nonlinear optics, where the light behaves nonlinearly e.g. two photons are absorbed and only one photon double the energy is being reemitted.[3]

One possible material class, which is showing such photophysical activity are coordination polymers (CPs). CPs describes the general term for inorganic-organic hybrid materials, which are normally composed of metal ions (inorganic part) bridged by linker molecules (organic part), forming a variety of architectures ranging from one-dimensional chains to 3D porous frameworks.[4-6] Depending on the valency of the metal ions and thereof the formed secondary building unit (SBU) consisting of metal-oxoclusters, different types of geometries i.a. tetrahedral, square-planar and octahedral architectures can be constructed, which determines the dimension of the CP.[7-8]

A property determining unit of CPs are their linker molecules, which are compromising donor functionalities, usually carboxylic acids or pyridyl-groups, connecting the SBUs as a linker to a chain or network.[5] Furthermore, the incorporation of linker molecules already shows the great potential that this material class offers to insert the properties of functional linkers into coordination polymers achieving a different photophysical response due to linker-linker interaction through aggregation (Fig. 1).[9]

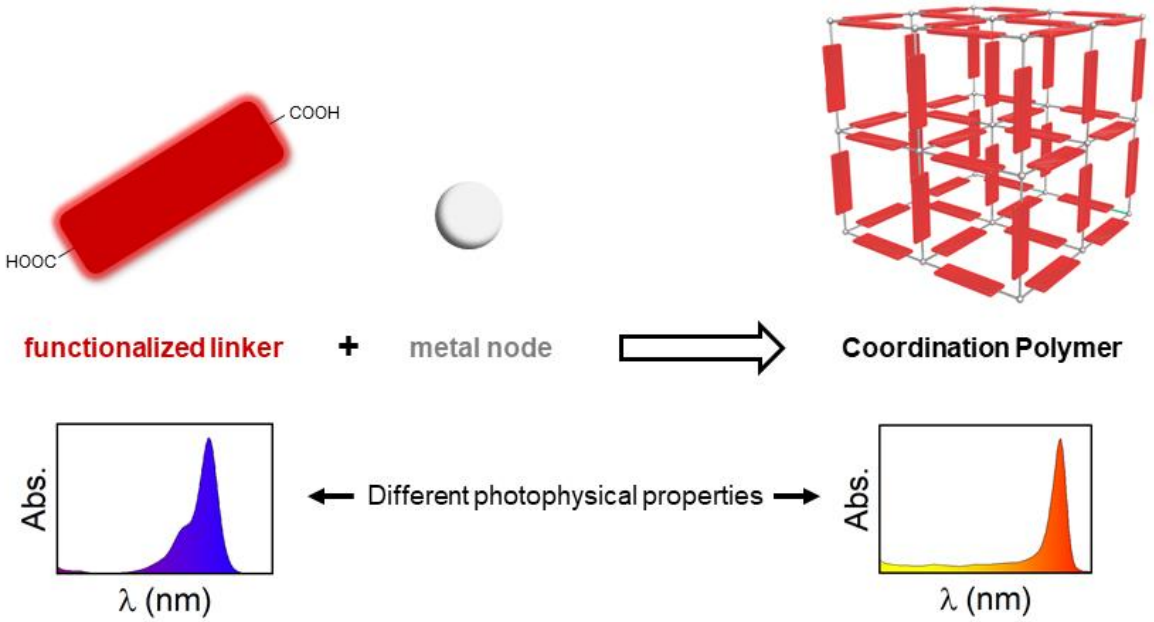

Fig. 1: General concept of the incorporation of functionalized linker molecules into coordination polymers in order to achieve different photophysical properties.

As chromophores intrinsically show outstanding photophysical properties, this dissertation deals with the general approach of chromophore-based linker molecules, which are incorporated into coordination polymers for enhanced optical properties towards nonlinear applications like two-photon absorption (TPA) (cf. Chapter **1.1**) as well as linear optics such as energy transfer and light harvesting (cf. Chapter **1.2**), which will be further elucidated in the following.

1.1 Multiphoton absorption active crystalline coordination polymers (CPs)

1.1.1 Nonlinear optics

Nonlinear optics (NLO) is one of the subdisciplines of modern physics, which has a tremendous influence on today's optics and laser physics.[10] NLO is the investigation of various kinds of light-induced phenomena of a material, that occurs by the nonlinearly interaction of light and matter and is typically only observed with high intensity laser lights.[11]

The origin of nonlinear optics was marked by the investigations of *Franken et al.* in 1961, where they first observed a second harmonic generation of blue light (λ = 347 nm) with a pulsed ruby laser (λ = 347 nm) into a quartz crystal, subsequent to the invention of the first working laser by *Maiman* in 1960.[12-13]

Up to now, there are several processes that belong to the group of NLO such as second harmonic generation (SHG), sum frequency generation (SFG) and two-photon absorption (TPA) (Fig. 2).[14]

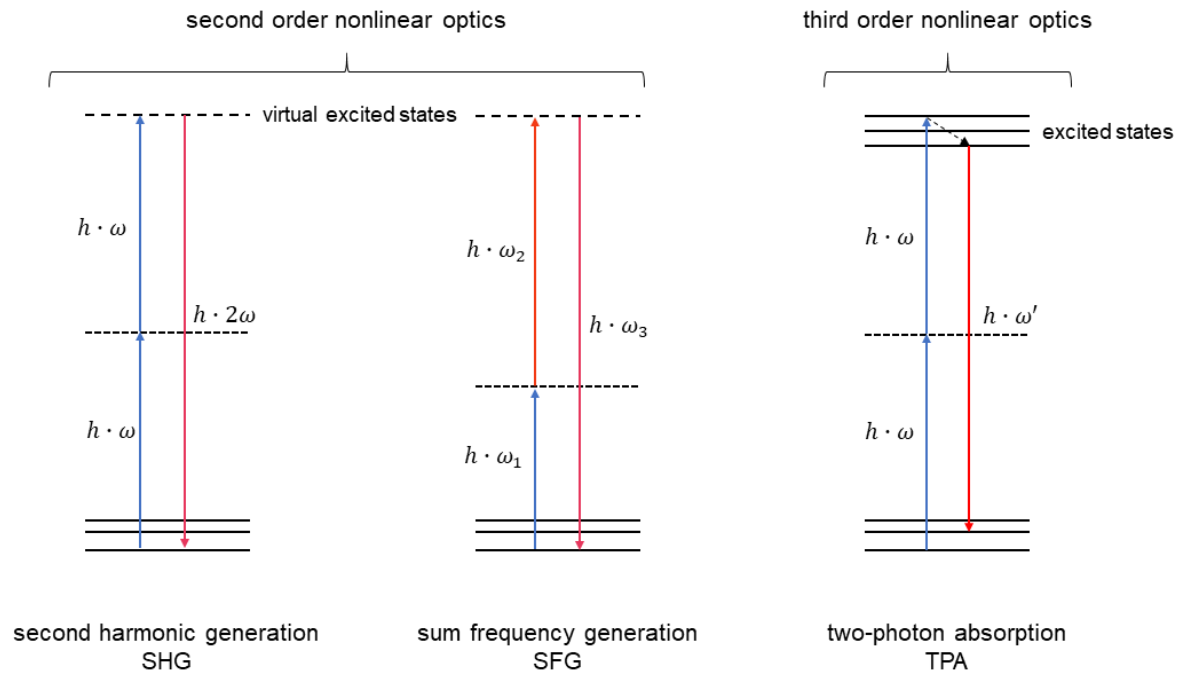

Fig. 2: Jablonski diagram for the NLO process of SHG (left), SFG (middle) and TPA (right).[15]

Thereby, SHG, also called frequency doubling, is a second order nonlinear optical process, where two photons with an optical frequency ω are mediated by two virtual states to a single photon with doubled frequency of 2ω.[16]

Furthermore, SFG is also a second order nonlinear optical process, in which two input laser beams with two different frequencies ω_1 and ω_2 are overlapped on a surface in order to create a third beam which has the sum frequency ω_3 of the two separate beams ($\omega_3 = \omega_1 + \omega_2$). This is also the main difference to the SHG, where only one input laser beams is used to generate the combined beam.[17]

The last process, which is one of the key-processes further discussed in the next chapter, is described as two-photon absorption (TPA), a third order nonlinear optical process where two photons are involved or multiphoton absorption (MPA), where three or more photons are absorbed.

Thereby, the main difference of TPA compared to SHG and SFG is that the electrons are excited to virtual states (dashed lines) with very short lifetimes, whereas for the TPA real eigenstates of the material are involved (continuous lines) with longer lifetimes possible.

1.1.2 Multiphoton absorption as a NLO process

The process of multiphoton absorption (MPA) was first analytically described by Maria Göppert-Mayer in 1931, with virtual eigenstates as a key factor for her theory. However, the probability to observe such a MPA process was too small with the light sources available at that time.[17] Enabled by the laser technology, Kaiser and Garrett were able to deliver the missing experimental proof 30 years later, with the first report of a two-photon excitation in a fluorescent CaF_2:Eu^{2+}-crystal in 1961.[18]

This process of multiphoton absorption can be described by two theories: the semiclassical and the quantum theory of radiation.[19-21]

Regarding the semiclassical theory, the media is specified by theory of quantum mechanics, whereas the induced light is defined by the Maxwell theory. However, the main feature in this theory is an explicit expression for the non-linear electric polarization of an optical medium. It is generally known, that the polarization vector $\vec{P}$ is defined by the summation of the light field-induced electric-dipole-moment of all molecules within an unit volume. If a weak light field from an incoherent light source is applied, $\vec{P}$ is proportional to the electrical field $\vec{\mathrm{E}}$, which leads to the following equation:

$$\vec{P} = \vec{P}^{(1)}(\omega) = \epsilon_0 \chi^{(1)}(\omega)\vec{E}(\omega) \tag{1.1}$$

Here $\chi^{(1)}$ is the first order susceptibility of a given medium and ϵ_0 is the free space permittivity. In general, $\chi^{(1)}(\omega)$ is a complex parameter in the form of a second-rank tensor, whereas its real part is described by the refractive index of the medium, while its imaginary part determines the linear one-photon absorption.[22] To consider the nonlinear absorption of strong monochromatic coherent light of frequency ω, the equation (1.1) is generalized to equation (2):

$$\vec{P} = \vec{P}^{(1)}(\omega) + \vec{P}^{(3)}(\omega) + \vec{P}^{(5)}(\omega) \ldots = \epsilon_0[\chi^{(1)}(\omega)\vec{E}(\omega) + \chi^{(3)}(\omega,\omega,-\omega)\vec{E}(\omega)\vec{E}^{*}(\omega)\vec{E}(\omega) + \chi^{(5)}(\omega,\omega,-\omega,\omega,-\omega)\vec{\mathrm{E}}(\omega)\vec{\mathrm{E}}^{*}(\omega)\vec{\mathrm{E}}(\omega)\vec{\mathrm{E}}^{*}(\omega)\vec{\mathrm{E}}(\omega) + \cdots \tag{1.2}$$

In equation (1.2), $\vec{\mathrm{E}}^{*}(\omega)$ is the complex conjugate of the electric field and $\chi^{(3)}(\omega,\omega,-\omega)$ the third order susceptibility of the nonlinear absorbing material.

Though, the semiclassical theory treats light waves as classical electromagnetic field with no quantized concept of photons, which means that it does not describe a rigorous concept of the elementary processes of MPA.[21] The better theory to describe such MPA processes is the quantum theory of radiation (Fig. 3).

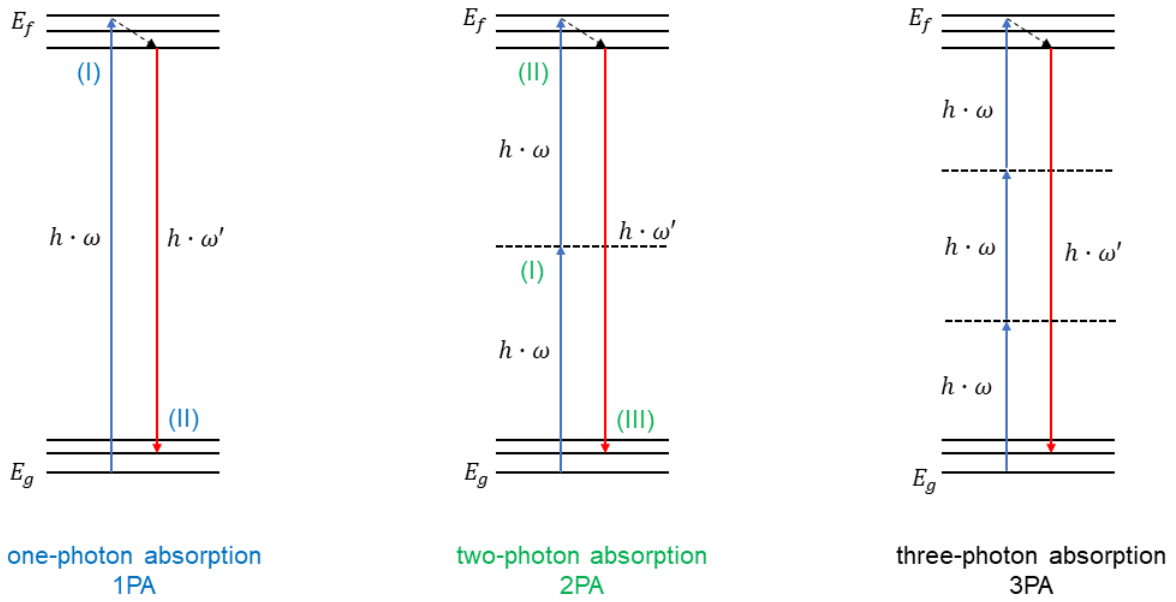

Fig. 3: Schematic representation of the 1PA, 2PA and 3PA process, whereby solid lines are representing real eigen states and dashed lines intermediate states; E_g is the ground state and E_f the final state.

For a one photon absorption process (1PA), one photon is absorbed (I), which excites the medium from the ground state E_g to the final state E_f, subsequently with relaxation back to E_g via emission of one photon (II). In contrast to 2PA, where the whole absorption process can be seen as a two-step event. At first one photon is absorbed with the energy $h\omega$ (I), whereby the medium leaves the E_g to a virtual intermediate state. In the next step another photon is absorbed exciting the medium from this virtual state to the real final state E_f (II), followed by a relaxation back to the ground state of only photon with the $h\omega'$ (III). The connection between the ground and the final state is the intermediate state, where the status of the molecule may stay in all its possible eigenstates, except E_g and E_f, with a certain probability of distribution. For this reason, the residence time of the initial state should be infinitely short. Thereby, this means that the virtual "two-step" process, is actual a one-step process, where both steps happen simultaneously.[21] The mechanism for three or more photons can be described accordingly, but the energy conservation has to be fulfilled in every case.

However, for the quantification of these processes, the attenuation of light beam passing through the optical with equation (1.3) has to be considered:[2, 21, 23]

$$\frac{dI(z)}{dz} = -\alpha I(z) - \beta I^2(z) - \gamma I^3(z) - \cdots \tag{1.3}$$

Here $I(z)$ is the intensity of the light source beam propagating the medium along the Z-axis, α, β and γ are the respective one-, two- and three-photon absorption coefficients. For a

two-photon process, it can be assumed that there is no linear absorption at the certain wavelength of the incident light and only 2PA takes place. Thus, equation (1.3) can be simplified and solved leading to equation (1.4):[21, 23]

$$\frac{dI(z)}{dz} = -\beta I^2(z) \;\rightarrow\; I(z,\lambda) = \frac{I_0(\lambda)}{1+\beta(\lambda)I_0(\lambda)z}\;(2PA) \tag{1.4}$$

where $I_0(\lambda)$ is the incident light intensity and $\beta(\lambda)$ is the wavelength dependant 2PA coefficient. This 2PA coefficient is a macroscopic parameter that is strongly dependent on the concentration, whereby $\beta(\lambda)$ in (1.4) can be further expressed (1.5):[2, 21, 23]

$$\beta(\lambda) = \sigma'^{(2)}(\lambda)N_0 = \sigma'^{(2)}(\lambda)N_A d_0 \times 10^{-3} \tag{1.5}$$

Thereby $\sigma'^{(2)}$ is the molecular two-photon cross section of the medium, N_0 is the molecular density, N_A is the Avogadro's number and d_0 is the molar concentration.
$\sigma'^{(2)}(\lambda)$ is a directly measurable variable, nevertheless it is common to use another parallel expression for the two-photon absorption which is given by equation (1.6):[2, 21, 23]

$$\sigma^{(2)}(\lambda) = \sigma'^{(2)}(\lambda) \cdot h\nu \tag{1.6}$$

with $h\nu$ as the photon energy of the incident laser beam.
These equations are needed for the quantification and interpretation of NLO processes. The second step is to find materials that are able to show such characteristics. Prominent material classes that are mostly studied in the context of such MPA activity are organic chromophores and inorganic nanoparticles. Although, these materials classes show great MPA properties, they suffer from several disadvantages like uncontrolled aggregation and low thermal stability, which already limits their applicability.[24] One possible material class, which could overcome those problems are crystalline coordination polymers (CPs), which will be further outlined in the following.[25-26]

1.1.3 The topology of Coordination Polymers (CPs)

One of the most prominent examples for this materials class of MOFs and CPs, the MOF-5 (in analogy to famous zeolite ZSM-5), was synthesized by the group of O. M. Yaghi in 1999, a $Zn_4(O)O_{12}C_6$ cluster connected via benzene-dicarboxylic acid (H_2BDC) forming a 3D framework (Fig. 4).[27]

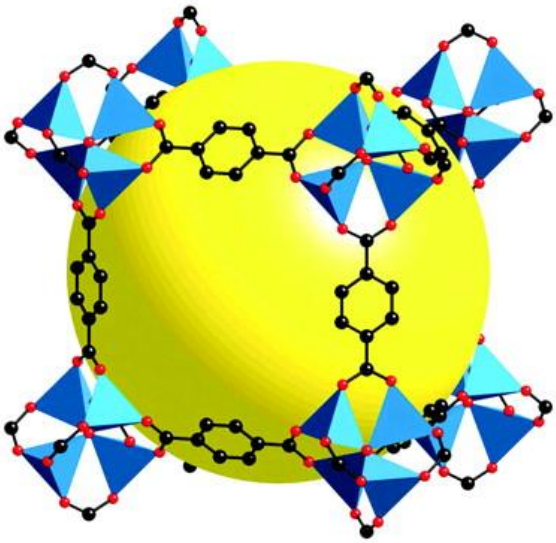

Fig. 4: Single-crystal x-ray analysis of MOF-5, with a yellow ball representing the cavity. Colour coding: Oxygen: Red sphere, Carbon: Black sphere, tetrahedral Zinc: blue tetrahedron.[27] Reprinted with permission from Nature Publishing Group, copyright 1999.

As a consequence, the synthesis and design of these novel materials were attracting more and more attention as they have shown to be applicable in gas storage, catalysis, biomedicine, optics and sensing caused by their unique structure properties.[28-38] Furthermore, this variety of properties led to more than 20.000 CP and MOF structures with similar amounts of novel network topologies, which already show the enormous potential of the materials class.[39] More specific subgroups of coordination polymers are (I) coordination networks (CNs), which are one dimensional coordination chains with cross-links to two or more individual chains, forming two or even three-dimensional networks and (II) metal-organic frameworks (MOFs), which are coordination networks with potential voids.[40-41] These MOFs were later classified by S. Kitagawa into 1st-generation MOFs, where the framework collapses upon solvent removal, 2nd-generation MOFs, where the Framework is stable upon solvent removal and 3rd-generation, where MOFs exhibit flexibility and responsivity (phase transition) upon solvent removal.[42]

However, several factors have to be taken into account which influence the properties of the CPs: choice of metal node and linker, coordination geometries of linker and SBU, secondary interactions like hydrogen bonding, π-π interactions or metal-to-ligand interactions determining the materials properties.[6] All of these interactions are dependent on the linker arrangement in the CP, which in turn leads to reticular chemistry, describing the chemistry of linking molecular building blocks to extended frameworks.[43-45] For a better abstraction of these connected networks, they can be simplified and classified by reducing their linkers and SBUs to their connectivity in order to create network topologies. It can be reduced as follows: MOF-5 has 2-connecting linker and a 6-connecting SBU, which forms a (2,6)-connecting network (Fig.

5). This connected net can now be searched in the topology database, where all of the known topology are listed in three letter codes, e.g. MOF-5 with its (2,6)-connecting net is listed as the **pcu** topology.[46]

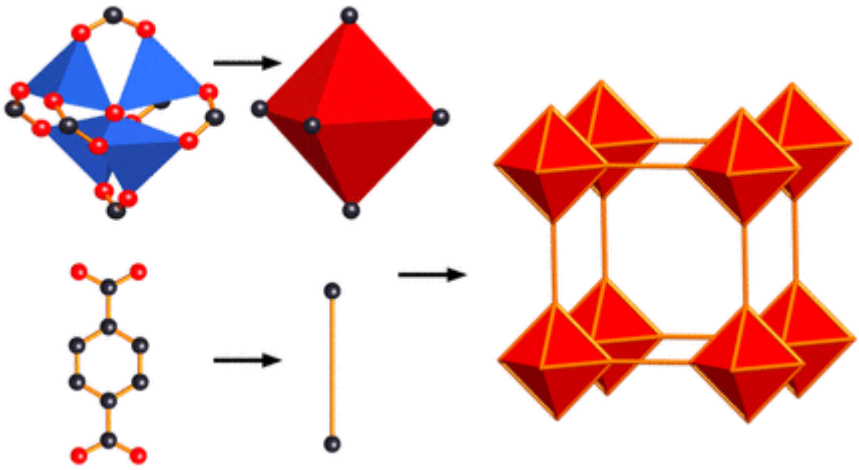

Fig. 5: Components of MOF-5 showing the 6-connecting SBU (red octahedron) and the 2-connecting linker (ball and stick) forming the (2,6)-connecting network.[46] Reprinted with permission from American Chemical Society, copyright 2014.

This topology now can be retained with different linkers, as long as the connectivity of the building blocks stays the same and the elongation does not lead to framework interpenetration. An exemplary study was performed by the group of Yaghi in 2002 with their IRMOF series, a study with the same SBU with different 2-connecting linker molecules leading to a series of 16 isoreticular **pcu** MOFs (Fig. 6).[47]

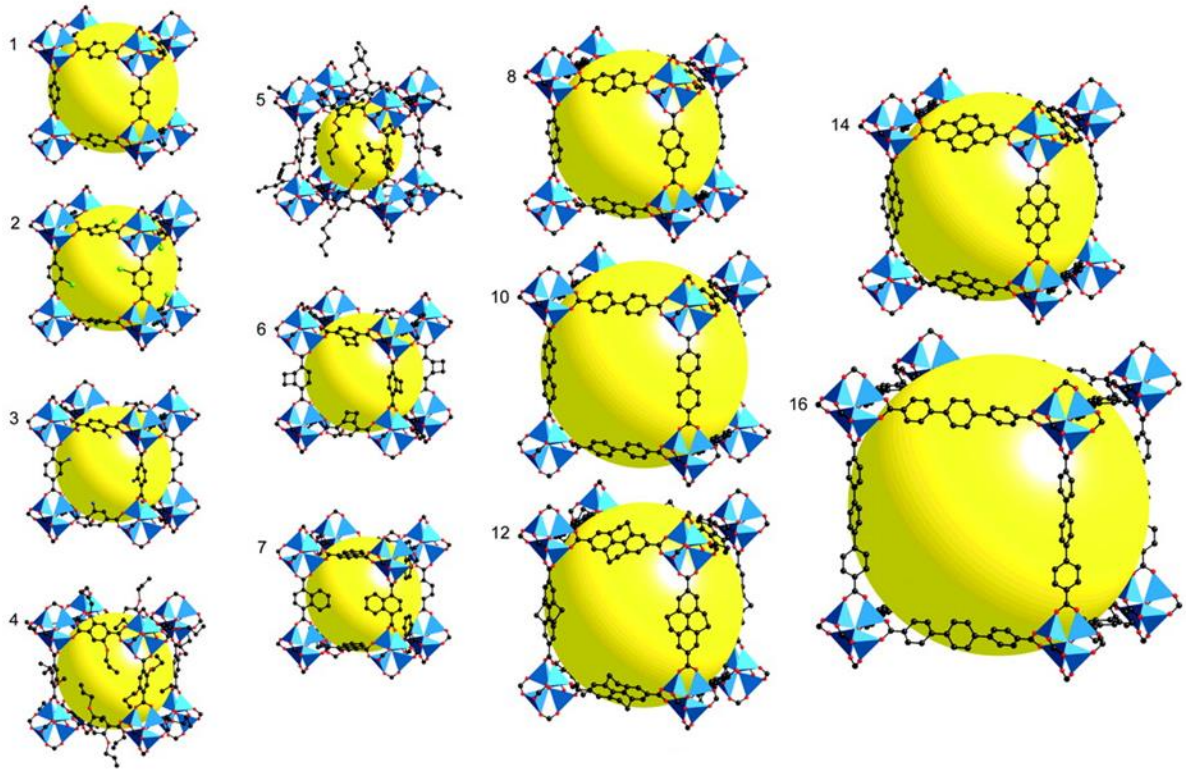

Fig. 6: Single crystal X-ray structures of the IRMOF series. Note: The doubly interpenetrated IRMOFs (9, 11, 13 and 15) are not shown. Colour coding: Oxygen: Red sphere, Carbon: Black sphere, Nitrogen: blue sphere, tetrahedral Zinc: blue tetrahedron.[47] Reprinted with permission from Science, copyright 2002.

With this crystal engineering tool by the choice of SBU and linker connectivity, different arrangements of chromophores inside the network can be achieved, in order to get a better property-structure relationship. Therefore, different design principles towards MPA active CPs have to be established.

1.1.4 Linker Design Principles for MPA active CPs

In contrast to simple CP synthesis which is only dependent on the Linker-SBU interaction, MPA active CPs can be designed in many ways, e.g. by using open shell metal precursors for the SBU, by introducing MPA active guests inside the pores, or by using MPA active linkers as chromophores.[48-50] However, this thesis focuses only on the synthesis of CPs with photophysical “silent” metals, where the MPA character originates from the linker molecule in order to deepen the understanding of a MPA-structure-property-relationship.

From an electronic structure and photophysical point of view, there is a strong correlation between an intramolecular charge transfer for the linker itself and multi-photon absorption.[51-52] This results in ideal molecular features for high MPA active chromophores. Since molecules with charge transfer processes show high MPA values, it seems that an electron-rich π-donor group, an electron poor π-acceptor or both of them are beneficial (Fig. 7).[53] Additionally, an

extent of the conjugated system has been identified to be important for a better charge separation through the chromophore.[54-56]

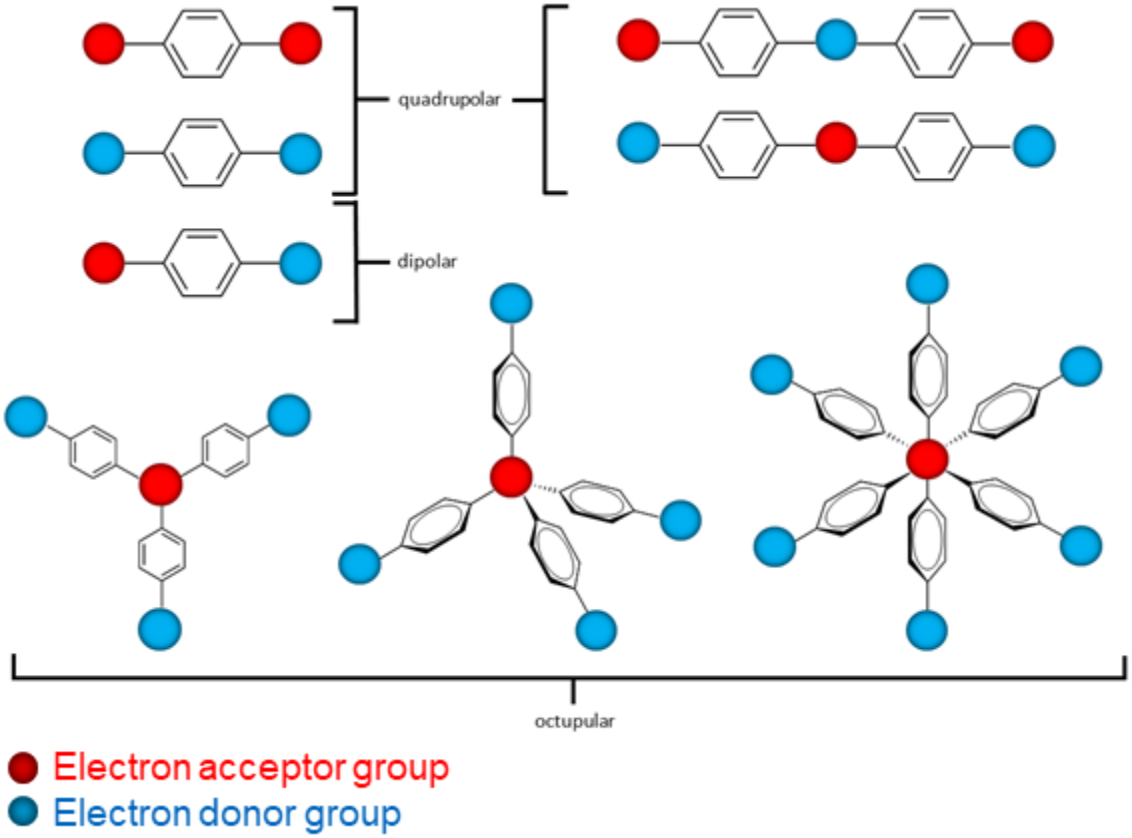

Fig. 7: Molecular structure motifs for MPA chromophores. Red ball = electron acceptor group, Blue ball = electron donor group. Note that for octupolar depictions the donor and acceptor groups can also be interchanged.[21]

Reinhardt et al. published three general types of molecular designs for chromophores: quadrupolar chromophores are symmetrical and consist of electron rich aromatic rings with either two donor or acceptor groups or one donor/acceptor group surrounded/enclosed/sandwiched by two acceptor/donor groups. Dipolar chromophores are asymmetrical molecules, consisting of electron rich aromatic rings with an electron donor and electron acceptor group.[57] The third type are octupolar chromophores, where the electron acceptor and donor groups are arranged spatially for example trigonal, tetrahedral and octahedral configuration.[58] These types could also be described applying the “push-pull” concept. Therefore, “push-push” means donor-donor interaction, whereas “pull-pull” defines acceptor-acceptor groups interactions, “pull-push-pull” and “push-pull-push”, or “push-pull” for the dipolar ones, as well as the push and pull arrangement for the octupolar molecules. As it follows, in the simplest way, a strong intramolecular charge transfer can be achieved by incorporating an electron donor and acceptor group bridged with an aromatic system.

As stated above, the chromophores itself suffer from divers limitations with respect to MPA activity, through uncontrolled aggregation in high concentrated solutions and low thermal stability.[24, 59] Therefore, the incorporation of these chromophores into CPs are perfect candidates to overcome those limitations. Additionally, the incorporation of linker molecules already increases the emissive properties due to the restriction of the radiationless energy channels caused by the restricted conformation of the linker between the metal centres.[60] This is one of the biggest advantages of MOFs and CPs compared to other materials. Additionally, in case of transition metals, metal-to-ligand charge transfer bands (MLCT) or ligand-to-metal charge transfer (LMCT) bands introduces new charge transfer bands, which can also render higher NLO properties than it would be found for the linker itself. But still, the NLO responses for CPs are primary defined by the ligand, if photophysically silent metals with closed electron shells are used.[58]

1.1.5 Benchmark MPA active CPs

The first reported MPA active CP was by Vittal and co-workers in 2015, where they incorporated a 4-connecting anthracene based linker An2py (*trans,trans*-9,10-bis(4-pyridylethenyl)anthracene), into a pillar-layered MOF, $[Zn_2(sdc)_2(An2Py)]$.[61] An2Py is a perfect role model for towards of MPA active ligands, as it is composed of pyridyl groups acting as electron withdrawing groups. Based on this work, the ligand An2Py and its derivatives represent themselves as a promising ligand motif for further studies.

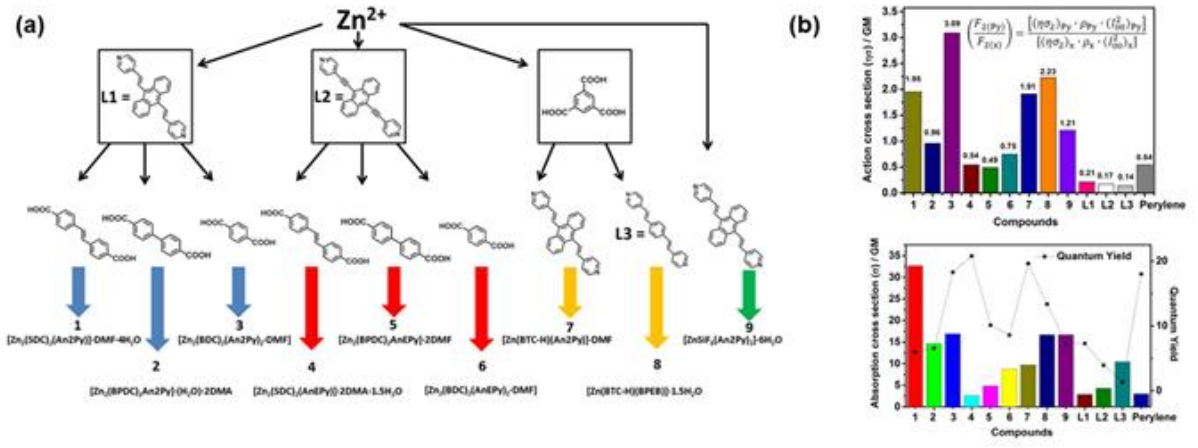

Fig. 8: (a) An overview of the used ligands in the construction of the MOFs in the study by Vittal and co-workers. (b) The measured TPA action cross-sections (upper panel) and TPA cross-sections (lower panel) of the respective MOFs.[62] Reprinted with permission from American Chemical Society, copyright 2017.

The group of Vittal and co-workers embarked upon a first systematic study to investigate structural effects on TPA properties of MOFs.[62] They synthesized and characterized a series

of nine MPA active MOFs (Fig. 8), all composed of 4-connecting A-π-D-π-A linkers (A = electron acceptor; D = electron donor) using a similar construction principle (pyridine working as electron acceptor group): An2Py, AnEPy (= *trans, trans*-9,10-bis-(4-pyridylethynyl)anthracene) and BPEB (= 1,4,-bis[2-(4-pyridyl)ethenyl]-benzene). Reaction of these bipyridine pillar linkers with different Zn^{II} precursor and co-ligands (BDC = benzene dicarboxylic acid, BPDC = biphenyl dicarboxylic acid, BTC = benzene tricarboxylic acid and SDC = *trans,trans*-4,4'-stilbene dicarboxylic acid) resulted in the respective series of pillar-layered MOFs: **1** = [Zn_2(SDC)(An2Py)], **2** = [Zn_2(BPDC)(An2Py)], **3** = [Zn_2(BDC)(An2Py)], **4** = [Zn_2(SDC)(AnEPy)], **5** = [Zn_2(BPDC)(AnEPy)], **6** = [Zn_2(BDC)(AnEPy)], **7** = [Zn(BTC-H)(An2Py)], **8** = [Zn(BTC-H)(BPEP)], **9** = [$ZnSiF_6$(An2Py)].

Nonetheless, the analysis of the collected two-photon responses showed no clear structural trend. The reason for the different behaviour results from a couple of interplaying factors, such as conjugation degree of the auxiliary linker, linker rotation within the frameworks or possible pores, induced by the systematic variation of the length and connectivity of the auxiliary ligand and the responding alternation in MOF structure. However, the nature of the 2PA cross sections of the used ligands (An2Py > AnEPy > BPEP) was transferred to the MOFs and all MOFs showed higher TP brightness than their respective ligands, which confirmed the success of incorporating chromophores as linkers inside the MOFs while enhancing its MPA activity.

In 2017, Fischer and co-workers studied a series of zirconium and hafnium based MOFs assembled from H_4TCPE (tetrakis[4-((4-carboxylato)phenyl)phenyl]ethylene) chromophore, PCN-128(Zr,Hf) and PCN-94(Zr, Hf). They systematically varied the parameters affecting/influencing the chromophores, such as the electron withdrawing capacity of the metal-oxo-clusters, the ligand deformation of linkers and the variation of underlying structure motifs (cubic vs. hexagonal space group symmetry) (Fig. 9).[63] Using the internal-standard MPEF method (IT-MPEF) with rhodamine B as standard, the authors measured strong two-photon excited fluorescence (2PEF) with action cross-section values reaching 3582 GM. They revealed a couple of governing parameters responsible for the enhanced NLO response: (I) differences in the charge distribution of the used linker, due to enhanced electron withdrawing of the metal-oxo clusters initiated by coordinating trifluoroacetic acid co-ligands; (II) structure depending framework forces, which lead to a ligand deformation accompanied by its 2PA properties; (III) higher TPA cross sections calculated for the unit-cells of the MOFs as a direct consequence of the spatial arrangement of chromophores within the framework.

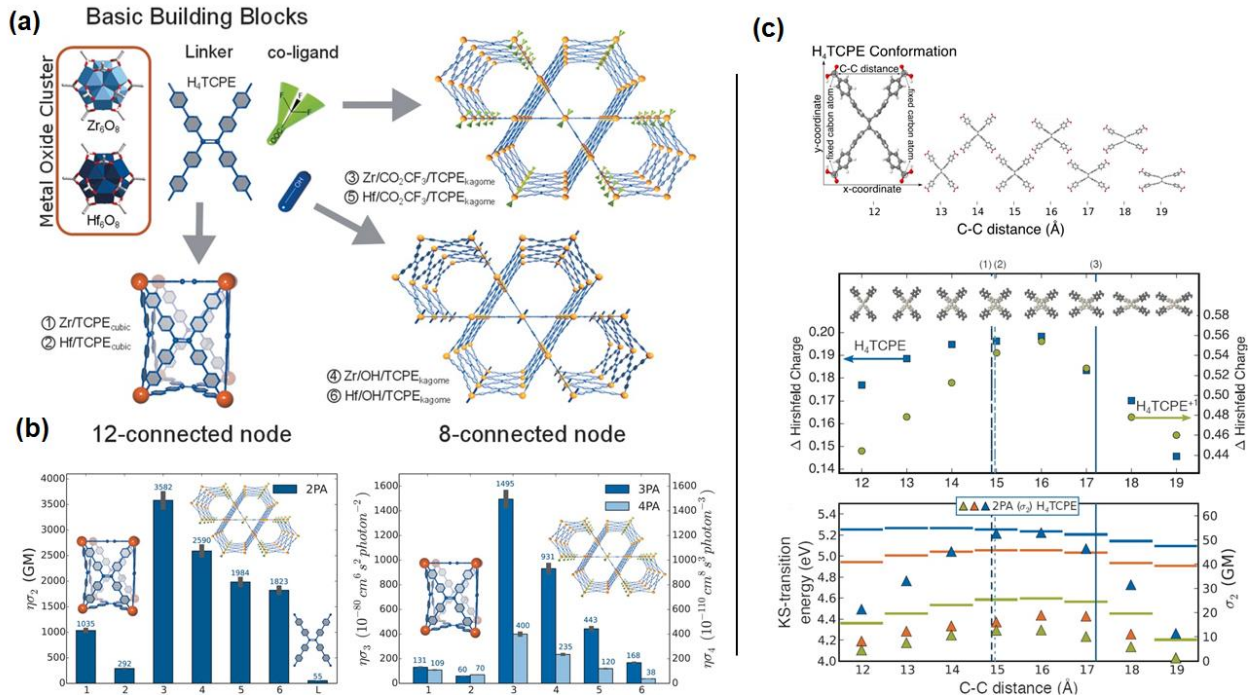

Fig. 9: (a) The depiction of the investigated materials by Fischer et al. (b) The measured 2,3, and 4PA action cross-sections of the MOFs. (c) An overview of the theoretical study towards linker deformation and charge polarization in the framework.[63] Reprinted with permission from John Wiley and Sons, copyright 2017.

A further step for establishing a structural-MPA-property relationship was conducted by Fischer and co-workers in 2019.[50] The authors investigated two CPs, $[Zn_2(TPBD)(DMAc)_2]$ and $[Cd_2(TPBD)(H_2O)_4]$, consisting of the push-pull linker H_4TPBD (tetrakisphenylphenylenediamine), which was designed following synthetic guidelines of multiphoton absorbers as stated in the beginning. According to the authors, the 3D-CP $[Cd_2(TPBD)(H_2O)_4]$ showed an one order of magnitude higher TPA efficiency than the 2D-CP $[Zn_2(TPBD)(DMAc)_2]$, which was explained as a result of denser packing, type and strength of excited state delocalization ultimately affecting the electronic structure of the CPs (Fig. 10).

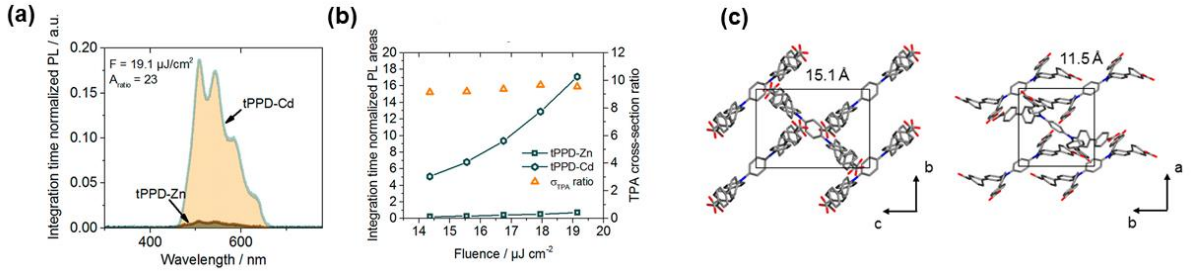

Fig. 10: (a) The measured TPEF spectra of $[Zn_2(TPBD)(DMAc)_2]$ and $[Cd_2(TPBD)(H_2O)_4$. (b) The integrated TPEF areas at different laser intensities and the corresponding TPA cross-section ratio. (c) The TPBD packing motifs in the CPs (left: $[Zn_2(TPBD)(DMAc)_2]$; right: $[Cd_2(TPBD)(H_2O)_4]$).[50] Reprinted with permissions from American Chemical Society, copyright 2019.

Very recently, Vittal and co-workers published another structure-activity study on the H_4tcpe linker molecule mixed with different stilbene based pillar ligands and zinc as metal precursor, in order to synthesize 5 MOFs with different pillar ligands (Fig. 11).[64] Thereby, the 2D MOF without a pillar ligand shows a two-photon absorption action cross section $\eta\sigma$ of up to 7 x 10^7 GM, which is three orders of magnitude higher than state-of-the-art organic lumophores and is up to now, the highest MPA cross section ever reported for MOFs and CPs. In comparison, the other MOFs with the additional pillar ligands in between only show lower two-photon absorption action cross section of roughly 100 GM. The authors explained this phenomenon by the additional aromatic cores between the chromophore layers introduced by pillar ligands, which is slowing down the charge transfer from layer to layer, whereas the MPA performance is decreasing.

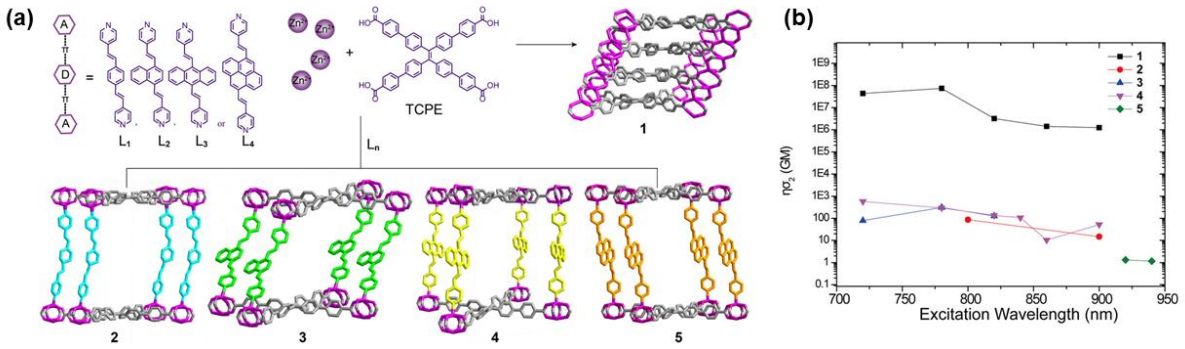

Fig. 11: (a) Depiction of the synthesized pillar layers CPs 1-5 by Vittal and co-workers. (b) Two-photon action cross section ησ of the synthesized CPs 1-5.[64] Reprinted with permissions from John Wiley and Sons, copyright 2022.

1.2 CPs as light harvesting materials

One of the biggest challenges, that mankind has to face, is anthropogenic global warming initiated through emission of greenhouse gases (e.g. CO_2, NO_x).[65] In contrast to that, the worldwide energy usage is rapidly increasing, which in turn leads to an enhanced scarcity of resources. Therefore, a conversion of these greenhouse gases back into valuable chemicals is in the focus of current research. However, a view in nature pinpoints a process, the photosynthesis, where plants, algae, bacteria and other organisms use the sunlight to convert CO_2. This biochemical process is one of the most fundamental processes assuring life on earth. Hereby, light-absorbing dyes such as chlorophyll are utilized to convert light energy into chemical energy. This energy is then used to create energy-rich organic compounds, primarily carbohydrates, from low-energy inorganic substances as carbon-dioxide and water.[66] The sum of all renewable energy, that would theoretically be available from all sources within one year, is equivalent to the amount of usable energy that reaches the earth in the form of sunlight

within one hour. This shows the enormous potential of the sun as an energy source, whereby in the long term, it will be of eminent importance for humanity to convert, use and store the energy provided by solar radiation in an affordable model. Therefore, mimicking the fundamental reactions of the natural photosynthesis by building and constructing an efficient, robust and economic artificial leaf is a significant task.[66-67]

There are two decisive steps of natural photosynthesis: the photochemical splitting of water and the reduction of CO_2, which take place in photosystem I and photosystem II.[66-68]

In palm cells the electron transfer takes place in the thylakoid membrane located in the inner part of the chloroplast (Fig. 12).

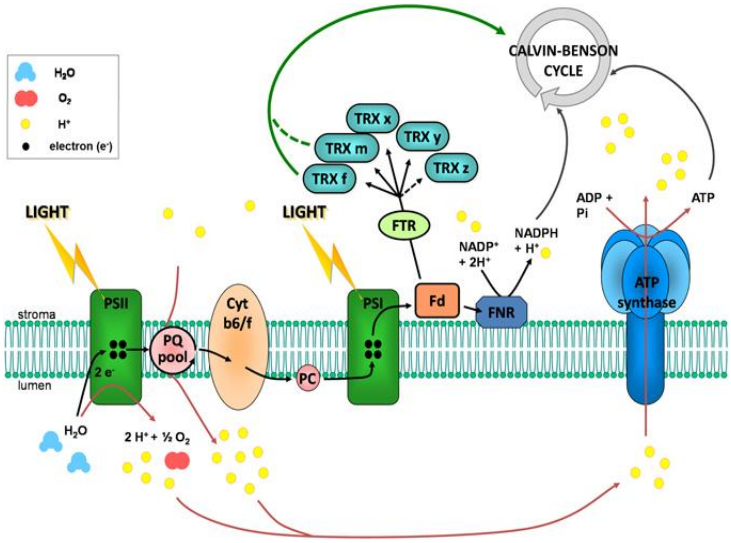

Fig. 12: Schematic representation of the electron transfer chain inside a thylakoid membrane.[69] Reprinted with permission from Frontiers in Plant Science, copyright 2013.

By absorbing light, electrons are first released from the reaction centers of the chlorophyll. These electrons are then transferred via various electron-transfer mediators of the photosystems, which starts a series of redox reactions. Thereby, the mediators are arranged spatially so that the electron transfer is directed from the inner to the outer part of the membrane.[70]

To mimic, use and apply these natural processes for synthetic photoactive materials, it is of great importance to understand the energy transfer inside, since this is the crucial step for a high efficiency process.

1.2.1 Types of Energy Transfers (ET) in CPs

Due to the synthetic bandwidth of MOF designs as indicated in the chapters above, functionalized chromophores can be directly utilized as linker molecules in CP synthesis. This enables the possibility of unique directed energy transfers (ET), a generic term for charge

transfer, inside the solid framework through four different pathways inside the solid framework: host-guest, ligand-to-metal, metal-to-metal and ligand-to-ligand (Fig. 13).[71-74]

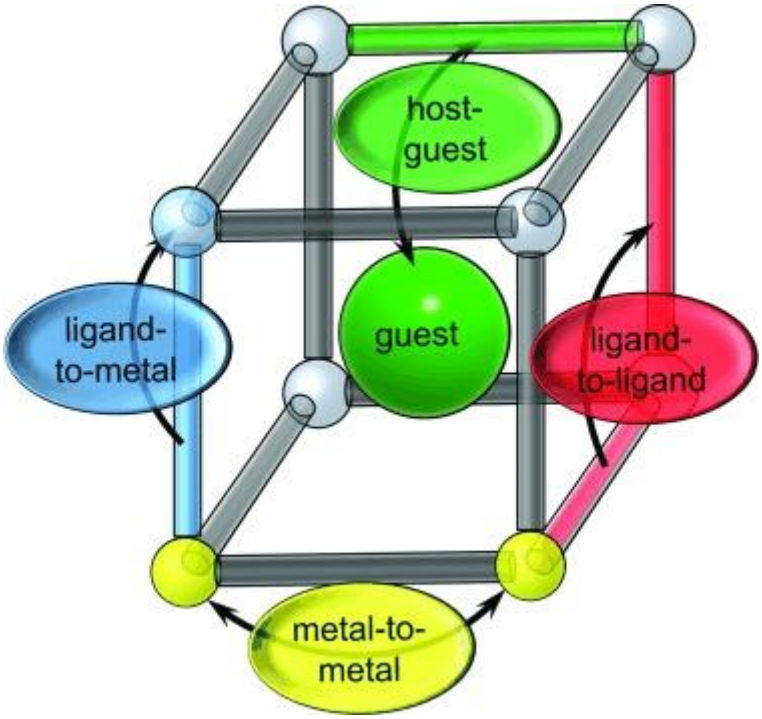

Fig. 13: A schematic representation of the different types of energy transfers inside the framework.[71] Reprinted with permission from John Wiley and Sons, copyright 2015.

Due to its pore structure, MOFs enable the possibility of inserting chromophore molecules as guests inside the framework. In turn, this leads to possible host-to-guest or guest-to-host ET processes. In 2013 Sun and co-workers studied this phenomenon of efficient host-guest interaction through adsorption of different dye molecules into a zeolitic MOF which increased the light harvesting properties and therefore the ET properties.[75]

Furthermore, MOFs are able to show ET between the metals, which was first reported by the groups of Lin and Mayer.[76-77] The authors reported a phosphorescent MOF [Ru(bpy)(4,4′-dcbpy)$_2$][PF_6]$_2$, which was doped with Os instead of Ru inside the linker molecule. This has the effect of an effective phosphorescence quenching by a Ru-to-Os energy migration.

Moreover, through the orbital overlap of linker and metals, MOFs have also the possibility of ligand-to-metal and metal-to-ligand ET. One major class towards this processes are lanthanide-based frameworks.[78-80] For these materials, typically the organic linker absorbs the light, then this energy is transferred to metal-ion and finally resulting in lanthanide-emission.[71] However, the ET, which follows the same principle as for the MPA based novel materials, are CPs that enable ligand-to-ligand ET. To observe this ET one set of chromophores are used as fluorophore donors and transfers the energy to the neighboured chromophores acceptors.[71] This concept was already established by groups of Hupp and Farha, where the authors

demonstrated this principle by achieving an efficient förster-resonance energy transfer (FRET) from the pillar ligand to the porphyrin based tetratopic linker.[81]

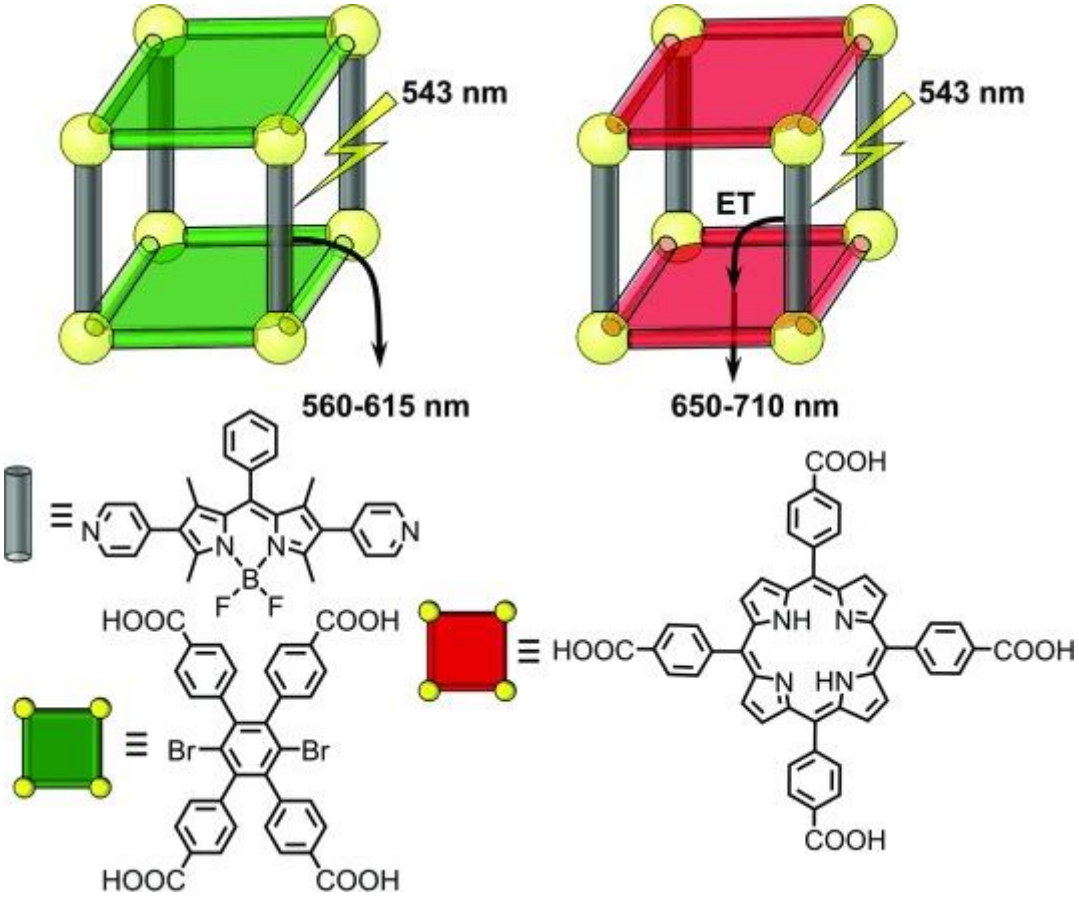

Fig. 14: Activation of the ET process by replacement of the tetratopic ligand (green) with the porphyrin-based linker red (red).[71] Reprinted with permission from John Wiley and Sons, copyright 2015.

However, to design those materials capable of ET process the underlying mechanisms have to be understood.

1.2.2 Förster and Dexter Energy transfer

Typically, weak chromophore couplings are observed in supramolecular materials like CPs and MOFs, whereas Förster and Dexter mechanisms are responsible for the ET.[82-83] Therefore, to describe the underlying processes a two-state model is proposed: the energy is transferred from an excited chromophore donor (**D***) to an acceptor chromophore in the ground state (**A**), which leads to a relaxation of the excited electron of the donor (**D**) and excitation of an electron of the acceptor (**A***) (Fig. 15).[72, 84]

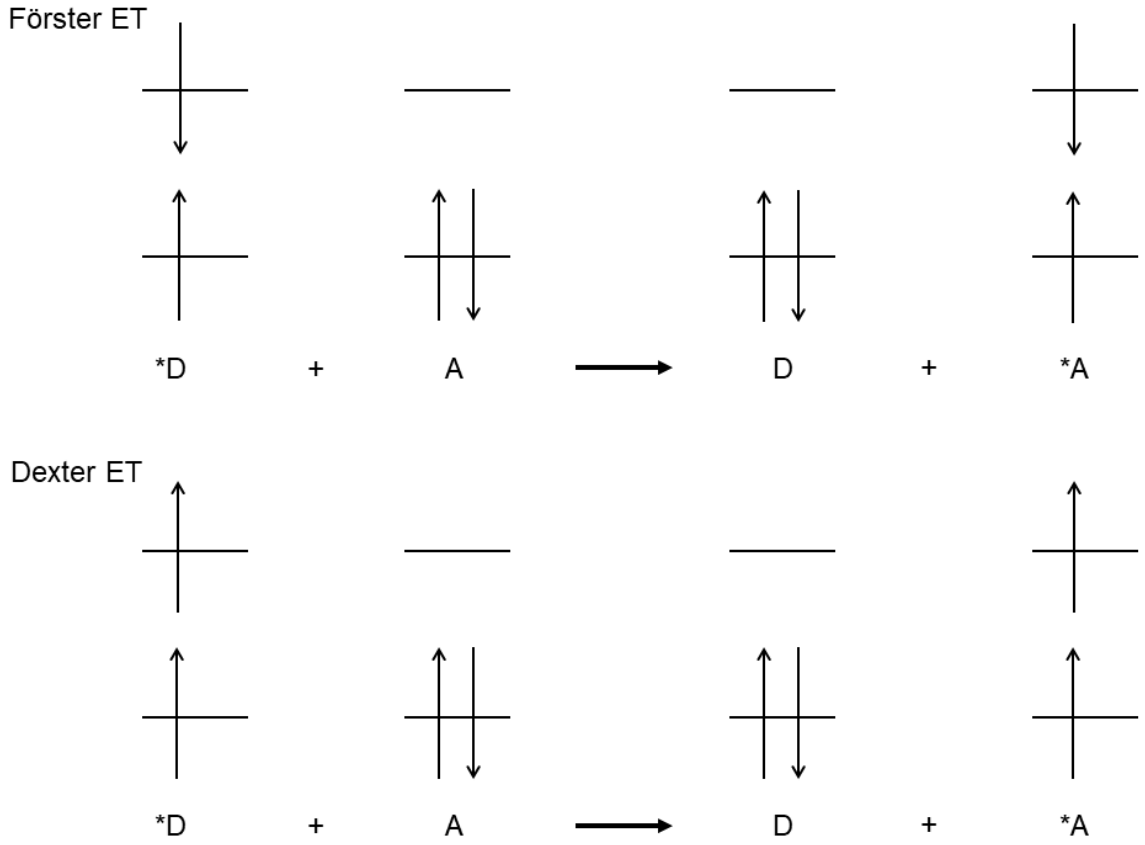

Fig. 15: Depiction of the singlet-singlet Förster (above) and triplet-triplet Dexter ET (below) mechanism.[71]

Nonetheless, the energy is transferred by dipole-dipole interactions without radiation and is therefore not transported via emission and absorption of photons.[71, 85] Thus, FRET is known to occur as a singlet-singlet transfer and can be typically observed in a chromophore distance range of 1-10 nm, whereas Dexter is a triplet-triplet transfer with a chromophore distance with less than 1 nm.[86]

The extent of the FRET, represented as the transfer rate k_{ET}, depends on the radiation emission rate of the donor dye k_D, its residence time in the excited state τ_D and in particular on the distance between donor and acceptor dye r. The efficiency of the ET decreases six orders of magnitude with respect to the distance between the two dyes. Hence, the transfer rate is also determined by the Förster radius R_0 of the donor-acceptor dye pair, whereby R_0 corresponds to the distance between both dyes at which the energy transfer is 50%.[84]

$$k_{ET} = \frac{1}{\tau_D}\left(\frac{R_0}{r}\right)^6 \tag{2.1}$$

Equation (2.1) underpins, that the distance r must be as small as possible in order to obtain an efficient transfer.[71] Additionally, the interplay between the distance orientation of the

chromophores is essential for a good ET. Therefore, the orientation factor k^2 will be defined as follows (2.2):

$$k^2 = (\cos\theta_{DA} - 3\cos\theta_D \cos\theta_A)^2 \qquad (2.2)$$

θ_{DA} represents the angle between the emission dipole of the donor dye and the absorption dipole of the acceptor dye. θ_D and θ_A are the angles between both dipoles and the connection vector between donor and acceptor dye. According to the definition of k^2 and in order to generate an optimal energy transfer, donor and acceptor chromophore should have parallel electronic oscillation planes (Fig. 16).[87]

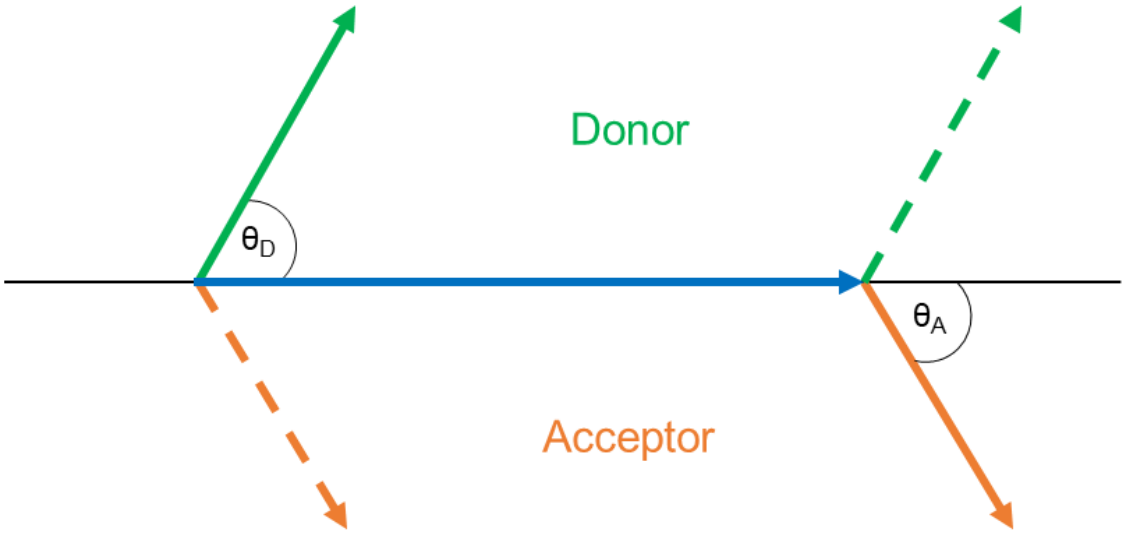

Fig. 16: Angle dependency of Donor and Acceptor of the FRET efficiency $\boldsymbol{k^2}$.[87]

In contrast to FRET, energy transfer rate k_{ET} of the Dexter-type ET is decays exponentially with increasing interchromophoric distance. Also, the integral J from the overlapping of the energy functions of donor and acceptor chromophore is a basic requirement for Dexter-type ETs.[71, 88] Equation (2.3) shows the dependency of k_{ET}, where L is the sum of D-A van der Waals radii.

$$k_{ET} = J \cdot e^{\frac{-2r}{L}} \qquad (2.3)$$

1.2.3 Influence of aggregation on the energy transfer

Additionally, in order to deepen the understanding of ET inside CPs, the influence of aggregation on the electronic coupling have to be considered, since with strong coupling between the chromophores conclusions on their ET can be drawn, e.g. weak coupling between chromophores, will also lead to a weak energy transfer rates between them. In 1963 Kasha proposed spectral effects with respect to the type of aggregation and its strength.[89] In the publication, Kasha classified two types of aggregation (H- and J-aggregates), which is predicted on coulomb coupling J_C^{pd} between molecule 1 and 2 (2.4):[90-92]

$$J_C^{pd} = \frac{\mu^2(1 - 3\cos^2\theta)}{4\pi\varepsilon R^3} \tag{2.4}$$

Thereby μ is dependent on the relative orientation θ of dipole moments. J-type aggregates, or "head-to-tail" orientation describes the aggregates, where the angle θ between the dipole moments is less than the "magic angle" of $\theta_M = 54.7°$ ($J_C^{pd} = 0$), which leads to a negative coulomb coupling ($J_C^{pd} < 0$). Consequently, for H-type aggregation, or head-to-head orientation, the angle θ is bigger than the "magic angle", whereby this leads to a positive coulomb coupling ($J_C^{pd} > 0$).[91]

This different behavior of coulomb coupling has a direct influence on the photophysical response since this coupling leads to two delocalized excited split states. These split states are linear combinations of two local excited states of each monomer (Fig. 17).

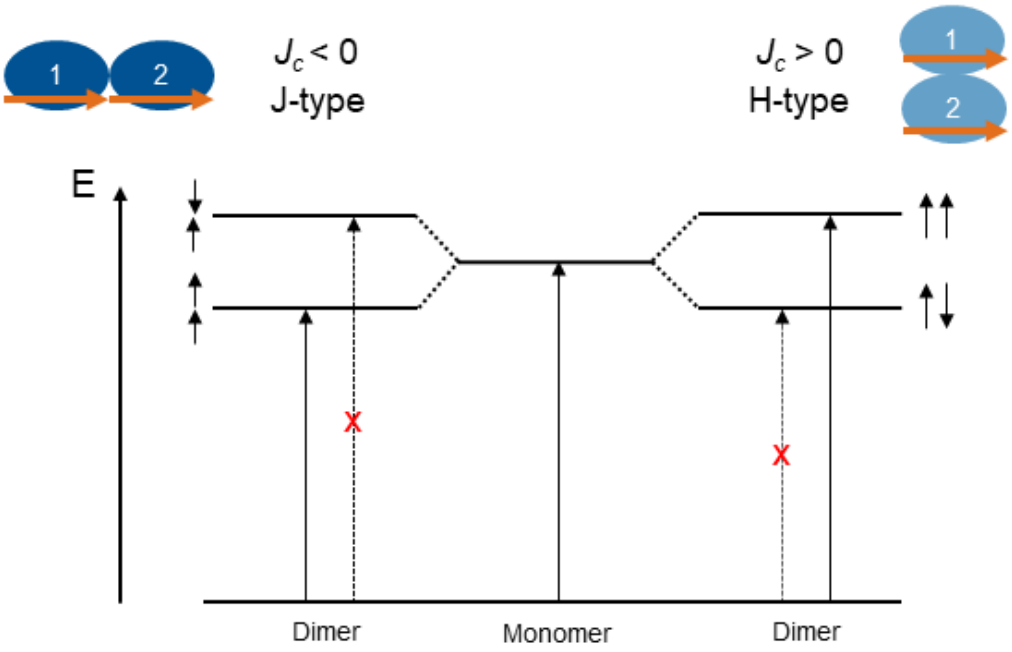

Fig. 17: Energy diagrams for J-type (left) and H-type (right) aggregate dimers.[89]

For J-aggregates, the negative coulomb coupling results in the symmetric state having lower energy than the antisymmetric state, whereas for H-type it is reversed. Consequently, the main absorption peak of J-type aggregates is red-shifted compared to the corresponding monomer. For H-type aggregates the antisymmetric state has the lowest energy level, but this state is forbidden, whereas the main absorption peak is blue-shifted compared to the monomer.[89, 91-92] Furthermore, the extent of shift and intensity of absorption, gives also information on the strength of the coupling, which is also an indicator for the ET inside the material.

1.2.4 Rylene Dyes as efficient light harvesting chromophores

Another decisive factor for the energy transfer inside the material, besides the orientation, is the choice of the chromophore itself. Due to the large delocalized π-electron system, Rylene dyes (R-n) and rylene diimides (RD-n) (Fig. 18) are an outstanding class of organic dye molecules, which were initially applied for industrial use as dyes and pigments in automotive finishes.[93] They consist of polycylic hydrocarbons that are connected by its smallest subunit naphthalene (R-1), whereas rylene diimides have additionally two diimide groups at the end positions of the chromophore.

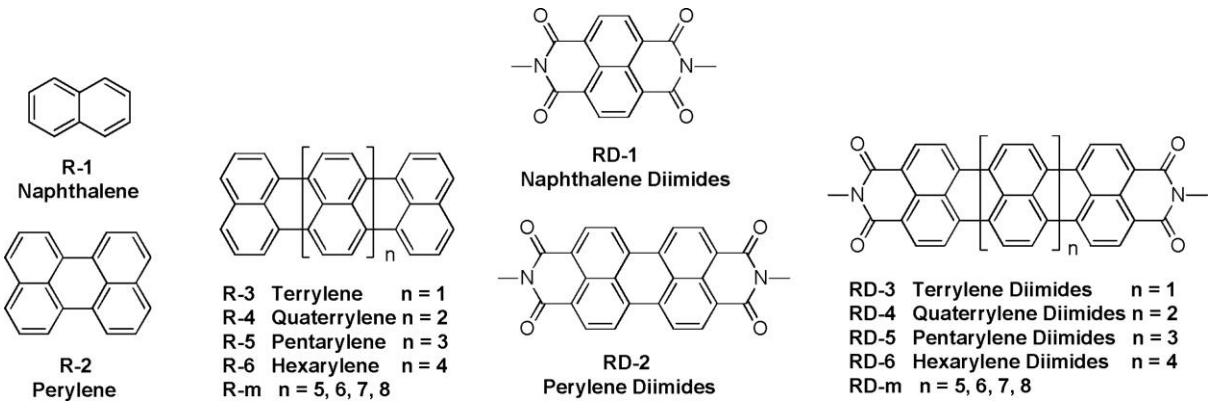

Fig. 18: Chemical structure of rylene dyes and their corresponding diimides.[94] Reprinted with permission from American Chemical Society, copyright 2016.

They became widely used in manifold applications in industry as well as in research, due to their outstanding properties such as their chemical, thermal and optical stability.[95-96]
In addition, they exhibit outstanding optoelectronic properties and are known to be excellent light-harvesting materials. Rylenes have also a strong visible light-absorption ability and show high fluorescence quantum yields in solution.[97] Furthermore, they reveal a big conjugated π-system as well as large molar absorption coefficients, which results in strong intermolecular coulomb coupling, which is as stated above a prerequisite for a good ET transfer.[98]
They are also comparably easy to modify, since the hydrogen at the bay position can be easily substituted with various side-groups influencing the photophysical properties as the π-stacking behaviour. This has also an impact on the chemical properties of the rylene chromophore, as plenary structure of the aromatic system to rotated aromatic rings (Fig. 19).[99]

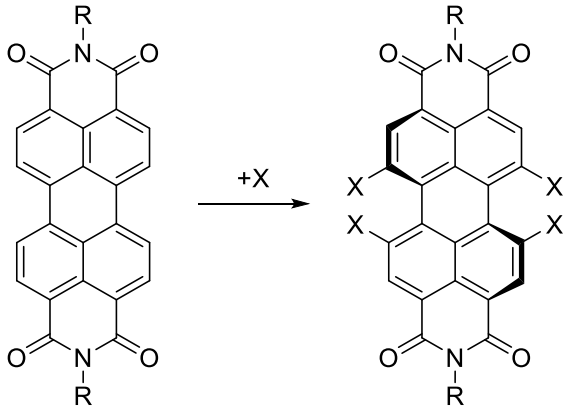

Fig. 19: Rotation of aromatic rings of the perylene diimide after equatorial substitution.

Taking all these photophysical properties into account, functionalized rylene dyes, or more specific perylene diimide dyes (PDI), represents themselves as perfect candidates towards light harvesting chromophores for the ET investigation inside the CP material.

1.2.5 Perylene diimide (PDI) based CPs

Due to their low solubility in common solvents and strong π-stacking, there are only a few examples of PDI derived coordination polymers.

In 2016 Duan et al. published the first example of a PDI based zinc coordination polymer, which is active in photoinduced aryl-halide reduction.[100]

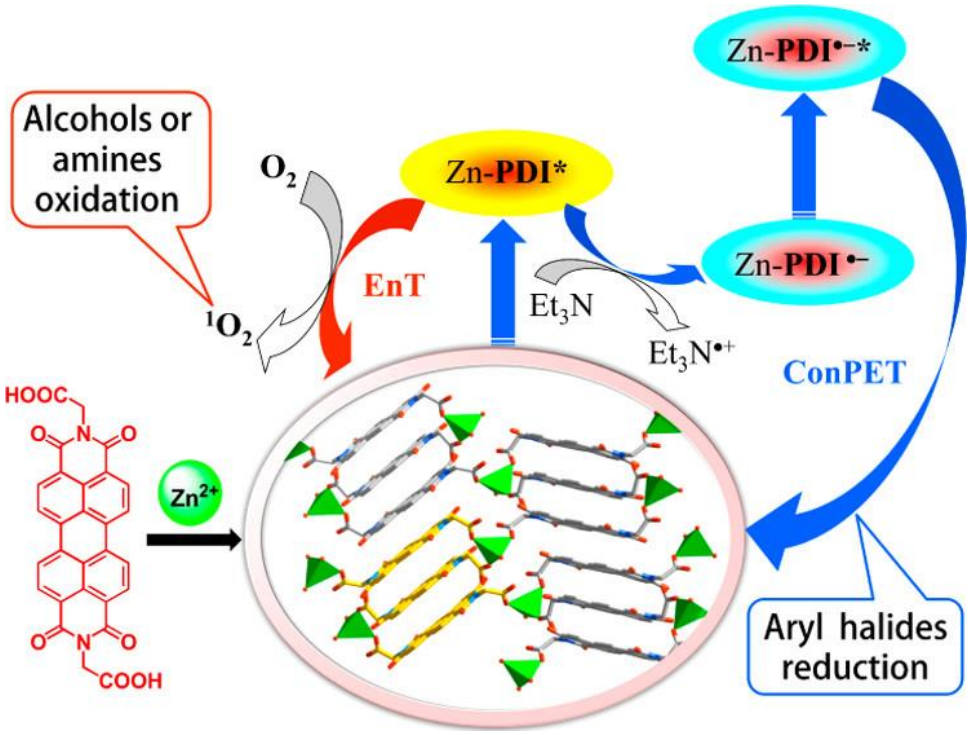

Fig. 20: Illustration of the halide reduction with the zinc-PDI based photocatalyst.[100] Reprinted with permission from American Chemical Society, copyright 2016.

The reaction mechanism of the photoreduction follows the principle of a consecutive photo-induced electron transfer (conPET) process with triethylamine as electron donor (Figure 20). First, the Zn-PDI is excited to Zn-PDI* upon light irradiation. Subsequently, the triethylamine donates an electron to the excited Zn-PDI*, which is then used to reduce the aryl halide. Furthermore, the CP shows a better performance towards the photoreduction compared to the linker itself, which is due to synergistic effects between the Zn ion and the linker.[100]

Furthermore, in 2018 Rodriguez and co-workers synthesized a 3D potassium based CP built from perylene-3,4,9,10-tetracarboxylate linker (Fig. 21).[101]

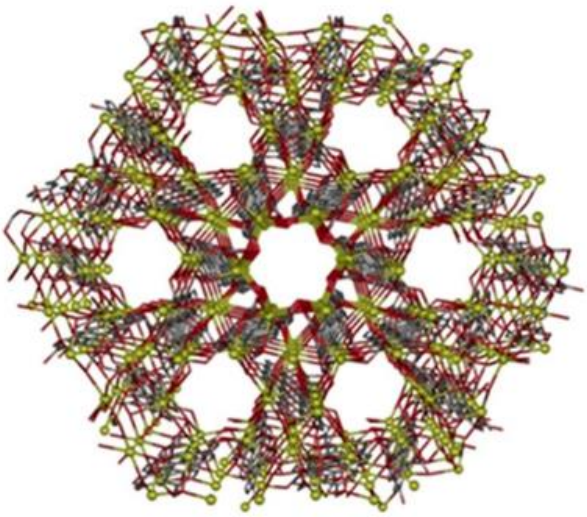

Fig. 21: Single-crystal x-ray structure of the potassium CP. Colour coding: Oxygen: red, Carbon: grey, Potassium: yellow.[101] Reprinted with permission from Nature Publishing Group, copyright 2018.

The synthesized CP shows intense photoluminescence with a blue-shift of the absorption band compared to the solvated linker. The authors explained this effect by the hindrance of π-stacking of the linker molecule, by its incorporation into the potassium framework.[101] Recently, Müllen and Yin et al. published a perylenediimide MOF, Zr-PDI, which is able to trap electron donors in order to generate stable radicals (Fig. 22).[102]

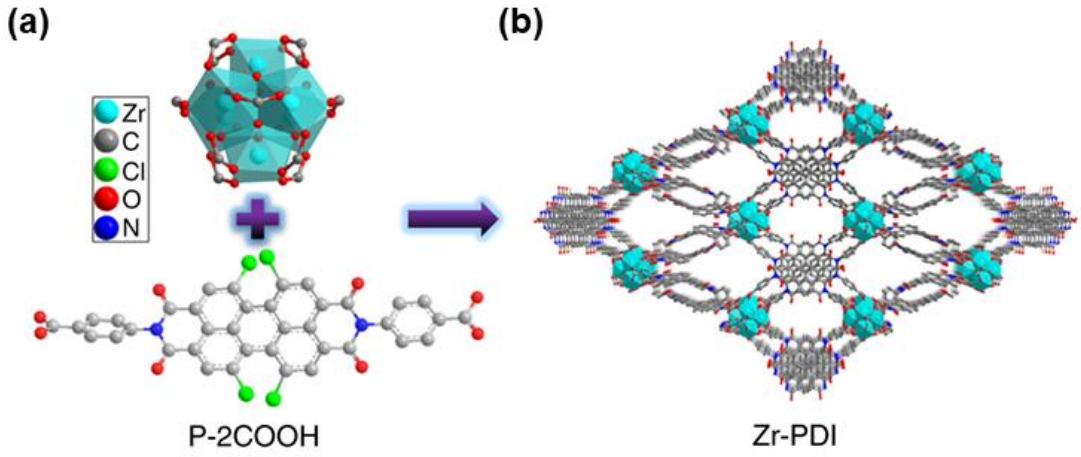

Fig. 22: (a) Structure of the zirconium cluster and the respective linker. (b) Single-crystal x-ray structure of Zr-PDI.[102] Reprinted with permission from Nature Publishing Group, copyright 2019.

Upon irradiation with an electron donor, the Zr-PDI also forms a Zr-PDI$^{\bullet-}$ radical through a PET process. However, the generated radicals are stable and stay unobstructed for nearly a month, which makes this MOF material a potential candidate as radical trapper in biomedicine and photothermal therapy.[102]

2 Objectives

Coordination polymers and metal-organic frameworks offer unique properties that are beneficial for photoelectronic applications since they are highly versatile through the possibility of the incorporation of different chromophores as linker. However, there are still unanswered research questions related to this topic, which are targeted within this thesis.

“How is the MPA activity of coordination polymers dependent on the (I) choice of linker and (II) their arrangement inside the framework?”
“What is the influence of the metal-ions of the secondary building units on the photophysical properties of the solid-state material?”
“Can the outstanding photocatalytic properties e.g. photosensitization of PDIs be retained while they are incorporated in coordination polymers?"

First, in order to synthesize MPA-active CPs, NLO active chromophore linkers have to be synthesized. Therefore, the well-investigated carbazoles as electron donor are bridged over π-systems, to construct linker molecules following the push/pull principle. Afterwards, these linkers were used for a solvothermal synthesis screening, to synthesize new coordination polymers. The first research question is targeted, by using different metal-salts with either the same or different linkers, to get more insights into a structural-photophysical-property relationship.
Furthermore, through synthesizing isostructural CPs with different metal salts using the crystal engineering tool of the reticular chemistry, the metal influence on the MPA properties are studied. Thereby, the key target towards the first two research questions is the systematic screening to find the optimal reaction conditions towards crystalline coordination polymers, which can later be used for Z-scan measurements.
The third research question is aiming towards the energy transfer inside CPs using PDIs as linker molecules. Therefore, as a first step a soluble PDI based linker is/will be synthesized. This could be achieved by the substitution of hydrogen atoms at the bay-position which leads to a rotation of the phenyl rings and thus decreases the π-stacking of the chromophore. Consequently, this soluble PDI linker is screened towards single-crystalline coordination polymers. As a last step, the synthesized materials are then tested towards possible retained photocatalytic properties, for which there was precedence in the literature on PDI based coordination complexes showing similar characteristics.

3 Summary and Discussion of Publications

3.1 A Nitrophenyl-Carbazole based Push-Push Linker as a Bulding Block for Non-Linear Optical Active Coordination Polymers: A Structural and Photophysical Study

To incorporate NLO active molecules as linkers inside coordination polymers, rigid donor and acceptor groups have to be identified. Therefore, carbazoles having electron donor properties were synthetically combined with the electron accepting nitro benzene in order to synthesize a dipolar push/pull chromophore. In this manuscript the synthesis and photophysical study of the novel chromophore dipropyl-9-(4-nitrophenyl)-carbazole-3,6-dicarboxylate (H_2CbzNO_2), designed for NLO active coordination polymers, is reported. The chromophore was characterized by ^{1}H-NMR and ^{13}C-NMR spectroscopy, LIFDI-MS, elemental analysis and single-crystal x-ray diffraction (SC-XRD). Thereby, SC-X-ray analysis of H_2CbzNO_2 revealed, that it crystallizes in the monoclinic crystal system *P* $2_1/c$ with antiparallel linker packing throughout the unit cell. The solvated chromophore exhibits an aromatic emission band at 360 nm as well as an intramolecular charge transfer emission band at 420 nm. This charge transfer band red-shifts with increasing solvent polarity with the characteristics of a twisted-intramolecular charge transfer transition (TICT) between the carbazole unit and the nitro group. Furthermore, in more polar surroundings this TICT-state will be further stabilized due to the increased dipole moment upon twisting of the chromophores alongside the C-N axis. As a consequence, the TICT state will stronger contribute to the emission (Fig. 23).

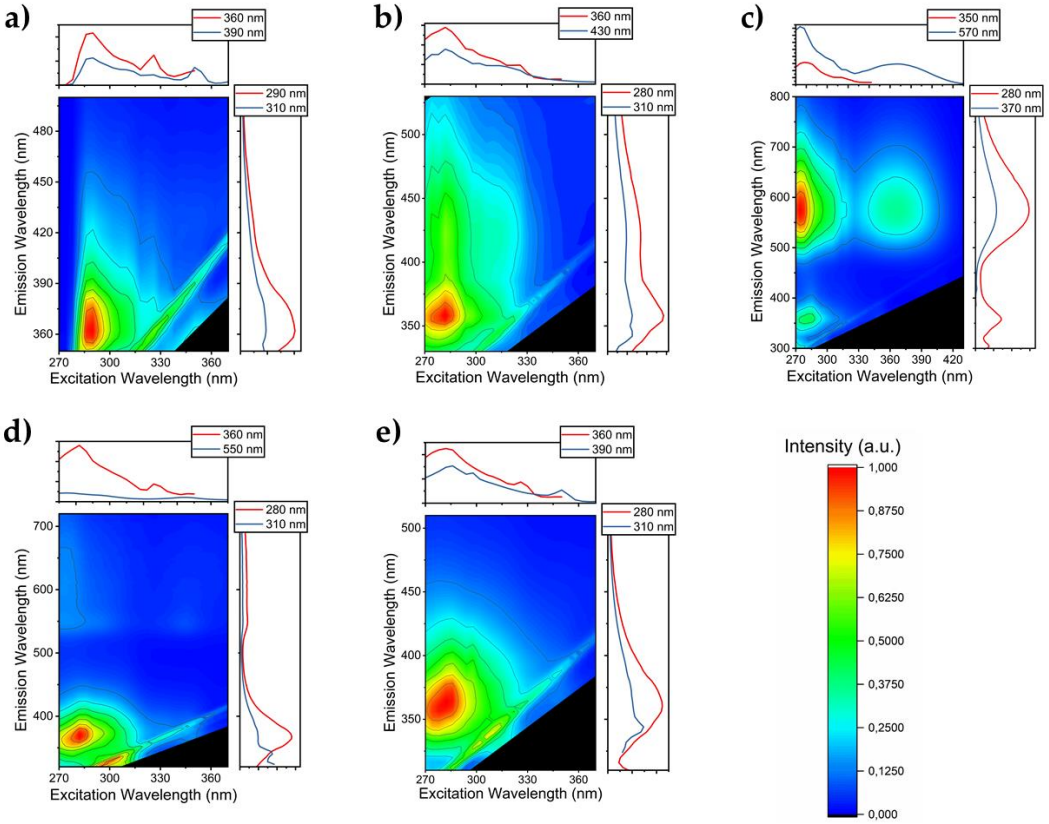

Fig. 23: Excitation-emission-matrices (EEM) of Pr_2CbzNO_2 in different solvents: a) toluene, b) THF, c) DCM, d) acetonitrile and e) ethanol**.**

However, in very polar solvents like ethanol and acetonitrile, this TICT state is potentially lowered leading to a charge-separation, which in turn is quenching the TICT fluorescence (Fig. 24).

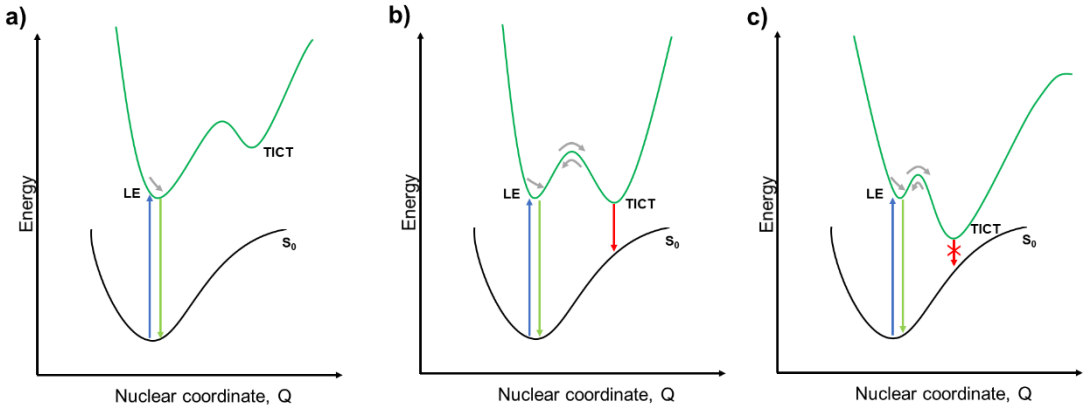

Fig. 24: A pictorial description of the interplay between LE and CT states in the push-pull chromophore and how the solvent reaction field shapes the excited state PES.

Additionally, Solid-state photoluminescence spectroscopy of the chromophore showed, that it is a green emitting chromophore with contributions from π-stacked excimer formation.

The conceptualization and original draft preparation of this manuscript, the experiments and the chemical characterization was performed by the author of this thesis. Methodology, review and editing was performed by the author of this thesis in collaboration with D. C. Mayer, E. Thyrhaug, A. Pöthig, J. Hauer and R. A. Fischer. UV/Vis and photoluminescence spectroscopy was done by E. Thyrhaug.

Weishäupl, S. J.; Mayer, D. C.; Thyrhaug, E.; Hauer, J.; Pöthig, A.; Fischer, R. A., A nitrophenyl-carbazole based push-pull linker as a building block for non-linear optical active coordination polymers: A structural and photophysical study. *Dyes and Pigments* **2021,** *186*, 109012.

ARTICLE IN PRESS

Dyes and Pigments xxx (xxxx) xxx

Contents lists available at ScienceDirect

Dyes and Pigments

journal homepage: http://www.elsevier.com/locate/dyepig

A nitrophenyl-carbazole based push-pull linker as a building block for non-linear optical active coordination polymers: A structural and photophysical study

Sebastian J. Weishäupl [a], David C. Mayer [a], Erling Thyrhaug [b], Jürgen Hauer [b], Alexander Pöthig [a,**], Roland A. Fischer [a,*]

[a] Chair of Inorganic and Metal–Organic Chemistry, Department of Chemistry & Catalysis Research Center, Technical University of Munich, Lichtenbergstraße 4, 85748, Garching, Germany

[b] Professorship of Dynamic Spectroscopy, Department of Chemistry & Catalysis Research Center, Technical University of Munich, Lichtenbergstraße 4, 85748, Garching, Germany

ARTICLE INFO

Keywords:
Chromophore
Emission
Metal-organic frameworks
Non-linear optics

ABSTRACT

Non-linear optical effects (NLO) such as multi-photon absorption, second harmonic generation (SHG) etc. have a wide range of applications. Nevertheless, the performance of many NLO-active organic dyes is limited by their thermal stability and photobleaching. These problems can be overcome by integrating the dyes into coordination polymers or metal-organic frameworks. Here, we present a structural and photophysical study of dipropyl-9-(4-nitrophenyl)-carbazole-3,6-dicarboxylate, a new "push-pull" organic dye molecule designed as a chromophore linker for NLO-active coordination polymers. Structure determination of a single-crystal showed that it crystallizes in a monoclinic crystal system $P\,2_1/c$. The solvated chromophore exhibits two aromatic absorption bands at 250 nm and 275 nm as well as broad long wavelength band at 350 nm, which we assign to an intramolecular charge transfer state. Photoluminescence measurements in solvents of different polarities revealed two main effects: In nonpolar solvents, the spectrum shows an emission band at 360 nm, whereas in solvents with a higher polarity, the emission maximum broadens and redshifts. Solid-state emission measurement of sample powder exhibits an emission band at 520 nm which is redshifted compared to the measurements in solution, due to excimer formation in the solid-state. The optical as well as solvation-related properties of the investigated pigment render it to be a versatile ligand in coordination polymers.

1. Introduction

Coordination polymers (CPs) and metal-organic frameworks (MOFs) featuring chromophore linkers as building blocks have been recognized as a promising solid-state material class for non-linear optical (NLO) applications, as their high chemical tunability, among other effects, enables to organize chromophore molecules in a defined oriented fashion [1].

To date, NLO studies on CPs and MOFs have been focusing on second- and third-harmonic generation (SHG, THG) as well as multi-photon absorption (MPA) properties [2–5]. These studies follow a common strategy, to assemble small NLO active organic building blocks in achieving highly functional crystalline solid-state materials, meanwhile surpassing often found drawbacks with classical NLO materials (e.g. limited performance, toxicity, photostability, non-polar arrangements etc.) [6,7]. Such an approach, however, requires comparatively small NLO-active chromophore linker molecules, with the desired optical properties and good crystallization tendencies.

NLO properties of chromophores have systematically been investigated within the electronic push-pull concept [8], which reveals a strong correlation between both the NLO-activity and the intramolecular charge transfer (ICT) characteristics and the size or structure of the charge transfer network. The NLO response was shown to be tailored by (i) connecting electron donors and acceptors of various electronic nature, (ii) assuring efficient donor-acceptor interaction (iii) extent, composition and steric arrangement of π-electron bridges (iv) reduction

* Corresponding author.
** Corresponding author.
E-mail addresses: alexander.poethig@tum.de (A. Pöthig), roland.fischer@tum.de (R.A. Fischer).

https://doi.org/10.1016/j.dyepig.2020.109012
Received 28 September 2020; Received in revised form 13 November 2020; Accepted 14 November 2020
Available online 21 November 2020

Please cite this article as: Sebastian J. Weishäupl, *Dyes and Pigments*, https://doi.org/10.1016/j.dyepig.2020.109012

of the bond-length alternation of the π-bridges and (v) planarization of the π-electron system [8,9].

In general, the photophysical (including NLO) properties of coordination polymers can be influenced by each of their components - both the organic linkers as well as the metal nodes as well as the excitonic coupling between the linker molecules [10]. For example, photoactive ions capable of metal-centered transitions can be used, e.g. lanthanides, steering the photophysical properties of the material solely by choice of the metal [11]. Often the situation is more complex, exhibiting a delicate interplay of (also photo-inactive) metal ions, especially transition metal ions, and chromophore linkers. Hereby, metal-to-ligand charge transfer (MLCT) as well as ligand-to-metal charge transfer (LMCT) can introduce new charge transfer bands, which possibly allow for a higher NLO response of the material compared to the isolated linker. As stated above, the emission properties of organic chromophores are well understood and can be specifically tailored towards desired applications. Therefore, tailoring the organic chromophores within linker platforms is also the method of choice for optimizing photoactive coordination compounds and networks. Additionally, there are two further advantages: First, the incorporation of linker molecules inside a framework usually increases their emission efficiency, through limitation of radiationless energy decays as a result of a restriction of conformational changes in the coordinated chromophore [12]. Second, by arranging the chromophores in a rigid framework a dense packing of the chromophores is enabled, whereas fluorescence quenching via aggregation (which is usually observed in highly concentrated solutions) is prevented [13]. Based on this, we identified dicarboxy-functionalized carbazoles as highly promising donor building blocks within the push-pull linker design of prospective NLO-photoactive coordination polymers or MOFs [14–16].

Herein, we report the synthesis and complete characterization of a new potential push-pull linker, comprising a carbazole donor and a $-NO_2$ acceptor group. Both are linked via a phenylene bridge, mimicking the well-studied showcase NLO chromophore *p*-nitroaniline (PNA) [17]. The carbazole moiety is equipped with carboxylic acid groups, which should enable an incorporation into framework structures. 9-(4-nitrophenyl)-carbazole-3,6-dicarboxylic acid (H_2CbzNO_2, **8**) was synthesized in a multi-step procedure starting from carbazole. The molecule was characterized by NMR spectroscopy, mass spectrometry and elemental analysis. Single-crystal X-ray diffraction (SCXRD) analysis reveals an antiparallel packing motif, minimizing the overall dipole-moment of the unit cell, a behavior often found for polar molecules [18,19]. Finally, the absorption and emission behavior were studied in solution as well as in solid state. The spectroscopic findings were corroborated with the help of electronic structure calculations at the level of time-dependent density functional theory (TD-DFT). The spectroscopic results and the theoretical calculations show the formation of an ICT state, proving H_2CbzNO_2 as a highly prospective NLO ligand for future CP and MOF synthesis.

2. Experimental

2.1. Material and methods

All purchased reagents were received from chemical suppliers and used without any further purification if not otherwise stated. All reactions with air and moisture sensitive compounds were carried out under standard Schlenk techniques using Argon 4.6 (Westfalen) or in a glove box (*UNIlab*, M. Braun). Required glass ware was flame-dried *in vacuo* prior to use. Elemental analysis was performed at the micro analytic laboratory at the Technical University of Munich. Analysis of C, H and N values was conducted by flash combustion method at 1800 °C. NMR spectra were recorded on a Bruker AV400 at room temperature at 400 MHz. ESI-MS was performed on a *LCQ fleet* and *MS* Q^+ from Thermo Fischer Scientific. LIFDI-MS spectra were measured at a Waters Micromass *LCT TOF* mass spectrometer equipped with an LIFDI ion source (LIFDI 700) from Linden CMS GmbH. Single-crystal X-ray diffraction data was collected on a BRUKER *D8 Venture* system equipped with a Mo TXS rotating anode (λ = 0.71073 Å) and a CMOS photon 100 detector. UV/VIS spectra were recorded on a double beam *Lambda 365* UV–Vis spectrophotometer from PerkinElmer. Fluorescence measurements were recorded on an *FS5* spectrofluorometer from Edinburgh Instruments. Cyclic voltammetry measurements were conducted on a BioLogic *SP-200*. Melting point analysis was performed on a Büchi *M-565*.

2.2. Computational methods

All quantum mechanical calculations were performed using the Gaussian09 software package [20]. The long-range corrected coulomb-attenuated exchange-correlation functional cam-B3LYP [21] and the basis set def2TZVP were employed as implemented in the software package. Theoretical absorption spectra were calculated on the level of time-dependent DFT using the above functional and basis set. No symmetry or internal coordinate constraints were applied during the optimization. The optimized geometry was verified as being a true minimum by the absence of negative eigenfrequencies in the vibrational frequency analysis.

2.3. Synthesis

3,6-Dibromocarbazole (2): A solution of *N*-bromosuccinimide (22.35 g, 125 mmol) in 50 mL DMF was slowly added through a syringe pump to a stirring solution of carbazole **1** (10 g, 59.80 mmol) in 20 mL DMF in an ice bath. After 24 h of reaction time, the mixture was poured into 600 mL ice water and then filtered through a suction filter to give a dark grey powder. The crude product was recrystallized with Ethanol to give a grey powder of 3,6-Dibromocarbazole **2** (18,68 g, 96%). ^{1}H NMR (400 MHz, 298K, DMSO-d_6) δ (ppm) = 7.47 (d, J = 8.6 Hz, 2H), 7.53 (dd, J = 2.0, 8.6 Hz, 2H), 8.43 (d, J = 1.9, 2H), 11.59 (s, 1H, N–H). ^{13}C NMR (101 MHz, 298K, DMSO-d_6) δ (ppm) = 110.96, 113.18, 123.35, 123.29, 128.70, 138.78.

Carbazole-3,6-Dicarbonitrile (3): 3,6-Dibromocarbazole **2** (9.75 g, 30.0 mmol) and dppf (100 mg, 0.18 mmol) were added to a 100 mL Schlenk flask and solved in 30 mL DMF and 0.3 mL water. The suspension was degassed via bubbling argon for 1 h through the mixture. Subsequently, $Zn(CN)_2$ (4.21 g, 36 mmol), zinc powder (78 mg, 1.2 mmol), $Zn(OAc)_2 \cdot 2\,H_2O$ (0.26 g, 1.2 mmol) and $Pd_2(dba)_3 \cdot$ dba (69.5 mg, 0,06 mmol) were added under a positive pressure of argon. This mixture was heated to 110 °C for 2 days. The suspension was subsequently cooled and then poured into a 100 mL mixture of $H_2O/NH_4Cl/NH_3$ (5/4/1) and filtered through a suction filter. The filter cake was washed with the same volume of the above mixture, toluene (3 x 30 mL) and MeOH (3 x 30 mL) to give a grey solid. The crude product was recrystallized with DMF to give a white solid (**3**) (5.2 g, 81%). ^{1}H NMR (400 MHz, 298K, DMSO-d_6) δ (ppm) = 7.72 (d, J = 8.5 Hz, 2H), 7.85 (d, J = 9.9 Hz, 2H), 8.80 (s, 2H), 12.38 (s, 1H, N–H). ^{13}C NMR (101 MHz, 298K, DMSO-d_6) δ (ppm) = 101.74, 112.84, 120.10, 121.85, 126.8, 129.93, 142.32.

Carbazole-3,6-dicarboxylic acid (4): Carbazole-3,6-Dicarbonitrile **3** (4.2 g, 19.3 mmol) was suspended in an aqueous NaOH solution (12.45 g in 150 mL). To this solution CuI (37,5 mg, 0.195 mmol) was added and then quickly heated to 125 °C for 2 days, until the starting material was dissolved. Afterwards active carbon was added, and the mixture was again heated to 125 °C for 2 h. After cooling, the suspension was filtered through celite, which was pre-washed with aq. NaOH-solution. The filtrate was acidified with 6 M HCl-solution to give a white precipitate. The precipitate was filtered, washed with water and then dried to give a withe solid (**4**) (4.0 g, 85%). ^{1}H NMR (400 MHz, 298K, $CDCl_3$) δ (ppm) = 7.60 (d, J = 8.5 Hz, 2H), 8.06 (d, J = 8.4 Hz, 2H), 8.85 (s, 2H), 12.04 (s, 1H, N–H), 12.69 (bs, 2H, COOH). ^{13}C NMR (101 MHz, 298K, DMSO-d_6) δ (ppm) = 111.13, 122.00, 122.27, 122.79, 127.65, 143.12, 167.94.

Dipropyl-carbazole-3,6-dicarboxylate (5): Carbazole-3,6-dicarboxylic acid **4** (4.0 g, 15.64 mmol) was suspended in 100 mL 1-propanol. To this suspension, conc. sulfuric acid (2 mL) was added and then refluxed at 110 °C for 24 h. After cooling, the suspension was concentrated on a rotary evaporator and extracted with 200 mL dichloromethane. The organic layer was washed with aq. $NaHCO_3$ (150 mL) and then dried with $MgSO_4$. The solvent was evaporated to give a yellowish solid (**5**) (4.5 g, 84%). ^{1}H NMR (400 MHz, 298K, $CDCl_3$) δ (ppm) = 1.09 (t, J = 7.4 Hz, 6H), 1.87 (h, J = 7.2 Hz, 4H), 4.36 (t, J = 6.7 Hz, 4H), 7.47 (d, J = 8.5 Hz, 2H), 8.18 (dd, J = 1.5 Hz, 2H), 8.86 (s, 2H). ^{13}C NMR (101 MHz, 298K, $CDCl_3$) δ (ppm) = 10.77, 22.40, 66.67, 110.64, 122.89, 123.19, 128.28, 142.85, 167.35.

Dipropyl-9-(4-nitrophenyl)-carbazole-3,6-dicarboxylate (Pr_2CbzNO_2) (6): Dipropyl-carbazole-3,6-dicarbox-ylate **5** (0.87 g, 2.56 mmol), 1-iodo-4-nitrobenzene (0.638 g, 2.56 mmol), K_3PO_4 (2.18 g, 10.3 mmol), *N,N′*-dimethylethylenediamine (0.18 mL, 1.67 mmol) and CuI (73.15 mg, 0.39 mmol) were dissolved in 20 mL dry toluene in a 50 mL Schlenk flask and heated to 115 °C for 2 days. After cooling, the suspension was dissolved in 100 mL aq. NH_4Cl, extracted with EtOAc (3 x 50 mL). The organic phase was combined and then dried with $MgSO_4$. The solvent was evaporated on a rotary evaporator to give an orange solid. The crude product was then subjected to column chromatography (100% dichloromethane, R_f = 0.75) to give a yellow powder (843 mg, 72%). mp 227 °C; ^{1}H NMR (400 MHz, 298K, $CDCl_3$) δ (ppm) = 1.09 (t, J = 7.4 Hz, 6H), 1.88 (h, J = 6.7 Hz, 4H), 4.37 (t, J = 6.7 Hz, 4H), 7.46 (d, J = 8.7 Hz, 2H), 7.81 (d, 8.9 Hz, 2H), 8.20 (dd, J = 1.4 Hz, 2H), 8.54 (d, J = 8.9 Hz, 2H), 8.92 (s, 2H). ^{13}C NMR (101 MHz, 298K, $CDCl_3$) δ (ppm) = 1.16, 10.75, 22.37, 66.86, 109.65, 123.30, 123.90, 124.39, 125.94, 127.45, 128.76, 143.35, 166.86. LIFDI-MS: m/z $[M]^{\bullet+}$: calculated for $C_{26}H_{24}O_6N_2$: 460.16; found: 459.55. EA: calculated for $C_{26}H_{24}O_6N_2$: C, 67.82; H, 5.25; N, 6.08; found: C, 67.35; H, 5.27; N, 5.87.

Dipropyl-9-(4-phenyl)-carbazole-3,6-dicarboxylate (Pr_2CbzH) (7): Dipropyl-carbazole-3,6-dicarboxylate (0.3 g, 0.88 mmol), iodobenzene (0.18 g, 0.88 mmol), K_3PO_4 (0.750 g, 3.54 mmol), DMEDA (0.06 mL, 0,58 mmol) and CuI (25.5 mg, 0.13 mmol) were dissolved in 10 mL dry toluene in a 50 mL Schlenk flask and heated to 115 °C for 3 days. After cooling, the suspension was dissolved in 60 mL aq. NH_4Cl-solution, extracted with EtOAc (4 x 30 mL). The organic phase was combined and then dried with $MgSO_4$. The solvent was evaporated on a rotary evaporator, to give a brown solid. The crude product was then subjected to column chromatography (100% dichloromethane, R_f = 0.8) to give a white powder (**6**) (295 mg, 80%). mp 133 °C; ^{1}H NMR (400 MHz, 298K, $CDCl_3$) δ (ppm) = 1.09 (t, J = 7.4 Hz, 6H), 1.88 (h, J = 6.7 Hz, 4H), 4.37 (t, J = 6.7 Hz, 4H), 7.46 (d, J = 8.7 Hz, 2H), 7.81 (d, 8.9 Hz, 2H) 8.20 (dd, J = 1.4 Hz, 2H), 8.54 (d, J = 8.9 Hz, 2H), 8.92 (s, 2H). ^{13}C NMR (101 MHz, 298K, $CDCl_3$) δ (ppm) = 1.16, 10.75, 22.37, 66.86, 109.65, 123.30, 123.90, 124.39, 125.94, 127.45, 128.76, 143.35, 166.86. EA: calculated for $C_{26}H_{25}O_4N$: C, 75.16; H, 6.07; N, 3.37; found: C, 74.99; H, 6.07; N, 3.52.

9-(4-nitrophenyl)-carbazole-3,6-dicarboxylic acid (H_2CbzNO_2) (8): Dipropyl-9-(4-nitrophenyl)-carbazole-3,6-dicarboxylate (500 mg, 1.2 mmol) was dissolved in 50 mL THF, aq. NaOH-solution (0.25 g in 10 mL water) and 7.5 mL MeOH. This mixture was refluxed for 12 h at 90 °C. After cooling, the solvent was evaporated and 100 mL water was added. The suspension was filtered and subsequently acidified with 3 M HCl-solution. The precipitate was filtered, washed thoroughly with water and then dried, to give a yellow solid (310 mg, 84%). ^{1}H NMR (400 MHz, 298K, DMSO-d_6) δ (ppm) = 7.59 (d, J = 9.0 Hz, 2H), 8.04 (d, J = 9.0 Hz, 2H), 8.11 (dd, J = 1.6 Hz, 8.7 Hz, 2H), 8.55 (d, J = 9.0 Hz, 2H), 9.00 (s, 2H), 12.89 (bs, 2H, COOH). ^{13}C NMR (101 MHz, 298K, DMSO-d_6) δ (ppm) = 110.12, 123.07, 123.11, 124.18, 125.76, 127.85, 128.49, 141.69, 142.76, 146.44, 167.48. ESI-MS: m/z [M − H]: calculated for $C_{20}H_{12}O_6N_2$: 375.313; found: 375.14. EA: calculated for $C_{20}H_{12}O_6N_2 \cdot 0.75\ H_2O$: C, 61.62; H, 3.49; N, 7.19; found: C, 61.80; H, 3.47; N, 7.02.

9-(4-phenyl)-carbazole-3,6-dicarboxylic acid (H_2CbzH) (9): The literature known compound 9-(4-phenyl)-carbazole-3,6-dicarboxylic acid [22] was synthesized in a saponifaction reaction, using the analogous reaction conditions to that described for **8**. ^{1}H NMR (400 MHz, 298K, DMSO-d_6) δ (ppm) = 7.43 (d, J = 8.7 Hz, 2H), 7.58–7.79 (m, 5H), 8.10 (dd, J = 1.6 Hz, 8.7 Hz, 2H), 8.98 (s, 2H), 12.82 (bs, 2H). ^{13}C NMR (101 MHz, 298K, DMSO-d_6) δ (ppm) = 109.87, 122.46, 123.01, 123.36, 127.00, 128.27, 128.65, 130.40, 135.78, 143.49, 167.62.

3. Results and discussion

3.1. Synthesis

The dipolar push-pull chromophore dipropyl-9-(4-nitrophenyl)-carbazole-3,6-dicarboxylate (Pr_2CbzNO_2) **6** was synthesized in a six step synthesis procedure starting from carbazole **1** (Fig. 1). Bromination of **1** yielded 3,6-dibromocarbazole **2**, which was subsequently reacted to carbazole-3,6-dicarbonitrile **3** in a modified *Negishi* coupling reaction [23,24]. Alkaline hydrolysis of **3** followed by acidic precipitation gave 3,6-carbazole-dicarboxylic acid **4**. It turned out that the low solubility and acidic behavior of **4** hampered N-hetero cross-coupling reactions of Buchwald-Hartwig or Ullman type. Consequently, to enhance the solubility of the carbazole donor precursor **4**, the corresponding propyl ester **5** was synthesized in an acid-catalyzed esterification reaction. Furthermore, different Ullmann and Buchwald-Hartwig coupling reaction attempts were screened under varying reactions conditions finally yielding the desired product **6** (compare the experimental part for a detailed procedure). A modified Ullmann reaction procedure following work by *Eddaoudi* et al. results in high yield and excellent purity [25]. As the compound should be used as a building block for CP synthesis in pursuing work, **6** was hydrolyzed by alkaline esterification finally giving the corresponding carboxylic acid **8**. Please note that all optical characterization methods discussed in the following paragraphs were conducted on **6** due to the higher solubility of the latter in differing organic solvents. The effects of the propyl ester group of **6** on optical properties are marginal, as the absorption and emission behavior are determined by the push-pull system, as will be shown in the following paragraphs.

3.2. Photophysical characterization in solution

3.2.1. UV/VIS spectroscopy

The photophysical properties of **6** were studied using UV/Vis spectroscopy in solvents of different polarity (Fig. 2a). In all solvents the absorption spectra show two strong absorption bands centered at 250 nm and 275 nm, as well as weaker bands around 300 nm and a characteristic broad absorption band centered at approximately 355 nm. We pursue two strategies to assign the origin of these spectral features: *i)* comparison with the spectra of the reference compound dipropyl-9-(4-phenyl)-carbazole-3,6-dicarboxylate (Pr_2CbzH) **7** (Fig. 2, yellow), and *ii)* comparison with quantum chemical calculations of the absorption spectrum.

Compound **6** and the reference **7** differ in molecular structure only by the *p*-nitro group (Fig. 2c), which implies that any spectral differences report on the influence of the nitro acceptor group on the molecular photophysics of the push-pull chromophore. The similarity of the short-wavelength range of the spectra suggest that the features below 300 nm can be assigned to π-π* transitions located at the carbazole moiety. In the long-wavelength range, however, we observe significant differences. In particular, the absorbance spectra of **7** have only minor bands red-shifted with respect to the π-π* transitions (Fig. 2). Thus, the long-wavelength band at **6** is clearly induced by the electron accepting $–NO_2$ group. While introducing electron-withdrawing groups may result in charge-transfer transitions, the modest solvatochromy of the band shows that these transitions are associated with only a minor change in permanent dipole moment.

To obtain further insight into the electronic structure of **6**, and to corroborate our assignments of the spectroscopic data, we perform a

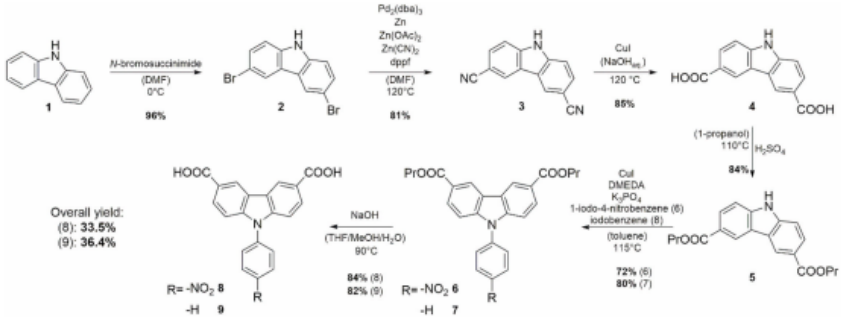

Fig. 1. Reaction scheme for the preparation of **8** (and **9**) showing the different conducted steps from commercially available starting materials.

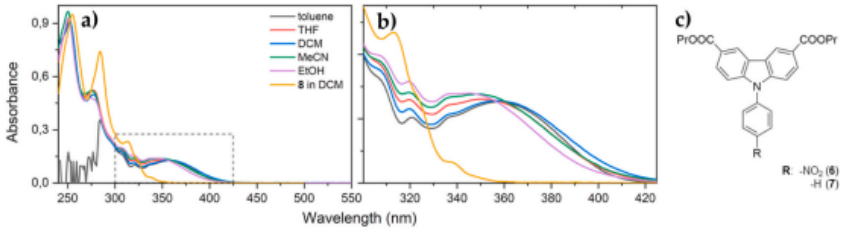

Fig. 2. a) Side-by-side comparison of the absorbances of **6** in different solvents with increasing polarity, from toluene to ethanol, as well as **7** in DCM. **b)** Zoom-in of the outlined area (dashed box) in the left panel focusing on the absorption of the charge transfer state. **c)** Molecular structure of chromophores **6** and **7**.

quantum chemical analysis of the compound's absorption spectra. This was done at the level of TD-DFT using the long-range corrected cam-B3LYP functional and def2TZVP as basis set (50 excited states, Fig. 3).

The calculated UV/VIS spectrum is in good accordance with the experimental absorbance spectrum and shows two main groupings of transitions in the UV region centered at 180 nm and 240 nm. Qualitative (visual) comparison of the most contributing Kohn-Sham molecular orbitals (KS-MOs) of these excitations show that these transitions are mostly of π-π* character and located at the carbazole moiety (not shown). The band at approximately 310 nm however, involves substantial transfer of charge-density towards the nitrobenzene moiety, and the $S_0 \rightarrow S_1$ transition can thus be assigned to a charge-transfer excitation. Fig. 3b shows the KS-MOs most strongly involved in the S_1 transition, where the transfer of electron density from the donating carbazole to the electron accepting nitro group upon photo excitation is clearly illustrated.

3.2.2. *Photoluminescence and excitation spectroscopy*

To unravel the emission properties of this new organic chromophore, we conducted a detailed photoluminescence (PL) spectroscopic investigation. Excitation-emission-matrices (EEM) of **6** were measured in order to study the excitation-wavelength dependent fluorescence behavior in different polar surroundings (Fig. 4). The collected data point towards a subtle interplay of a locally excited (LE) state at the carbazole moiety and a twisted intramolecular charge-transfer (TICT) state involving the carbazole donor and nitro acceptor as a function of solvent polarity (Fig. 5). The EEMs reveal the formation of two contributions. In solvents of low polarity (toluene, Fig. 4a) the spectra show a

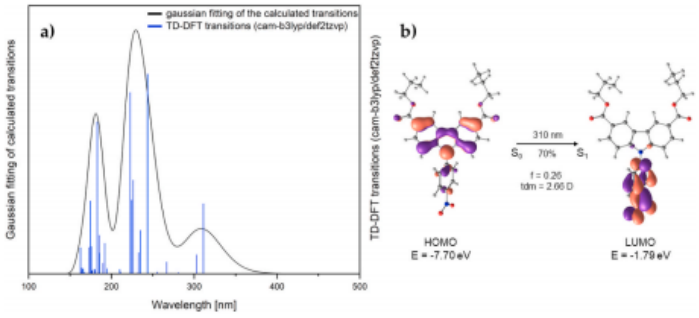

Fig. 3. a) Theoretical UV/VIS spectrum of **6** (50 excited states, gaussian broadening) **b)** Charge transfer excitation of **6** located from the carbazole moiety to the phenyl ring (S1, 310 nm, oscillator strength f, transition dipole moment tdm [D], HOMO (left) → LUMO (right)).

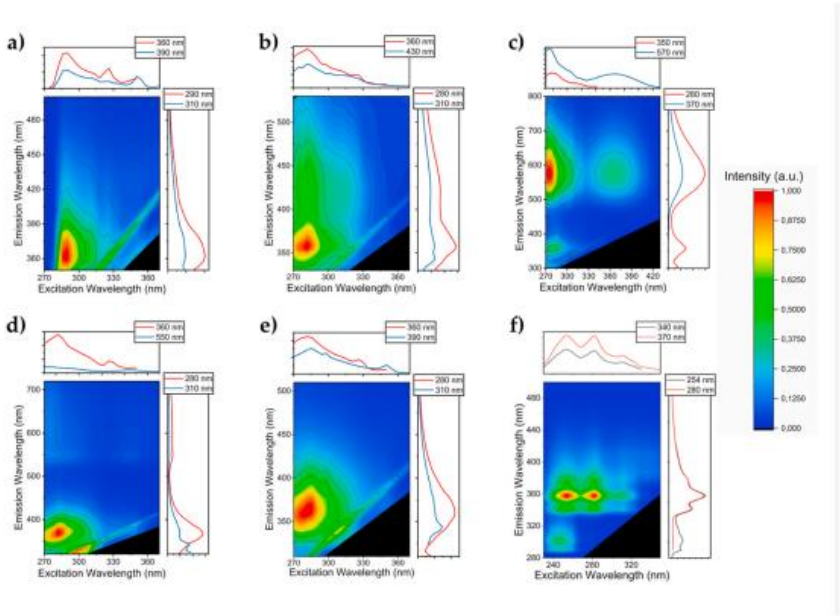

Fig. 4. Excitation-emission-matrices (EEM) of **6** in different solvents: **a)** toluene, **b)** THF, **c)** DCM, **d)** MeCN and **e)** EtOH as well as **7** in DCM for comparison, **f)**. Note the different scaling of the x/y axis for clarity reasons.

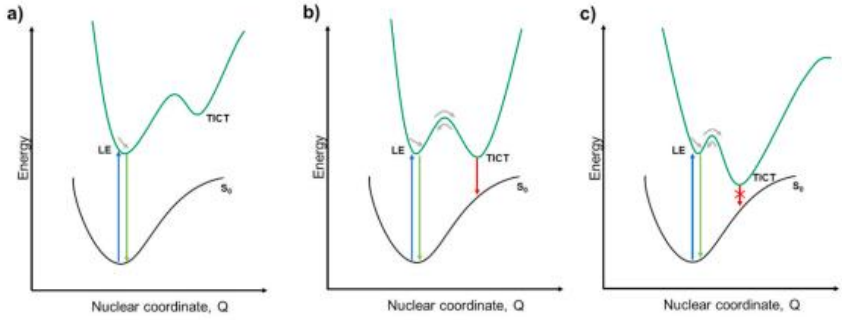

Fig. 5. A pictorial description of the interplay between LE and CT states in the push-pull chromophore **6** and how the solvent reaction field shapes the excited state PES. a) In non-polar solvents, the lowest state will hold π-π^* character. b) In more polar solvents the TICT state will be lowered due to stabilization by the reaction field, resulting in an equilibration with the LE state. c) Finally, at strong-polar solvents the TICT state gets close to the S_0 surface, resulting in a large increase in non-radiative relaxation, preventing its contribution to emission.

single emissive state, with a PL maximum at ~ 360 nm. By increasing the solvent's polarity, an additional emission band appears which redshifts and broadens distinctively (~ 430 nm in THF, Fig. 4b; ~ 570 nm in DCM). Finally, in very polar and protic solvents such as ethanol, the long-wavelength contribution vanishes (Fig. 4d and e). The EEMs show no long-wavelength contribution to the emission signal, and the spectra are remarkably similar to the spectra in low-polar solvents. To gain further insights, we also measured an EEM of **7**, following a similar strategy as presented in the UV/Vis spectroscopic studies with the aim to understand the influence of the $-NO_2$ substituent. Interestingly, the EEM of **7** in DCM reveal two emission bands, with lowest-energy transitions at (~290 nm) and (~360 nm), respectively.

Taken the above into consideration, the dual-emission behavior of **6** can be understood within a TICT-model. In less polar solvents the lowest energy state will show LE character with a narrow PL band and a maximum at approximately 360 nm. Via comparison of EEMs of **6** and **7** displayed in Fig. 4, we assign this LE state to be largely located at the carbazole moiety. However, in more polar surroundings TICT states will be stabilized, due to the increased dipole moment through twisting of the chromophore alongside the C–N single bond. Consequently, the TICT state will contribute stronger to the emission band - which is most pronounced in DCM. Finally, in very polar and protic surroundings (here acetonitrile and ethanol) the TICT state is potentially lowered to a strong extent, with the typical reduction in transition moment due to the

extensive charge-separation, likely leading to essentially complete quenching of the TICT emission. Instead, the EEMs clearly show that only the LE emission remains in these cases. Fig. 5 displays the interplay of LE and TICT states of **6** in different polar surroundings. Note that such an approach of describing the excited state dynamics is commonly used for push-pull chromophores [26–28]. In summary, the static excitation and emission spectroscopic analysis of **6** reveals a highly interesting photophysical behavior of the linker molecule, in particular showing a strong dependency on the polarity of the chromophore environment. Presumably, these effects can be exploited further in sensor systems (e.g., guest molecule detection) through controlled chromophore packing in a coordination polymer.

3.3. Crystal structure analysis

Single crystals suitable for single crystal X-ray diffraction (SCXRD) analysis were obtained by slow diffusion of pentane into a concentrated solution of **6** in chloroform. Fig. 6a shows the molecular structure of **6** and its packing along the crystallographic a and b-axis (Fig. 6b and **c**). The material crystallizes in the monoclinic space group $P\ 2_1/c$ with a single molecule of **6** in the asymmetric unit and four molecules per unit cell (Z = 4). The mean bond lengths found for the molecular structure from SCXRD analysis lay in ranges as expected for organic molecules of such types (Table S1). The carbazole unit and the nitrophenylene group hold a torsional angle of 52.50°. Interestingly, the $-NO_2$ group and the phenylene ring have a dihedral angle of almost 0°, proofing both molecule fragments to lay in a single plane. As can nicely been seen in Fig. 6b, the polar molecule crystallizes diametral in the *ac*-plane, minimizing the overall dipole moment of the unit cell. Furthermore, the molecule propagates along the crystallographic *b*-axis in a co-planar fashion, with a mean center-to-center distance of ~ 3.4 Å. Additional intermolecular hydrogen bonds of the type C_{arom}-H···O involving the ester group and the nitrophenylene group with characteristic distances ranging from 2.4 Å to 2.8 Å, contribute to the overall packing as found in the crystal structure. In summary, the SCXRD analysis reveals that the packing motif of **6** is mainly governed by electrostatic as well as intermolecular interactions (minimization of dipole moments, π-π interactions of the carbazole moiety and C_{arom}-H···O interactions).

3.4. Solid-state photoluminescence and excitation spectroscopy

In order to characterize the photophysical properties in the solid-state, powder samples of **6** were investigated with solid-state fluorescence and excitation spectroscopy. Fig. 7a shows the emission spectrum measured at different excitation wavelengths (280 nm and 425 nm, respectively) with an emission band located at 540 nm for both excitations. This is different, compared to the photoluminescence measurements in solution, where two emission bands can be seen: a LE band at 360 nm, as well as a solvent dependent red-shifting ICT. Furthermore, the solid-state spectrum shows two contributing transitions, as apparent from the excitation spectrum (red line in Fig. 7a), which we assign to carbazole based π-π* transitions (280 nm) and the charge transfer state (425 nm). To support our assignments, we also measured emission and excitation spectra for powdered **7** and compared it to **6** (Fig. 7b). Interestingly, **7** shows very similar emission - centered at 520 nm- but the excitation spectrum reveals only one absorptive transition. Based on these findings and the packing of the carbazole moieties into dimers with a distance of ~3.4 Å in the crystal structure, the solid-state emission of **6** (and **7**) appears to originate from a π-stacked sandwich excimer formation, which has been observed 2001 in photoluminescence studies on carbazole dimers [29].

For a future incorporation of the chromophore in a CP, a similar effect can be expected, since a high chromophore density without fluorescence quenching should be achievable. On top, an additional advantage of these coordination materials compared to the crystallized linker itself is, that the photophysical properties can be potentially controlled via defined arrangement of the chromophores, whereas this is intrinsically limited in an organic crystal. This leads to a remarkable enlargement of the playfield of organic chromophores, deliberately packed and arranged in solid-state materials, thereby steering the photophysical properties of the solid-state material.

4. Conclusions

In conclusion, we have synthesized a novel dipolar "push-pull" chromophore dipropyl-9-(4-nitrophenyl)-carbazole-3,6-dicarboxylate via an modified *Ullmann*-coupling reaction, which should be used in further studies for the synthesis of NLO active CPs and MOFs. The chromophore was characterized by ^{1}H NMR and ^{13}C NMR spectroscopy, LIFDI-MS and elemental analysis as well as SCXRD. The optical studies of chromophore **6** in solution showed two aromatic absorption bands at 250 nm and 275 nm as well as a broad long wavelength absorption band at 350 nm with characteristics of an ICT transition. The PL measurements in solvents of differing polarity, revealed an interesting interplay between locally excited states, centered at the carbazole moiety, and a twisted intramolecular charge transfer state between the carbazole

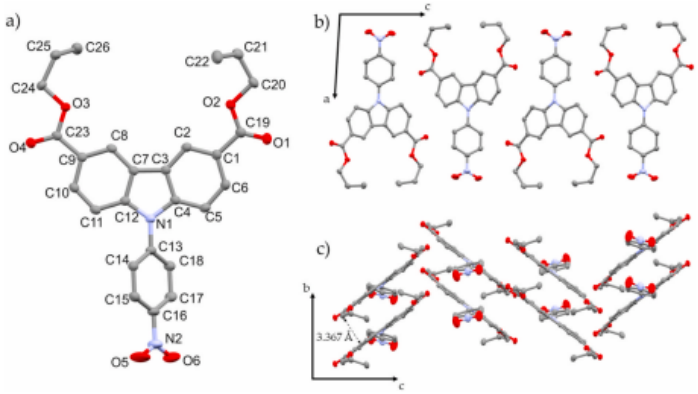

Fig. 6. Hydrogen atoms are omitted for clarity. **a)** ORTEP representation of the single-crystal structure of **6** with thermal ellipsoids shown at the 50% probability level. **b)** Alternating packing of **6** alongside the a/c plane. **c)** Co-planar packing of **6** alongside the b/c plane with a mean chromophore distance of 3.367 Å.

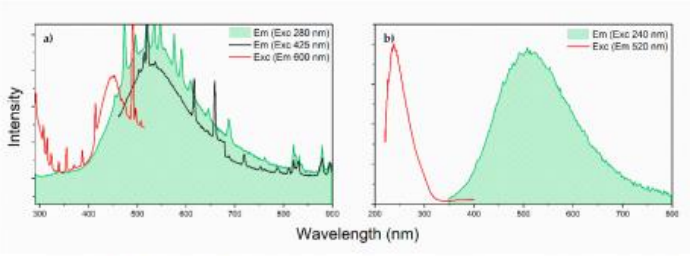

Fig. 7. **a)** Solid-State emission (blue and yellow line, λ_{ex} = 280 nm, 425 nm) and excitation spectrum (red line, λ_{em} = 600 nm) of **6**. **b)** Solid-State emission (yellow line, λ_{ex} = 240 nm) and excitation spectrum (red line, λ_{em} = 520 nm) of **7**. (For interpretation of the references to colour in this figure legend, the reader is referred to the Web version of this article.)

donor and the nitro acceptor group. The solid-state emission measurements exhibited **6** as a greenish emitter with contributions from π-stacked excimer formation. Taking all these photophysical properties in account, the newly synthesized dipolar "push-pull" chromophore presents itself as a highly interesting building block to study within a structural-photophysical-property-relationship investigation on potential NLO active CPs or MOFs in the future.

Author contributions

Conceptualization and writing - original draft preparation, S.J.W., methodology, S.J.W., D.C.M., E.T. and A.P., writing – review and editing, D.C.M., E.T., J.H., A.P. and R.A.F., project administration, R.A.F. All authors have given approval to the final version of the manuscript.

Funding

The authors would like to thank the German Research Foundation (DFG) for funding within the frame of EXC 2089 Cluster of Excellence and the Priority Programme "COORNETs" (SPP 1928).

Declaration of competing interest

The authors declare that they have no known competing financial interests or personal relationships that could have appeared to influence the work reported in this paper.

Acknowledgments

The TUM is very greatly acknowledged for institutional funding. S.J. W. and D.C.M. thank the TUM Graduate School for financial support. The authors would like to thank Leibniz Supercomputing Centre of the Bavarian Academy of Sciences and Humanities for provision of computing time.

Appendix A. Supplementary data

Supplementary data to this article can be found online at https://doi.org/10.1016/j.dyepig.2020.109012.

References

[1] Markey K, Krüger M, Seidler T, Reinsch H, Verbiest T, De Vos DE, Champagne B, Stock N, van der Veen MA. Emergence of nonlinear optical activity by incorporation of a linker carrying the p-nitroaniline motif in MIL-53 frameworks. J Phys Chem C 2017;121(45):25509–19.

[2] Medishetty R, Nalla V, Nemec L, Henke S, Mayer D, Sun H, Reuter K, Fischer RA. A new class of lasing materials: intrinsic stimulated emission from nonlinear optically active metal–organic frameworks. Adv Mater 2017;29(17):1605637.

[3] Medishetty R, Nemec L, Nalla V, Henke S, Samoć M, Reuter K, Fischer RA. Multi-photon absorption in metal–organic frameworks. Angew Chem Int Ed 2017;56(46): 14743–8.

[4] Mayer DC, Manzi A, Medishetty R, Winkler B, Schneider C, Kieslich G, Pöthig A, Feldmann J, Fischer RA. Controlling multiphoton absorption efficiency by chromophore packing in metal–organic frameworks. J Am Chem Soc 2019;141 (29):11594–602.

[5] Liu M, Quah HS, Wen S, Yu Z, Vittal JJ, Ji W. Efficient third harmonic generation in a metal–organic framework. Chem Mater 2016;28(10):3385–90.

[6] Pietryga JM, Park Y-S, Lim J, Fidler AF, Bae WK, Brovelli S, Klimov VI. Spectroscopic and device aspects of nanocrystal quantum dots. Chem Rev 2016; 116(18):10513–622.

[7] He GS, Tan L-S, Zheng Q, Prasad PN. Multiphoton absorbing Materials: molecular designs, characterizations, and applications. Chem Rev 2008;108(4):1245–330.

[8] Bureš F. Fundamental aspects of property tuning in push–pull molecules. RSC Adv 2014;4(102):58826–51.

[9] Spangler Charles W. Recent development in the design of organic materials for optical power limiting. J Mater Chem 1999;9(9):2013–20.

[10] Medishetty R, Zareba JK, Mayer D, Samoc M, Fischer RA. Nonlinear optical properties, upconversion and lasing in metal-organic frameworks. Chem Soc Rev 2017;46(16):4976–5004.

[11] Eliseeva SV, Pleshkov DN, Lyssenko KA, Lepnev LS, Bünzli J-CG, Kuzmina NP. Highly luminescent and triboluminescent coordination polymers assembled from lanthanide β-diketonates and aromatic bidentate O-donor ligands. Inorg Chem 2010;49(20):9300–11.

[12] Hu Z, Huang G, Lustig WP, Wang F, Wang H, Teat SJ, Banerjee D, Zhang D, Li J. Achieving exceptionally high luminescence quantum efficiency by immobilizing an AIE molecular chromophore into a metal–organic framework. Chem Commun 2015;51(15):3045–8.

[13] Jiang Y, Wang Y, Hua J, Tang J, Li B, Qian S, Tian H. Multibranched triarylamine end-capped triazines with aggregation-induced emission and large two-photon absorption cross-sections. Chem Commun 2010;46(26):4689–91.

[14] Venkateswararao A, Thomas KRJ, Lee C-P, Li C-T, Ho K-C. Organic dyes containing carbazole as donor and π-linker: optical, electrochemical, and photovoltaic properties. ACS Appl Mater Interfaces 2014;6(4):2528–39.

[15] Ledwon P. Recent advances of donor-acceptor type carbazole-based molecules for light emitting applications. Org Electron 2019;75:105422.

[16] Hongji J, Jian S, Jinlong Z. A review on synthesis of carbazole-based chromophores as organic light-emitting materials. Curr Org Chem 2012;16(17):2014–25.

[17] Nalwa HS, Watanabe T, Miyata S. A comparative study of 4-nitroaniline, 1,5-diamino-2,4- dinitrobenzene and 1,3,5-triamino-2,4,6-trinitrobenzene and their molecular engineering for second-order nonlinear optics. Opt Mater 1993;2(2): 73–81.

[18] Liao Y, Eichinger BE, Firestone KA, Haller M, Luo J, Kaminsky W, Benedict JB, Reid PJ, Jen AKY, Dalton LR, Robinson BH. Systematic study of the Structure−Property relationship of a series of ferrocenyl nonlinear optical chromophores. J Am Chem Soc 2005;127(8):2758–66.

[19] Liao Y, Bhattacharjee S, Firestone KA, Eichinger BE, Paranji R, Anderson CA, Robinson BH, Reid PJ, Dalton LR. Antiparallel-aligned neutral-ground-state and zwitterionic chromophores as a nonlinear optical. Mater J Am Chem. Soc 2006;128 (21):6847–53.

[20] Frisch MJ, Trucks GW, Schlegel HB, Scuseria GE, Robb MA, Cheeseman JR, Scalmani G, Barone V, Petersson GA, Nakatsuji H, Li X, Caricato M, Marenich AV, Bloino J, Janesko BG, Gomperts R, Mennucci B, Hratchian HP, Ortiz JV, Izmaylov AF, Sonnenberg JL, Williams, Ding F, Lipparini F, Egidi F, Goings J, Peng B, Petrone A, Henderson T, Ranasinghe D, Zakrzewski VG, Gao J, Rega N, Zheng G, Liang W, Hada M, Ehara M, Toyota K, Fukuda R, Hasegawa J, Ishida M, Nakajima T, Honda Y, Kitao O, Nakai H, Vreven T, Throssell K, Montgomery Jr JA, Peralta JE, Ogliaro F, Bearpark MJ, Heyd JJ, Brothers EN, Kudin KN, Staroverov VN, Keith TA, Kobayashi R, Normand J, Raghavachari K, Rendell AP, Burant JC, Iyengar SS, Tomasi J, Cossi M, Millam JM, Klene M, Adamo C, Cammi R, Ochterski JW, Martin RL, Morokuma K, Farkas O, Foresman JB, Fox DJ. Gaussian 9. Wallingford, CT: Rev. B.01; 2009.

[21] Yanai T, Tew DP, Handy NC. A new hybrid exchange–correlation functional using the Coulomb-attenuating method (CAM-B3LYP). Chem Phys Lett 2004;393(1):51–7.
[22] Chen H-F, Chi L-C, Hung W-Y, Chen W-J, Hwu T-Y, Chen Y-H, Chou S-H, Mondal E, Liu Y-H, Wong K-T. Carbazole and benzimidazole/oxadiazole hybrids as bipolar host materials for sky blue, green, and red PhOLEDs. Org Electron 2012;13(11):2671–81.
[23] Bag PP, Wang D, Chen Z, Cao R. Outstanding drug loading capacity by water stable microporous MOF: a potential drug carrier. Chem Commun 2016;52(18):3669–72.
[24] Weseliński ŁJ, Luebke R, Eddaoudi M. A convenient preparation of 9H-Carbazole-3,6-dicarbonitrile and 9H-Carbazole-3,6-dicarboxylic acid. Synthesis 2014;46(5):596–9.
[25] Guillerm V, Weseliński ŁJ, Belmabkhout Y, Cairns AJ, D'Elia V, Wojtas Ł, Adil K, Eddaoudi M. Discovery and introduction of a (3,18)-connected net as an ideal blueprint for the design of metal–organic frameworks. Nat Chem 2014;6:673.
[26] Farztdinov VM, Schanz R, Kovalenko SA, Ernsting NP. Relaxation of optically excited p-nitroaniline: semiempirical quantum-chemical calculations compared to femtosecond experimental results. J Phys Chem 2000;104(49):11486–96.
[27] Sasaki S, Drummen GPC, Konishi G-i. Recent advances in twisted intramolecular charge transfer (TICT) fluorescence and related phenomena in materials chemistry. J Mater Chem C 2016;4(14):2731–43.
[28] Grabowski ZR, Rotkiewicz K, Rettig W. Structural changes accompanying intramolecular electron Transfer: focus on twisted intramolecular charge-transfer states and structures. Chem Rev 2003;103(10):3899–4032.
[29] Tani K, Tohda Y, Takemura H, Ohkita H, Ito S, Yamamoto M. Synthesis and photophysical properties of [3.3](3,9)carbazolophanes. Chem Commun 2001;(19):1914–5.

3.2 Coordination Polymers based on Carbazole-Derived Chromophore Linkers for Optimized Multiphoton Absorption: A Structural and Photophysical Study

Coordination polymers are a prominent material class towards NLO activity, since they are known to be chemical and thermal robust. Hereby, we report the synthesis and characterization of three novel highly MPA active coordination polymers $Zn_2(sbcd)(DMAc)_2(H_2O)_{1.5}$, $Sr(fbcd)(DMAc)_{0.25}(H_2O)_{3.5}$ and $Ba(fbcd)(DMAc)_{2.5}(H_2O)_{1.5}$, based on two carbazole-containing chromophore linkers: the previously reported 9,9'-stilbene-bis-carbazole-3,6-dicarboxylic acid (H_4sbcd) and the new 2,7-fluorene-9,9'-dimethyl-bis-carbazole-3,6-dicarboxylic acid (H_4fbcd). Thereby, the organic linkers were synthesized in a multi-step synthesis procedure with an Ullmann C-N coupling as a main reaction. The reported materials were investigated using ^{1}H-NMR/ ^{13}C-NMR spectroscopy, LIFDI-MS, elemental analysis and single-crystal X-ray diffraction. X-ray structure determination revealed, that the zinc-based CP crystallizes in a *sql* network topology with the triclinic unit *P* -1, whereas the isostructural barium and strontium-based CP are showing a 4,8-connecting net topology with the triclinic unit cell *P* -1 for strontium and a monoclinic unit cell *P* $2_1/n$ for barium. Steady-state spectroscopy of the coordination polymers compared to the solvated linker molecules revealed a redshift of approximately 50 nm, which presumably emerges from excitonic interactions of the chromophores inside the framework. Furthermore, Z-scan measurements of the synthesized materials with a fully automated setup based on a broadband (femtosecond) oscillator to obtain excitation wavelength dependant two-photon excitation spectra were performed. The Z-scan results showed large two-photon cross sections $\sigma^{(2)}$ in the range of 2100 to 33300 GM, which is an enhancement of three orders of magnitude compared to the solvated linkers (Fig. 25).

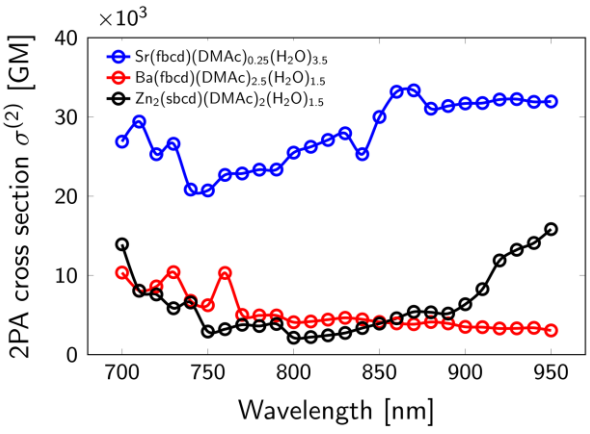

Fig. 25: Comparison of the two-photon absorption cross sections of the three coordination polymers. Color coding: Blue = $Sr(fbcd)(DMAc)_{0.25}(H_2O)_{3.5}$, Red = $Ba(fbcd)(DMAc)_{2.5}(H_2O)_{1.5}$, Black = $Zn_2(sbcd)(DMAc)_2(H_2O)_{1.5}$.

Thereby, Sr(fbcd)$(DMAc)_{0.25}(H_2O)_{3.5}$ showed the highest 2PA cross section, which seems to originate from the smaller carbazole-carbazole distance compared to the isostructural barium CP, which is mainly responsible for the MPA activity (Fig. 26).

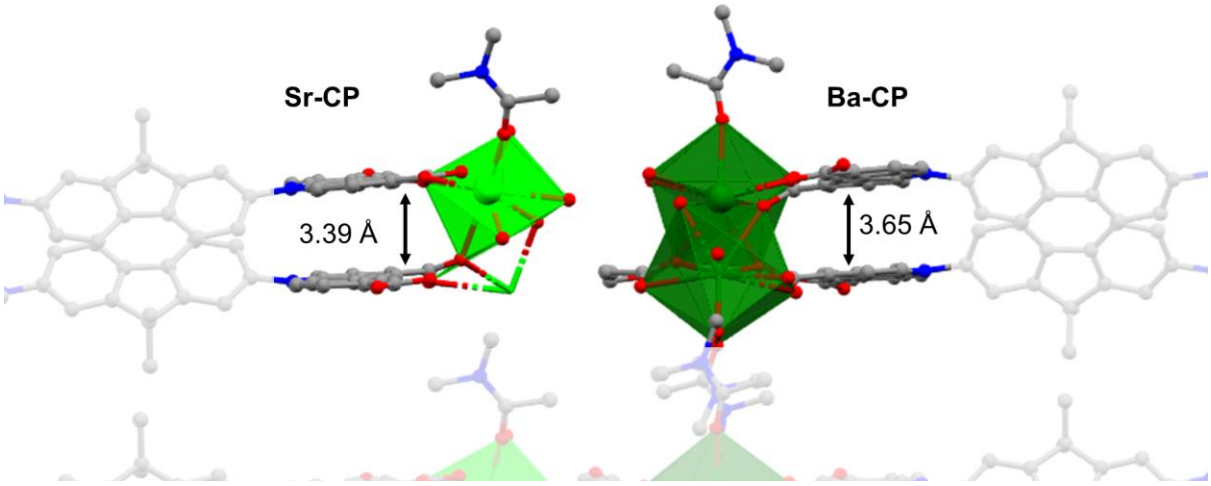

Fig. 26: Smaller carbazole-carbazole distance of the Sr-CP compared to Ba-CP leading to a higher 2PA cross section.

Furthermore, strontium is a “harder” ion than barium, which can in principle polarize the charge transfer character more and therefore render higher MPA cross sections.

This manuscript was written by two shared first authors and edited by six co-authors. The synthesis, structural characterization (PXRD, SC-XRD and Pawley fitting) and steady state spectroscopy was done by the author of this thesis under the supervision of R. A. Fischer. Z-scan measurements were performed Y. Cui and H. Syed. Furthermore, S. N. Deger supported the material synthesis in the context of his research internship and Bachelor’s thesis which were conducted under supervision of this author.

S. J. Weishäupl[†], Y. Cui[†], S. Deger, H. Syed, A. Pöthig, A. Ovsianikov, J. Hauer and R. A. Fischer, *Chemistry of Materials*, **2022**.

[†] These authors contributed equally to this work.

CHEMISTRY OF MATERIALS

pubs.acs.org/cm Article

Coordination Polymers Based on Carbazole-Derived Chromophore Linkers for Optimized Multiphoton Absorption: A Structural and Photophysical Study

Sebastian J. Weishäupl,[⊥] Yang Cui,[⊥] Simon N. Deger, Hamad Syed, Aleksandr Ovsianikov, Jürgen Hauer,* Alexander Pöthig,* and Roland A. Fischer*

Cite This: https://doi.org/10.1021/acs.chemmater.2c01525 Read Online

ACCESS | Metrics & More | Article Recommendations | Supporting Information

ABSTRACT: Multiphoton absorption (MPA), as a subgroup of non-linear optical effects, is of high interest in modern materials research since it has a great applicability in optoelectronics. However, most of the commonly used materials featuring MPA properties are chromophore molecules, which are limited by their thermal stability and uncontrolled aggregation in high-concentration solutions. A prominent material class which could in principle overcome these problems are metal−organic frameworks and coordination polymers (CPs) as they can be modularly tuned to possess chemical and thermal stability. In addition, by incorporating chromophores as linkers in the framework, their molecular properties can be retained or even enhanced. In this article, we report the synthesis and characterization of three new and highly MPA-active CPs, $Zn_2(sbcd)(DMAc)_2(H_2O)_{1.5}$, $Sr(fbcd)(DMAc)_{0.25}(H_2O)_{3.5}$, and $Ba(fbcd)(DMAc)_{2.5}(H_2O)_{1.5}$, based on two carbazole-containing chromophore linkers: a previously reported 9,9′-stilbene-bis-carbazole-3,6-dicarboxylic acid (H_4sbcd) and the new 2,7-fluorene-9,9′-dimethyl-bis-carbazole-3,6-dicarboxylic acid (H_4fbcd). Single-crystal structure analysis of the zinc-based CP reveals a *sql* network, whereas the barium- and strontium-based CPs are isostructural, showing a 4,8-c network topology. Z-scan analysis of the networks shows large two-photon absorption cross-sections $\sigma^{(2)}$ of 2100 to 33,300 GM, which is an enhancement of up to 3 orders of magnitude in comparison to the solvated linker and is also one of the highest MPA-cross-sections reported for CPs up to date.

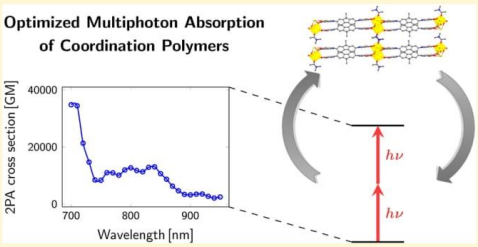

INTRODUCTION

Non-linear optics (NLO) is the study of light-induced phenomena with above-linear scaling with respect to the incident light intensity.[1] NLO-related effects such as second-harmonic generation or multiphoton absorption (MPA) have a wide range of applications ranging from 3D-data storage and optical limiting to bio-imaging.[2] In this respect, coordination polymers (CPs) or metal−organic frameworks (MOFs) featuring chromophore linkers are a promising material class as they are known to be chemically versatile and stable even under intense light conditions.[3−5]

CPs or MOFs are a hybrid material class comprising inorganic metal nodes—often built from metal-oxo-clusters—bridged by organic linkers often having dicarboxylic acids or pyridyls as donor groups.[6] The versatility in the choice of linker and metal nodes explains the enormous variability of these materials. Molecular linker properties, for example, regarding photo- or electrocatalytic activity, can be transferred directly into a solid framework, preserving the properties of the monomer unit. Furthermore, interactions of the molecules within the framework allow for additional and directed modifications of the linker properties.[7]

Accordingly, MPA-active molecules inside an MOF can show an enhanced MPA cross-section as compared to the uncoordinated molecule.[8−11] This enhancement can be explained by structural rigidity and multi-chromophore effects such as excitonic coupling, all of which are due to the special steric arrangements of the linkers in the MOF. The relative orientation of the linkers can also be engineered using different metals or different additives in order to synthesize a variety of topologies to directly influence the optical properties of the MOF.[12−14] Additionally, an appropriate choice of metal centers may open charge transfer channels such as ligand-to-metal charge transfer or metal-to-ligand charge transfer.[15] Such extra decay channels may heavily influence the photophysical properties of the solid-state material.

Received: May 20, 2022
Revised: July 19, 2022

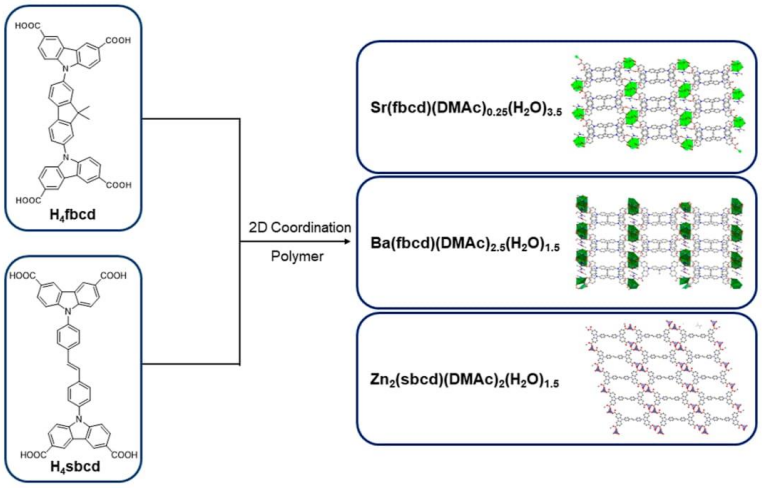

Figure 1. Overview of the synthesized and characterized materials in this work.

The properties of the linker molecule are another decisive factor when synthesizing MPA-active MOFs or CPs. For example, a strong intramolecular charge-transfer character is known to be beneficial for a large MPA cross-section.[16,17] Hence, chromophores bearing electron-pushing groups (electron donor), electron-pulling groups (electron acceptor), or both connected with large aromatic systems are molecular designs sought after when aiming for an MPA-active linker.[18,19] In this context, carbazoles show desirable properties as they act as electron donors.[20,21] From the point of view of optoelectronic research, carbazoles are well established systems due to their chemical stability, robustness, and generally desirable electronic properties.

In this article, we report the synthesis and photophysical characterization of two carbazole-based MPA-active chromophore linkers, namely, the new 2,7-fluorene-9,9′-dimethyl-bis-carbazole-3,6-dicarboxylic acid (H_4fbcd) and 9,9′-stilbene-bis-carbazole-3,6-dicarboxylic acid (H_4sbcd), which were recently reported first by Krause et al. for gas sorption studies incorporated in a copper MOF in 2020.[22] Furthermore, three different CPs were successfully synthesized employing a solvothermal synthesis strategy, resulting in single-crystalline materials of $Zn_2(sbcd)(DMAc)_2(H_2O)_{1.5}$, $Sr(fbcd)(DMAc)_{0.25}(H_2O)_{3.5}$, and $Ba(fbcd)(DMAc)_{2.5}(H_2O)_{1.5}$ with the above-mentioned linkers incorporated (Figure 1). Their corresponding crystal structures were determined, revealing that all materials are 2D CPs: the zinc-based stilbene CP crystallizes in the *sql* topology, whereas the fluorene-based main-group metal CPs crystallize in a 4,8-c net topology with two linker molecules anti-parallel arranged to each other. Z-scan measurements of the synthesized materials were performed with a fully automated setup based on a tunable femtosecond oscillator to obtain excitation-wavelength-dependent two-photon excitation spectra.[23] The results on the CP materials showed large two-photon absorption cross-sections $\sigma^{(2)}$ in the range of 2100−33,300 GM, which is an enhancement of up to 3 orders of magnitude as compared to the free linker in solution. Hence, MOFs or CPs with specifically designed linker molecules represent ideal candidates for MPA-active materials.

EXPERIMENTAL SECTION

Material and Methods. All purchased reagents were received from chemical suppliers and used without any further purification if not otherwise stated. Dipropyl-9-(4-nitrophenyl)-carbazole-3,6-dicarboxylate was synthesized following the previous published synthesis procedure.[20] All reactions with air- and moisture-sensitive compounds were carried out under standard Schlenk techniques using Argon 4.6 (Westfalen) or in a glovebox (*UNIlab*, M. Braun). Required glassware was flame-dried in vacuo prior to use. Elemental analysis was performed at the micro analytic laboratory at the Technical University of Munich. Analysis of C, H, and N values was conducted by the flash combustion method at 1800 °C. NMR spectra were recorded on a Bruker AV400 at room temperature at 400 MHz. LIFDI-MS data were recorded on an *Exactive Plus* Orbitrap system by Thermo Fisher Scientific equipped with an ion source (LIFDI) from LINDEN CMS GmbH.[24] Single-crystal X-ray diffraction (SC-XRD) data were collected on a BRUKER *D8 Venture* system equipped with a Mo TXS rotating anode (λ = 0.71073 Å) and a CMOS photon 100 detector (for detailed information, see the Supporting Information). Capillary PXRD measurements were recorded in transmission geometry on a Stoe *STADI P* diffractometer equipped with Mo radiation (λ = 0.7093 Å), a curved Ge(111) monochromator, and a Dectris Mythen 1K detector. UV/Vis spectra in solution were recorded on a double-beam *Lambda 365* UV−Vis spectrophotometer from PerkinElmer. Diffuse reflectance UV/vis measurements of sample powder were performed on a Shimadzu *UV-3600 Plus* UV−Vis−NIR spectrophotometer by fixing it between two quartz glass slides. Fluorescence measurements were recorded on an *FS5* spectrofluorometer from Edinburgh Instruments either in solution (linker) or in a PMMA matrix (CPs). IR measurements were conducted on a PerkinElmer *Frontier* FT-IR spectrometer. Excitation-wavelength-dependent Z-scans were performed using a femtosecond oscillator as part of an experimental setup designed previously.[23]

Synthesis. *4,4′-Dibromostilbene 2*. To a suspension of zinc powder (6.00 g, 90.69 mmol, 5.60 equiv) in THF (150 mL) at 0 °C, slowly, $TiCl_4$ (5 mL, 8.61 g, 45.34 mmol, 2.80 equiv) is added via a syringe. Subsequently, the reaction mixture is heated to 80 °C, and bromobenzaldehyde (3.00 g, 16.2 mmol, 1.00 equiv) and THF (50 mL) is added and heated for 5 h at reflux. After completion, saturated

https://doi.org/10.1021/acs.chemmater.2c01525
Chem. Mater. XXXX, XXX, XXX−XXX

$NaHCO_3$ solution is added dropwise at room temperature. Afterward, the organic layer is separated and the water is extracted with chloroform (3 × 100 mL). The combined organic layers are dried with magnesium sulfate, filtered, and then concentrated on a rotary evaporator to yield a white solid (2.56 g, 93%). ^{1}H NMR (400 MHz, $CDCl_3$): δ (ppm) 7.02 (s, 2H), 7.36 (d, J = 8.47 Hz, 4H), 7.48 (d, J = 8.45 Hz, 4H).

4,4′-Diiodostilbene ***3***. 2.5 M nBuLi solution (5.45 mL, 13.6 mmol, 4.60 equiv) was slowly dropped into a mixture of *trans*-4,4′-dibromostilbene (6) (1.00 g, 2.96 mmol, 1.00 equiv) in THF (150 mL) at −78 °C. Then the yellow solution was stirred at −78 °C for 4 h. Afterward, it was warmed up to 0 °C, whereby the color of the solution was changed from yellow to grayish yellow. The reaction mixture was cooled down again to −78 °C, and a solution of iodine (2.82 g, 11.1 mmol, 3.75 equiv) in THF (48 mL) was added. Finally, the reddish-brown solution was quenched with a solution of sodium thiosulfate (2 spatulas $Na_2S_2O_3$ in 150 mL H_2O) and filtrated through a glass filter. The filter cake was then washed multi-times with water and dried at 100 °C to get a yellowish solid (1.07 g, 100%). ^{1}H NMR (400 MHz, $CDCl_3$): δ (ppm) 7.04 (d, 4H), 7.26 (d, J = 14.2 Hz), 7.70 (dd, J = 8.3, 1.9 Hz, 4H).

Dipropyl-9,9′-(stilbyl)-bis-(carbazole-3,6-dicarboxylate) ***4*** *(Pr_4sbcd)*. Dipropyl-carbazole-3,6-dicarboxylate (0.785 g, 2.32 mmol, 2 equiv), 4,4′-iodostilbene (0.5 g, 1.16 mmol, 1 equiv), K_3PO_4 (1.97 g, 9.26 mmol, 8 equiv), DMEDA (0.186 mL, 1.74 mmol, 1.5 equiv), and CuI (66 mg, 0.34 mmol, 0.3 equiv) were dissolved in 15 mL of dry toluene in a 50 mL Schlenk flask and heated to 115 °C for 3 days. After cooling, the suspension was dissolved in 60 mL of aq. NH_4Cl solution, extracted with chloroform (3 × 50 mL). The organic phases were combined and then dried with $MgSO_4$. The solvent was evaporated on a rotary evaporator to give a brown solid. The crude product was then dissolved in 5 mL of dichloromethane (DCM) and added dropwise to 35 mL of MeCN in a centrifuge tube. The precipitate was collected by centrifugation and washed with MeCN twice to give pale-yellow powder. Subsequently, the raw product is then subjected to column chromatography (DCM 100%) to give an off-white powder (810 mg, 0.94 mmol, 82%). ^{1}H NMR (400 MHz, $CDCl_3$): δ (ppm) 1.12 (t, J = 7.4 Hz, 12H, CH_3), 1.89 (h, J = 7.2 Hz, 8H), 4.38 (t, J = 6.7 Hz, 8H), 7.26 (d, 4H), 7.49 (d, J = 8.5 Hz, 4H), 7.69 (d, J = 14.2 Hz, 2H), 7.86 (dd, J = 8.3, 1.9 Hz, 4H), 8.23 (dd, J = 1.5 Hz, 4H), 8.89 (s, 4H). ^{13}C NMR (101 MHz, 298 K, $CDCl_3$) δ (ppm) 10.76, 22.43, 66.72, 109.94, 123.18, 123.41, 123.48, 127.52, 128.40, 128.42, 129.05, 136.14, 137.35, 144.27, 167.20. LIFDI-MS: m/z $[M]^+$ calcd for $C_{54}H_{50}N_2O_8$, 854.3562; found, 854.3545. EA calcd for $C_{54}H_{50}N_2O_8$: C, 75.86; H, 5.89; N, 3.28; found: C, 74.76; H, 5.87; N, 3.45.

9,9′-(Stilbyl)-bis-(carbazole-3,6-dicarboxylic acid) ***5*** *(H_4sbcd)*. To a solution of Pr_4sbcd (450 mg, 0.59 mmol, 1.00 equiv) in 150 mL of THF and 15 mL of MeOH, an aqueous NaOH solution (2.5 g in 250 mL of water) is added and heated for 18 h at 90 °C. After completion of the reaction, THF and MeOH are removed under vacuum on a rotary evaporator. Subsequently, the aqueous phase is acidified with a 2 N HCl solution till it reacts acidic. The resulting white precipitate is filtered, washed with water, and then dried, giving a white powder (335 mg, 0.48 mmol, 85%). ^{1}H NMR (400 MHz, 298 K, DMSO-d_6) δ (ppm) 7.52 (d, 4H), 7.61 (s, 2H) 7.74 (d, 4H), 8.02 (d, 4H), 8.12 (dd, 4H), 8.99 (s, 4H), 12.81 (s, 4H); ^{13}C NMR (101 MHz, 298 K, DMSO-d_6) δ (ppm) 110.03, 122.56, 123.03, 123.05, 123.45, 127.26, 128.32, 128.43, 128.79, 137.18, 143.44, 167.63; LIFDI-MS: m/z $[M]^+$ calcd for $C_{42}H_{26}N_2O_8$, 686.1684; found, 686.1667. EA calcd for $C_{42}H_{26}N_2O_8$: C, 73.46; H, 3.82; N, 4.08. Found: C, 70.87; H, 4.2; N, 4.02.

2,7-Diiodofluorene ***6***. A Schlenk flask is filled with 5.00 g (30.05 mmol, 1.00 equiv) of fluorene, 40.70 mL of acetic acid, 8.15 mL of water, and 1.22 mL of conc. H_2SO_4 and heated up to 80 °C to dissolve fluorene completely. Subsequently, the mixture is cooled down to 60 °C, treated with 5.10 g (20.08 mmol, 0.67 equiv) of I_2 and 2.30 g (10.09 mmol, 0.34 equiv) of H_5IO_6, and stirred for 4 h. The violet-red solution is filtered and recrystallized with 100 mL *n*-hexane. The precipitation is dried to a fine orange-yellow powder. ^{1}H NMR (400 MHz, $CDCl_3$): δ (ppm) 7.87 (d, J = 1.5 Hz, 2H), 7.70 (dd, J = 8.0, 1.6 Hz, 2H), 7.49 (d, J = 8.0 Hz, 2H), 3.83 (s, 2H).

2,7-Diiodo-9,9-dimethyl fluorene ***7***. In a Schlenk flask, 4.17 g (9.97 mmol, 1.00 equiv) of 2,7-diiodofluorene is dissolved in 30 mL of dry THF and cooled down to 0 °C. Afterward, 2.56 g (26.64 mmol, 2.67 equiv) of Na^{t}OBu is added to the mixture and stirred at room temperature for 2 h. At 0 °C, the mixture is treated with 1.86 mL (29.88 mmol, 3.00 equiv) of MeI and stirred overnight at room temperature. Subsequently, the dark-yellow solution is filtered with Celite and evaporated to a bright orange-yellow powder. The crude product is recrystallized with 30 mL of toluene to give an orange-brown powder. ^{1}H NMR (400 MHz, $CDCl_3$): δ (ppm) 7.74 (d, J = 1.6 Hz, 2H), 7.66 (dd, J = 8.0, 1.6 Hz, 2H), 7.43 (d, J = 8.0 Hz, 2H), 1.45 (s, 6H).

Dipropyl-2,7-flourene-9,9-dimethyl-bis-carbazole-3,6-dicarboxylate ***8*** *(Pr_4fbcd)*. 9,9-Dimethyl-2,7-diiodofluorene (500 mg, 1.12 mmol, 1.00 equiv), carbazole-3,6-dipropyl-ester (761 mg, 2.24 mmol, 2.00 equiv), CuI (64.04 mg, 0,336 mmol, 0.3 equiv), DMEDA (0.18 mL, 1.68 mmol,1.5 equiv), and K_3PO_4 (1.90 g, 8.97 mmol, 8.00 equiv) are dissolved in 15 mL of dry toluene to give a yellow suspension, which is heated to 115 °C for 2 days under an argon atmosphere. The resulting brown solution is extracted with chloroform (3 × 50 mL) and NH_4Cl solution, the organic phases are combined and dried with $MgSO_4$, and the solvent is subsequently removed under vacuum. The resulting brown solid is redissolved in a small amount of DCM and is then poured dropwise into 35 mL of acetonitrile. The white precipitate is then centrifuged and washed three times with acetonitrile. The remaining off-white solid is then subjected to column chromatography (DCM 100%) to give a white powder (732 mg, 0.84 mmol, 75%). ^{1}H NMR (400 MHz, $CDCl_3$): δ (ppm) 1.11 (t, J = 7.5 Hz, 12H), 1.66 (s, 6H), 1.89 (h, J = 7.2 Hz, 8H), 4.38 (t, J = 6.7 Hz, 8H), 7.48 (d, J = 8.7 Hz, 4H), 7.61 (dd, J = 8.0, 1.9 Hz, 2H), 7.68 (d, J = 1.9 Hz, 2H), 8.07 (d, J = 8.0 Hz, 2H), 8.21 (dd, J = 8.6, 1.7 Hz, 4H), 9.00−8.96 (m, 4H). ^{13}C NMR (400 MHz, $CDCl_3$): 10.76, 22.39, 27.20, 47.81, 66.68, 109.90, 121.69, 121.95, 123.17, 123.34, 123.36, 128.38, 136.10, 138.48, 144.37, 156.14, 167.16. LIFDI-MS: m/z $[M]^+$ calcd for $C_{55}H_{52}N_2O_8$, 868.3718; found, 868.3694. EA calcd for $C_{55}H_{52}N_2O_8$: C, 76.02; H, 6.03; N, 3.22. Found: C, 75.20; H, 5.92; N, 3.21.

2,7-Fluorene-9,9-dimethyl-bis-carbazole-3,6-dicarboxylic Acid ***9*** *(H_4fbcd)*. To a solution of Pr_4fbcd (450 mg, 0.57 mmol, 1.00 equiv) in 150 mL of THF and 15 mL of MeOH, an aqueous NaOH solution (2.5 g in 250 mL of water) is added and heated for 18 h at 90 °C. After completion of the reaction, THF and MeOH are removed under vacuum on a rotary evaporator. Subsequently, the aqueous phase is acidified with a 2 N HCl solution until it reacts acidic. The resulting white precipitate is filtered, washed with water, and then dried, giving a white powder (336 mg, 0.48 mmol, 84%). ^{1}H NMR (400 MHz, DMSO): δ (ppm) 1.63 (s, 6H), 7.52 (d, J = 8.6 Hz, 2H), 7.72 (dd, J = 8.0, 1.9 Hz, 2H), 8.01 (d, J = 1.9 Hz, 2H), 8.14 (dd, J = 8.7 Hz, 1.7 Hz, 4H), 8.30 (d, J = 8.1 Hz, 2H), 9.01 (d, J = 1.7 Hz, 4H). ^{13}C NMR (400 MHz, DMSO-d_6): δ (ppm) 27.40, 47.51, 110.04, 121.82, 122.31, 122.53, 123.04, 123.42, 126.14, 128.34, 135.25, 137.89, 143.62, 156.08, 167.63. LIFDI-MS: m/z $[M]^+$ calcd for $C_{43}H_{28}N_2O_8$, 700.1840; found, 700.1830. EA calcd for $C_{43}H_{28}N_2O_8$: C, 73.71; H, 4.03; N, 4.00. Found: C, 70.07; H, 4.25; N, 2.97.

Zn_2(sbcd)(DMAc)$_2$(H_2O)$_{1.5}$. In a 4 mL screw cap vial, 10 mg of H_4sbcd and 11.12 mg of $Zn(NO_3)_2$ (3 equiv) were dissolved in a DMAc/water mixture (2/0.5 mL) and heated at 90 °C for 2 days. The resulting precipitate was filtered, washed with DMAc, and dried to give white frost-flower shaped crystals (6.6 mg, 45%). EA calcd for $Zn_2C_{42}H_{32}N_2O_8{\cdot}2C_4H_9O{\cdot}1.5H_2O$: C, 58.67; H, 4.33; N, 5.47; Zn, 12.77. Found: C, 58.71; H, 4.52; N, 5.81; Zn, 12.3.

Sr(fbcd)(DMAc)$_{0.25}$(H_2O)$_{3.5}$. In a 4 mL screw cap vial, 10 mg of H_4fbcd and 9.24 mg of $Sr(NO_3)_2$ (3 equiv) were dissolved in a DMAc/water mixture (2/0.5 mL) and heated at 100 °C for 2 days. The resulting precipitate was filtered, washed with DMAc, and dried to give a white crystalline needle (5.2 mg, 42%). EA calcd for $SrC_{43}H_{26}N_2O_8{\cdot}0.25C_4H_9O{\cdot}3.5H_2O$: C, 60.46; H, 3.89; N, 3.6. Found: C, 60.67; H, 4.08; N, 3.62.

https://doi.org/10.1021/acs.chemmater.2c01525
Chem. Mater. XXXX, XXX, XXX−XXX

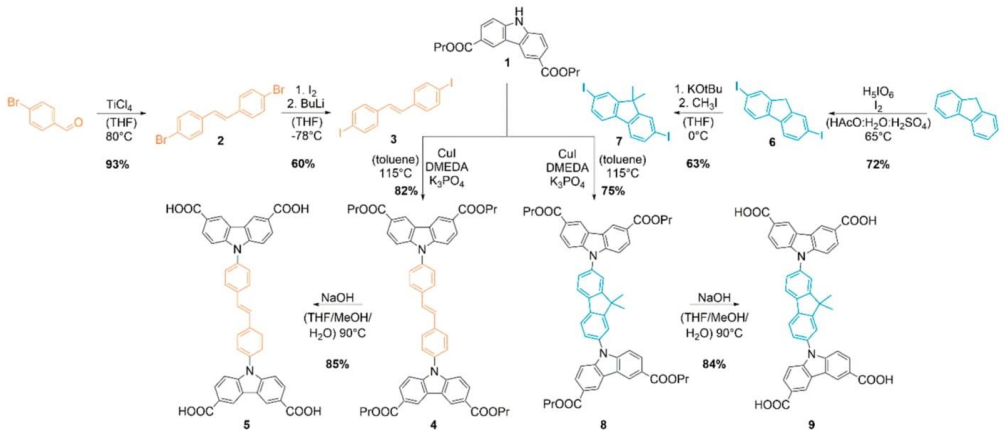

Figure 2. Multi-step synthesis procedure toward the carbazole-based linkers H_4sbcd **5** and H_4fbcd **9**.

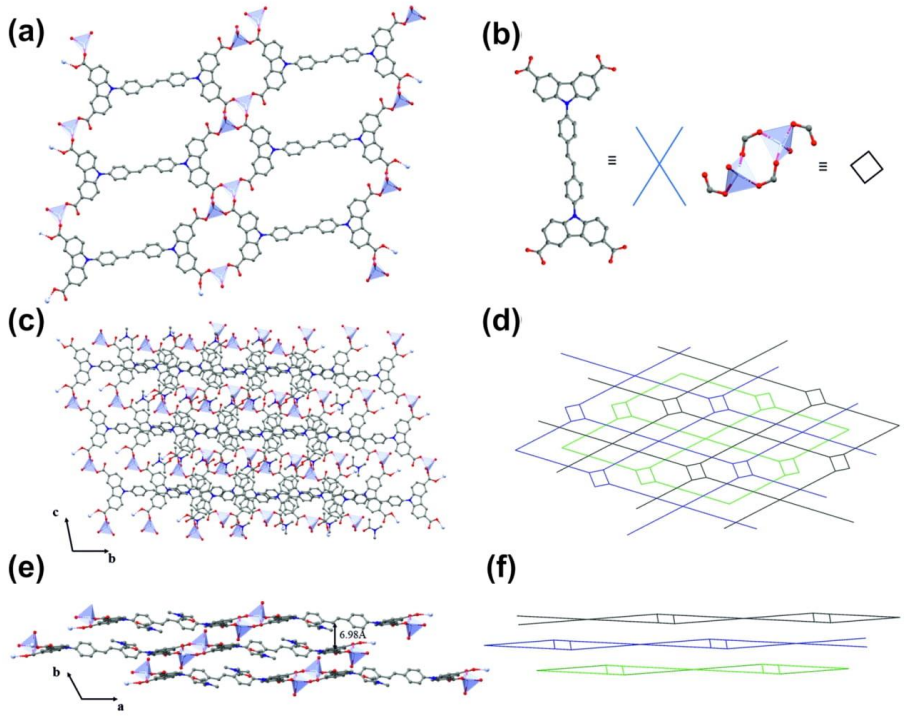

Figure 3. (a) Depiction of a monolayer cut-out of the Zn_2(sbcd)$(DMAc)_2(H_2O)_{1.5}$ 2D-CP. (b) Depiction of the SBU containing two Zn^{2+} atoms with four coordinated oxygen atoms and representation of the four-connecting stilbene linker. (c) Depiction of the crystal structure of the network alongside the *a*-axis. (d) Schematic representation of the underlying network topology of the *sql*-network topology alongside the *a*-axis. (e) Depiction of the parallel packing of the network layers with a mean chromophore distance of 6.98 Å alongside the *ab*-plane. (f) Schematic representation of the underlying network topology along the *c*-axis. Note: hydrogen atoms are omitted for clarity. Color coding: gray = carbon, blue = nitrogen, red = oxygen, and light gray = zinc.

https://doi.org/10.1021/acs.chemmater.2c01525
Chem. Mater. XXXX, XXX, XXX−XXX

Ba(fbcd)(DMAc)$_{2.5}$(H$_2$O)$_{1.5}$. In a 4 mL screw cap vial, 10 mg of H_4fbcd and 11.12 mg of $Ba(NO_3)_2$ (3 equiv) were dissolved in a DMAc/water mixture (2/0.25 mL) and heated at 100 °C for 2 days. The resulting precipitate was filtered, washed with DMAc, and dried to give white crystalline needles (6.7 mg, 43%). EA calcd for $BaC_{43}H_{26}N_2O_8 \cdot 2.5C_4H_9O \cdot 1.5H_2O$: C, 58.9; H, 4.8; N, 6.01. Found: C, 58.9; H, 4.87; N, 6.01.

■ RESULTS AND DISCUSSION

Synthesis of the Carbazole-Based Donor−π−Donor-Linker Molecules. The synthesis of the chromophore units (Figure 2) that were incorporated in the CP starts with the carbazole donor **1** synthesis, which was previously published by our group in 2020 (cf. Supporting Information).[20] Being a reliable synthesis method for C−N hetero-coupling reactions for carbazoles, the *Ullmann* reaction using copper as a metal catalyst was employed. Therefore, first, the halogenated aromatic cores have to be synthesized in order to subsequently couple them with the carbazole moiety.

For the synthesis of the stilbene core, a *McMurry* reaction with 4-bromobenzaldehyde using titanium tetrachloride as a reduction agent was performed, yielding 4,4′-dibromostilbene **2** according to a synthesis procedure by Jeong and co-workers.[25] In principle, **2** could be used directly for a subsequent *Ullmann* reaction as it was reported earlier by Krause et al. in 2020.[22] However, we found that the reaction time of 10 days can be significantly reduced via an additional synthetic step to substitute the bromine atoms with iodine, making the molecule more reactive toward the coupling. Within this improved synthesis, a bromine−iodine exchange reaction was performed using butyllithium for the bromine−metal exchange, followed by addition of iodine solution in THF for the metal−iodine exchange to yield **3**. Finally, via *Ullmann* reaction following our previously reported protocol, the stilbene core is coupled to the carbazole moiety using a copper catalyst ligated with two molecules of *N*,*N*-dimethylethylenediamine, leading to **4** in good purity and yields. As a last step toward the final linker, the ester groups are saponificated via alkaline hydrolysis reaction with NaOH, yielding **5** in excellent purity.

For the synthesis of the fluorene core, first, the terminal 2 and 7 positions were subjected to a substitution reaction using a periodic acid and elemental iodine in a solvent mixture of acetic acid, water, and sulfuric acid toward **6**, in accordance with Tsutsui and co-workers from 2001.[26] Afterward, the two protons at position 9 of the synthesized 2,7-diiodofluorene have to be substituted since they would hinder the following *Ullmann* reaction due to their acidic character. This was done according to an adapted synthesis procedure from a publication by West et al., where first the fluorene is deprotonated with potassium-*tert*-butoxide and afterward by adding methyliodine as an electrophilic reagent, yielding 9,9′-dimethyl-2,7-diiodofluorene **7**.[27] The aromatic core is then also coupled with the carbazole moiety using the same conditions and the same work-up procedure as for **4**, resulting in excellent yields and purity for **8** and later on after alkaline hydrolysis for **9**.

SC-XRD Analysis of the Coordination Polymers. *SC-XRD Analysis of Zn$_2$(sbcd)(DMAc)$_2$(H$_2$O)$_{1.5}$*. After 2 days reaction time of a one-batch solvothermal synthesis using $Zn(NO_3)_2$, DMAc, and water, small frost flower-shaped single crystals could be obtained, which were analyzed via SC-XRD. It revealed that the CP $Zn_2(sbcd)(DMAc)_2(H_2O)_{1.5}$ crystallizes in the triclinic space group *P*-1 with its unit cell parameters of a = 9.256(3) Å, b = 11.735(4) Å, and c = 12.319(4) Å and the respective cell angles of α = 73.267(10)°, β = 78.637(8)°, and γ = 68.362° with two linker-node moieties per unit cell (Z = 2).

In Figure 3a, a monolayer cut-out of the CP is depicted, showing that two carboxylic acid group atoms connect two zinc centers, forming a Zn_2O_8 cluster as a secondary building unit (SBU) with two water molecules on the top of each tetrahedron (Figure 3b). These SBUs in turn connect four linker molecules, which leads to a 2D sheet-like *sql*-network topology. Alongside the *b*/*c*-plane, the shifted stacking of each layer can be seen in Figure 3c, which means that the carbazole units are lying over the stilbene moieties. This is further illustrated in a schematic representation of the whole network in Figure 3d. This can also be observed in Figure 3e,f alongside the *c*-axis, where the side view of the packing is depicted, which reveals an interchromophoric distance of 6.98 Å.

In Figure 4, the powder X-ray diffractogram of $Zn_2(sbcd)(DMAc)_2(H_2O)_{1.5}$ is depicted, which shows a high degree of crystallinity and intense reflections at 3.75, 4.50, 6.11, 9.95, 7.58, 9.02, and 10.11°. Pawley fit on the data reveals an R_{wp} value of 5.01% and a goodness of fit (GoF) of 4.95, which shows that the proposed structure model is in good agreement with the bulk material.

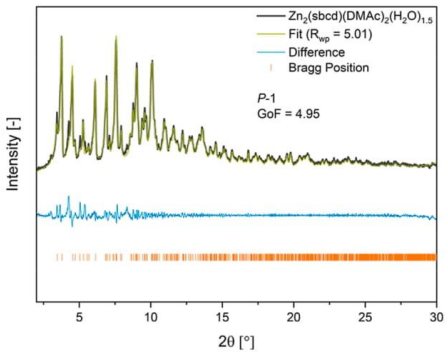

Figure 4. Plot of the powder XRD data of the $Zn_2(sbcd)(DMAc)_2(H_2O)_{1.5}$ network (dark gray), the simulated Pawley fit (green), the difference plot (blue), and the Bragg positions (orange).

SC-XRD Analysis of Sr(fbcd)(DMAc)$_{0.25}$(H$_2$O)$_{3.5}$ and Ba(fbcd)(DMAc)$_{2.5}$(H$_2$O)$_{1.5}$. After 2 days of solvothermal synthesis using H_4fbcd as a linker mixed with either strontium or barium in a dimethylacetamide/water mixture, needle-shaped single crystals suitable for SC-XRD could be obtained. Analysis of single crystals of the strontium CP revealed that it crystallizes in the triclinic space *P*-1 with the unit cell lengths of a = 10.076(3) Å, b = 12.140(3) Å, and c = 23.401(6) Å and cell angles of α = 93.793(7)°, β = 90.197(8)°, and γ = 93.276(8)° with two linker-node moieties per unit cell (Z = 2). The barium-based CP crystallizes in the monoclinic space group $P2_1/n$ with the cell axis lengths of a = 12.1780(10) Å, b = 20.5805(17) Å, and c = 46.760(4) Å and its monoclinic angle of β = 90.270(2)° with four linker-node moieties per unit cell (Z = 4).

https://doi.org/10.1021/acs.chemmater.2c01525
Chem. Mater. XXXX, XXX, XXX−XXX

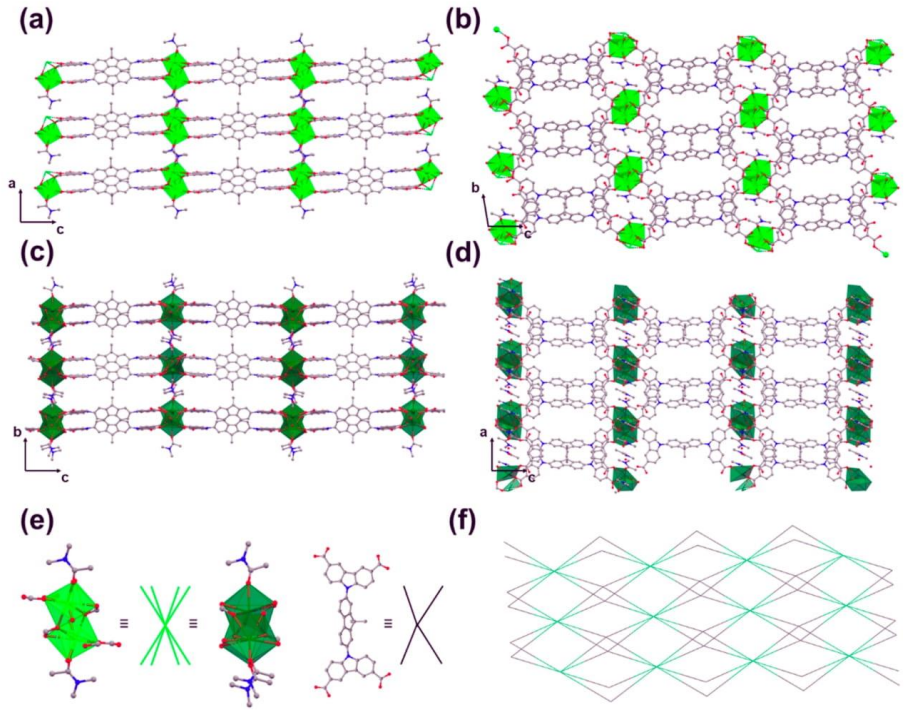

Figure 5. (a) Side view alongside the *a*/*c*-plane of the 2D coordination network of $Sr(fbcd)(DMAc)_{0.25}(H_2O)_{3.5}$. (b) Depiction of a monolayer cut-out of $Sr(fbcd)(DMAc)_{0.25}(H_2O)_{3.5}$ along the *a*-axis. (c) Side view alongside the *b*/*c*-plane of the 2D coordination network of $Ba(fbcd)(DMAc)_{2.5}(H_2O)_{1.5}$. (d) Depiction of a monolayer cut-out of $Ba(fbcd)(DMAc)_{2.5}(H_2O)_{1.5}$ along the *b*-axis. (e) Depiction of the Sr_2O_{12} SBU (left) containing two coordinated DMAc molecules and the Ba_2O_{15} SBU (right) containing three coordinated DMAc molecules and representation of the four-connecting fluorene-based linker. (f) Schematic representation of the underlying 4,8-c network topology for both CPs. Note: hydrogen atoms are omitted for clarity. Color coding: gray = carbon, blue = nitrogen, red = oxygen, light green = strontium, and dark green = barium.

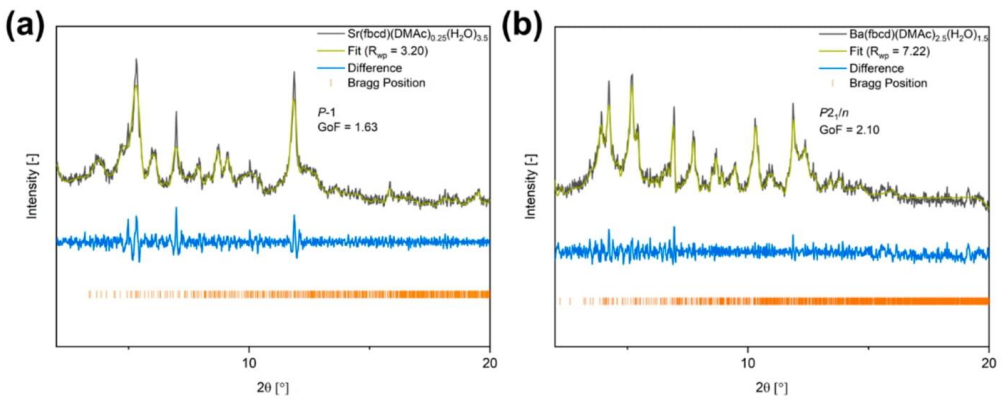

Figure 6. Plot of the measured powder XRD data (dark gray), the simulated Pawley fit (green), the difference plot (blue), and the Bragg positions (orange) of (a) $Sr(fbcd)(DMAc)_{0.25}(H_2O)_{3.5}$ and (b) $Ba(fbcd)(DMAc)_{2.5}(H_2O)_{1.5}$.

https://doi.org/10.1021/acs.chemmater.2c01525
Chem. Mater. XXXX, XXX, XXX−XXX

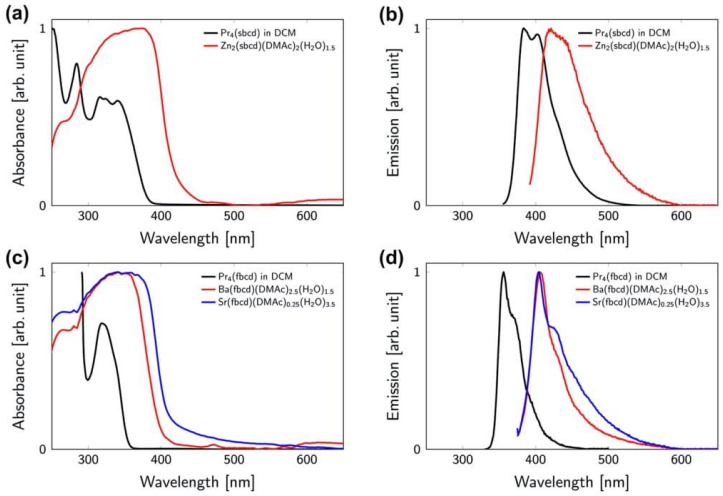

Figure 7. (a) UV/vis spectra of the linker Pr_4(sbcd) in DCM solution (black) and its corresponding zinc CP (red) in the solid state. (b) Emission spectra of the linker Pr_4(sbcd) in DCM solution (black) and its corresponding CP (red) in the solid state. (c) UV/vis spectra of the linker Pr_4(fbcd) in DCM solution (black) and its corresponding strontium CP (blue) and barium CP (red) in the solid state. (d) Emission spectra of the linker Pr_4(fbcd) in DCM solution (black) and its corresponding strontium CP (blue) and barium CP (red) in the solid state.

In Figure 5a, $Sr(fbcd)(DMAc)_{0.25}(H_2O)_{3.5}$ 2D layers are depicted, which are parallel-packed alongside the *a*/*c*-plane with an intralayer chromophore distance of 3.39 Å and an interlayer distance of 10.08 Å. This monolayer can be seen in Figure 5b, which shows a parallel packing of always pairs of two chromophores with an inversed fluorene center. For the barium-based $Ba(fbcd)(DMAc)_{2.5}(H_2O)_{1.5}$ CP, the same packing of chromophores is observed with a slightly larger intralayer chromophore distance of 3.65 Å and a smaller interlayer distance of 9.044 Å (Figure 5c,d). However, their overall topology of a 4,8-c network (Figure 5f) is the same for both CPs, which renders them being isostructural. A main difference can be observed in their SBUs because the strontium-based SBU has two strontium ions with two dimethylacetamide molecules coordinated at each metal forming a Sr_2O_{12} metal-oxo-cluster, whereas the barium-based CP has a Ba_2O_{15} metal oxo-cluster with three dimethylacetamide molecules coordinated to the SBU (Figure 5e).

In Figure 6, the measured powder X-ray diffractogram of the CPs is depicted, which also shows a high degree of crystallinity for both materials. The strontium-based CP shows intense reflections at 5.32, 6.98, and 11.97°, whereas the barium-based CP shows 4.23, 5.18, 6.94, 7.73, 10.29, and 11.87°. Pawley fit on both networks reveals a R_{wp} value of 3.20% for Sr-CP and 7.22% for Ba-CP as well as a goodness of fit (GoF) of 1.63 and 2.10, respectively, which indicates that structure models agree very well with the respective bulk material.

Photophysical Characterization of the CPs and Their Linkers. *Steady-State Spectroscopy of CPs and Linkers.* For a primary investigation of the photophysical properties of the synthesized materials, steady-state spectroscopy was performed (Figure 7) along with IR spectroscopy (cf. Figure S10). The absorption spectrum of the stilbene-based linker molecule shows four absorption bands located at 250, 270, 320, and 350 nm, which can be mainly attributed to $n-\pi^*$ and $\pi-\pi^*$ transitions as the linker molecule is dominated by its aromatic core structure (Figure 7a). However, the absorption spectrum of the respective CP shows a red shift of absorption bands of approximately 50 nm, leading to a broad strong absorption around 400 nm. When we assume that the solvent-related effects to the absorption spectra are negligible (Figure S18) and note that the linker and CP spectra were measured in DCM and in the solid state, respectively, the observed red shift can be explained by the excitonic interaction of the chromophores within the CP as the same trend can be seen for solid linker powder (Figure S19). In this environment, the interchromophore distance is strongly reduced as compared to the solvated, isolated chromophores.[28] A red shift of a similar magnitude is also observed when comparing the emission spectrum of the free linker with the emission spectrum of the CP in Figure 7b. We note that the transition in the visible range (above 550 nm in Figure 7a) is due to scattered light and does not represent a molecular transition; accordingly, the stilbene-based CP is a white powder. The absorption spectrum of the fluorene-based linker molecule shows two absorption bands located at 290 and 320 nm, tentatively attributed to transitions of the aromatic rings of the fluorene linker. The respective CP absorption spectra are broadened and featureless as compared to the linker. This holds true regardless of the choice of metal, that is, Sr or Ba (Figure 7c). The emission spectra however reveal a clear 50 nm red shift of the CPs (Figure 7d).

Z-Scan Measurements. Nonlinear optical properties of CPs $Zn_2(sbcd)(DMAc)_2(H_2O)_{1.5}$, $Sr(fbcd)(DMAc)_{0.25}(H_2O)_{3.5}$, and $Ba(fbcd)(DMAc)_{2.5}(H_2O)_{1.5}$ were characterized using the open-aperture Z-scan technique,[23,29] which is a method that allows one to extract two-photon absorption coefficient β by fitting the measured Z-scan traces (see the Supporting Information for more details). Afterward, values of two-photon

https://doi.org/10.1021/acs.chemmater.2c01525
Chem. Mater. XXXX, XXX, XXX−XXX

Table 1. Two-Photon Absorption (Action) Cross-Sections of the Reported CPs/MOFs over Excitation Wavelengths Ranging from 550 to 960 nm

CPs/MOFs	2PA cross-section $\sigma^{(2)}$ (10^3 GM)	2PA action cross-section $\eta\sigma^{(2)}$ (10^3 GM)	literature
$Zn_2(sbcd)(DMAc)_2(H_2O)_{1.5}$	2.137−15.838		this work
$Sr(fbcd)(DMAc)_{0.25}(H_2O)_{3.5}$	20.724−33.355		this work
$Ba(fbcd)(DMAc)_{2.5}(H_2O)_{1.5}$	3.054−10.415		this work
$Zn_2(benzoate)_4(An2Py)_2$	0.89		36
$Zr/CO_2CF_3/TCPE_{kagome}$		3.582	30
$Zr/OH/TCPE_{kagome}$		2.59	30
$Zr_6O_4(OH)_8(ETTC)_2(H_2O)_4$		2.217	37
Zn_2(TCPPE) (complex 1)		1.2×10^3 to 7.4×10^4	38

absorption cross-section $\sigma^{(2)}$ can be calculated accordingly and expressed in the unit of Göppert-Mayer GM (1 GM = 10^{-50} $cm^4 \cdot s \cdot photon^{-1} \cdot molecule^{-1}$). All three CP samples were prepared in a PMMA film with a thickness of c.a. 0.05 mm attached on a 1 mm thick quartz glass substrate; the calculated concentrations are in the range of 28−55 mM (see sample preparation, Supporting Information Section S8).

The preparation of MOF/CP samples for a given nonlinear characterization technique has proved to be challenging. Medishetty et al. and Quah et al. performed the measurements based on solid-state multiphoton excited fluorescence (SSMPEF) by packing MOF powders in a thin quartz cuvette to measure the MPA-induced fluorescence detected orthogonally with respect to the excitation beam.[30,31] In order to do so, one needs to find a standard sample as a reference (e.g., solid perylene or rhodamine dyes). In our method, we disperse the fine ground CP crystals in the PMMA film, which brings us several advantages. As compared to solid-state powders, the sample concentration can be defined more properly. This is advantageous for the Z-scan technique as it is transmission-based and sets demands for an optimal concentration regime. In the context of the measurements presented here, Z-scan is advantageous as the two-photon absorption cross-sections are measured directly and no reference sample is required. Unlike Z-scan, fluorescence-based methods (e.g., SSMPEF) require information of quantum efficiency η to calculate the 2PA cross-section $\sigma^{(2)}$. If η is not known, 2PA action cross-section $\eta\sigma^{(2)}$ is a commonly accepted parameter to quantify 2PA cross-section (Table 1).

The excitation range of the employed femtosecond oscillator is from 700 to 950 nm. $Zn_2(sbcd)(DMAc)_2(H_2O)_{1.5}$ gives $\sigma^{(2)}$ values in the range of 2137−15,838 GM. The H_4fbcd-based CPs $Sr(fbcd)(DMAc)_{0.25}(H_2O)_{3.5}$ (20,724−33,355 GM) and $Ba(fbcd)(DMAc)_{2.5}(H_2O)_{1.5}$ (3054−10,415 GM) exhibit $\sigma^{(2)}$ values that are 1 order of magnitude higher (Figure 8). Furthermore, $Sr(fbcd)(DMAc)_{0.25}(H_2O)_{3.5}$ shows two-photon cross-section values that are outcompeting most of the common state-of-the-art materials like organic lumophores, which normally show cross-sections in the range of 1×10^3 to 1×10^5 GM.[32,33] Additionally, for H_4tcpe-based MOFs (H_4tcpe = tetrakis[4-(4-carboxyphenyl)phenyl]ethylene), Medishetty et al. observed a maximum $\eta\sigma^{(2)}$ value of 3582 GM (Table 1). The appreciable enhancement of two-photon absorption of three CPs discussed here is attributed to the replacement of H_4tcpe (55 GM) with linkers exhibiting higher 2PA cross-sections, for example, H_4fbcd (170 GM).[30] When retaining H_4fbcd as a linker but selecting different metal ions, strontium-based materials exhibit a 3-fold increase of $\sigma^{(2)}$ values when compared to the barium CP. Both barium and strontium have the same charge, but the latter has a smaller ion

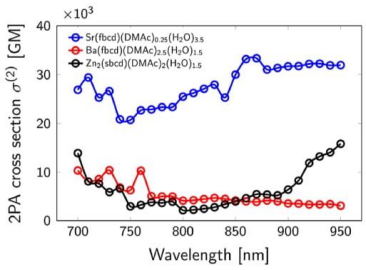

Figure 8. Comparison of the two-photon absorption cross-sections of the three CPs. Color coding: blue = $Sr(fbcd)(DMAc)_{0.25}(H_2O)_{3.5}$, red = $Ba(fbcd)(DMAc)_{2.5}(H_2O)_{1.5}$, and black = $Zn_2(sbcd)(DMAc)_2(H_2O)_{1.5}$. The error is estimated as 10%, mainly from the laser stabilities[23] and the determination of sample thicknesses.

radius, making strontium a "harder" ion; strontium can in turn polarize the chromophore more, which leads to an increase of the charge-transfer character of the chromophore. Similar effects are reported in the literature, showing that the choice of metal ions has an influence on the charge-transfer character.[34] When examining the structure of $Sr(fbcd)(DMAc)_{0.25}(H_2O)_{3.5}$ and $Ba(fbcd)(DMAc)_{2.5}(H_2O)_{1.5}$, we find that the carbazole−carbazole distance between the layers is decreased in the strontium case (3.39 vs 3.65 Å). It is the carbazole units that define the charge-transfer character of the ligand and therewith the 2PA cross-section.[14,35] Therefore, we hypothesize that the above-mentioned structural differences are another factor explaining the altered two-photon activity observed for the two CPs.

■ CONCLUSIONS AND OUTLOOK

In conclusion, we have synthesized and photophysically characterized two MPA-active chromophores, H_4sbcd and H_4fbcd, which were successfully incorporated into three MPA-active CPs. These CPs ($Zn_2(sbcd)(DMAc)_2(H_2O)_{1.5}$, $Sr(fbcd)(DMAc)_{0.25}(H_2O)_{3.5}$, and $Ba(fbcd)(DMAc)_{2.5}(H_2O)_{1.5}$) were investigated through single-crystal XRD, revealing that the three CPs are 2D CPs. The zinc-based CP shows an *sql*-network topology, whereas the main group CPs show a 4,8-c net topology. Steady-state spectroscopy of the free linkers compared to networks displays a red shift of the absorption and emission bands, which is due to dipole interactions of the chromophores inside the solid framework. Investigation of the MPA properties using the Z-scan technique showed that the three CPs exhibit high two-photon absorption cross-sections $\sigma^{(2)}$ of 10,415−33,355 GM, which are among highest cross-sections reported for MPA-active CPs (Table 1).[37] Very

https://doi.org/10.1021/acs.chemmater.2c01525
Chem. Mater. XXXX, XXX, XXX−XXX

recently, Vittal and co-workers synthesized five MOF complexes utilizing H_4tcpe.[38] Surprisingly, one of the obtained complexes showed extremely large $\eta\sigma^{(2)}$ values ($\approx 1.2 \times 10^6$ to 7.4×10^7 GM), which are among the highest $\eta\sigma^{(2)}$ values reported for MOFs/CPs up to date (Table 1).

As a perspective, we aim to further develop the MPA efficiency of these CP materials by combining the presented strong multiphoton absorbing chromophores (H_4sbcd and H_4fbcd) with the topological approach published by Vittal and co-workers,[38] which will potentially lead to modular tunable MPA materials significantly outcompeting the state of the art.

■ ASSOCIATED CONTENT

Supporting Information

The Supporting Information is available free of charge at https://pubs.acs.org/doi/10.1021/acs.chemmater.2c01525.

Additional synthetic procedures; NMR spectra; IR and TGA; Z-scan data processing; and single-crystal X-ray data (PDF)

Crystallographic data of Sr(fbcd) (CIF)

Crystallographic data of Zn(sbcd) (CIF)

Crystallographic data of Ba(fbcd) (CIF)

Accession Codes

Crystallographic data are available from the Cambridge Crystallographic Data Centre under the CCDC deposition numbers 2173885 (Zn(sbcd)), 2173886 (Sr(fbcd)), and 2173887 (Ba(fbcd)).

■ AUTHOR INFORMATION

Corresponding Authors

Jürgen Hauer − *Professorship for Dynamic Spectroscopy, Technical University of Munich, 85748 Garching, Germany;* orcid.org/0000-0002-6874-6138; Email: juergen.hauer@tum.de

Alexander Pöthig − *Chair of Inorganic and Metal−Organic Chemistry, Department of Chemistry & Catalysis Research Center, Technical University of Munich, 85748 Garching, Germany;* orcid.org/0000-0003-4663-3949; Email: alexander.poethig@tum.de

Roland A. Fischer − *Chair of Inorganic and Metal−Organic Chemistry, Department of Chemistry & Catalysis Research Center, Technical University of Munich, 85748 Garching, Germany;* orcid.org/0000-0002-7532-5286; Email: roland.fischer@tum.de

Authors

Sebastian J. Weishäupl − *Chair of Inorganic and Metal−Organic Chemistry, Department of Chemistry & Catalysis Research Center, Technical University of Munich, 85748 Garching, Germany*

Yang Cui − *Professorship for Dynamic Spectroscopy, Technical University of Munich, 85748 Garching, Germany; Department of Physics, Technical University of Munich, 85748 Garching, Germany;* orcid.org/0000-0003-2116-7611

Simon N. Deger − *Chair of Inorganic and Metal−Organic Chemistry, Department of Chemistry & Catalysis Research Center, Technical University of Munich, 85748 Garching, Germany*

Hamad Syed − *3D Printing and Biofabrication Group, Institute of Materials Science and Technology, Technische Universität Wien (TU Wien), 1060 Vienna, Austria*

Aleksandr Ovsianikov − *3D Printing and Biofabrication Group, Institute of Materials Science and Technology, Technische Universität Wien (TU Wien), 1060 Vienna, Austria*

Complete contact information is available at: https://pubs.acs.org/10.1021/acs.chemmater.2c01525

Author Contributions

$^{\perp}$S.J.W. and Y.C. contributed equally to this work.

Author Contributions

Conceptualization and writing, original draft preparation, S.J.W. and Y.C.; synthesis and characterization, S.J.W. and S.N.D.; photophysical characterization, S.J.W., Y.C., and H.S.; methodology, S.J.W., Y.C., J.H., and A.P.; writing, review, and editing, J.H., A.O., A.P., and R.A.F.; project administration, R.A.F. All authors have given approval to the final version of the manuscript.

Funding

The authors would like to thank the German Research Foundation (DFG) for funding within the frame of EXC 2089 Cluster of Excellence and the Priority Programme "COORNETs" (SPP 1928).

Notes

The authors declare no competing financial interest.

■ ACKNOWLEDGMENTS

The TUM is very greatly acknowledged for institutional funding. S.J.W. and Y.C. would like to thank the TUM Graduate School for financial support. S.J.W. would like to thank Johannes Voigtland for experiments and Silva Kronawitter for measurement support. Y.C. would like to thank Franziska Chalupa-Gantner for measurement support.

■ REFERENCES

(1) Munn, R. W. Nonlinear optical phenomena. In *Principles and Applications of Nonlinear Optical Materials*; Munn, R. W., Ironside, C. N., Eds.; Springer Netherlands: Dordrecht, 1993; pp 5−19.

(2) Medishetty, R.; Zaręba, J. K.; Mayer, D.; Samoć, M.; Fischer, R. A. Nonlinear optical properties, upconversion and lasing in metal−organic frameworks. *Chem. Soc. Rev.* **2017**, *46*, 4976−5004.

(3) Mingabudinova, L. R.; Vinogradov, V. V.; Milichko, V. A.; Hey-Hawkins, E.; Vinogradov, A. V. Metal−organic frameworks as competitive materials for non-linear optics. *Chem. Soc. Rev.* **2016**, *45*, 5408−5431.

(4) Zaręba, J. K.; Nyk, M.; Samoć, M. Nonlinear Optical Properties of Emerging Nano- and Microcrystalline Materials. *Adv. Opt. Mater.* **2021**, *9*, 2100216.

(5) Shi, R.; Han, X.; Xu, J.; Bu, X.-H. Crystalline Porous Materials for Nonlinear Optics. *Small* **2021**, *17*, 2006416.

(6) Zhou, J. R. L.; Long, O. M.; Yaghi, O. M. Introduction to Metal−Organic Frameworks. *Chem. Rev.* **2012**, *112*, 673−674.

(7) Wang, Q.; Astruc, D. State of the Art and Prospects in Metal−Organic Framework (MOF)-Based and MOF-Derived Nanocatalysis. *Chem. Rev.* **2020**, *120*, 1438−1511.

(8) Allendorf, M. D.; Bauer, C. A.; Bhakta, R. K.; Houk, R. J. T. Luminescent metal−organic frameworks. *Chem. Soc. Rev.* **2009**, *38*, 1330−1352.

(9) Hu, Z.; Huang, G.; Lustig, W. P.; Wang, F.; Wang, H.; Teat, S. J.; Banerjee, D.; Zhang, D.; Li, J. Achieving exceptionally high luminescence quantum efficiency by immobilizing an AIE molecular chromophore into a metal−organic framework. *Chem. Commun.* **2015**, *51*, 3045−3048.

(10) Wei, Z.; Gu, Z.-Y.; Arvapally, R. K.; Chen, Y.-P.; McDougald, R. N.; Ivy, J. F.; Yakovenko, A. A.; Feng, D.; Omary, M. A.; Zhou, H.-

C. Rigidifying Fluorescent Linkers by Metal−Organic Framework Formation for Fluorescence Blue Shift and Quantum Yield Enhancement. *J. Am. Chem. Soc.* **2014**, *136*, 8269−8276.
(11) Shustova, N. B.; Ong, T.-C.; Cozzolino, A. F.; Michaelis, V. K.; Griffin, R. G.; Dincă, M. Phenyl Ring Dynamics in a Tetraphenylethylene-Bridged Metal−Organic Framework: Implications for the Mechanism of Aggregation-Induced Emission. *J. Am. Chem. Soc.* **2012**, *134*, 15061−15070.
(12) Mayer, D. C.; Manzi, A.; Medishetty, R.; Winkler, B.; Schneider, C.; Kieslich, G.; Pöthig, A.; Feldmann, J.; Fischer, R. A. Controlling Multiphoton Absorption Efficiency by Chromophore Packing in Metal−Organic Frameworks. *J. Am. Chem. Soc.* **2019**, *141*, 11594−11602.
(13) Mayer, D. C.; Zaręba, J. K.; Raudaschl-Sieber, G.; Pöthig, A.; Chołuj, M.; Zaleśny, R.; Samoć, M.; Fischer, R. A. Postsynthetic Framework Contraction Enhances the Two-Photon Absorption Properties of Pillar-Layered Metal−Organic Frameworks. *Chem. Mater.* **2020**, *32*, 5682−5690.
(14) Weishäupl, S. J.; Mayer, D. C.; Cui, Y.; Kumar, P.; Oberhofer, H.; Fischer, R. A.; Hauer, J.; Pöthig, A. Recent advances of multiphoton absorption in metal−organic frameworks. *J. Mater. Chem. C* **2022**, *10*, 6912−6934.
(15) Vogler, A.; Kunkely, H. Charge Transfer Excitation of Coordination Compounds. Generation of Reactive Intermediates. In *Photosensitization and Photocatalysis Using Inorganic and Organometallic Compounds*; Kalyanasundaram, K., Grätzel, M., Eds.; Springer Netherlands: Dordrecht, 1993; pp 71−111.
(16) He, X.; Xu, B.; Liu, Y.; Yang, Y.; Tian, W. Effect of intramolecular charge transfer on the two-photon absorption behavior of multibranched triphenylamine derivations. *J. Appl. Phys.* **2012**, *111*, 053516.
(17) Jia, J.; Wu, X.; Zhang, X.; Wang, Y.; Yang, J.; Fang, Y.; Song, Y. Effect of intramolecular charge transfer on nonlinear optical properties of chalcone derivatives: a visual description of the charge transfer process. *Phys. Chem. Chem. Phys.* **2022**, *24*, 955−965.
(18) Dar, A. H.; Gowri, V.; Gopal, A.; Muthukrishnan, A.; Bajaj, A.; Sartaliya, S.; Selim, A.; Ali, M. E.; Jayamurugan, G. Designing of Push−Pull Chromophores with Tunable Electronic and Luminescent Properties Using Urea as the Electron Donor. *J. Org. Chem.* **2019**, *84*, 8941−8947.
(19) He, G. S.; Tan, L.-S.; Zheng, Q.; Prasad, P. N. Multiphoton Absorbing Materials: Molecular Designs, Characterizations, and Applications. *Chem. Rev.* **2008**, *108*, 1245−1330.
(20) Weishäupl, S. J.; Mayer, D. C.; Thyrhaug, E.; Hauer, J.; Pöthig, A.; Fischer, R. A. A nitrophenyl-carbazole based push-pull linker as a building block for non-linear optical active coordination polymers: A structural and photophysical study. *Dyes Pigm.* **2021**, *186*, 109012.
(21) Sippola, R. J.; Hadipour, A.; Kastinen, T.; Vivo, P.; Hukka, T. I.; Aernouts, T.; Heiskanen, J. P. Carbazole-based small molecule electron donors: Syntheses, characterization, and material properties. *Dyes Pigm.* **2018**, *150*, 79−88.
(22) Krause, S.; Evans, J. D.; Bon, V.; Senkovska, I.; Ehrling, S.; Iacomi, P.; Többens, D. M.; Wallacher, D.; Weiss, M. S.; Zheng, B.; Yot, P. G.; Maurin, G.; Llewellyn, P. L.; Coudert, F.-X.; Kaskel, S. Engineering micromechanics of soft porous crystals for negative gas adsorption. *Chem. Sci.* **2020**, *11*, 9468−9479.
(23) Steiger, W.; Gruber, P.; Theiner, D.; Dobos, A.; Lunzer, M.; Van Hoorick, J.; Van Vlierberghe, S.; Liska, R.; Ovsianikov, A. Fully automated z-scan setup based on a tunable fs-oscillator. *Opt. Mater. Express* **2019**, *9*, 3567−3581.
(24) Muhr, M.; Heiß, P.; Schütz, M.; Bühler, R.; Gemel, C.; Linden, M. H.; Linden, H. B.; Fischer, R. A. Enabling LIFDI-MS measurements of highly air sensitive organometallic compounds: a combined MS/glovebox technique. *Dalton Trans.* **2021**, *50*, 9031−9036.
(25) Li, Q.; Shin, S. M.; Moon, D.; Jeong, K. S.; Jeong, N. Chiral porous metal−organic frameworks from chiral building units with different metrics. *CrystEngComm* **2013**, *15*, 10161−10164.
(26) Lee, S. H.; Nakamura, T.; Tsutsui, T. Synthesis and Characterization of Oligo(9,9-dihexyl-2,7-fluorene ethynylene)s: For Application as Blue Light-Emitting Diode. *Org. Lett.* **2001**, *3*, 2005−2007.
(27) West, K.; Wang, C.; Batsanov, A. S.; Bryce, M. R. Carbon-rich molecules: synthesis and isolation of aryl/heteroaryl terminal bis(butadiynes)(HC−C−C−C−Ar−C−C−C−CH) and their applications in the synthesis of oligo(arylenebutadiynylene) molecular wires. *Org. Biomol. Chem.* **2008**, *6*, 1934−1937.
(28) Valkunas, L.; Abramavicius, D.; Mančal, T. Quantum States of Molecules and Aggregates. In *Molecular Excitation Dynamics and Relaxation*; Wiley, 2013; pp 101−132.
(29) Sheik-Bahae, M.; Said, A. A.; Van Stryland, E. W. High-sensitivity, single-beam *n_2* measurements. *Opt. Lett.* **1989**, *14*, 955−957.
(30) Medishetty, R.; Nemec, L.; Nalla, V.; Henke, S.; Samoć, M.; Reuter, K.; Fischer, R. A. Multi-Photon Absorption in Metal−Organic Frameworks. *Angew. Chem., Int. Ed.* **2017**, *56*, 14743−14748.
(31) Quah, H. S.; Chen, W.; Schreyer, M. K.; Yang, H.; Wong, M. W.; Ji, W.; Vittal, J. J. Multiphoton harvesting metal−organic frameworks. *Nat. Commun.* **2015**, *6*, 7954.
(32) Kim, H. M.; Rae Cho, B. Two-photon materials with large two-photon cross sections. Structure−property relationship. *Chem. Commun.* **2009**, 153−164.
(33) Sadowski, B.; Kita, H.; Grzybowski, M.; Kamada, K.; Gryko, D. T. π-Expanded Dipyrrolonaphthyridinediones with Large Two-Photon Absorption Cross-Section Values. *J. Org. Chem.* **2017**, *82*, 7254−7264.
(34) Few, S.; Frost, J. M.; Kirkpatrick, J.; Nelson, J. Influence of Chemical Structure on the Charge Transfer State Spectrum of a Polymer:Fullerene Complex. *J. Phys. Chem. C* **2014**, *118*, 8253−8261.
(35) Jagatap, B. N.; Meath, W. J. Contributions of permanent dipole moments to molecular multiphoton excitation cross sections. *J. Opt. Soc. Am. B* **2002**, *19*, 2673−2681.
(36) Liu, M.; Quah, H. S.; Wen, S.; Li, Y.; Vittal, J. J.; Ji, W. Multiphoton absorption and two-photon-pumped random lasing in crystallites of a coordination polymer. *J. Phys. Chem. C* **2018**, *122*, 777−781.
(37) Chen, C. X.; Yin, S. Y.; Wei, Z. W.; Qiu, Q. F.; Zhu, N. X.; Fan, Y. N.; Pan, M.; Su, C. Y. Pressure-Induced Multiphoton Excited Fluorochromic Metal−Organic Frameworks for Improving MPEF Properties. *Angew. Chem.* **2019**, *131*, 14517−14523.
(38) Liu, N.; Chen, Z.; Fan, W.; Su, J.; Lin, T.; Xiao, S.; Meng, J.; He, J.; Vittal, J. J.; Jiang, J. Highly Efficient Multiphoton Absorption of Zinc-AIEgen Metal−Organic Frameworks. *Angew. Chem., Int. Ed.* **2022**, *61*, e202115205.

https://doi.org/10.1021/acs.chemmater.2c01525
Chem. Mater. XXXX, XXX, XXX−XXX

3.3 A Perylenediimide-Based Zinc-Coordination Polymer for Photosensitized Singlet-Oxygen Generation

Perylenediimides (PDI) are well-known organic dyes caused by their outstanding optoelectronical applicability. However, there are only a few examples of PDI based coordination polymers, which are used for photocatalysis. In this manuscript, we report the synthesis and characterization of a novel zinc based 2-coordination polymer Zn(tpbd)$(DMF)_3$ with the already literature known linker molecule 1,6,7,12-tetrachloroperylenediimide-*N,N'*-di-benzoic acid (H_2tpbd). The CP and the respective linker were fully investigated including single crystal x-ray diffraction. SC-x-ray analysis revealed that both linker and CP crystallize in the monoclinic space group C 2/*c* with a strong aggregation of the incorporated linker. Absorption measurements of the CP shows, that absorption band are red- and blue-shifting compared to the solvated linker, which can be attributed to H-type aggregation and additional charge transfer of the framework, leading also to a limited quantum efficiency. Finally, Zn(tpbd)$(DMF)_3$ and H_2tpdb was tested for photosensitization of triplet oxygen to singlet at 512 nm using 1,3-diphenylisobenzofurane (DBPF) as trapping agent**.**

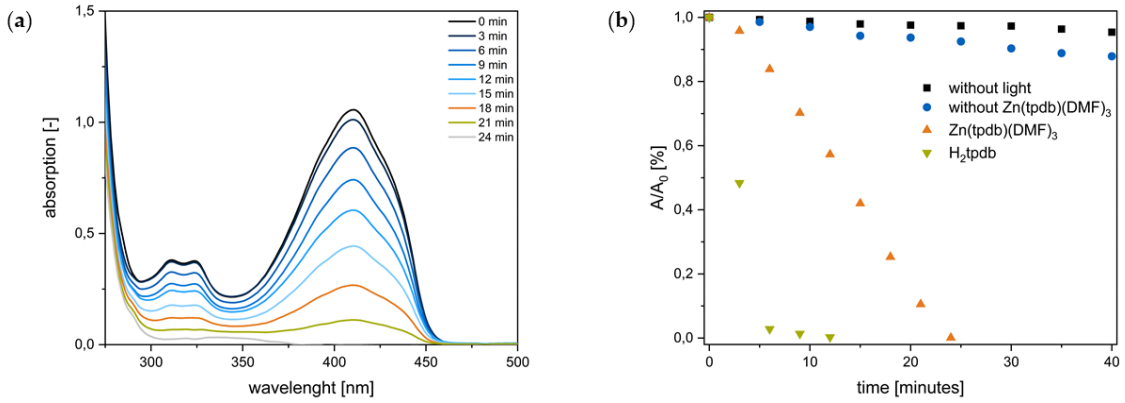

Fig. 27: (a) Stacked UV/Vis spectra of 1,3-diphenylisobenzofurane (DBPF) showing the decrease in absorption over time for the reaction with the Zn-based CP used as photosensitizer with a 512 nm LED. (b) decrease of the absorption maxima of DBPF at 416 nm with the CP and the respective linker as well as the control experiments.

Thereby, the H_2tpdb shows activity towards photosensitization, which can be retained upon incorporation in CP. This is, up to now, the first example of a PDI-based CP successfully tested towards singlet oxygen generation.

This manuscript was written by two shared-first authors and edited by R. A. Fischer and A. Pöthig. The conceptualization and methodology were done by the author of this thesis in

cooperation with S. N. Deger and A. Pöthig. The synthesis and the photocatalytic experiments were performed by S. N. Deger in the context of his Master's thesis under the supervision of this author. The structural and photophysical characterization was done by the author of this thesis.

Reprinted with permission from *Energies* in 2022.[105]

Deger, S. N.[†]; Weishäupl, S. J. [†]; Pöthig, A.; Fischer, R. A., A Perylenediimide-Based Zinc-Coordination Polymer for Photosensitized Singlet-Oxygen Generation. *Energies* **2022,** *15* (7), 2437.

[†] These authors contributed equally to this work.

energies

MDPI

Article

A Perylenediimide-Based Zinc-Coordination Polymer for Photosensitized Singlet-Oxygen Generation

Simon N. Deger †, Sebastian J. Weishäupl †, Alexander Pöthig * and Roland A. Fischer *

Chair of Inorganic and Metal-Organic Chemistry, Catalysis Research Center, Ernst-Otto-Fischer-Straße 1, 85748 Garching, Germany; simon.deger@tum.de (S.N.D.); sebastian.weishaeupl@tum.de (S.J.W.)
* Correspondence: alexander.poethig@tum.de (A.P.); roland.fischer@tum.de (R.A.F.)
† These authors contributed equally to this work.

Abstract: In the face of anthropogenic global warming the design and synthesis of materials, which enable energy transfer processes using sunlight as an energy source, are of high interest. Perylenediimides are a highly absorbing class of chromophores suitable for sunlight absorption and conversion. Therefore, metal–organic frameworks (MOFs) and coordination polymers (CPs) with incorporated organic perylene chromophores are highly interesting materials both for applied, but also fundamental, photophysical research. MOFs/CPs have the advantage of a modular adjustability of interchromophoric distances and angles, and the choice of metal nodes can be used to further tune the material towards the desired photophysical properties. In the present paper, we present a study using a reported organic perylenediimide (PDI) chromophore (H_2tpdb) as a linker to be incorporated into coordination polymer and test towards applicability within the photochemical $^1O_2$ generation. In detail, a novel zinc 2D -coordination polymer Zn(tpdb)$(DMF)_3$ is reported, which is synthesized using a solvothermal synthesis with $Zn(NO_3)_2$ and a ditopic organic perylene linker. Both the linker and Zn-CP are fully characterized, including SC-XRD, showing a strong aggregation of tightly packed chromophores in the solid state. The photophysical properties are examined and discussed, including the observed shifts within the absorption spectra of the CP are compared to the linker in solution. These shifts are mainly attributed to the for PDIs known H-type aggregation and an additional charge transfer in the framework structure, causing a limited quantum yield of the emission. Finally, the photosensitization of triplet oxygen to singlet oxygen using 1,3-diphenylisobenzofurane (DBPF) as a trapping agent is investigated both for the free linker and the Zn-CP, showing that the perylene chromophore is an efficient photosensitizer and its activity can, in principle, be retained after its incorporation in the coordination polymer.

Keywords: perylene diimide; metal–organic framework; singlet oxygen; photosensitizer; H-type aggregation

Citation: Deger, S.N.; Weishäupl, S.J.; Pöthig, A.; Fischer, R.A. A Perylenediimide-Based Zinc-Coordination Polymer for Photosensitized Singlet-Oxygen Generation. *Energies* **2022**, *15*, 2437. https://doi.org/10.3390/en15072437

Academic Editor: Claudio Mele

Received: 18 February 2022
Accepted: 21 March 2022
Published: 25 March 2022

1. Introduction

In the light of anthropogenic global warming, a conversion of greenhouse gases (e.g., CO_2 and NO_x) into valuable chemicals is the focus of current research [1]. In nature, light-absorbing dyes, such as chlorophyll, are utilized to convert light into energy-rich organic compounds, primarily carbohydrates, from low-energy inorganic substances, such as carbon dioxide and water [2,3].

Therefore, translating the fundamental reactions of natural photosynthesis into an efficient, robust, and economic *artificial leaf* is a significant task [2,4,5]. In order to be able to design and fabricate high-performance synthetic materials, a deep understanding of related energy transfer processes inside these compounds is of utmost importance.

Metal–organic frameworks (MOFs) are a class of porous, polymeric, and multifunctional hybrid materials. They consist of metal ions and organic bridging ligands, and therefore the respective research is located at the interface between molecular coordination

chemistry and materials science [6]. In the presented study, the metal ions serve as nodes of a crystalline lattice. They govern the structure and topology of the material n combination with the directionality of the organic linkers [7].

Additionally, the wide range of possible metal nodes as well as the different design concepts of the organic linker molecules offer a variety of magnetic, electrical, optical, and catalytic properties that can be incorporated into these materials. For instance, MOFs have been applied in catalysis, gas storage, telecommunications, photovoltaics, or sensor technology applications [8–13].

With respect to the photochemical properties of the material, MOF chemistry offers a precise control of pore size and interchromophoric distances and angles, therefore, in principle, providing synthetic tools to fundamentally study energy-transfer processes and the reactivity of the material [9,14].

Concerning the choice of chromophore linkers, rylene dyes are a very prominent class of organic dye molecules. Initially applied for industrial use as red dyes and as pigments in automotive finishes [15], they became widely used in manifold industrial applications as well as in modern research [16], due to their outstanding chemical, thermal, and optical stability [17–19]. In addition, they exhibit remarkable optoelectronic properties, e.g., as excellent light-harvesting materials, since they strongly absorb visible light with high fluorescence quantum yields in solution [20]. Furthermore, they possess a large conjugated π-system, as well as high molar absorption coefficients, which results in strong intermolecular coupling [21].

One of the potential photochemical applications of perylene dyes is the photosensitized singlet-oxygen generation, e.g., within photodynamic therapy [22]. In this process, the photosensitizer, in this case the perylene chromophore, is excited and transfers the absorbed energy to a triplet oxygen $^3O_2$ to generate singlet oxygen $^1O_2$ [23]. As a consequence, the generated $^1O_2$ has a higher reactivity and electrophilicity than $^3O_2$, which makes it more applicable in photochemical and photobiological processes, since the singlet oxygen rapidly reacts with nearby biomolecules leading to destructive reactions, which then causes, for example, the death of cancer cells [24,25]. Such an incorporation of organic chromophores into a rigid framework for photosensitization reactions is already successfully applied for many porphyrin-based metal–organic frameworks [26–28].

Herein, we present the synthesis and characterization of a new 2D zinc coordination-polymer Zn(tpbd)$(DMF)_3$ with the already known perylenediimide (PDI)-based linker molecule 1,6,7,12-tetrachloroperylenediimide-N,N′-di(benzoic acid) (H_2tpdb). Similarly *Hupp* et al. reported a crystalline PDI-zinc framework in 2009, with a different powder pattern, and therefore crystal phase, to the material reported in the present work [29]. Single-crystal X-ray diffraction analysis (SC-XRD) of the materials revealed parallel chromophore packing featuring interchromophoric distances of 3.6 Å, showing a red and blue shifting of the absorption band known indicating as head-to-head aggregation.

Finally, the material was tested in the photosensitization reaction of triplet oxygen to generate singlet oxygen using 1,3-diphenylisobenzofurane as $^1O_2$ trapper, proving that Zn(tpdb)$(DMF)_3$ can be used as an effective material in photochemical reactions. This makes the herein presented material the first example of a PDI-based coordination polymer that is used for photosensitized singlet-oxygen generation.

2. Experimental

2.1. Materials and Method

All utilized chemicals were received from common chemical suppliers and were used without further purification. All air-sensitive reactions were carried out under argon atmosphere (Argon 4.6) using the standard Schlenk techniques. The determination of the elemental composition was performed by the flash combustion method at 1800 °C, conducted by the Microanalytical Lab at the Technical University of Munich. NMR spectra were measured on a Bruker AV400 at ambient temperature at 400 MHz. UV/Vis spectroscopical measurements in solution were performed using a PerkinElmer *Lambda 365*

UV/Vis spectrometer equipped with a xenon lamp. UV/Vis spectroscopical measurements for solid-state samples were performed on a SHIMADZU *UV-3600 Plus* with Ba_2SO_4 as blank. Solution as well as solid-state fluorescence measurements were carried out using an Edinburgh Instruments *FS5* spectrofluorometer equipped with a xenon lamp. BET measurements were performed on a 3Flex Physisorption from Micromeritics Instrument Corp. (Norcross, GA, USA). Single-crystal XRD measurements were conducted in the SC-XRD laboratory of the Catalysis Research Center at the Technical University of Munich (for details cf. Supplementary Materials).

2.2. Synthesis

1,6,7,12-tetrachloro-perylene-3,4,9,10-tetracarboxylic anhydride 1: the synthesis was performed according to a literature-known synthesis [30]. In a 100 mL Schlenk flask, 1 g of perylene-3,4,9,10-tetracarboxylic acid anhydride 1 (2.5 mmol, 1 eq.) and 0.17 g of iodine (0.68 mmol, 0.27 eq.) in 6.55 mL of chlorosulfonic acid were stirred for 2 days at 70 °C under argon atmosphere. After completion, the reaction mixture was slowly poured into 500 mL of ice water. Subsequently, the precipitating orange solid was filtered, washed with water, and dried to produce a bright orange powder (1.32 g, 2.49 mmol, 99%). ^{1}H-NMR (400 mHz, CDCl3): δ (ppm) = 8.75 (s, 4H).

1,6,7,12-tetrachloroperylenediimide-N,N′-di-benzoic acid (H_2tpbd) 2: the synthesis was performed with a modified literature synthesis [31]. In a 100 mL round bottom flask, 1 g of **1** (1.89 mmol, 1 eq.) and 3.88 g of 4-aminobenzoic acid 3 (28.3 mmol, 15 eq.) were dissolved in 25 mL of propionic acid and stirred for 2 days at 160 °C. After the completion of the reaction, the reaction mixture was poured into 100 mL of water and subsequently filtered off. The filtrate is washed with 100 mL of water/methanol (1:1), and afterwards the orange solid was dried to constant weight (1.1 g, 1.89 mmol, 79%).

^{1}H-NMR (400 mHz, DMSO-d6): δ (ppm) = 13.20 (s, 2H, COOH), 8.64 (s, 4H), 8.16–8.12 (m, 4H), 7.61–7.56 (m, 4H).

Zn(tpdb)$(DMF)_3$ 3: in a 4 mL screw-cap vial, $Zn(NO_3)_2$ (15.0 mg, 0.05 mmol, 3.8 eq.) and H_2tpbd **2** (10.0 mg, 0.013 µmol. 1 eq.) were dissolved in 3 mL of DMF. Afterwards, the solution was sonicated and placed for 96 h at 90 °C in an oven. The precipitated solid was then filtered and dried to constant weight to produce orange needles of Zn(tpbd)$(DMF)_3$ **3** (4.13 mg, 0.0039 mmol, 30%).

Elemental analysis (%) calc. for Zn(tpdb)$(DMF)_3$: C, 53.17; H, 3.17; N, 6.66; Zn, 6.22; Cl, 13.49; found C, 53.57; H, 2.78; N, 6.03; Zn, 6.2; Cl, 13.0.

2.3. $^1O_2$ Evolution Experiments

In a glovebox, a 20 mL phototube was filled with 1.25 mg (4.62 mmol, 1 eq.) of DBPF and 1 eq. of the respective photosensitizer **2** or **3**. A total of 5 mL of dried acetonitrile was added with argon counter flow, and subsequently the suspension was stirred for 30 min in the dark to achieve the adsorption/desorption equilibrium under an oxygen atmosphere. Afterwards, an LED with a wavelength of 512 nm was used and at defined time intervals, aliquots of the reaction solution were obtained, diluted, and investigated byUV/Vis-spectroscopy.

3. Results and Discussion

3.1. Linker and CP Synthesis

The PDI-based linker **2** was synthesized in a two-step synthesis procedure starting from perylene-3,4,9,10-tetracarboxylic acid anhydride (Figure 1). In the first step, the bay area positions of the perylene core were chlorinated to twist the aromatic system and later enhance the solubility of the linker for CP synthesis [32]. Subsequently, **1** was reacted with 4-amino benzoic acid to obtain an orange powder of H_2tpbd **2** in good yields of 79% and excellent purity.

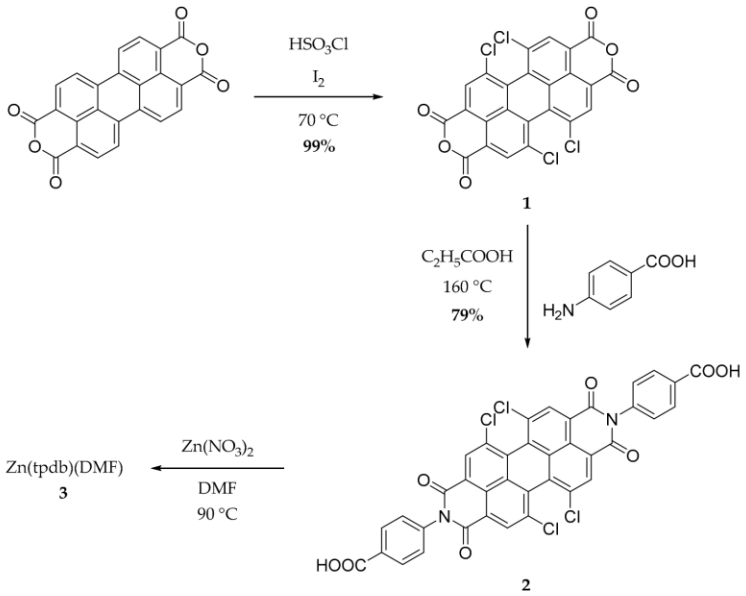

Figure 1. Three-step synthesis procedure to obtain **3**, starting from perylene-3,4,9,10-tetracarboxylic acid anhydride.

Then, 10 mg of **2** were used in a solvothermal synthesis reaction towards novel coordination polymers with 3.8 eq. of $Zn(NO_3)_2$ in 3 mL of DMF for 4 days at 90 °C in an oven. Following this, orange single crystals of $Zn(tpdb)(DMF)_3$ **3** were obtained, which were filtered off and washed with DMF.

In comparison to the other CPs or MOFs, the solvothermal synthesis applied here is comparably uncomplicated (compare Table 1), as it requires no preformation of SBUs or additional additives (e.g., MeOH, trifluoroacetic acid).

Table 1. Table of different literature-known MOF synthesis approaches.

MOF Name	Linker	Metal Salt	Temperature	Solvent	Additives	Refs.
MOF-5, IRMOF(2-20)	R_1-7-BDC, 2,6-NDC, BPDC, HPDC, PDC, TPDC	$Zn(NO_3)_2$	85° to 105 °C	(DMF/DEF), chlorobenzene	H_2O_2, NEt_3	[6,33]
$[Zn_2(TPOM)(NDC)_2]$	TPOM, H_2NDC	$Zn(NO_3)_2$	100 °C	DMF	H_2O	[34]
{[Zn(μ-4-hzba)2]2·4(H2O)}n	4-hydrazinebenzoic acid	$Zn(OAc)_2$	110 °C	EtOH	H_2O	[35]

3.2. Crystal Structure Analysis of H_2tpbd

Small single crystals of H_2tpbd for single-crystal X-ray diffraction (SCXRD) analysis were obtained by controlled crystal growth through the slow diffusion of pentane into a linker solution of 2 (THF). In Figure 2a, the molecular structure, as well as the packing alongside the crystallographic *a* and *c* axis, are depicted (Figure 2b,c).

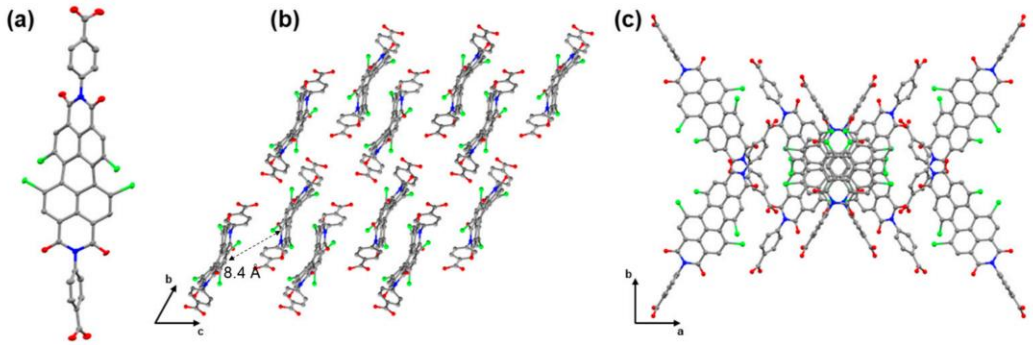

Figure 2. (**a**) ORTEP representation of the molecular structure of the linker molecule H_2tpbd **2** in the solid state, with displacement ellipsoids shown at the 50% probability level. (**b**) Parallel packing of **2** alongside the *b*-*c* plane showing a mean linker distance of 8.4 Å. (**c**) Packing of the **2** alongside the a-b plane showing an alternating arrangement along the *c*-axis. Hydrogen atoms and co-crystallized solvent are omitted for clarity. Color coding: gray = carbon, blue = nitrogen, red = oxygen, and green = chlorine.

The chromophore molecule crystallizes in the monoclinic space group C 2/*c* with unit cell lengths of *a* = 35.229(4) Å, *b* = 12.367(13) Å and *c* = 21.757(3) Å, and monoclinic angle β = 119.954(6)°. The asymmetric unit shows a single molecule of the PDI linker, accompanied by two co-crystallized THF molecules. As expected, the substituted PDI core twists by 35°, compared to the unsubstituted PDI chromophores, caused by the steric demand of the chlorine atoms [32]. This also has an impact on the solubility, since π stacking of the benzene rings is less favored, which makes the molecule more soluble. Interestingly, one of the benzene rings of the benzoic acid group is rotated out of the PDI-imide moiety by roughly 90°, whereas the opposing one shows a respective torsion angle of 78°. The view along the *a*-axis shows the parallel packing of the linker molecules (Figure 2b), with a center-to-center chromophore distance of 8.4 Å. Additionally, in Figure 2c, the alternating packing of the PDI along the a-b plane is depicted.

3.3. Crystal Structure Analysis of Zn(tpbd)(DMF)$_3$

The SC-XRD analysis of the synthesized coordination polymer revealed that the material crystallizes in the monoclinic space group C 2/*c* with unit cell parameters of *a* = 50.894(3) Å, *b* = 19.971(12) Å and *c* = 16.31(10) Å, as well as monoclinic angle β = 91.825(2)°. Two linker molecules and two zinc atoms are present in the asymmetric unit.

In Figure 3a,b the 2D crystalline network is depicted along the *c*-axis and the *b*-axis, showing the linker molecules being arranged as parallel, as well as head-to-tail oriented, to each other. This can also be seen from the topology analysis shown in Figure 3c,d, revealing a four-connecting uninodal net, with an alternating packing that is similar to the linker in the solid state. Additionally, each zinc atom bridges two linkers and additionally coordinates two dimethylformamide molecules, forming a tetrahedral zinc-oxo cluster (Figure 3e). In Figure 3f, the head-to-head chromophore packing of the chromophore is depicted, with a distance of 3.6 Å, and a head-to-tail center of gravity distance of 27.3 Å, which has a great influence on the photophysical behavior of the material.

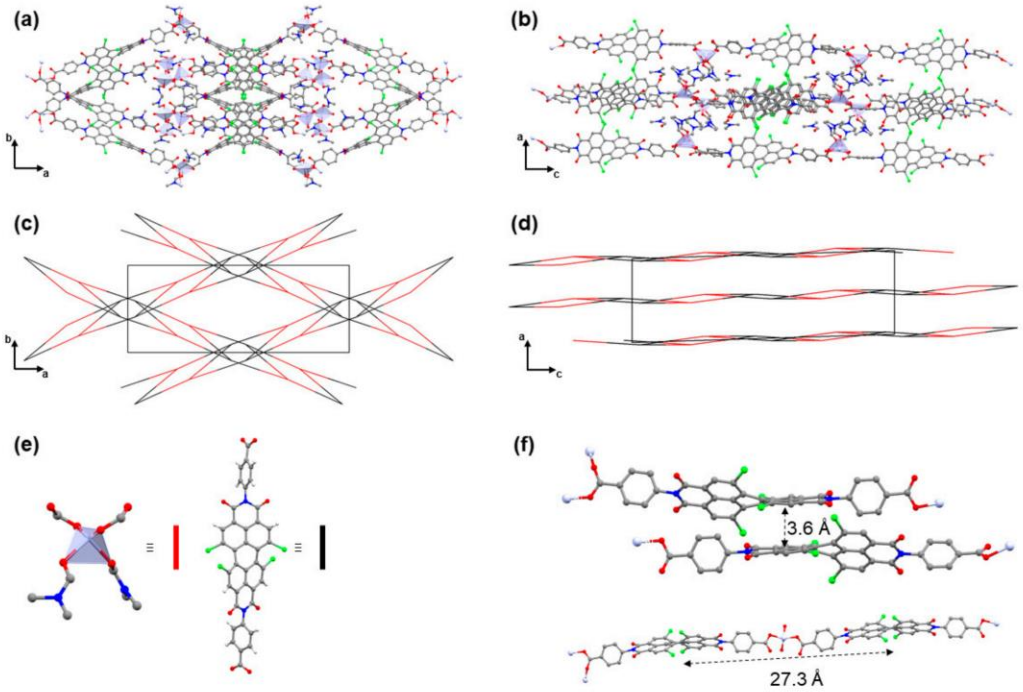

Figure 3. (**a**) Depiction of the crystal structure of the Zn(tpbd)(DMF)$_3$ network along the *c*-axis. (**b**) Parallel packing of chromophore linkers in the 2D framework along the a-c plane. (**c**) Underlying network topology of the 4-c uninodal net alongside the *c*-axis (color coding cf. Figure 3e). (**d**) Depiction of the parallel packing of the underlying network along the *b*-axis (color coding cf. Figure 3e). (**e**) Zn^{2+}-containing tetrahedral SBU (zinc = gray, carbon = dark gray, oxygen = red, and nitrogen = blue), and the representation of the two-connecting linkers. (**f**) Depiction of the head-to-head and head-to-tail arrangement of the linker molecule inside the framework. Hydrogen atoms are omitted for clarity. Color coding: gray = carbon, blue = nitrogen, red = oxygen, green = chlorine, and light gray = zinc.

The powder X-ray diffractogram of the coordination polymer is depicted in Figure 4, which shows high crystallinity and pronounced reflections at 3.59°, 7.01°, and 10.75°, compared to the already-known literature compound presented by *Hupp* et al., showing reflections at 7°, 21°, and 39°. Furthermore, the previously published material showed a high surface area, whereas Zn(tpdb) shows no porosity (cf. Figure S8), proving that the reported material in the present study is a novel framework. Pawley fitting on this data revealed only a small deviation of the fitted curve and measured data, and an R_{wp} of 2.59% and a GoF of 1.92, which supports the determined structure model.

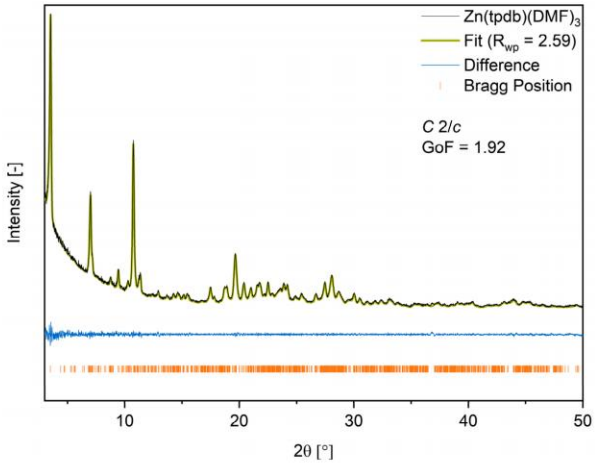

Figure 4. Experimental powder X-ray diffractogram of the Zn(tpdb)-CP (gray), the simulated Pawley fit on the measured data (green), the difference plot (blue), and the Bragg positions (orange).

3.4. Photophysical Characterization of H_2tpdb and Zn(tpdb)(DMF)$_3$

Following the structural investigation of Zn(tpdb)(DMF)$_3$ and H_2tpdb, the photophysical properties of both compounds were examined. The UV/Vis spectrum of **2** shows an absorption band with a maximum absorption at 516 nm, which is comparable to other common perylene chromophores [32]. In contrast, the absorption properties of the CP are different (cf. Figure 5). The respective UV/Vis spectrum shows additional absorption bands with bathochromic and hypochromic shifts. Therefore, the light absorption improved upon the incorporation of the chromophore into the MOF, thus covering a broader spectral range of the electromagnetic spectrum.

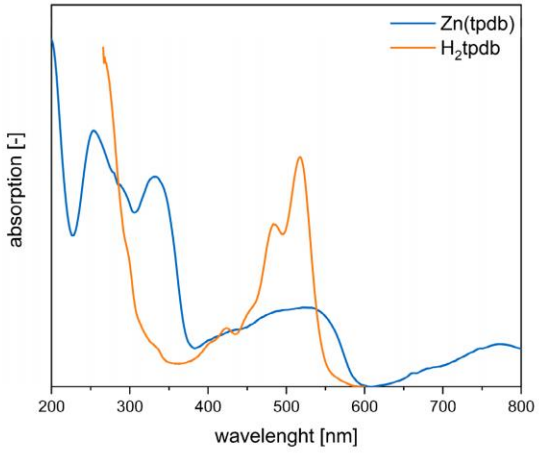

Figure 5. Solid state UV/Vis spectrum of **3** (blue) in comparison to **2** (orange) in the DMF solution. This shows a shift in the spectra of the absorption band of **3**, compared to the absorption band of **2**. Additional to the original absorption band of **2**, **3** shows absorption bands at 760 nm, 260 nm, and 440 nm, which are shifting hypsochromic and bathochromic.

The two mainly discussed aggregation types are the head-to-tail (J-type) and head-to-head (H-type) aggregates (Figure 6) [21].

H-type aggregates promote n-type mobility, which is helpful in electronic devices, while J-type aggregates elevate exciton mobility for optical devices and applications [22]. Furthermore, H-type aggregates are associated with a hypsochromic shift of the bands in the spectrum and J-type aggregates with a bathochromic shift (cf. Figure 6) [23].

Thus, the UV/Vis spectrum of Zn(tpdb)$(DMF)_3$ points towards H-type aggregation behavior, as the absorption band at 516 nm shifts hypsochromic (cf. Figure 5). Furthermore, bathochromic shifting compared to the absorption band of **2** can be observed in the absorption bands of **3**. This shift in the spectrum can be most likely attributed to a charge transfer in the head-to-tail direction of the chromophores (along the crystallographic *c*-axis), since the transition dipole moments of the chromophores are aligned longitudinally to each other (Figure 3f). Additionally, J-type aggregates might be a possible explanation, but are supposed to be unlikely for PDI dyes in extended MOF structures [36,37].

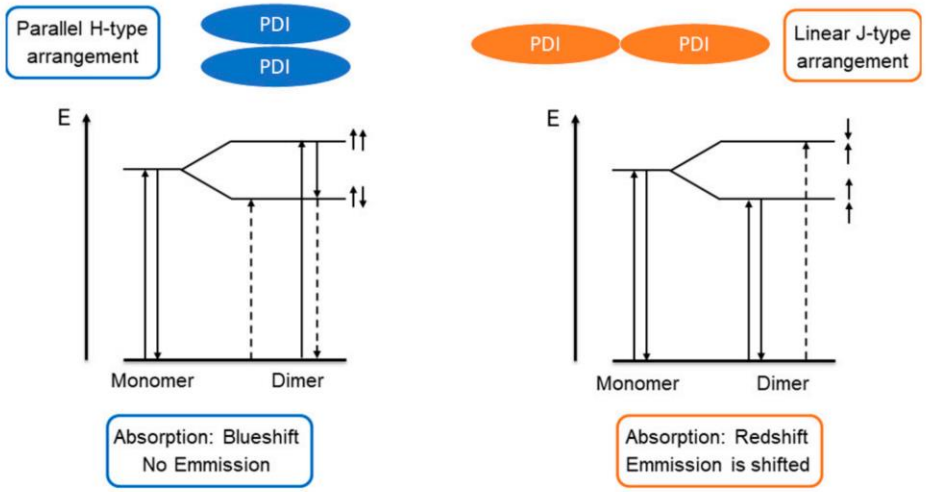

Figure 6. Jablonski diagram of the comparison of the absorption and emission behavior of J- and H-type aggregates [38].

These attributions are supported by an inspection of the emission spectra of **2** and coordination polymer **3** (Figure S4). The CP shows a low-emission intensity when compared to **2**, which can be explained by the high contribution of H-type aggregates, as observed in the UV/Vis spectrum. In general, H-type aggregates quench the emission of the chromophores and promote radiationless energy decay after an internal conversion to the lowest excited state following *Kasha's rule* (Figure 6) [39]. The remaining emission of **3**, despite the presence of H-type aggregates, might be explained by the defects or emission from the surface of the CP, as in both cases, the H-type aggregation might be disturbed.

3.5. Photosensitization Studies

Since we observed the dominant influence of H-type aggregation in **3** within the photophysical studies, the evolution of singlet oxygen under visible light irradiation was tested as the aggregation behavior was shown to be advantageous, compared to unaggregated chromophores in MOFs in the evolution of $^1O_2$ [40]. This reaction has already been reported for different kinds of PDI assemblies, for example, polymers and metal–organic polyhedrons [41,42]. It has also been successfully transferred into MOFs [43], and we present the first example of a PDI linker-based CP within this application.

The activity of the photosensitizer is monitored with 1,3-diphenylisobenzofurane (DBPF), as it is a known $^1O_2$-trapping agent and the reaction can be monitored via UV/Vis spectroscopy following the decrease in the absorption intensity of the aromatic band of DBPF at 416 nm (Figure 7) [44].

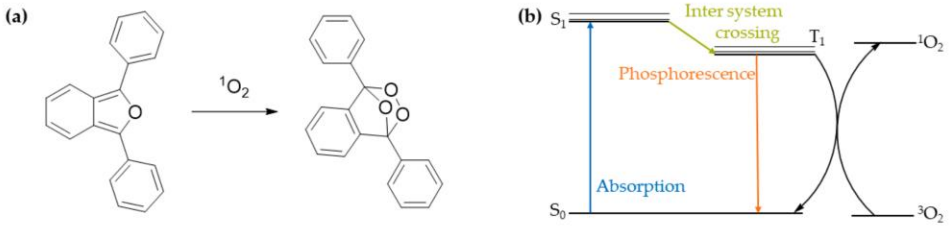

Figure 7. Schematic representation of the photosensitized oxygen activation process applied in this work: (**a**) reaction of $^1O_2$ with 1,3-Diphenylisobenzofuran (DBPF) to obtain the peroxide bridged UV/Vis inactive species. (**b**) Jablonski diagram of the excitation from the $^3O_2$-to-$^1O_2$ trough inter-system crossing enhanced by H-type aggregates adapted from [45].

First, **2** was studied to observe if the chromophore shows any activity. Using a 1:1 molar ratio of linker DBPF in MeCN under argon, an oxygen atmosphere was applied after measuring the first data point, and, subsequently, further data points were recorded after fixed time intervals. Then, **2** was observed to show a high activity towards singlet-oxygen generation, as can be observed in the UV/Vis spectrum (Figure 8a and Figure S5). After six minutes, DBPF is completely consumed by $^1O_2$ generated by the dispersed linker in MeCN. To check if this activity is retained in the coordination polymer, the performance of **3** was tested using the same conditions described for **2**. To our delight, we were able to observe that **3** also successfully generates $^1O_2$ upon light irradiation, as the absorption band of DBPF completely seizes (Figure 8b). We checked that **3** was still stable after the reaction and it remained in a crystalline state (Figure S10). Additionally, control experiments were carried out to test the stability of DBPF under light irradiation and in the presence of **3** without light. These show the stability of DBPF under the chosen conditions (Figure 8a, Figures S7 and S8). In direct comparison, the photosensitization process using **3** is approximately three times slower compared to the **2** (Figure 8a), potentially caused by diffusion limitations within the dispersed CP particles. This is in accordance with previous studies, which also compared the homogenous catalysis of PDI chromophores to a heterogenous catalyst incorporating the same PDIs, showing a decreased $^1O_2$-evolution activity upon incorporation [42]. This is also consistent with several other studies, which show that the use of solid materials decelerates the $^1O_2$ exciation [46]. However, to the best of our knowledge, this is the first example of a PDI-based CP being successfully used as a photosensitizer for singlet-oxygen generation. In general, the incorporation into CPs or MOFs offers key advantages towards future material development, including the modulation of chromophore alignment and material porosity, to specifically address the aggregation and potential diffusion limitations.

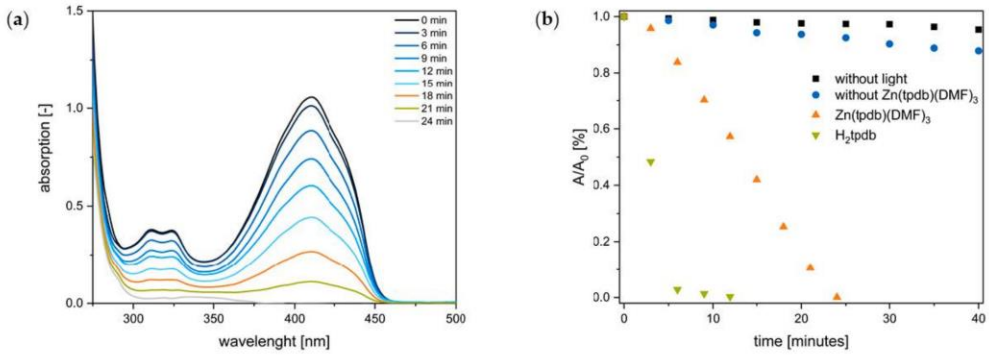

Figure 8. UV/Vis spectroscopic data monitoring the photosensitized $^1O_2$ evolution using linker **2** and CP **3**: (**a**) stacked UV/Vis spectra of 1,3-diphenylisobenzofurane (DBPF) showing the decrease in absorption over time for the reaction with the **3** used as a photosensitizer with a 512 nm LED. (**b**) Decrease in the absorption maxima of DBPF at 416 nm measured from the share of starting absorption at t = 0 min. The decrease in the absorption of DBPF with **3** and linker **2** under light irradiation are presented. In comparison, the control experiments of the DBPF solution with only **3** (black) or only light irradiated (blue) are shown over the duration of 40 min. (**a**) Stacked UV/Vis spectra of DBPF showing the decrease in absorption over time for the reaction with **3** used as a photosensitizer.

4. Conclusions

We synthesized and structurally characterized a new 2D-coordination polymer Zn(tpdb)$(DMF)_3$ **3** based on a PDI-based ditopic linker H_2tpdb **2**. The photophysical properties of the linker and the CP were investigated, revealing a low quantum yield of the luminescence of the CP compared to that of the linker, most likely being caused by H-type aggregation associated with radiationless energy decay within the CP. However, the CP shows desirable absorption properties, since the material covers a broad range of the electromagnetic spectrum desired in mimicking the photosynthesis. Therefore, both the linker and CP were investigated concerning their activity in the photosensitized $^1O_2$ evolution, which is known to be promoted by the aggregation of chromophores. Ultimately, the linker shows activity, which can be retained upon its incorporation into the PDI-based CP, although it is slowed down by a factor of approximately three. Nevertheless, to the best of our knowledge, this is the first example of a PDI-based CP successfully employed for singlet-oxygen generation.

Supplementary Materials: The following supporting information can be downloaded at: https://www.mdpi.com/article/10.3390/en15072437/s1, Figure S1: Thermal gravimetric analysis of Zn(tpdb) from 25 °C to 800 °C with a rate of 10 K min^{-1}. The weight loss of 10% starting at 150 °C indicates the loss of weight the in the structure included water. The subsequent weight loss of 5% starting at 300 °C corresponds to the stored DMF in the structure. The CP structure is then stable until 400 °C. At this temperature, the CP starts to decompose. Figure S2: ^{1}H-NMR of 1,6,7,12-tetrachloro-perylene-3,4,9,10-tetracarboxylic anhydride (1) in $CDCl_3$ showing a single singulett, according to the H atoms in the bay area of the perylene. Figure S3: ^{1}H-NMR of 1,6,7,12-tetrachloroperylenediimide-N,N′-di-benzoic acid (2) in DMSO-d6 showing a singlet at 13.2 ppm for the carboxylic acid groups and an additional singlet at 8.64 ppm for the H atoms in the bay area of the perylene. Additionally, two multipletts can be observed, accounting for the aromatic H atoms of the benzoic acid at 8.15 ppm and 7.59 ppm. Figure S4: Comparison of the emission behavior of 2 and 3. The linker shows a much stronger emission than the CP (compare QY(H_2tpbd) = 0.9 vs. QY(Zn(tpbd)) = < 0.01), suggesting H-type aggregated perylenes, which show a high n-type mobility and quenching of the absorbed light energy, not allowing for directed energy transfer. Figure S5: UV/Vis of the decrease in absorption intensity of DBPF during the reaction with $^1O_2$ produced by linker 2. Figure S6: Control experiment of DBPF

with CP 3 and without light irradiation over the duration of 40 min. Figure S7: Control experiment of DBPF without CP 3 and with light irradiation over the duration of 40 min. Figure S8: BET data of $Zn(tpdb)(DMF)_3$ showing the low surface area of it because of missing pores and the layer structure of the 2D coordination polymer. (a) Semi-log plot of the nitrogen isotherm at 77 K of $Zn(tpdb)(DMF)_3$. (b) BET plot with linear-fit control parameters and calculated monolayer capacity (Q_m). Figure S9: IR data of (a) linker 2 and (b) CP 3. Figure S10: PXRD of the CP after catalysis.

Author Contributions: Conceptualization and writing—original draft preparation, S.N.D., S.J.W., methodology, S.N.D, S.J.W., and A.P., writing—review and editing, A.P. and R.A.F., project administration, R.A.F. All authors have read and agreed to the published version of the manuscript.

Funding: This research was funded by the German Research Foundation (DFG) [EXC 2089] and the Priority Programme COORNETs [SPP 1928].

Acknowledgments: The TUM is greatly acknowledged for institutional funding. S.D. and S.J.W. thank the TUM Graduate School for financial support.

Conflicts of Interest: The authors declare no conflict of interest.

References

1. Barnett, T.P.; Pierce, D.W.; Schnur, R. Detection of Anthropogenic Climate Change in the World's Oceans. *Science* **2001**, *292*, 270–274. [CrossRef] [PubMed]
2. Janna Olmos, J.D.; Kargul, J. A quest for the artificial leaf. *Int. J. Biochem. Cell Biol.* **2015**, *66*, 37–44. [CrossRef] [PubMed]
3. Whittingham, C.P. The chemical mechanism of photosynthesis. *Bot. Rev.* **1952**, *18*, 245–290. [CrossRef]
4. Michl, J. Towards an artificial leaf? *Nat. Chem.* **2011**, *3*, 268–269. [CrossRef]
5. Nocera, D.G. The Artificial Leaf. *Acc. Chem. Res.* **2012**, *45*, 767–776. [CrossRef]
6. Li, H.; Eddaoudi, M.; O'Keeffe, M.; Yaghi, O.M. Design and synthesis of an exceptionally stable and highly porous metalorganic framework. *Nature* **1999**, *402*, 276–279. [CrossRef]
7. Dhakshinamoorthy, A.; Asiri, A.M.; García, H. Metal–Organic Framework (MOF) Compounds: Photocatalysts for Redox Reactions and Solar Fuel Production. *Angew. Chem. Int. Ed.* **2016**, *55*, 5414–5445. [CrossRef]
8. Medishetty, R.; Nemec, L.; Nalla, V.; Henke, S.; Samoć, M.; Reuter, K.; Fischer, R.A. Multi-Photon Absorption in Metal–Organic Frameworks. *Angew. Chem. Int. Ed.* **2017**, *56*, 14743–14748. [CrossRef]
9. Zhu, J.; Shaikh, S.; Mayhall, N.; Morris, A. Energy Transfer in Metal-Organic Frameworks. In *Elaboration and Applications of Metal-Organic Frameworks*; World Scientific: Singapore, 2018; Volume 2, pp. 581–654.
10. Lephalala, M.; Kanchi, S.; Sabela, M.I.; Bisetty, K. Electrochemical Enzymatic Biosensing of Neotame Supported by Computational Methods. *Electroanalysis* **2020**, *32*, 2669–2680. [CrossRef]
11. Sajjadi, S.; Khataee, A.; Bagheri, N.; Kobya, M.; Şenocak, A.; Demirbas, E.; Karaoğlu, A.G. Degradation of diazinon pesticide using catalyzed persulfate with Fe_3O_4@MOF-2 nanocomposite under ultrasound irradiation. *J. Ind. Eng. Chem.* **2019**, *77*, 280–290. [CrossRef]
12. Şenocak, A.; Khataee, A.; Demirbas, E.; Doustkhah, E. Ultrasensitive detection of rutin antioxidant through a magnetic micro-mesoporous graphitized carbon wrapped Co nanoarchitecture. *Sens. Actuators B Chem.* **2020**, *312*, 127939. [CrossRef]
13. Şenocak, A.; Tümay, S.O.; Ömeroğlu, İ.; Şanko, V. Crosslinker polycarbazole supported magnetite MOF@CNT hybrid material for synergetic and selective voltammetric determination of adenine and guanine. *J. Electroanal. Chem.* **2022**, *905*, 115963. [CrossRef]
14. Kent, C.A.; Mehl, B.P.; Ma, L.; Papanikolas, J.M.; Meyer, T.J.; Lin, W. Energy Transfer Dynamics in Metal−Organic Frameworks. *J. Am. Chem. Soc.* **2010**, *132*, 12767–12769. [CrossRef]
15. Würthner, F. Perylene bisimide dyes as versatile building blocks for functional supramolecular architectures. *Chem. Commun.* **2004**, 1564–1579. [CrossRef] [PubMed]
16. Troeger, A.; Ledendecker, M.; Margraf, J.T.; Sgobba, V.; Guldi, D.M.; Vieweg, B.F.; Spiecker, E.; Suraru, S.-L.; Würthner, F. p-Doped Multiwall Carbon Nanotube/Perylene Diimide Derivative Photoelectrochemical Cells for Photocurrent Generation. *Adv. Energy Mater.* **2012**, *2*, 536–540. [CrossRef]
17. Zhao, F.-J.; Zhang, G.; Ju, Z.; Tan, Y.-X.; Yuan, D. The Combination of Charge and Energy Transfer Processes in MOFs for Efficient Photocatalytic Oxidative Coupling of Amines. *Inorg. Chem.* **2020**, *59*, 3297–3303. [CrossRef] [PubMed]
18. Almuhana, A.R.Y.; Langer, P.; Griffin, S.L.; Lodge, R.W.; Rance, G.A.; Champness, N.R. Retention of perylene diimide optical properties in solid-state materials through tethering to nanodiamonds. *J. Mater. Chem. C* **2021**, *9*, 10317–10323. [CrossRef]
19. Haddow, S.L.; Ring, D.J.; Bagha, H.; Pearce, N.; Nowell, H.; Blake, A.J.; Lewis, W.; McMaster, J.; Champness, N.R. Perylene Diimide Triple Helix Formation in the Solid State. *Cryst. Growth Des.* **2018**, *18*, 802–807. [CrossRef]
20. Weissman, H.; Shirman, E.; Ben-Moshe, T.; Cohen, R.; Leitus, G.; Shimon, L.J.W.; Rybtchinski, B. Palladium Complexes of Perylene Diimides: Strong Fluorescence Despite Direct Attachment of Late Transition Metals to Organic Dyes. *Inorg. Chem.* **2007**, *46*, 4790–4792. [CrossRef]

21. Dinçalp, H.; Kızılok, Ş.; İçli, S. Fluorescent macromolecular perylene diimides containing pyrene or indole units in bay positions. *Dye. Pigment.* **2010**, *86*, 32–41. [CrossRef]
22. DeRosa, M.C.; Crutchley, R.J. Photosensitized singlet oxygen and its applications. *Coord. Chem. Rev.* **2002**, *233-234*, 351–371. [CrossRef]
23. Tanaka, F.; Tsumura, K.; Furuta, T.; Iwamoto, K.; Okamoto, M. Efficiencies of singlet oxygen production and rate constants for oxygen quenching in the S1 state of dicyanonaphthalenes and related compounds. *Photochem. Photobiol. Sci.* **2008**, *7*, 56–62. [CrossRef] [PubMed]
24. Pibiri, I.; Buscemi, S.; Palumbo Piccionello, A.; Pace, A. Photochemically Produced Singlet Oxygen: Applications and Perspectives. *ChemPhotoChem* **2018**, *2*, 535–547. [CrossRef]
25. Chen, J.; Keltner, L.; Christophersen, J.; Zheng, F.; Krouse, M.; Singhal, A.; Wang, S.-s. New Technology for Deep Light Distribution in Tissue for Phototherapy. *Cancer J.* **2002**, 8. [CrossRef] [PubMed]
26. Wang, J.; Zhang, X.; Liu, Y.; Wang, Z.; Wang, P.; Zheng, Z.; Cheng, H.; Dai, Y.; Huang, B. Enhanced singlet oxygen production over a photocatalytic stable metal organic framework composed of porphyrin and Ag. *J. Colloid Interface Sci.* **2021**, *602*, 300–306. [CrossRef]
27. Ling, P.; Cheng, S.; Chen, N.; Gao, F. Singlet-oxygen generated by a metal–organic framework for electrochemical biosensing. *J. Mater. Chem. B* **2021**, *9*, 4670–4677. [CrossRef] [PubMed]
28. Park, J.; Jiang, Q.; Feng, D.; Zhou, H.-C. Controlled Generation of Singlet Oxygen in Living Cells with Tunable Ratios of the Photochromic Switch in Metal–Organic Frameworks. *Angew. Chem. Int. Ed.* **2016**, *55*, 7188–7193. [CrossRef]
29. Nelson, A.P.; Farha, O.K.; Mulfort, K.L.; Hupp, J.T. Supercritical Processing as a Route to High Internal Surface Areas and Permanent Microporosity in Metal−Organic Framework Materials. *J. Am. Chem. Soc.* **2009**, *131*, 458–460. [CrossRef]
30. Yoshinaga, K.; Swager, T.M. Fluorofluorescent perylene bisimides. *Synlett* **2018**, *29*, 2509–2514.
31. Addicott, C.; Oesterling, I.; Yamamoto, T.; Müllen, K.; Stang, P.J. Synthesis of a Bis(pyridyl)-Substituted Perylene Diimide Ligand and Incorporation into a Supramolecular Rhomboid and Rectangle via Coordination Driven Self-Assembly. *J. Org. Chem.* **2005**, *70*, 797–801. [CrossRef]
32. Würthner, F.; Saha-Möller, C.R.; Fimmel, B.; Ogi, S.; Leowanawat, P.; Schmidt, D. Perylene Bisimide Dye Assemblies as Archetype Functional Supramolecular Materials. *Chem. Rev.* **2016**, *116*, 962–1052. [CrossRef]
33. Eddaoudi, M.; Kim, J.; Rosi, N.; Vodak, D.; Wachter, J.; O'Keeffe, M.; Yaghi, O.M. Systematic Design of Pore Size and Functionality in Isoreticular MOFs and Their Application in Methane Storage. *Science* **2002**, *295*, 469–472. [CrossRef]
34. Lv, R.; Li, H.; Su, J.; Fu, X.; Yang, B.; Gu, W.; Liu, X. Zinc Metal–Organic Framework for Selective Detection and Differentiation of Fe(III) and Cr(VI) Ions in Aqueous Solution. *Inorg. Chem.* **2017**, *56*, 12348–12356. [CrossRef] [PubMed]
35. Basu, U.; Otto, S.; Heinze, K.; Gasser, G. Biological Evaluation of the NIR-Emissive Ruby Analogue [Cr(ddpd)2][BF4]3 as a Photodynamic Therapy Photosensitizer. *Eur. J. Inorg. Chem.* **2019**, *2019*, 37–41. [CrossRef]
36. Eder, T.; Stangl, T.; Gmelch, M.; Remmerssen, K.; Laux, D.; Höger, S.; Lupton, J.M.; Vogelsang, J. Switching between H- and J-type electronic coupling in single conjugated polymer aggregates. *Nat. Commun.* **2017**, *8*, 1641. [CrossRef] [PubMed]
37. McCarthy, B.D.; Hontz, E.R.; Yost, S.R.; Van Voorhis, T.; Dincă, M. Charge Transfer or J-Coupling? Assignment of an Unexpected Red-Shifted Absorption Band in a Naphthalenediimide-Based Metal–Organic Framework. *J. Phys. Chem. Lett.* **2013**, *4*, 453–458. [CrossRef]
38. Herbst, S.; Soberats, B.; Leowanawat, P.; Stolte, M.; Lehmann, M.; Würthner, F. Self-assembly of multi-stranded perylene dye J-aggregates in columnar liquid-crystalline phases. *Nat. Commun.* **2018**, *9*, 2646. [CrossRef]
39. Gierschner, J.; Lüer, L.; Milián-Medina, B.; Oelkrug, D.; Egelhaaf, H.-J. Highly Emissive H-Aggregates or Aggregation-Induced Emission Quenching? The Photophysics of All-Trans para-Distyrylbenzene. *J. Phys. Chem. Lett.* **2013**, *4*, 2686–2697. [CrossRef]
40. Feng, X.; Wang, X.; Wang, H.; Wu, H.; Liu, Z.; Zhou, W.; Lin, Q.; Jiang, J. Elucidating J-Aggregation Effect in Boosting Singlet-Oxygen Evolution Using Zirconium–Porphyrin Frameworks: A Comprehensive Structural, Catalytic, and Spectroscopic Study. *ACS Appl. Mater. Interfaces* **2019**, *11*, 45118–45125. [CrossRef]
41. He, L.; Cai, L.-X.; Li, M.-H.; Zhang, G.-L.; Zhou, L.-P.; Chen, T.; Lin, M.-J.; Sun, Q.-F. Designing a highly stable coordination-driven metallacycle for imaging-guided photodynamic cancer theranostics. *Chem. Sci.* **2020**, *11*, 7940–7949. [CrossRef]
42. Blacha-Grzechnik, A.; Drewniak, A.; Walczak, K.Z.; Szindler, M.; Ledwon, P. Efficient generation of singlet oxygen by perylene diimide photosensitizers covalently bound to conjugate polymers. *J. Photochem. Photobiol. A Chem.* **2020**, *388*, 112161. [CrossRef]
43. Meng, A.-N.; Chaihu, L.-X.; Chen, H.-H.; Gu, Z.-Y. Ultrahigh adsorption and singlet-oxygen mediated degradation for efficient synergetic removal of bisphenol A by a stable zirconium-porphyrin metal-organic framework. *Sci. Rep.* **2017**, *7*, 6297. [CrossRef] [PubMed]
44. Rossi, L.M.; Silva, P.R.; Vono, L.L.R.; Fernandes, A.U.; Tada, D.B.; Baptista, M.S. Protoporphyrin IX Nanoparticle Carrier: Preparation, Optical Properties, and Singlet Oxygen Generation. *Langmuir* **2008**, *24*, 12534–12538. [CrossRef] [PubMed]
45. Hynek, J.; Chahal, M.K.; Payne, D.T.; Labuta, J.; Hill, J.P. Porous framework materials for singlet oxygen generation. *Coord. Chem. Rev.* **2020**, *425*, 213541. [CrossRef]
46. Wahlen, J.; De Vos, D.E.; Jacobs, P.A.; Alsters, P.L. Solid Materials as Sources for Synthetically Useful Singlet Oxygen. *Adv. Synth. Catal.* **2004**, *346*, 152–164. [CrossRef]

4 Conclusion and Outlook

The research conducted in the context of this PhD-thesis can be divided into two parts, namely chromophore based MPA active coordination polymers and the synthesis of PDI based coordination polymers for photocatalytic applications.

4.1 Chromophore based MPA active coordination polymers

In the first part of this thesis, the successful synthesis and photophysical characterization of the novel dipolar push/pull chromophore dipropyl-9-(4-nitrophenyl)-carbazole-3,6-dicarboxylic acid (H_2CbzNO_2) were demonstrated. Optical studies of the solvated chromophore showed a broad long wavelength absorption with contributions of a TICT transition. This is further underpinned by the fact, that the absorption band is red-shifting with increasing solvent polarity. PL spectroscopy of the solid-state powder reveals an emission band located at 520 nm, which originates from excimer formation.

Additionally, we have synthesized three novel highly MPA active CPs derived from the carbazole containing chromophores 9,9'-stilbene-bis-carbazole-3,6-dicarboxylic acid (H_4sbcd) and the new 2,7-fluorene-9,9'-dimethyl-bis-carbazole-3,6-dicarboxylic acid (H_4fbcd). The structure of the novel CPs (Zn_2(sbcd)$(DMAc)_2(H_2O)_{1.5}$, Sr(fbcd)$(DMAc)_{0.25}(H_2O)_{3.5}$ and Ba(fbcd)$(DMAc)_{2.5}(H_2O)_{1.5}$) was investigated using single-crystal x-ray diffraction revealing that the materials are 2D coordination polymers. Thereby, the zinc-based CP shows a *sql* network topology, whereas the main-group based CPs are showing a 4,8-connecting net. Steady-state spectroscopy of the network exhibits a red-shift of the absorption and the emission bands, which can be attributed to excitonic dipole interactions. Investigation of the MPA properties using the Z-Scan technique showed high two-photon cross sections with $\sigma^{(2)}$ of 10415-33355 GM, which is also one of the highest cross sections ever reported for CPs.

As a perspective, in order to further enhance the MPA efficiency of the CPs, the here presented strong MPA chromophores H_4fbcd and H_4sbcd can be combined with the topological approach recently published by Vittal and co-workers,[106] which will potentially render even higher MPA active coordination polymers.

4.2 Perylene based coordination polymers for photocatalytic applications

In the second part of this thesis, the synthesis and characterization of a new 2D-coordination polymer $Zn(tpbd)(DMF)_3$ based on the PDI linker H_2tpdb were shown. Steady state spectroscopy of the CP was performed revealing a low quantum efficiency compared to the solvated linker, which is based on the H-aggregation formation and therefore quenching the fluorescence. Furthermore, due to the good absorption properties covering a broad range of the electromagnetic spectrum, both the CP and the linker were investigated towards a photosensitization reaction at 512 nm of triplet oxygen to singlet oxygen using 1,3-diphenylisobenzofurane (DBPF) as trapping agent. Thereby, the linker shows a great activity as photosensitizer, which can be retained upon incorporation in the coordination polymer. This is also, to the best of our knowledge, the first example of a PDI based coordination polymers that shows such activity.

In future studies, this photocatalytic activity can be further exploited by either using different substrates to react with the photocatalyst, or by using the generated singlet oxygen for organic synthesis reactions. Furthermore, the synthesized materials can be investigated towards their MPA activity, since perylenes are known for high MPA cross sections.

5 Supporting Information

5.1 Supporting Information for Manuscript I

Supporting Information

For

A Nitrophenyl-Carbazole based Push-Pull Linker as a Building Block for Non-Linear Optical Active Coordination Polymers: A Structural and Photophysical Study

Sebastian J. Weishäupl [1], David C. Mayer [1], Erling Thyrhaug [2], Jürgen Hauer [2], Alexander Pöthig [1], and Roland A. Fischer [1]**

[1] Chair of Inorganic and Metal−Organic Chemistry, Department of Chemistry & Catalysis Research Center, Technical University of Munich, Lichtenbergstraße 4, 85748 Garching, Germany;

[2] Professorship of Dynamic Spectroscopy, Department of Chemistry & Catalysis Research Center, Technical University of Munich, Lichtenbergstraße 4, 85748 Garching, Germany; e-mail@e-mail.com

* Correspondence: roland.fischer@tum.de (RAF)

Table of contents

1 NMR spectroscopy

1.1 Dipropyl-9-(4-nitrophenyl)-carbazole-3,6-dicarboxylate (**6**)

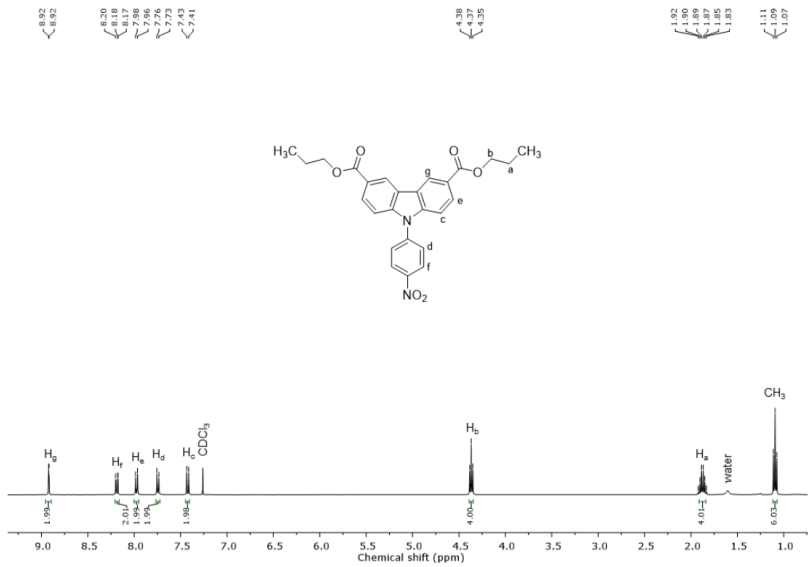

Figure S1: ^{1}H-NMR spectrum of dipropyl-9-(4-nitrophenyl)-carbazole-3,6-dicarboxylate in $CDCl_3$.

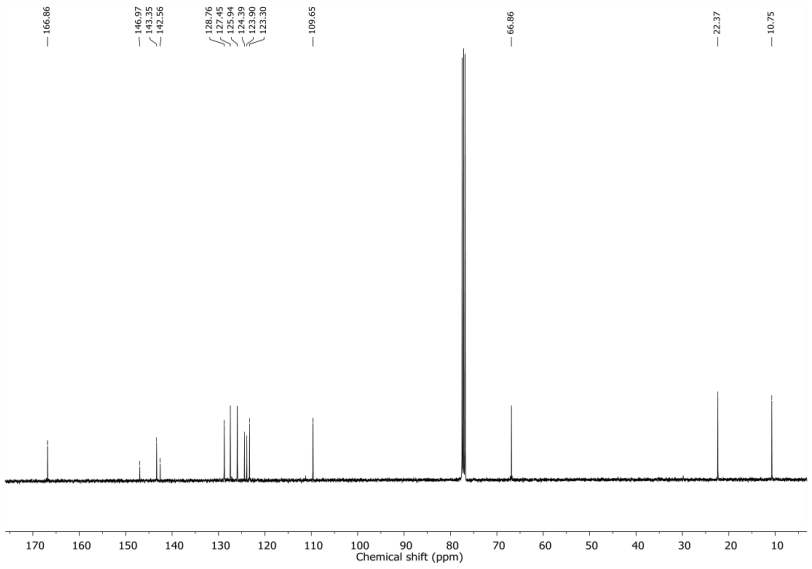

Figure S 2: ^{13}C-NMR of dipropyl-9-(4-nitrophenyl)-carbazole-3,6-dicarboxylate (Pr_2CbzNO_2) in $CDCl_3$.

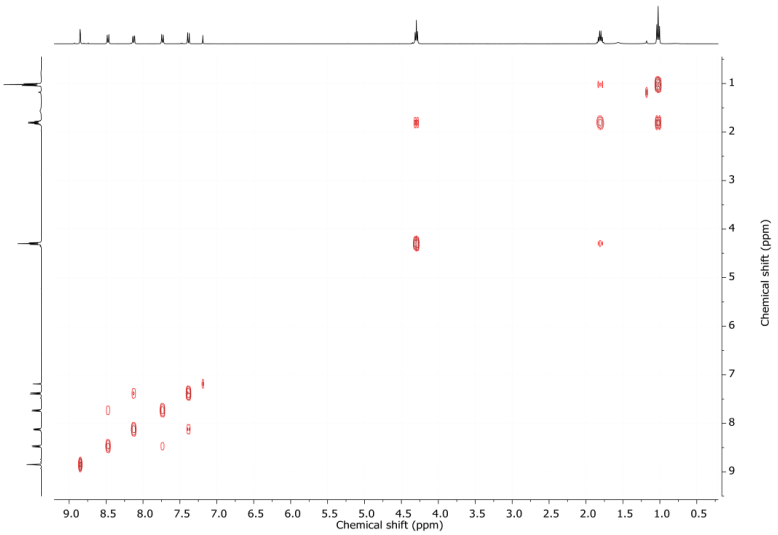

Figure S3: COSY-spectrum of dipropyl-9-(4-nitrophenyl)-carbazole-3,6-dicarboxylate (Pr_2CbzNO_2) in $CDCl_3$.

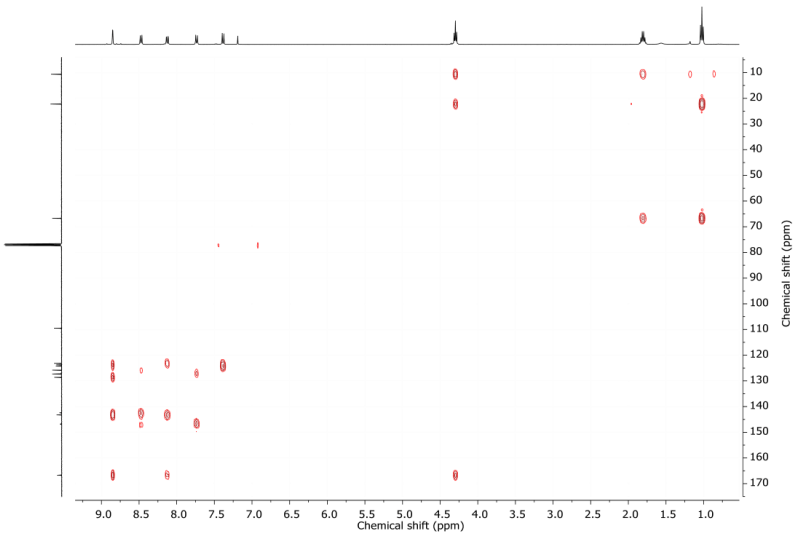

Figure S4: HMBC-spectrum of dipropyl-9-(4-nitrophenyl)-carbazole-3,6-dicarboxylate (Pr_2CbzNO_2) in $CDCl_3$.

1.2 9-(4-nitrophenyl)-carbazole-3,6-dicarboxylic acid (**8**)

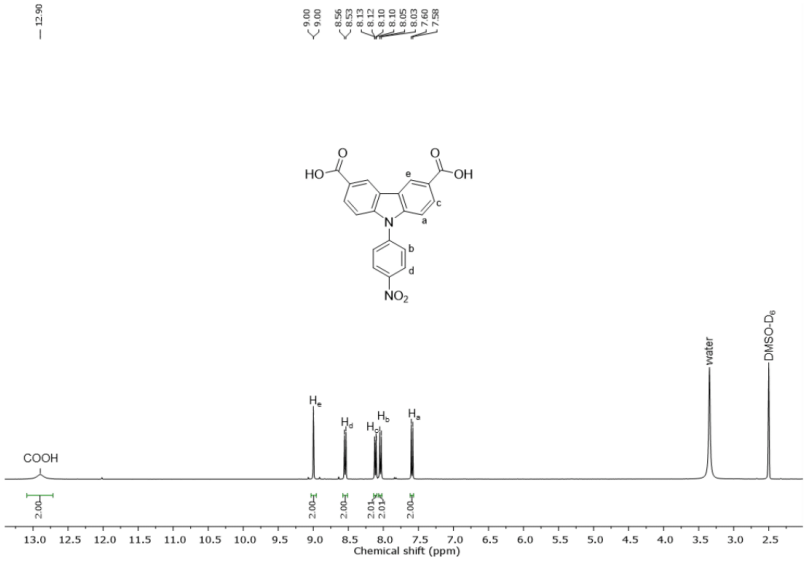

Figure S5: ^{1}H-NMR of 9-(4-nitrophenyl)-carbazole-3,6-dicarboxylic acid in DMSO-d_6.

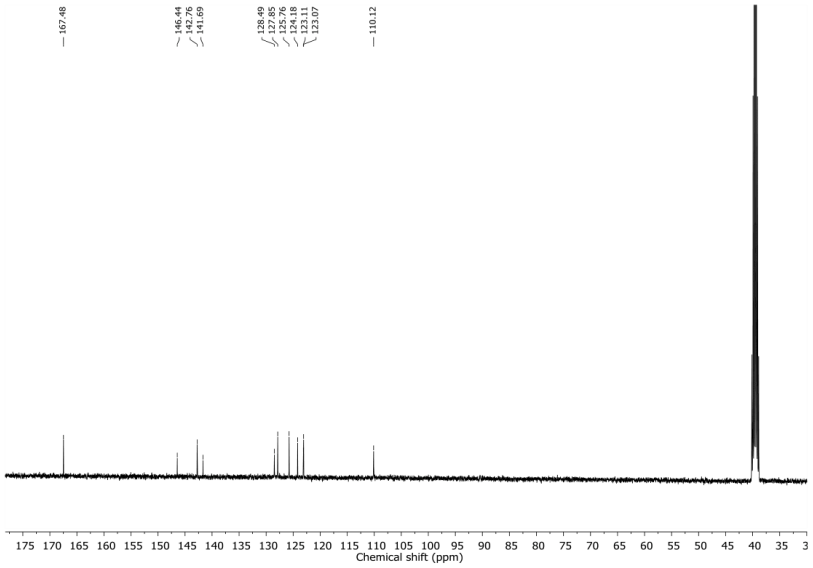

Figure S6: ^{13}C-NMR of 9-(4-nitrophenyl)-carbazole-3,6-dicarboxylic acid (H_2CbzNO_2) in DMSO-d_6.

5

2 Cyclic voltammetry measurements

2.1 Cyclic voltammetry of compound **6**

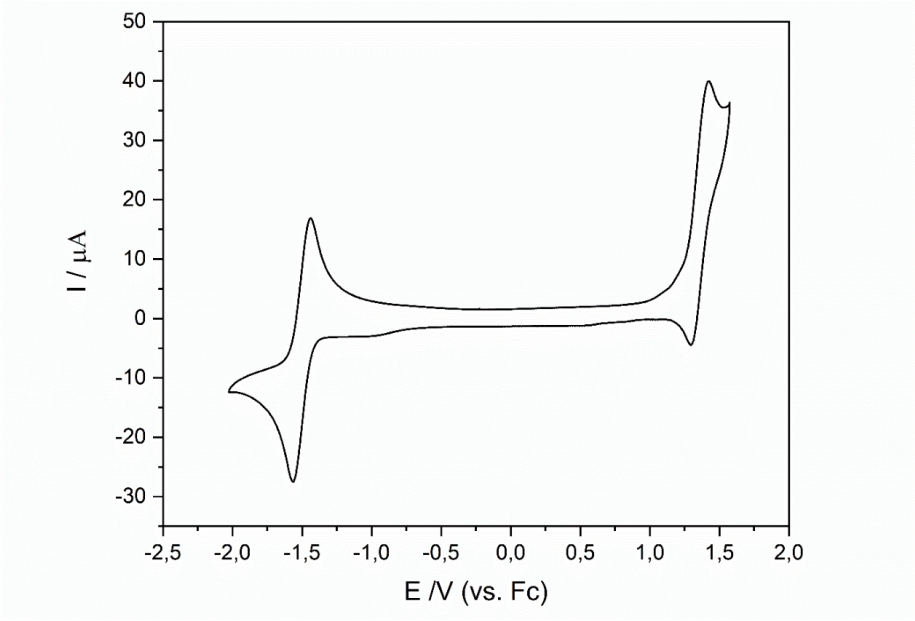

Figure S7: CV of compound **6** (1mM) in DCM using $TBAPF_6$ as electrolyte (0.1M) with a scan rate of 100mV/s. The CV was measured using two glassy carbon electrodes and an $Ag/AgNO_3$-reference.

3 Crystallographic data

Single crystals of the compound were grown by slowly diffusion of a pentane solution to a dichloromethane solution of dipropyl-9-(4-nitrophenyl)-carbazole-3,6-dicarboxylate. The crystals grow as clear, bright-yellow small needles with an approximately size of 10 x 25 x 40 µm. X-ray intensity data of the compound was collected at 100(2)K using a Bruker D8 Venture diffractometer equipped with a Helios optic monochromator, a Photon 100 CMOS detector and a Mo IMS microsource (Mo-K_α radiation). The raw area detector data frames were reduced and corrected for absorption effects using the SAINT and SADABS programs with multi-scan absorption correction. Final unit cell parameters were determined by least-squares refinement of the respective independent reflections taken from the data sets. The structure was solved by intrinsic phasing with SHELXT. Difference Fourier calculations and full-matrix least-squares refinements against F^2 were performed by SHELXL-2014/7 (Sheldrick, 2014). All non-hydrogen atoms were refined with anisotropic displacement parameters. Hydrogen atoms

could not be located in the Fourier maps and were calculated in ideal positions using a riding model (d(C-H) = 0.95 Å, $U_{ISO}(H) = U_{EQ}(C)$). CCDC deposition number: 2032744.

3.1 Crystal structure report of 9-(4-nitrophenyl)-carbazole-3,6-dicarboxylic acid (**7**)

Identification code	WeiSe1 AP8498-100	
Chemical formula	$C_{26}H_{24}N_2O_6$	
Formula weight	460.47	
Temperature	100(2)K	
Wavelength	0.710173 Å	
Crystal size	0.010 x 0.025 x 0.040 mm	
Crystal habit	yellow fragment	
Crystal system	monoclinic	
Space group	P 1 21/c 1	
Unit cell dimensions	a = 16.7529(16) Å	α = 90°
	b = 4.2179(4) Å	β = 94.227(3)°
	c = 31.624(3) Å	γ = 90°
Volume	2228.5(4) Å	
Z	4	
Density (calculated)	1.372 g/cm^3	
Absorption coefficient	0.098 mm^{-1}	
F(0000)	968	
Diffractometer	Bruker D8 Venture Duo IMS	
Theta range for data collection	2.44 to 25.35°	
Index ranges	-20<=h<=20, -5<=k<=5, -38<=I<=38	
Reflections collected	80119	

Independent reflections	4053 [R(int) = 0.0417]
Coverage of independent reflections	99.9%
Absorption correction	Multi-Scan
Refinement method	Full-matrix least-squares on F^2
Refinement program	SHELXL-2014/7 (Sheldrick, 2014)
Function minimized	$\Sigma\, w(F_0^2-F_c^2)^2$
Data / restrains / parameters	4053 / 0 / 403
Goodness-of-fit on F^2	1.076
Δ/σ_{max}	0.001
Final R indices	3538 data; I>2σ(I) R1 = 0.0367, wR2 = 0.0844
	All data R1 = 0.0445, wR2 = 0.0902
Weighting scheme	$w = 1/[\sigma^2(F_0^2)+(0.0352P)^2+1.3271P]$
	where $P = (F_0^2+2F_c^2)/3$
Largest diff. peak and hole	0.0192 and -0.247 eÅ^{-3}
RMS. Deviation from mean	0.040 eÅ^{-3}

3.2 Bond lengths of 9-(4-nitrophenyl)-carbazole-3,6-dicarboxylic acid (**7**)

Table S1: Table of Bond lengths of 9-(4-nitrophenyl)-carbazole-3,6-dicarboxylic acid in the crystal structure.

O1-C19	1.2148(18)	N1-C12	1.3941(18)
N1-C4	1.3948(18)	N1-C13	1.4232(18)
C1-C2	1.393(2)	C1-C6	1.404(2)
C1-C19	1.482(2)	O2-C19	1.3411(18)
O2-C20	1.4638(18)	N2-O5	1.225(2)
N2-O6	1.2262(19)	N2-C16	1.4701(19)
C2-C3	1.393(2)	C2-H3	0.968(16)
O3-C23	1.3435(17)	O3-C24	1.4570(18)
C3-C4	1.4131(19)	C3-C7	1.452(2)
O4-C23	1.2146(17)	C4-C5	1.392(2)
C5-C6	1.377(2)	C5-H2	0.986(16)

C6-H1	0.980(18)	C8-C9	1.394(2)
C8-C7	1.395(2)	C8-H4	0.985(16)
C7-C12	1.4122(19)	C9-C10	1.405(2)
C9-C23	1.480(2)	C10-C11	1.377(2)
C10-H5	0.984(16)	C11-C12	1.389(2)
C11-H6	0.962(16)	C18-C17	1.384(2)
C18-C13	1.391(2)	C18-H7	0.974(17)
C17-C16	1.380(2)	C17-H8	0.941(18)
C16-C15	1.382(2)	C15-C14	1.379(2)
C15-H10	0.950(18)	C14-C13	1.397(2)
C14-H9	0.970(16)	C22-C21	1.520(2)
C22-H17	1.02(3)	C22-H16	1.01(2)
C22-H15	1.00(2)	C21-C20	1.503(2)
C21-H14	1.00(2)	C21-H13	1.002(18)
C20-H11	0.993(19)	C20-H12	1.004(17)
C24-C25	1.503(2)	C24-H23	0.993(19)
C24-H24	0.970(17)	C26-C25	1.517
C26-H18	1.04(2)	C26-H19	1.04(3)
C26-H20	0.99(2)	C25-H22	1.030(17)
C25-H21	1.02(2)		

4 EEMs of dipropyl-9-(4-nitrophenyl)-carbazole-3,6-dicarboxylate (**6**) and dipropyl-9-(4-phenyl)-carbazole-3,6-dicarboxylate (**7**)

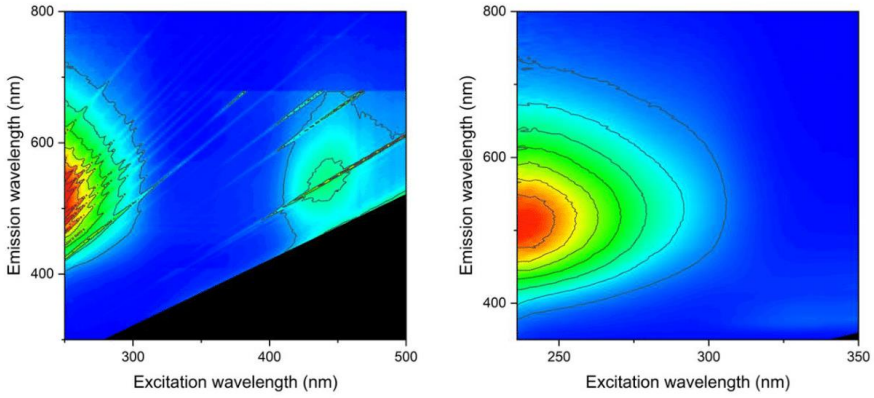

Figure S8: Excitation-emission-matrices (EEM) of **6** (left) and **7** (right) in solid state. Note the different scaling of the x/y axis for clarity reasons.

5 DFT calculations

5.1 *GaussView* representation of dipropyl-9-(4-nitrophenyl)-carbazole-3,6-dicarboxylate (**6**)

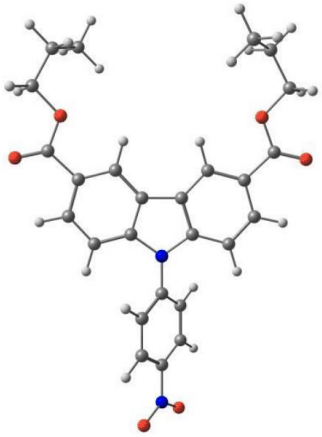

Figure S9: *Gaussview* representation of **6**. Color coding of the atoms: red = oxygen; grey = carbon; white = hydrogen; blue = nitrogen.

5.2 Coordinates and Energies of the *Gaussian09*-calculations of **6**

Atom	X	Y	Z
O	-1.797153000	5.264794000	-0.156326000
H	0.537228000	4.456950000	-0.097216000
N	1.788132000	-0.000054000	-0.000394000
C	-1.031932000	3.014536000	-0.078759000
O	-3.306671000	3.618648000	-0.069957000
H	2.362519000	2.786593000	-0.051986000
N	7.411738000	-0.000076000	0.000218000
C	-1.374909000	1.672661000	-0.046720000
O	-3.306821000	-3.618492000	0.069997000
H	-2.415172000	1.381330000	-0.035437000
C	-0.367934000	0.722344000	-0.027207000
O	-1.797386000	-5.264669000	0.157206000
H	-2.415239000	-1.381222000	0.035680000
C	0.976088000	1.127639000	-0.044912000
O	7.972627000	-0.621804000	0.876497000
H	0.537029000	-4.456969000	0.096957000
C	1.329422000	2.471084000	-0.061917000
O	7.972822000	0.621680000	-0.875917000
H	2.362396000	-2.786693000	0.051122000
C	0.312805000	3.399826000	-0.081557000
C	-1.374984000	-1.672586000	0.046763000
H	5.834514000	1.188300000	-1.767051000
C	-0.367968000	-0.722318000	0.027024000
H	3.346689000	1.173514000	-1.785288000
C	-1.032060000	-3.014476000	0.078787000
H	3.346310000	-1.173667000	1.784844000
C	0.312661000	-3.399834000	0.081295000
H	5.834130000	-1.188480000	1.767109000
C	1.329313000	-2.471140000	0.061366000
H	-4.207722000	5.299684000	0.716864000
C	3.892798000	0.670286000	-1.000205000
H	-6.846999000	-2.674118000	-1.373758000
C	5.272991000	0.678191000	-0.999461000
H	-5.832287000	3.877879000	2.164566000
C	5.942114000	-0.000078000	0.000052000
H	-5.107791000	2.416201000	1.498973000
C	5.272769000	-0.678346000	0.999421000
H	-6.846976000	2.673768000	1.373110000
C	3.892578000	-0.670440000	0.999873000
H	-5.761749000	3.166155000	-0.821166000
C	3.197928000	-0.000069000	-0.000237000
H	-6.465191000	4.620731000	-0.146115000
C	0.976034000	-1.127679000	0.044434000
H	-4.275615000	5.158709000	-1.037796000
C	-2.054322000	4.090059000	-0.106212000
H	-5.832021000	-3.878389000	-2.164652000

C	-2.054495000	-4.089946000	0.106575000
H	-4.207882000	-5.299841000	-0.716127000
C	-5.877280000	3.170051000	1.334702000
H	-6.465378000	-4.620429000	0.146216000
C	-5.677639000	3.878023000	0.003269000
H	-5.762005000	-3.165619000	0.820851000
C	-4.355498000	4.598543000	-0.105939000
H	-5.107806000	-2.416416000	-1.499428000
C	-4.355689000	-4.598309000	0.106338000
H	-4.275931000	-5.158055000	1.038467000
C	-5.877248000	-3.170286000	-1.335035000
C	-5.677793000	-3.877782000	-0.003325000

Sum of electronic and thermal enthalpies = -1565.394954 a.u.

Sum of electronic and thermal free Energies = -1565.492690 a.u.

5.3 Excitation energies and oscillator strengths of compound **6**

Excited State 1:	Singlet-A	3.9855 eV	311.09 nm	f=0.2607	<S**2>=0.000
111 -> 122	-0.28814				
116 -> 122	-0.12101				
121 -> 122	0.59890				
121 -> 126	0.10876				
Excited State 2:	Singlet-A	4.0941 eV	302.84 nm	f=0.0703	<S**2>=0.000
111 -> 122	0.58643				
111 -> 126	-0.14450				
111 -> 127	-0.18367				
121 -> 122	0.29055				
Excited State 3:	Singlet-A	4.4154 eV	280.80 nm	f=0.0034	<S**2>=0.000
120 -> 124	0.34392				
121 -> 123	0.58244				
Excited State 4:	Singlet-A	4.5640 eV	271.66 nm	f=0.0008	<S**2>=0.000
109 -> 122	0.65276				
109 -> 126	-0.15550				
109 -> 127	-0.19140				
Excited State 5:	Singlet-A	4.6186 eV	268.45 nm	f=0.0000	<S**2>=0.000
120 -> 122	0.46999				
120 -> 123	0.36803				

120 -> 126 0.13128

121 -> 124 -0.30026

Excited State 6: Singlet-A 4.6481 eV 266.74 nm f=0.0436 <S**2>=0.000

120 -> 122 0.44039

120 -> 123 -0.25690

120 -> 126 0.15681

121 -> 124 0.43208

Excited State 7: Singlet-A 4.8594 eV 255.14 nm f=0.0061 <S**2>=0.000

115 -> 122 -0.43802

116 -> 125 -0.22050

121 -> 125 0.48096

Excited State 8: Singlet-A 5.0896 eV 243.60 nm f=0.7448 <S**2>=0.000

114 -> 124 0.11110

115 -> 122 -0.11488

119 -> 123 0.14866

120 -> 122 -0.21502

120 -> 123 0.42006

120 -> 126 0.22255

120 -> 127 -0.11775

121 -> 124 0.35401

121 -> 128 0.12883

Excited State 9: Singlet-A 5.2788 eV 234.87 nm f=0.1618 <S**2>=0.000

116 -> 122 -0.16987

120 -> 124 0.45790

121 -> 123 -0.36130

121 -> 126 -0.29426

Excited State 10: Singlet-A 5.3311 eV 232.57 nm f=0.0785 <S**2>=0.000

115 -> 122 0.46393

119 -> 122 -0.10740

121 -> 124 0.13008

121 -> 125 0.47635

Excited State 11: Singlet-A 5.3480 eV 231.83 nm f=0.0018 <S**2>=0.000

117 -> 122 -0.11704

117 -> 123 -0.10573

117 -> 126 -0.37446

117 -> 127 0.16046

117 -> 135 0.11702

118 -> 124 0.48513

118 -> 142 -0.12283

Excited State 12: Singlet-A 5.3507 eV 231.72 nm f=0.0021 <S**2>=0.000

117 -> 124 0.48670

117 -> 142 -0.12310

118 -> 122 -0.11787

118 -> 123 -0.10600

118 -> 126 -0.37639

118 -> 127 0.16147

118 -> 135 0.11763

Excited State 13: Singlet-A 5.4773 eV 226.36 nm f=0.3489 <S**2>=0.000

114 -> 122 0.14415

116 -> 122 0.56946

121 -> 122 0.14671

121 -> 126 -0.24069

121 -> 127 0.14527

Excited State 14: Singlet-A 5.5237 eV 224.46 nm f=0.2746 <S**2>=0.000

116 -> 122 0.21121

119 -> 124 0.14797

120 -> 124 0.36886

120 -> 128 -0.10603

121 -> 123 -0.11975

121 -> 126 0.47458

Excited State 15: Singlet-A 5.5668 eV 222.72 nm f=0.6757 <S**2>=0.000

114 -> 124 0.11363

119 -> 123 0.23458

119 -> 126 -0.11697

120 -> 122 -0.12043

120 -> 123 -0.31226

120 -> 126 0.44430

120 -> 127 -0.10697

121 -> 124 -0.21910

121 -> 128 0.14899

Excited State 16: Singlet-A 5.8831 eV 210.75 nm f=0.0064 <S**2>=0.000

120 -> 125 0.68850

Excited State 17: Singlet-A 5.9014 eV 210.09 nm f=0.0155 <S**2>=0.000

115 -> 122 0.11307

119 -> 122 0.65648

119 -> 126 0.12667

120 -> 126 0.10227

Excited State 18: Singlet-A 6.1712 eV 200.91 nm f=0.0004 <S**2>=0.000

119 -> 123 0.41653

120 -> 126 -0.38380

121 -> 128 0.35876

Excited State 19: Singlet-A 6.2297 eV 199.02 nm f=0.0003 <S**2>=0.000

115 -> 125 0.11508

116 -> 126 -0.12950

116 -> 127 -0.10372

119 -> 124 -0.30653

120 -> 128 0.20216

121 -> 122 -0.12270

121 -> 126 0.20619

121 -> 127 0.46274

Excited State 20: Singlet-A 6.3733 eV 194.54 nm f=0.0189 <S**2>=0.000

110 -> 122 0.57247

115 -> 122 0.14716

115 -> 127 -0.10328

116 -> 125 -0.30701

Excited State 21: Singlet-A 6.4608 eV 191.90 nm f=0.1135 <S**2>=0.000

114 -> 122 -0.10451

114 -> 123 -0.12093

115 -> 125 0.19899

116 -> 127 -0.10108

119 -> 124 0.41672

119 -> 125 -0.11475

120 -> 128 -0.17943

121 -> 126 -0.15449

121 -> 127 0.37616

Excited State 22: Singlet-A 6.5263 eV 189.98 nm f=0.0386 <S**2>=0.000

116 -> 124 0.12643

119 -> 123 0.45515

119 -> 126 0.19618

121 -> 128 -0.43780

Excited State 23: Singlet-A 6.6833 eV 185.51 nm f=0.0769 <S**2>=0.000

112 -> 122 -0.17557

114 -> 122 0.55523

114 -> 126 0.10943

115 -> 125 -0.13434

116 -> 122 -0.19137

119 -> 124 0.22423

Excited State 24: Singlet-A 6.7007 eV 185.03 nm f=0.1429 <S**2>=0.000

110 -> 122 0.38432

114 -> 125 0.10773

115 -> 122 -0.18155

115 -> 126 0.15632

115 -> 127 0.23983

116 -> 125 0.43438

Excited State 25: Singlet-A 6.7814 eV 182.83 nm f=0.5662 <S**2>=0.000

114 -> 122 0.22293

115 -> 125 0.52291

119 -> 124 -0.16096

119 -> 125 -0.14979

120 -> 128 -0.15525

121 -> 127 -0.19305

Excited State 26: Singlet-A 6.8069 eV 182.15 nm f=0.0000 <S**2>=0.000

100 -> 123 0.10097

117 -> 122 -0.16429

117 -> 123 0.63028

118 -> 128 -0.19299

Excited State 27: Singlet-A 6.8243 eV 181.68 nm f=0.0003 <S**2>=0.000
117 -> 128 -0.19224
118 -> 122 -0.21167
118 -> 123 0.62646
Excited State 28: Singlet-A 6.8425 eV 181.20 nm f=0.0006 <S**2>=0.000
117 -> 122 0.66914
117 -> 123 0.14293
Excited State 29: Singlet-A 6.8518 eV 180.95 nm f=0.0001 <S**2>=0.000
118 -> 122 0.65734
118 -> 123 0.18642
Excited State 30: Singlet-A 6.8775 eV 180.27 nm f=0.0152 <S**2>=0.000
113 -> 124 0.10844
114 -> 122 -0.12103
114 -> 123 -0.17603
115 -> 125 0.11774
116 -> 123 0.25847
119 -> 124 0.16704
120 -> 128 0.51143
Excited State 31: Singlet-A 6.9207 eV 179.15 nm f=0.0163 <S**2>=0.000
114 -> 124 -0.19892
116 -> 124 0.22168
119 -> 126 0.44868
119 -> 127 -0.10210
121 -> 124 -0.10188
121 -> 128 0.33015
121 -> 130 0.12294
Excited State 32: Singlet-A 7.0063 eV 176.96 nm f=0.0106 <S**2>=0.000
114 -> 124 -0.17546
119 -> 126 -0.11352
120 -> 122 -0.11031
120 -> 126 0.16193
120 -> 127 0.62005
Excited State 33: Singlet-A 7.0353 eV 176.23 nm f=0.0123 <S**2>=0.000
119 -> 126 -0.12534

121 -> 129 -0.20500

121 -> 130 0.58074

121 -> 136 0.24794

Excited State 34: Singlet-A 7.0602 eV 175.61 nm f=0.1014 <S**2>=0.000

114 -> 123 0.15253

115 -> 125 0.21372

116 -> 123 -0.21287

116 -> 127 -0.11206

119 -> 124 0.14784

119 -> 125 0.53362

Excited State 35: Singlet-A 7.1034 eV 174.54 nm f=0.2709 <S**2>=0.000

112 -> 122 0.10157

112 -> 123 0.18489

112 -> 126 0.12737

113 -> 124 -0.21418

114 -> 123 -0.29677

116 -> 123 0.31287

119 -> 125 0.36971

Excited State 36: Singlet-A 7.1698 eV 172.93 nm f=0.0972 <S**2>=0.000

112 -> 124 0.37058

113 -> 122 -0.24427

113 -> 123 -0.15124

113 -> 126 -0.30832

113 -> 127 0.10511

114 -> 124 0.28026

119 -> 126 0.20823

120 -> 127 0.11926

Excited State 37: Singlet-A 7.1818 eV 172.64 nm f=0.0004 <S**2>=0.000

96 -> 122 0.10525

112 -> 122 -0.21432

112 -> 123 -0.12473

112 -> 126 -0.25372

113 -> 124 0.39944

116 -> 123 0.24937

119 -> 124 -0.10124

119 -> 125 0.11703

120 -> 128 -0.21756

Excited State 38: Singlet-A 7.2253 eV 171.60 nm f=0.0060 <S**2>=0.000

95 -> 122 0.20489

96 -> 122 0.47252

98 -> 122 0.15996

101 -> 122 -0.18129

104 -> 122 0.19425

106 -> 122 0.23492

121 -> 127 -0.10948

Excited State 39: Singlet-A 7.2438 eV 171.16 nm f=0.0013 <S**2>=0.000

112 -> 124 -0.31399

113 -> 122 0.10089

114 -> 124 0.40950

116 -> 124 -0.21153

119 -> 126 0.20960

120 -> 127 0.20942

Excited State 40: Singlet-A 7.3214 eV 169.35 nm f=0.0006 <S**2>=0.000

113 -> 124 -0.10811

114 -> 123 0.47166

114 -> 126 0.11285

116 -> 123 0.34562

116 -> 126 -0.22110

119 -> 124 0.13774

Excited State 41: Singlet-A 7.3994 eV 167.56 nm f=0.0053 <S**2>=0.000

121 -> 129 0.59399

121 -> 130 0.19733

121 -> 132 0.23392

121 -> 140 -0.11204

Excited State 42: Singlet-A 7.4106 eV 167.31 nm f=0.0000 <S**2>=0.000

120 -> 129 0.48202

120 -> 130 -0.37798

120 -> 132 0.15838

120 -> 136 -0.25560

Excited State 43: Singlet-A 7.4535 eV 166.34 nm f=0.0005 <S**2>=0.000

111 -> 124 0.12238

111 -> 125 0.67841

Excited State 44: Singlet-A 7.4745 eV 165.88 nm f=0.0186 <S**2>=0.000

103 -> 123 -0.24019

105 -> 123 0.13277

108 -> 123 -0.10903

115 -> 123 0.56371

116 -> 124 0.12272

Excited State 45: Singlet-A 7.4954 eV 165.41 nm f=0.0181 <S**2>=0.000

114 -> 124 0.25789

115 -> 123 -0.11695

115 -> 126 0.11236

116 -> 124 0.52774

116 -> 125 -0.15291

119 -> 126 -0.19799

Excited State 46: Singlet-A 7.5598 eV 164.01 nm f=0.0208 <S**2>=0.000

103 -> 124 -0.14870

112 -> 122 0.15907

114 -> 122 0.12788

114 -> 123 0.13373

115 -> 124 0.19913

116 -> 123 0.15263

116 -> 126 0.41698

116 -> 127 0.13581

119 -> 128 -0.13718

121 -> 135 -0.11549

121 -> 137 0.10292

Excited State 47: Singlet-A 7.5659 eV 163.87 nm f=0.0070 <S**2>=0.000

100 -> 122 -0.10537

100 -> 123 -0.10750

100 -> 126 -0.19511

103 -> 124 0.34443

105 -> 124 -0.20484

108 -> 124 0.23336

114 -> 126 -0.10168

115 -> 124 -0.16841

116 -> 126 0.19935

Excited State 48: Singlet-A 7.5673 eV 163.84 nm f=0.0094 <S**2>=0.000

100 -> 124 -0.25393

103 -> 122 0.16318

103 -> 123 0.22613

103 -> 126 0.17205

105 -> 123 -0.12798

105 -> 126 -0.11137

107 -> 124 -0.11048

108 -> 123 0.12439

108 -> 126 0.11697

115 -> 123 0.31816

115 -> 126 -0.22861

117 -> 124 -0.10443

Excited State 49: Singlet-A 7.6105 eV 162.91 nm f=0.0011 <S**2>=0.000

120 -> 129 0.37937

120 -> 130 0.43703

120 -> 132 0.21724

120 -> 136 0.21015

120 -> 140 -0.10147

Excited State 50: Singlet-A 7.6228 eV 162.65 nm f=0.0971 <S**2>=0.000

103 -> 123 -0.13727

113 -> 122 0.43087

114 -> 124 0.12762

115 -> 126 -0.29342

115 -> 127 -0.26291

116 -> 124 0.13117

116 -> 125 0.18457

5.2 Supporting Information for Manuscript II

Supporting Information

For

Coordination Polymers Based on Carbazole-Derived Chromophore Linkers for Optimized Multiphoton Absorption: A Structural and Photophysical Study

Sebastian J. Weishäupl [1†], Yang Cui [2,3†], Simon Deger [1], Hamad Syed [4], Alexander Pöthig [1], Aleksandr Ovsianikov [4], Jürgen Hauer[2] and Roland A. Fischer [1*]*

[1] Chair of Inorganic and Metal−Organic Chemistry, Department of Chemistry & Catalysis Research Center, Technical University of Munich, Lichtenbergstraße 4, 85748 Garching, Germany;

[2] Professorship for Dynamic Spectroscopy, Technical University of Munich, Lichtenbergstraße 4, 85748 Garching, Germany;

[3] Department of Physics, Technical University of Munich, James-Franck-Straße 1, 85748 Garching, Germany;

[4] 3D Printing and Biofabrication Group, Institute of Materials Science and Technology, Technische Universität Wien (TU Wien), Getreidemarkt 9/308, Vienna 1060, Austria;

[†] These authors contributed equally to this work.

* Correspondence: roland.fischer@tum.de (RAF), alexander.poethig@tum.de (AP), juergen.hauer@tum.de (JH)

1. Synthetic procedures of the carbazole precursor

All reactions were carried out following our 2020 already published synthesis procedure.

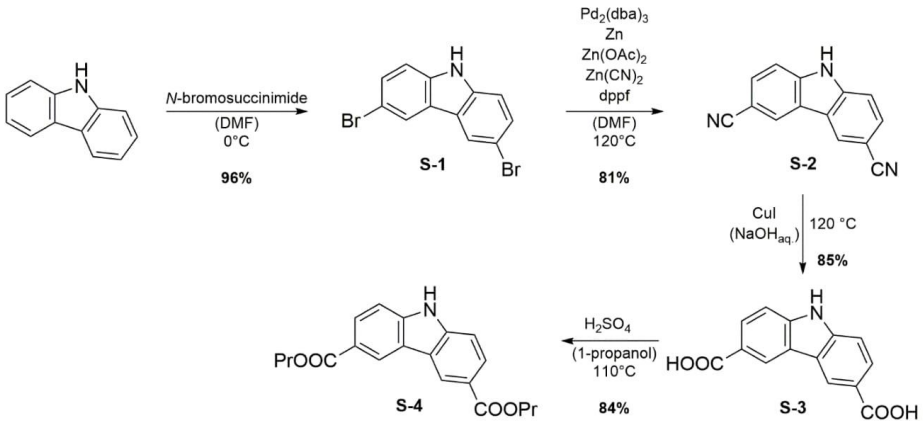

Fig. S1: Synthesis route towards the carbazole precursor.

3,6-Dibromocarbazole (**S-1**): A solution of N-bromosuccinimide (22.35 g, 125 mmol) in 50 mL DMF was slowly added through a syringe pump to a stirring solution of carbazole (10 g, 59.80 mmol) in 20 mL DMF in an ice bath. After 24 hours of reaction time, the mixture was poured into 600 mL ice water and then filtered through a suction filter to give a dark grey powder. The crude product was recrystallized with Ethanol to give a grey powder of 3,6-Dibromocarbazole (18,68 g, 96%). ^{1}H-NMR (400 MHz, 298K, DMSO-d_6) δ (ppm) = 7.47 (d, J = 8.6 Hz, 2H), 7.53 (dd, J = 2.0, 8.6 Hz, 2H), 8.43 (d, J = 1.9, 2H), 11.59 (s, 1H, N-H). ^{13}C-NMR (101 MHz, 298K, DMSO-d_6) δ (ppm) = 110.96, 113.18, 123.35, 123.29, 128.70, 138.78.

Carbazole-3,6-Dicarbonitrile (**S-2**): 3,6-Dibromocarbazole (9.75 g, 30.0 mmol) and dppf (100 mg, 0.18 mmol) were added to a 100 mL Schlenk flask and solved in 30 mL DMF and 0.3 mL water. The suspension was degassed via bubbling argon for 1 hour through the mixture. Subsequently, $Zn(CN)_2$ (4.21 g, 36 mmol), zinc powder (78 mg, 1.2 mmol), $Zn(OAc)_2 \cdot 2\ H_2O$ (0.26 g, 1.2 mmol) and $Pd_2(dba)_3 \cdot$ dba (69.5 mg, 0,06 mmol) were added under a positive pressure of argon. This mixture was heated to 110 °C for 2 days. The

suspension was subsequently cooled and then poured into a 100 mL mixture of $H_2O/NH_4Cl/NH_3$ (5/4/1) and filtered through a suction filter. The filter cake was washed with the same volume of the above mixture, toluene (3 x 30 mL) and MeOH (3 x 30 mL) to give a grey solid. The crude product was recrystallized with DMF to give a white solid (5.2 g, 81%). ^{1}H-NMR (400 MHz, 298K, DMSO-d_6) δ (ppm) = 7.72 (d, J = 8.5 Hz, 2H), 7.85 (d, J = 9.9 Hz, 2H), 8.80 (s, 2H), 12.38 (s, 1H, N-H). ^{13}C-NMR (101 MHz, 298K, DMSO-d_6) δ (ppm) = 101.74, 112.84, 120.10, 121.85, 126.8, 129.93, 142.32.

Carbazole-3,6-dicarboxylic acid (**S-3**): Carbazole-3,6-Dicarbonitrile (4.2 g, 19.3 mmol) was suspended in an aqueous NaOH solution (12.45 g in 150 mL). To this solution CuI (37,5 mg, 0.195 mmol) was added and then quickly heated to 125 °C for 2 days, until the starting material was dissolved. Afterwards active carbon was added, and the mixture was again heated to 125 °C for 2 hours. After cooling, the suspension was filtered through celite, which was pre-washed with aq. NaOH-solution. The filtrate was acidified with 6M HCl-solution to give a white precipitate. The precipitate was filtered, washed with water and then dried to give a withe solid (4.0 g, 85%). ^{1}H-NMR (400 MHz, 298K, $CDCl_3$) δ (ppm) = 7.60 (d, J = 8.5 Hz, 2H), 8.06 (d, J = 8.4 Hz, 2H), 8.85 (s, 2H), 12.04 (s, 1H, N-H), 12.69 (bs, 2H, COOH). ^{13}C-NMR (101 MHz, 298K, DMSO-d6) δ (ppm) = 111.13, 122.00, 122.27, 122.79, 127.65, 143.12, 167.94.

Dipropyl-carbazole-3,6-dicarboxylate (**S-4**): Carbazole-3,6-dicarboxylic acid 4 (4.0 g, 15.64 mmol) was suspended in 100 mL 1-propanol. To this suspension, conc. sulfuric acid (2 mL) was added and then refluxed at 110 °C for 24 hours. After cooling, the suspension was concentrated on a rotary evaporator and extracted with 200 mL dichloromethane. The organic layer was washed with aq. NaHCO3 (150 mL) and then dried with MgSO4. The solvent was evaporated to give a yellowish solid (4.5 g, 84%). ^{1}H NMR (400 MHz, 298K, CDCl3) δ (ppm) = 1.09 (t, J = 7.4 Hz, 6H), 1.87 (h, J = 7.2 Hz, 4H), 4.36 (t, J = 6.7 Hz, 4H), 7.47 (d, J = 8.5 Hz, 2H), 8.18 (dd, J = 1.5 Hz, 2H), 8.86 (s, 2H). ^{13}C-NMR (101 MHz, 298K, $CDCl_3$) δ (ppm) = 10.77, 22.40, 66.67, 110.64, 122.89, 123.19, 128.28, 142.85, 167.35.

2. NMR spectroscopy

2.1 Pr_4sbcd

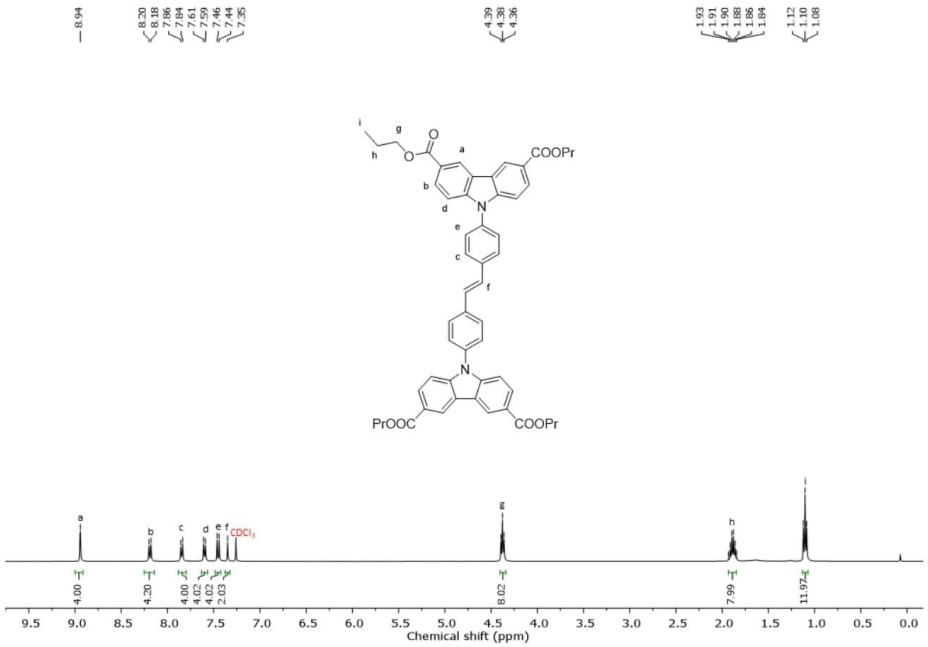

Fig. S2: ^{1}H-NMR of Pr_4sbcd with the respective chemical shifts in $CDCl_3$.

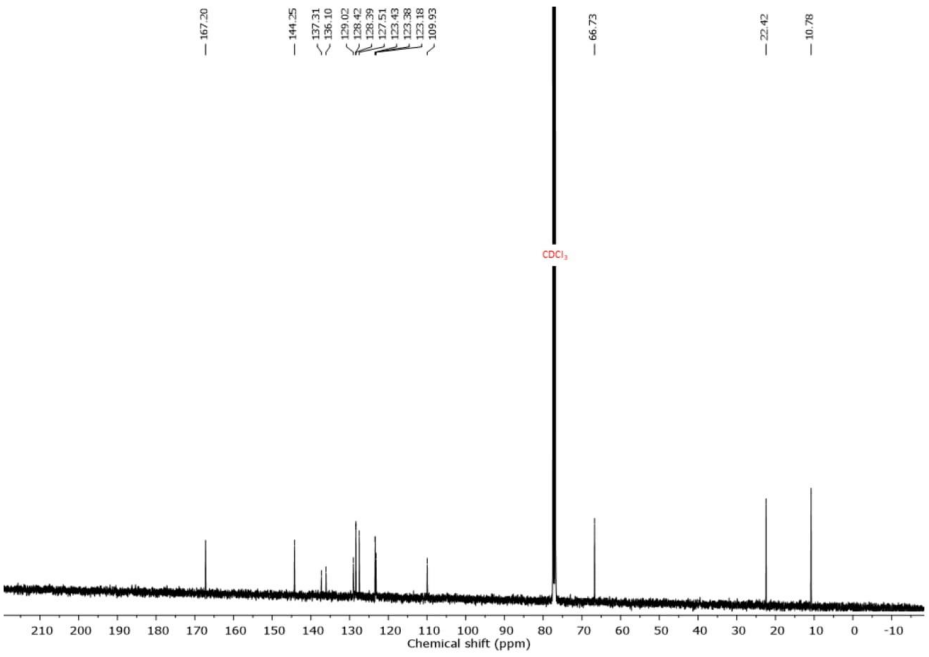

Fig. S3: ^{13}C-NMR of Pr_4sbcd with the respective chemical shifts in $CDCl_3$.

2.2 H_4sbcd

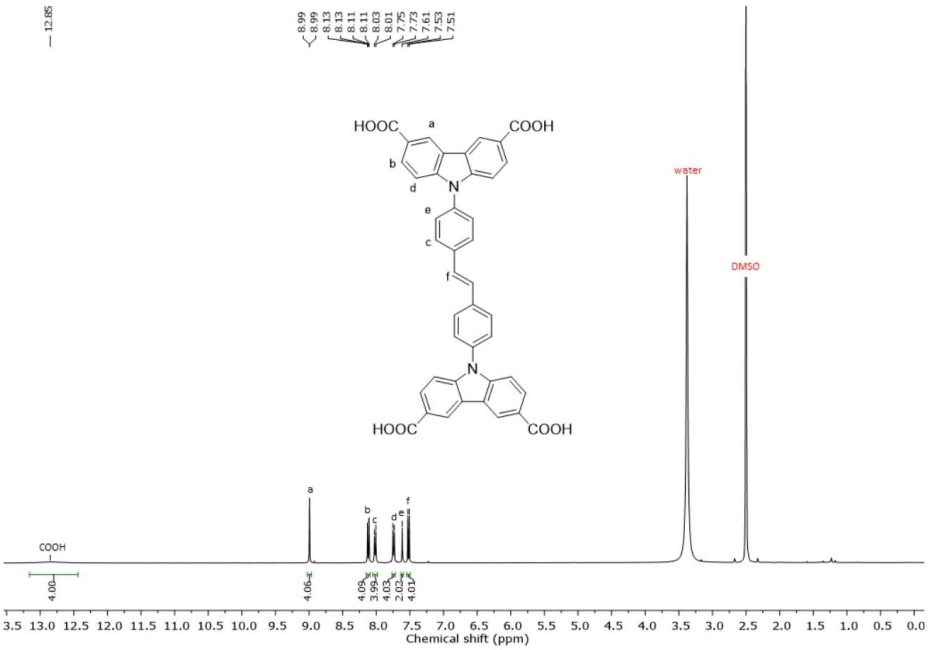

Fig. S4: ^{1}H-NMR of H_4sbcd with the respective chemical shifts in DMSO-d_6.

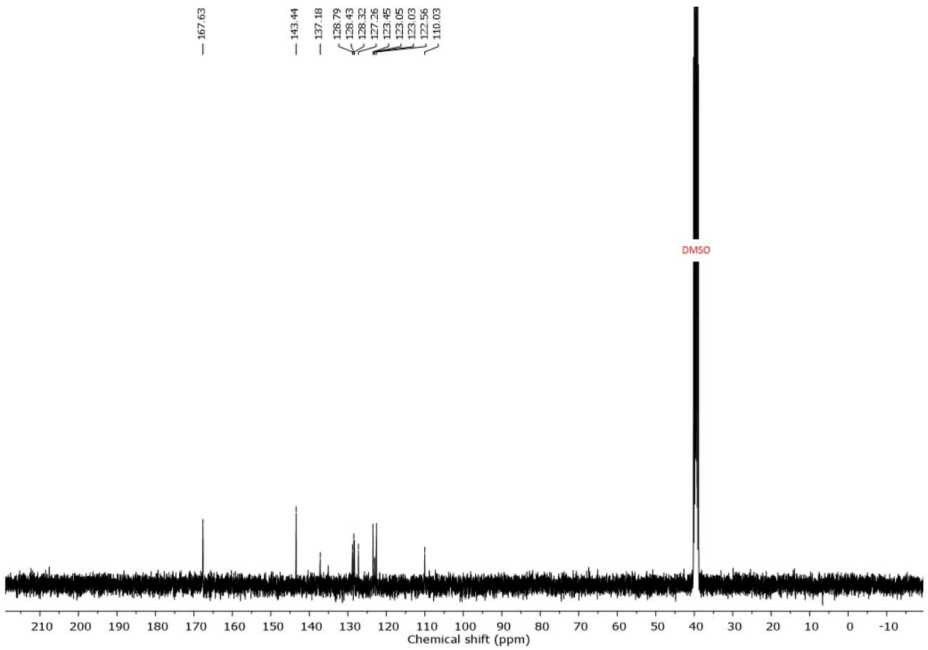

Fig. S5: ^{13}C-NMR of H_4sbcd with the respective chemical shifts in DMSO-d_6.

2.3 Pr_4fbcd

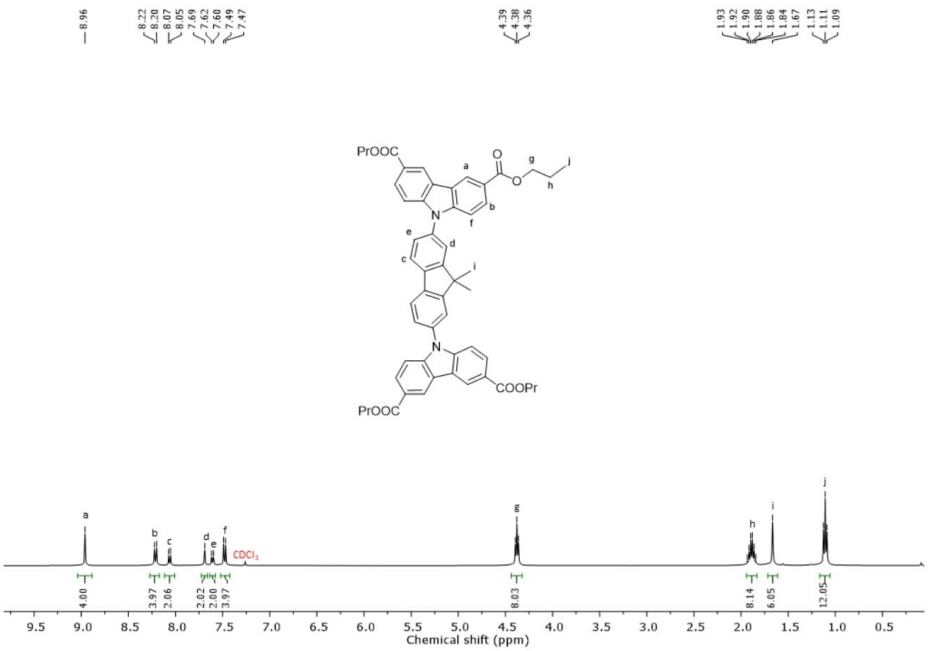

Fig. S6: ^{1}H-NMR of Pr_4fbcd with the respective chemical shifts in $CDCl_3$.

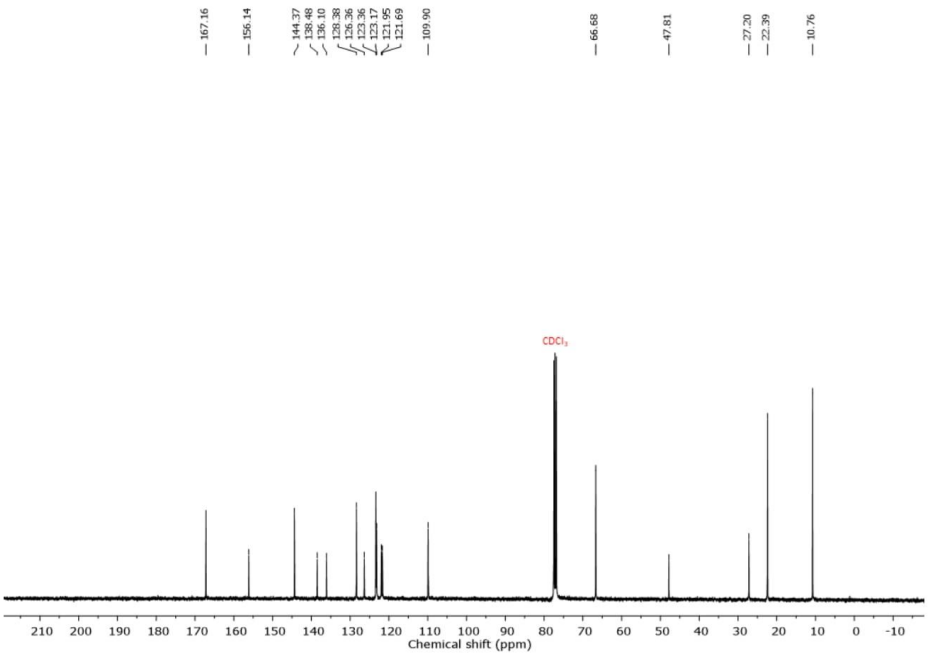

Fig. S7: ^{13}C-NMR of Pr_4fbcd with the respective chemical shifts in $CDCl_3$.

2.4 H_4fbcd

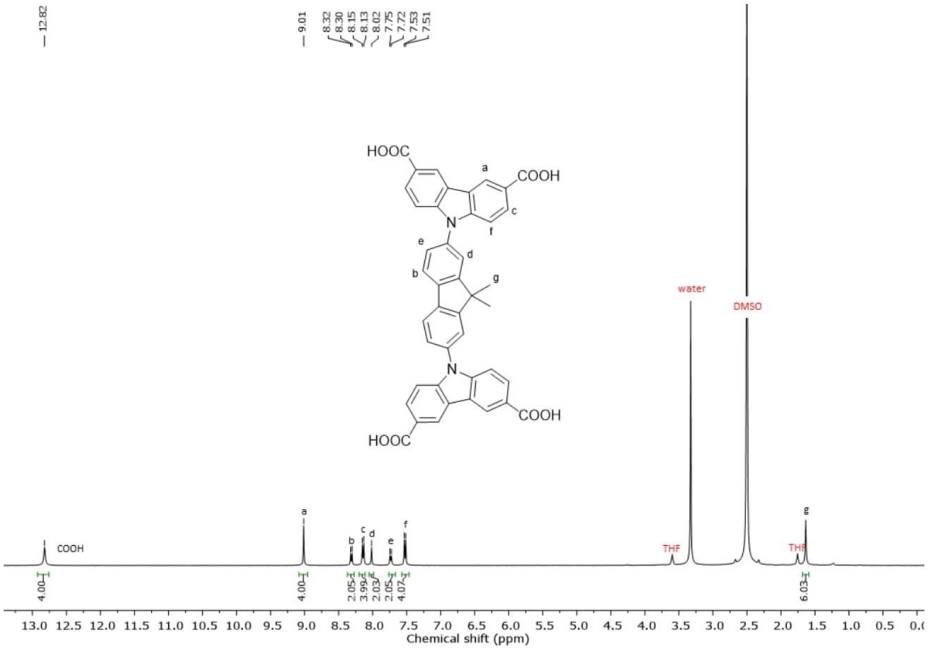

Fig. S8: ^{1}H-NMR of H_4fbcd with the respective chemical shifts in DMSO-d_6.

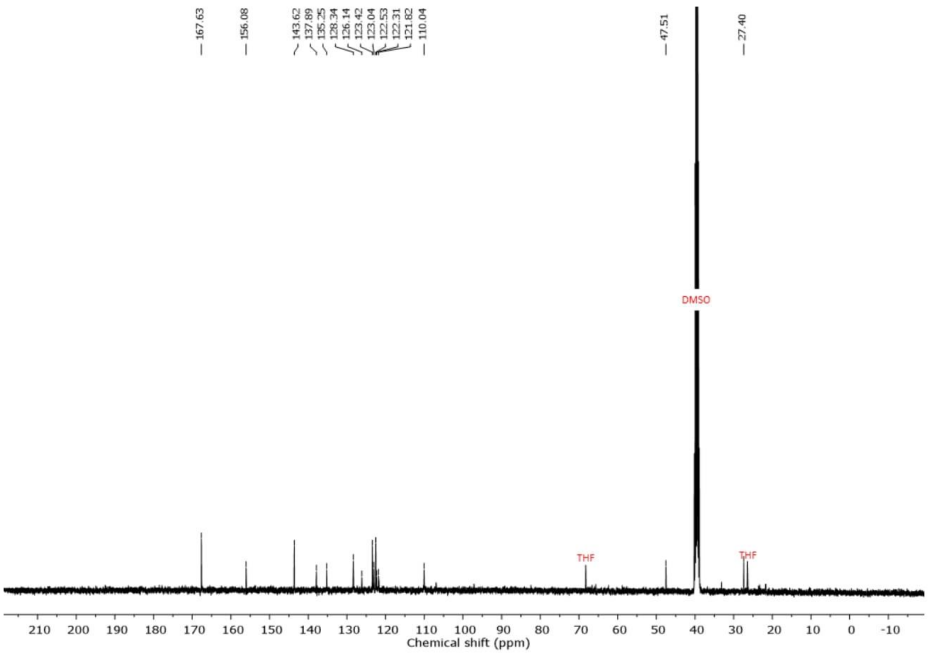

Fig. S9: ^{13}C-NMR of H_4fbcd with the respective chemical shifts in DMSO-d_6.

3. IR analysis of the coordination polymers and their linkers

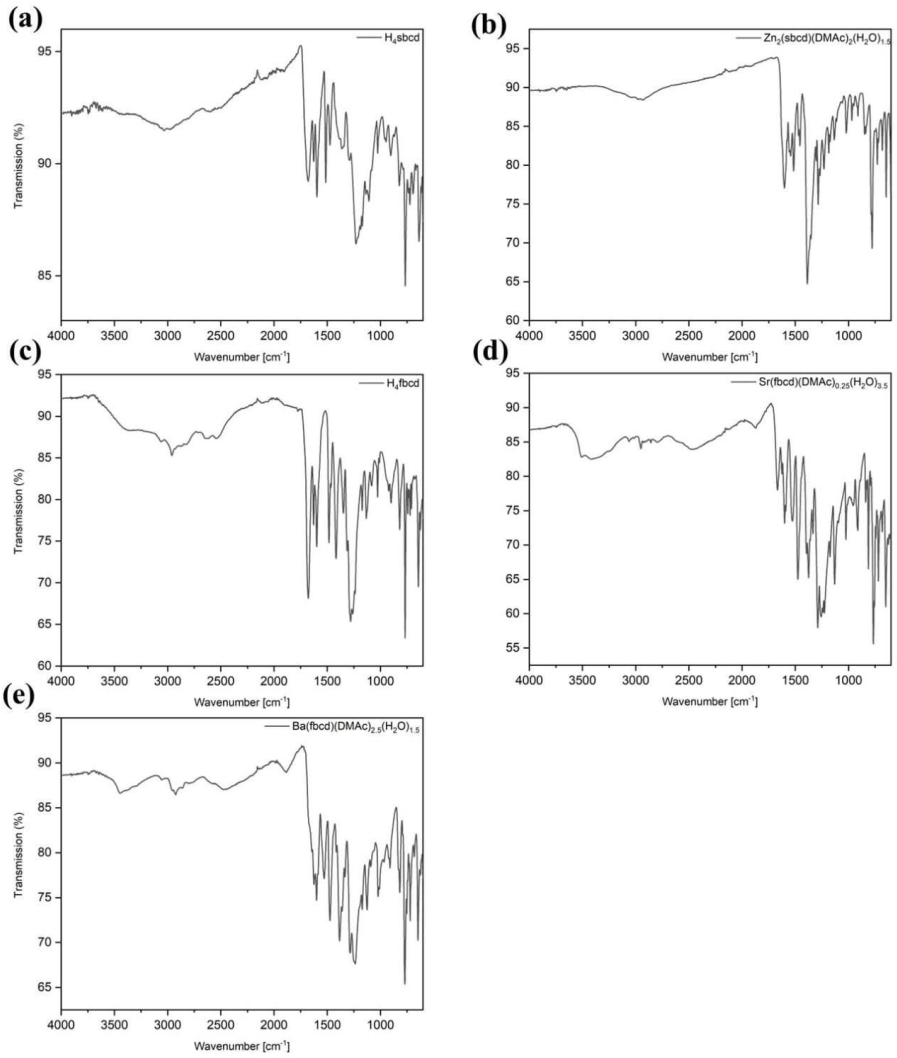

Fig. S10: IR spectrum of (a) H_4fbcd, (b) Zn_2(sbcd)$(DMAc)_2(H_2O)_{1.5}$, (c) H_4fbcd, (d) Sr(fbcd)$(DMAc)_{0.25}(H_2O)_{3.5}$ and (e) Ba(fbcd)$(DMAc)_{2.5}(H_2O)_{1.5}$.

4. Thermogravimetric analysis (TGA) of the coordination polymers

The TGA was carried out with a TGA/DSC 3+ STAR system from METTLER TOLEDO, to which a gas analysis system from THERMOStar was connected. The sample was filled into a crucible, which was tared beforehand, and the sample was weighed in the device.

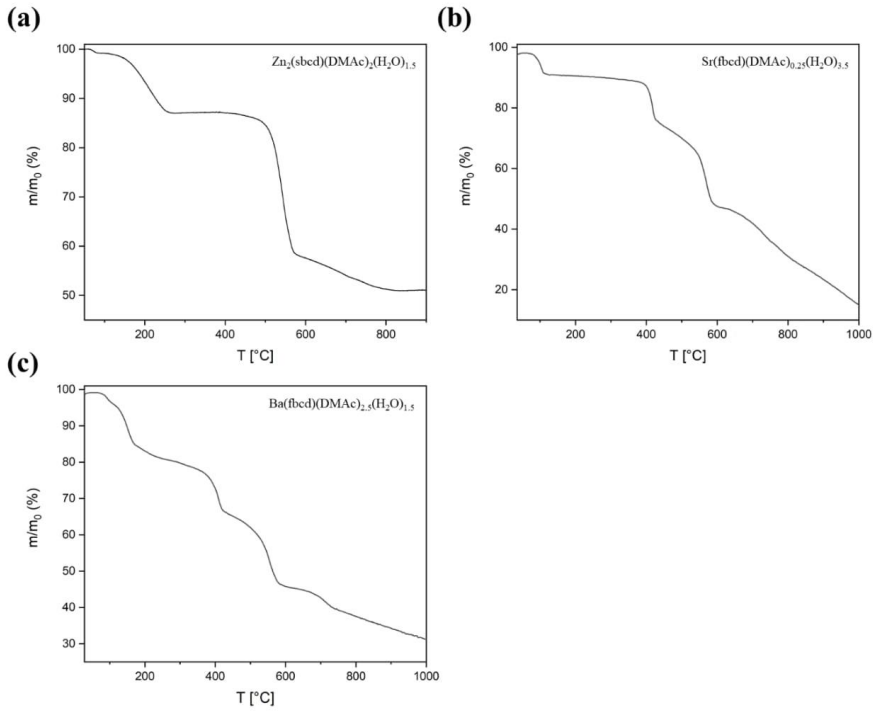

Fig. S11: TGA of the three coordination polymers (a) $Zn_2(sbcd)(DMAc)_2(H_2O)_{1.5}$, (b) $Sr(fbcd)(DMAc)_{0.25}(H_2O)_{3.5}$ and (c) $Ba(fbcd)(DMAc)_{2.5}(H_2O)_{1.5}$ with a heating rate of 10 K/min.

5. Z-scan data processing

The Z-scan setup is based on a high power femtosecond tunable oscillator (MaiTai DeepSee, Spectra Physics, Santa Clara, USA) with wavelength ranging from 690 to 1040 nm at a repetition rate of 81 MHz. The estimated pulse duration of the laser was 70 fs at 800 nm (central wavelength) and increased to 113 fs at lower wavelengths. The average power of the pulse (c.a. 70 fs) was about 3 W. The combination of Brewster-angle polarizer and half-wave plate were employed to tune the input power to the sample. The laser was directed to the custom-built mechanical chopper (142 Hz rotation frequency gives 78 μs on-time) and it decreases the exposure time of the sample to eliminate thermal effects. The laser pulses were focused onto the coordination polymers film samples by an achromatic doublet lens with focal length of 200 mm (AC254-200-B, Thorlabs). The sample was fixed on the motorized translation stage (LCS16-025-2(4)5, SMAC) and moved along the beam propagation direction *z* through monitoring the transmitted light from the sample by a photodiode (PDA100A-EC, Thorlabs) along with an oscilloscope (DS4024, Rigol). Moreover, a reference photodiode was used to compensate the signal fluctuations.[1] Nonlinear absorption studies were carried out by open-aperture Z-scan at various wavelengths from 700 nm to 950 nm with a spectral increment of 10 nm to comprehensively figure out the spectral dependent nonlinear absorption.

The measured Z-scan trace was fitted using the following equation

$$T_{\text{norm.}}(z) = 1 - \frac{1}{2\sqrt{2}} \frac{\beta I_0 L_{\text{eff}}}{1 + (\frac{z}{z_R})^2} \quad (1)$$

where

$$L_{\text{eff}} = \frac{1 - e^{-\alpha d}}{\alpha} \quad (2)$$

and

$$I_0 = 4\sqrt{\frac{\ln 2}{\pi}} \frac{P_{\text{avg}}}{M^2 \lambda z_R R \tau} \quad (3)$$

Two-photon absorption (2PA) coefficient β can be then extracted by fitting Equation (1), and, 2PA cross section $\sigma^{(2)}$ is calculated by

$$\sigma^{(2)}(\lambda) = \frac{hc}{\lambda}\frac{\beta(\lambda)}{N_{\mathrm{A}}\rho \times 10^{-3}}\ (\mathrm{cm^4\ s\ photon^{-1}\ molecule^{-1}}) \quad (4)$$

Related parameters are listed below:

$T_{\mathrm{norm.}}(z)$: normalized transmittance in terms of sample positon z

β: two-photon absorption coefficient

I_0: on-axis intensity of the laser

L_{eff}: effective optical path

z_{R}: Rayleigh length of the focusing beam

α: linear (one-photon) absorption coefficient

d: sample thickness

P_{avg}: average power of the laser

M^2: beam quality factor

λ: excitation wavelength

R: repetition rate of the pulsed laser

τ: laser pulse duration

h: Planck constant

c: speed of light in vacuum

N_{A}: Avogadro constant

ρ: sample concentration

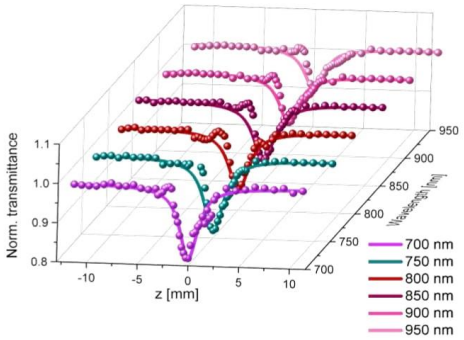

Fig. S12: Z-scan traces and data fitting for $Ba(fbcd)(DMAc)_{2.5}(H_2O)_{1.5}$ at different excitation wavelengths.

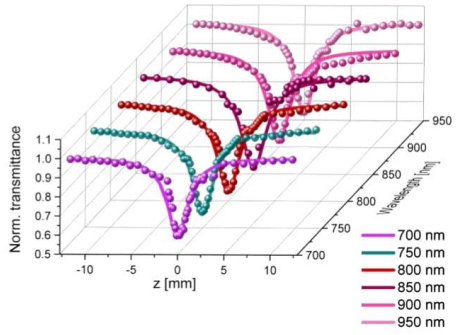

Fig. S13: Z-scan traces and data fitting for $Sr(fbcd)(DMAc)_{0.25}(H_2O)_{3.5}$ at different excitation wavelengths.

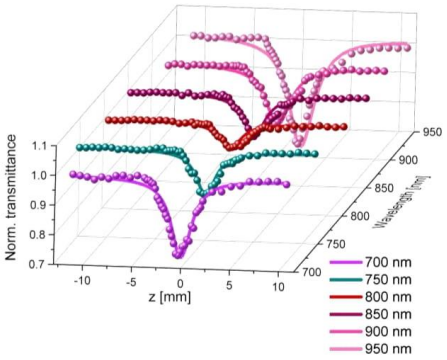

Fig. S14: Z-scan traces and data fitting for $Zn_2(sbcd)(DMAc)_2(H_2O)_{1.5}$ at different excitation wavelengths.

Table S1: Two-photon absorption coefficients $\beta(\lambda)$ in the unit of cm/GW and two-photon absorption cross-section values $\sigma^{(2)}(\lambda)$ in the unit of GM at different excitation wavelengths are tabulated. On-axis laser intensity for each samples are: $Zn_2(sbcd)(DMAc)_2(H_2O)_{1.5}$, 20–28 GW/cm^2; $Ba(fbcd)(DMAc)_{2.5}(H_2O)_{1.5}$, 28–39 GW/cm^2; $Sr(fbcd)(DMAc)_{0.25}(H_2O)_{3.5}$, 13–21 GW/cm^2..

Wavelength [nm]	$Zn_2(sbcd)(DMAc)_2(H_2O)_{1.5}$		$Ba(fbcd)(DMAc)_{2.5}(H_2O)_{1.5}$		$Sr(fbcd)(DMAc)_{0.25}(H_2O)_{3.5}$	
	β	$\sigma^{(2)}$	β	$\sigma^{(2)}$	β	$\sigma^{(2)}$
700	11.4	13922.80	6.2	10360.56	31	26885.96
710	6.7	8066.91	4.9	8073.24	34.4	29415.20
720	6.4	7599.59	5.3	8609.86	30	25297.51
730	5	5855.89	6.5	10415.49	32	26614.04
740	5.7	6585.69	4.3	6797.18	25.4	20839.91
750	5.66	2918.17	4	6238.03	25.6	20723.68
760	2.86	3216.68	6.7	10312.68	28.4	22687.87
770	3.4	3774.58	3.3	5012.68	29	22865.50
780	3.3	3617.09	3.3	4949.30	30	23347.95
790	3.58	3874.42	3.34	4946.48	30.4	23362.57
800	2	2136.90	2.8	4094.37	33.6	25497.08
810	2.1	2216.16	2.9	4187.32	35	26235.38
820	2.34	2439.73	3.1	4422.54	36.6	27097.95
830	2.66	2740.09	3.3	4650.70	38.2	27938.60
840	3.3	3358.72	3.2	4456.34	35	25299.71

850	3.9	3922.80	3	4128.17	42	30000
860	4.62	4592.90	2.9	3945.07	47	33179.82
870	5.5	5405.04	2.86	3845.49	47.8	33355.26
880	5.5	5343.28	3.1	4121.13	45	31045.32
890	5.4	5186.82	3	3942.25	46	31381.58
900	6.7	6364.38	2.7	3509.44	47	31703.22
910	8.8	8267.63	2.7	3470.85	47.6	31754.36
920	12.8	11888.83	2.6	3305.63	48.8	32200.29
930	14.4	13237.26	2.64	3319.72	49.4	32251.46
940	15.5	14097.79	2.72	3384.51	49.4	31907.89
950	17.6	15838.39	2.48	3053.52	50	31951.75

6. Single crystal X-ray diffraction

X-ray intensity data of the compound was collected at 100K using a Bruker D8 Venture diffractometer equipped with a Helios optic monochromator, a Photon 100 CMOS detector and a Mo IMS microsource (Mo-K_α radiation). The raw area detector data frames were reduced and corrected for absorption effects using the SAINT and SADABS programs with multi-scan absorption correction. Final unit cell parameters were determined by fast fourier transform refinement of the respective independent reflections taken from the data sets. The structure was solved by autostructure with SHELXT. Difference Fourier calculations and full-matrix least-squares refinements against F^2 were performed by SHELXL-2014/7 (Sheldrick, 2014). All non-hydrogen atoms were refined with anisotropic displacement parameters. Hydrogen atoms were refined by a mixture of independent and constrained refinement.

6.1 Single-crystal report of $Zn_2(sbcd)(DMAc)_2(H_2O)_{1.5}$ (CCDC deposition number:)

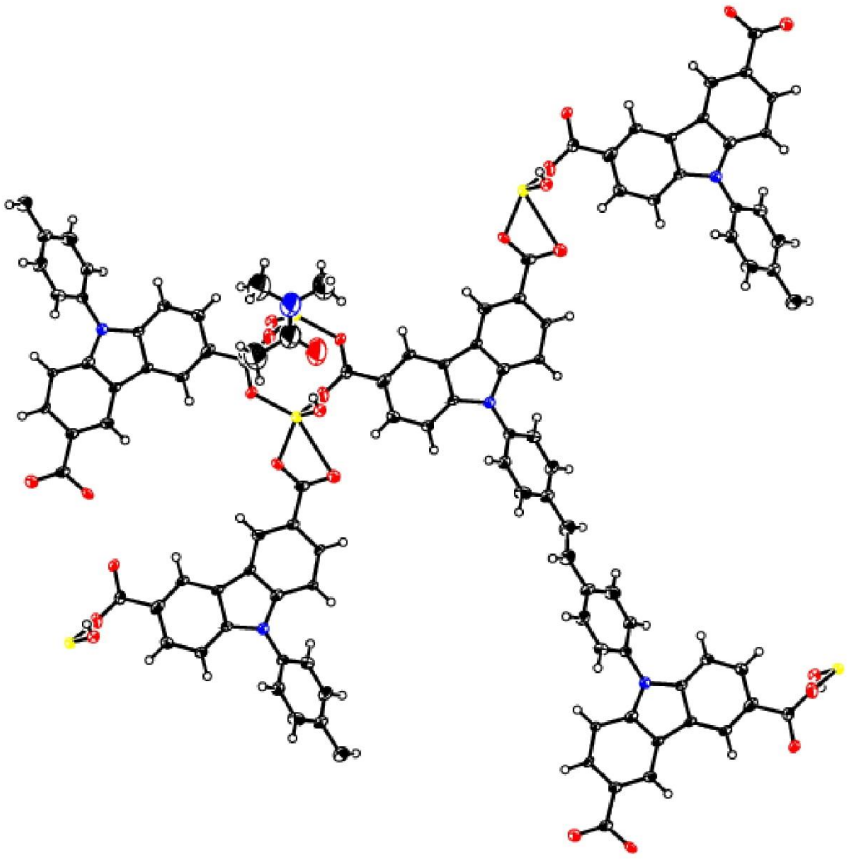

Fig. S15: ORTEP representation of the single-crystal structure of $Zn_2(sbcd)(DMAc)_2(H_2O)_{1.5}$ with thermal ellipsoids shown at the 50% probability level.

Crystal data	znsbcd_0m
Chemical formula	$C_{21}H_{11}NO_5Zn \cdot C_4H_9NO$
M_r	509.82

Crystal system, space group	Triclinic, *P* -1
Temperature (K)	103
a, *b*, *c* (Å)	9.256 (3), 11.735 (4), 12.319 (4)
α, β, γ (°)	73.267 (10), 78.637 (8), 68.362 (10)
V (Å^3)	1184.9 (7)
Z	2
Radiation type	Mo *K*α
μ (mm^{-1})	1.08
Crystal size (mm)	0.29 × 0.12 × 0.07
Data collection	
Diffractometer	Bruker Photon CMOS
Absorption correction	Multi-scan *SADABS* 2016/2, Bruker, 2016
T_{min}, T_{max}	0.550, 0.745
No. of measured, independent and observed [$I > 2\sigma(I)$] reflections	13863, 4247, 2440
R_{int}	0.116
$(\sin \theta/\lambda)_{max}$ (Å^{-1})	0.602
Refinement	
$R[F^2 > 2\sigma(F^2)]$, $wR(F^2)$, S	0.128, 0.349, 1.06
No. of reflections	4247
No. of parameters	315
No. of restraints	36
H-atom treatment	H atoms treated by a mixture of independent and constrained refinement
	W = 1/[Σ^2(*F*O^2) + (0.1315*P*)^2 + 18.4592*P*] WHERE *P* = (*F*O^2 + 2*F*C^2)/3
$\Delta\rho_{max}$, $\Delta\rho_{min}$ (e Å^{-3})	1.71, −0.94

6.2 Single-crystal report of $Sr(fbcd)(DMAc)_{0.25}(H_2O)_{3.5}$ (CCDC deposition number:)

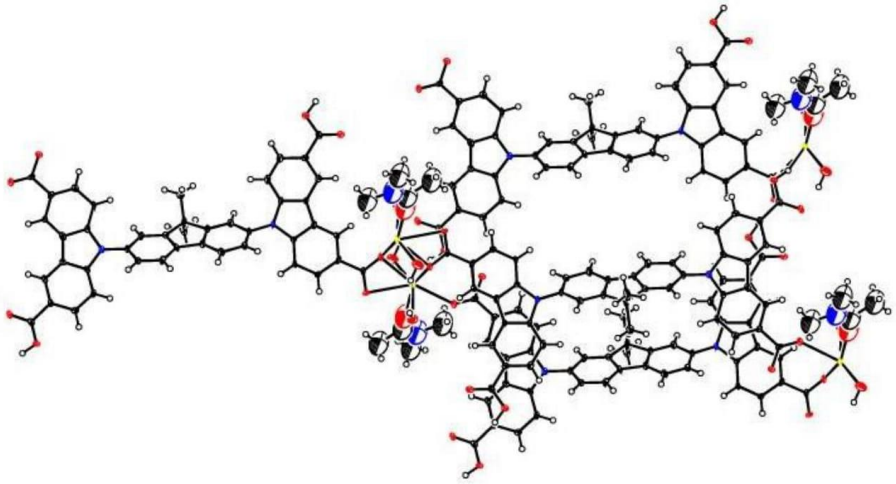

Fig. S16: ORTEP representation of the single-crystal structure of $Sr(fbcd)(DMAc)_{0.25}(H_2O)_{3.5}$ with thermal ellipsoids shown at the 50% probability level.

Crystal data	weise43_0ma_sq
Chemical formula	$C_{43}H_{26}N_2O_8Sr \cdot 2(OH) \cdot (C_4H_9NO)$
M_r	907.42
Crystal system, space group	Triclinic, *P* -1
Temperature (K)	100
a, *b*, *c* (Å)	10.076 (3), 12.140 (3), 23.401 (6)
α, β, γ (°)	93.793 (7), 90.197 (8), 93.276 (8)
V (Å^3)	2851.5 (13)
Z	2
Radiation type	Mo *K*α
μ (mm^{-1})	1.00

Crystal size (mm)	0.25 × 0.01 × 0.01
Data collection	
Diffractometer	Bruker Photon CMOS
Absorption correction	Multi-scan *SADABS* 2016/2, Bruker, 2016
T_{min}, T_{max}	0.660, 0.739
No. of measured, independent and observed [$I > 2\sigma(I)$] reflections	122464, 11211, 8779
R_{int}	0.112
$(\sin \theta/\lambda)_{max}$ (Å^{-1})	0.617
Refinement	
$R[F^2 > 2\sigma(F^2)]$, $wR(F^2)$, S	0.116, 0.324, 1.02
No. of reflections	11211
No. of parameters	572
No. of restraints	79
H-atom treatment	H atoms treated by a mixture of independent and constrained refinement
	W = 1/[$\Sigma^2(FO^2)$ + (0.172P)^2 + 35.4396P] WHERE P = (FO^2 + 2FC^2)/3
$\Delta\rho_{max}$, $\Delta\rho_{min}$ (e Å^{-3})	7.39, −1.36

6.3 Single-crystal report of Ba(fbcd)(DMAc)$_{2.5}$(H_2O)$_{1.5}$ (CCDC deposition number:)

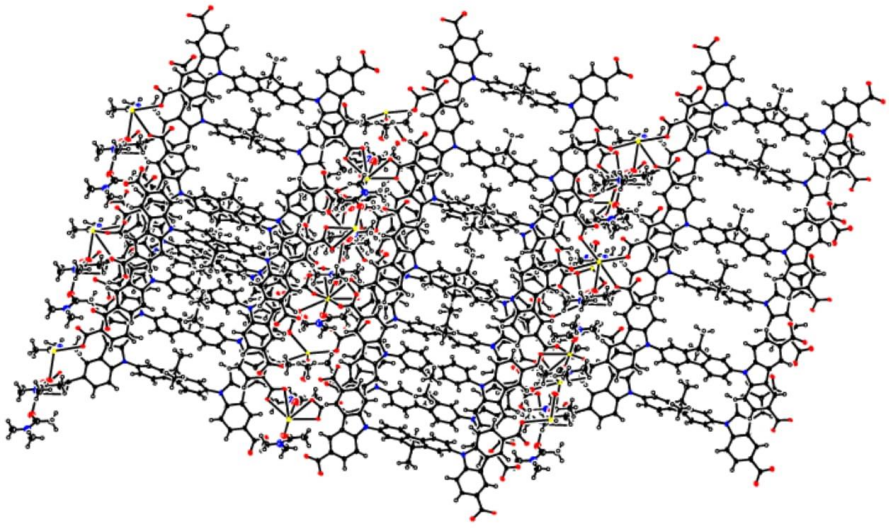

Fig. S17: ORTEP representation of the single-crystal structure of Ba(fbcd)(DMAc)$_{2.5}$(H$_2$O)$_{1.5}$ with thermal ellipsoids shown at the 50% probability level.

Crystal data	weise40_m_0m_sq
Chemical formula	$C_{86}H_{48}Ba_2N_4O_{16}\cdot 3(C_4H_9NO)\cdot(H_2O)$
M_r	1963.33
Crystal system, space group	Monoclinic, *P* 2$_1$/*n*
Temperature (K)	100
a, *b*, *c* (Å)	12.178 (1), 20.5805 (17), 46.760 (4)
β (°)	90.270 (2)
V (Å^3)	11719.3 (17)
Z	4
Radiation type	Mo *K*α
μ (mm^{-1})	0.73
Crystal size (mm)	0.25 × 0.01 × 0.01

Data collection	
Diffractometer	Bruker Photon CMOS
Absorption correction	Multi-scan *SADABS* 2016/2, Bruker, 2016
T_{min}, T_{max}	0.702, 0.745
No. of measured, independent and observed [$I > 2\sigma(I)$] reflections	312603, 23047, 21570
R_{int}	0.050
$(\sin\theta/\lambda)_{max}$ (Å^{-1})	0.617
Refinement	
$R[F^2 > 2\sigma(F^2)]$, $wR(F^2)$, S	0.075, 0.180, 1.16
No. of reflections	23047
No. of parameters	1233
No. of restraints	351
H-atom treatment	H atoms treated by a mixture of independent and constrained refinement
	W = 1/[$\Sigma^2(FO^2)$ + (0.0225P)^2 + 172.6567P] WHERE P = (FO^2 + 2FC^2)/3
$\Delta\rho_{max}$, $\Delta\rho_{min}$ (e Å^{-3})	2.78, −3.72

7. Steady-state spectroscopy of likers and CPs

7.1 Solvent-dependent absorption spectra of Pr_4sbcd linker

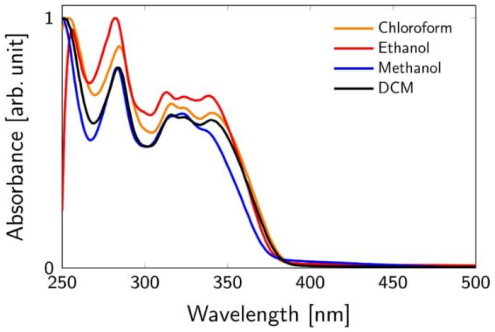

Fig. S18: UV/VIS absorption spectra of Pr_4sbcd measured in different solvents

7.2 Diffuse reflectance spectra of linkers and their corresponding CPs

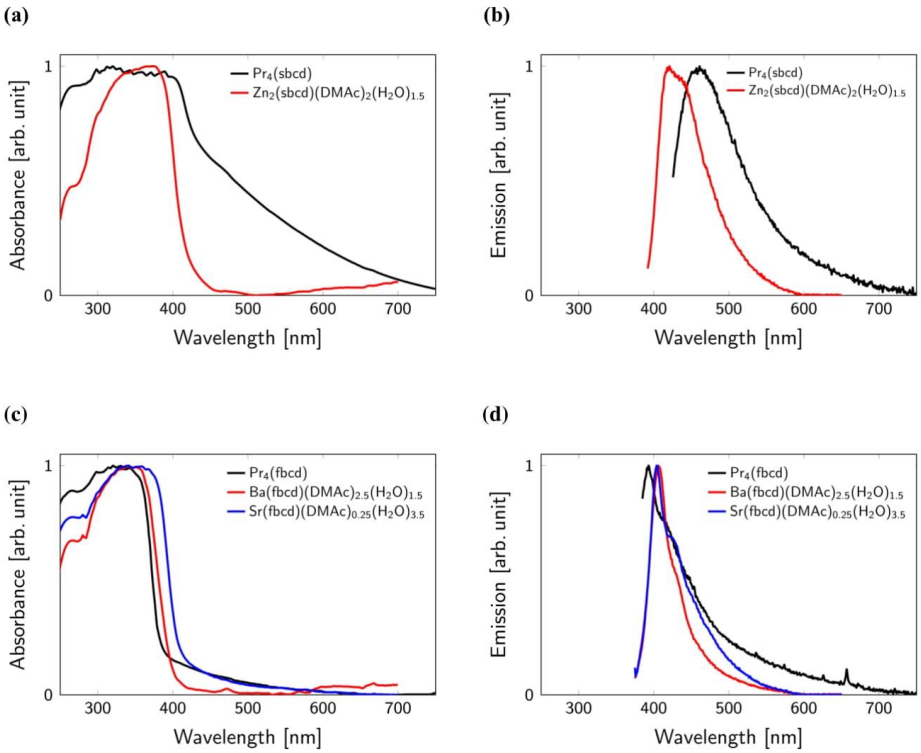

Fig S19: Diffuse reflectance spectra of solid-state linkers and corresponding solid-state CPs. (a) UV/Vis spectra of the linker Pr_4(sbcd) (black) and its corresponding zinc-CP (red) in solid-state. (b) Emission spectra of the linker Pr_4(sbcd) (black) and its corresponding CP (red) in solid-state. (c) UV/Vis spectra of the linker Pr_4(fbcd) (black) and its corresponding strontium-CP (blue) and barium-CP (red) in solid-state. (d) Emission spectra of the linker Pr_4(fbcd) (black) and its corresponding strontium-CP (blue) and barium-CP (red) in solid-state.

8. Sample preparation of CPs for the Z-scan measurements

All three CP crystalline powders are finely grinded to the uniform powders. Each CP powder was weighted (see Table S2) and mixed with 0.5 g PMMA (1.18 g/mL) powder into 5 mL DCM and was stirred for 2h in the solution. Afterwards PMMA films of the resulting dispersions were produced using the "doctor blading" technique with subsequent evaporation of the DCM.

Table S2: Parameters used to calculate the concentration of CPs in PMMA-film state.

CPs	Molecular weight [g/mol]	Mass [mg]	Concentration [mol/L]
$Zn_2(sbcd)(DMAc)_2(H_2O)_{1.5}$	1014.41	16.7	0.0389
$Ba(fbcd)(DMAc)_{2.5}(H_2O)_{1.5}$	1080.30	13.0	0.0284
$Sr(fbcd)(DMAc)_{0.25}(H_2O)_{3.5}$	871.13	20.2	0.0547

9. References

1. Steiger, W.; Gruber, P.; Theiner, D.; Dobos, A.; Lunzer, M.; Van Hoorick, J.; Van Vlierberghe, S.; Liska, R.; Ovsianikov, A., Fully automated z-scan setup based on a tunable fs-oscillator. *Opt. Mater. Express* **2019,** *9* (9), 3567-3581.

5.3 Supporting Information for Manuscript III

Supporting Information

A Perylenediimide-based Zinc-Coordination Polymer for Photosensitized Singlet-Oxygen Generation

Simon N. Deger [1,†], Sebastian J. Weishäupl [1,†], Alexander Pöthig [1*], and Roland A. Fischer [1,*]

[1] Chair of Inorganic and Metal-Organic Chemistry, Catalysis Research Center, Ernst-Otto-Fischer-Straße 1, 85748 Garching, Germany.
[†] These authors contributed equally to this work.
[*] Correspondence: roland.fischer@tum.de.

1. Analytical Methods

Surface Area Determination (BET)

Adsorption measurements with N2 (99.999 vol%) at 77 K were carried out on a 3Flex Physisorption from Micromeritics Instrument Corp., which uses a manometric method to determine the amount adsorbed under an equilibrated gas pressure.
Adsorption data was processed using the 3Flex Software Version 5.01 by Micromeritics Instrument Corp. and plotted in OriginPro 2019b by OriginLab Corp. To create open access data, prevent issues with data mining, and facilitate machine learning, all isotherms are presented as adsorption information files in the SI [1]. The conversion of measurement files was performed using an open access web application. [2]

The activated samples were transferred into pre-weighed sample tubes and capped with Micromeritics Check Seals. The samples were subsequently heated at 60 °C for 12 hours under a dynamic vacuum of ~ 10–3 mbar using SmartVac Prep by Micromeritics Instrument Corp. to ensure the absence of unwanted adsorbates and identical pre-measurement states of all the samples. The mass of the adsorbent was then recorded. The free space of the sample tube was determined prior to measuring each adsorption isotherm using helium (99.999 vol%). A water bath was used to maintain temperatures from 5–25 °C; a liquid nitrogen bath was used for measurements at 77 K.

Nuclear Magnetic Resonance Spectroscopy (NMR)

^{1}H-NMR spectra were recorded on a *BRUKER AVIII 400 US* with 400 MHz (^{1}H). The chemical shifts δ were referenced on the residue of the proton signals of the used solvents and specified in parts per million (ppm). The determined data are shown in the following presented sequence: chemical shift in ppm (multiplicity, coupling constant, integral, and assignment). The following abbreviations were used in the assignment of the signals: s – singulett, m – multiplett.

Powder X-Ray Diffraction (PXRD)

Powder X-ray diffraction measurements were carried out on a Rigaku MiniFlex 600-C diffractometer. The diffractometer is equipped with a 600 W X-ray tube and a D/teX Ultra silicon strip detector and a scan width of 2Θ = 3–50°.

Solid State UV/Vis (SS-UV/Vis)

The UV/Vis spectra of solids were recorded on a UV-3600 Plus from SHIMADZU at a wavelength range of 200 nm–800 nm. The sample was sandwiched between two quartz microscope plates from Alfa Aesar and measured at room temperature.

UV/Vis Spectroscopy

UV/Vis spectra were measured on a Lambda 365 UV/Vis Spectrometer form Perkin Elmer at a wavelength range of 0–900 nm. The spectrometer uses a tungstenhalogen and deuterium interface.

Elemental Analysis

The elemental analysis was carried out in the Microanalytical Laboratory at the Technical University of Munich. The analyses for carbon, chlorine hydrogen, nitrogen, and zinc were carried out with a flash 88 combustion method at 1800 °C with an ELEMENTAL analyzer from HEK-ATECH. All data are presented in %.

Thermogravimetric Analysis (TGA)

The TGA was carried out with a TGA/DSC 3+ STAR system from METTLER TOLEDO, to which a gas analysis system from THERMOStar was connected. The sample was filled into a crucible, which was tared beforehand, and the sample was weighed in the device.

Single-Crystal X-Ray Diffraction (SC-XRD)

X-ray intensity data of the compound was collected at 100(2)K using a Bruker D8 Venture diffractometer equipped with a Helios optic monochromator, a Photon 2 CPAD detector, and a Mo IMS micro source (Mo-K_α radiation) (compound 2) or a Photon 100 CMOS detector and a TXS rotating anode (Mo-K_α radiation) (compound 3). The raw area detector data frames were reduced and corrected for absorption effects using the SAINT and SADABS programs with multi-scan absorption correction. Final unit cell parameters were determined by fast Fourier transform refinement of the respective independent reflections ontained from the data sets. The structure was solved using SHELXT. Difference Fourier calculations and full-matrix least-squares refinements against F^2 were performed by SHELXL-2014/7 (Sheldrick, 2014). All non-hydrogen atoms were refined with anisotropic displacement parameters. Hydrogen atoms were calculated in ideal positions using a riding model.

Fluorescence Spectroscopy

A FS5 Spectrofluorometer from Edinburgh Instruments was used for the fluorescence measurements. As the light source, a 150 W CW ozone-free xenon arc lamp was used and a Czerny–Turner design monochromator with a dual grating turret. The detector used was a Photomultiplier R928P with a spectral coverage of 200 nm–900 nm.

2. Synthetic Procedures

1,6,7,12-tetrachloro-perylene-3,4,9,10-tetracarboxylic anhydride 1: the synthesis was performed according to a literature-known synthesis. [18] In a 100 mL Schlenk flask, 1 g of perylene-3,4,9,10-tetracarboxylic acid anhydride 1 (2.5 mmol, 1 eq.) and 0.17 g of iodine (0.68 mmol, 0.27 eq.) in 6.55 mL of chlorsulfonic acid were stirred for 2 days at 70 °C under argon atmosphere. After completion, the reaction mixture was slowly poured into 500 mL of ice water. Subsequently, the precipitating orange solid was filtered, washed with water, and dried to produce a bright orange powder (1.32 g, 2.49 mmol, 99%). ^{1}H-NMR (400 mHz, CDCl3): δ (ppm) = 8.74 (s, 4H).

1,6,7,12-tetrachloroperylenediimide-N,N'-di-benzoic acid (H_2tpbd) 2: the synthesis was performed with a modified literature synthesis [19]. In a 100 mL round bottom flask, 1 g of **1** (1.89 mmol, 1 eq.) and 3.88 g 4-aminobenzoic acid 3 (28.3 mmol, 15 eq.) were dissolved in 25 mL of propionic acid and stirred for 2 days at 160°C. After the completion of the reaction, the reaction mixture was poured into 100 mL of water and subsequently filtered off. The filtrate was washed with 100 mL of water/methanol (1:1), and afterwards the orange solid was dried to constant weight (1.1 g, 1.89 mmol, 82%).
^{1}H-NMR (400 mHz, DMSO-d6): δ (ppm) = 13.20 (s, 2H, COOH), 8.64 (s, 4H), 8.21- 8.05 (m, 4H), 7.65-7.56 (m, 4H).

Zn(tpdb)(DMF)$_3$ 3: in a 4 mL screw-cap vial, $Zn(NO_3)_2$ (15.0 mg, 0.05 mmol, 3.8 eq.) and H_2tpbd **2** (10.0 mg, 0.013 µmol. 1 eq.) were dissolved in 3 mL of DMF. Afterwards, the solution was sonicated and placed for 96 h at 90°C in an oven. The precipitated solid was then filtered and dried to constant weight to produce orange needles of Zn(tpbd)(DMF)$_3$ **3** (4.13 mg, 0.0039 mmol, 30%)
Elemental analysis (%) calc. for Zn(tpdb)(DMF)$_3$: C, 53.17; H, 3.17; N, 6.66; Zn, 6.22; Cl, 13.49; found C, 53.57; H, 2.78; N, 6.03; Zn, 6.2; Cl, 13.0.

$^1O_2$-Evolution Experiments

In a glovebox, a 20 mL phototube was filled with 1.25 mg (4.62 mmol, 1 eq.) of DBPF and 1 eq. of the respective photosensitizer **2** or **3**. A total of 5 mL of dried acetonitrile was added with argon counter flow and subsequently the suspension was stirred for 30 minutes in the dark to achieve the adsorption/desorption equilibrium under oxygen atmosphere. Afterwards, an LED with a wavelength of 512 nm was turned on and, at defined time intervals, aliquots of the reaction solution were obtained, diluted, and investigated, and UV/Vis spectra were recorded.

3. Supplementary Figures

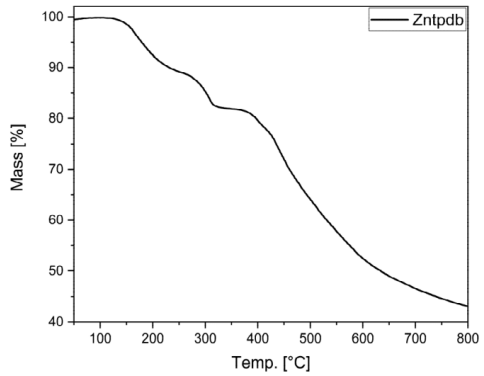

Figure S1. Thermal gravimetric analysis of Zn(tpdb)$(DMF)_3$ from 25°C to 800°C with a rate of 10 K min−1. The weight loss of 10% starting at 150°C indicates that the loss in the structure included water. The subsequent weight loss of 5% starting at 300°C corresponds to the stored DMF in the structure. The MOF structure is then stable until 400°C. At this temperature, the MOF starts to decompose.

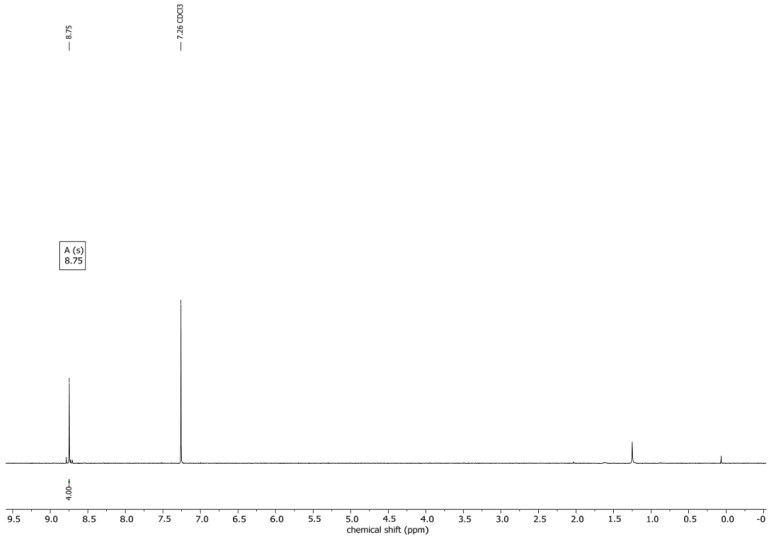

Figure S2. ^{1}H-NMR of 1,6,7,12-tetrachloro-perylene-3,4,9,10-tetracarboxylic anhydride **(1)** in $CDCl_3$ showing a single singulett, according for the H atoms in the bay area of the perylene.

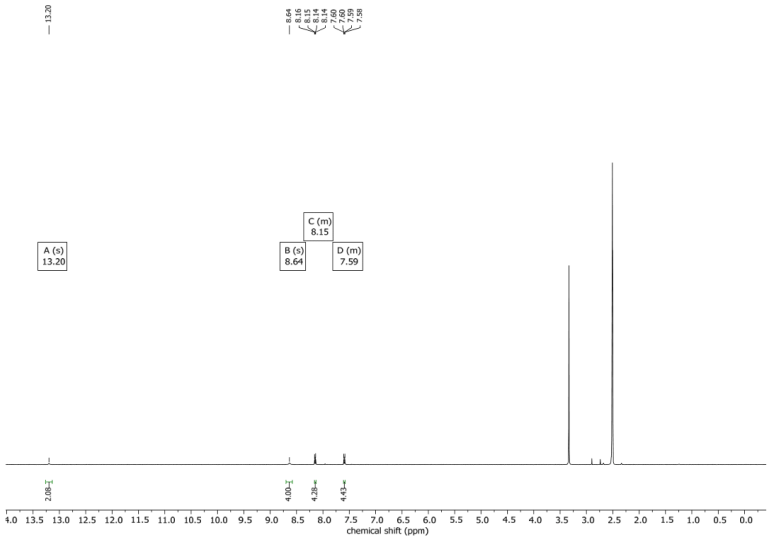

Figure S3. ^{1}H-NMR of 1,6,7,12-tetrachloroperylenediimide-N,N'-di-benzoic acid **(2)** in DMSO-d6 showing a singulett at 13.2 ppm for the carboxylic acid groups, and an additional singulet at 8.64 ppm for the H atoms in the bay area of the perylene. Additionally, two multipletts can be seen, accounting for the aromatic H atoms of the benzoic acid at 8.15 ppm and 7.59 ppm.

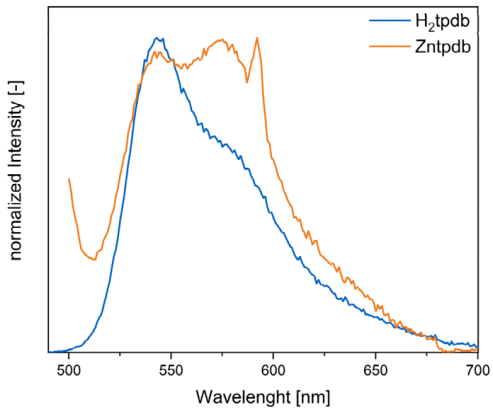

Figure S4. Comparison of the emission behavior of **2** and **3.** The linker shows a much stronger emission than the MOF (compare QY(H2tpbd) = 0,9 vs. QY(Zn(tpbd)) = < 0,01), suggesting H-type aggregated perylenes, which show a high n-type mobility and quenching of the absorbed light energy, not allowing for directed energy transfer.

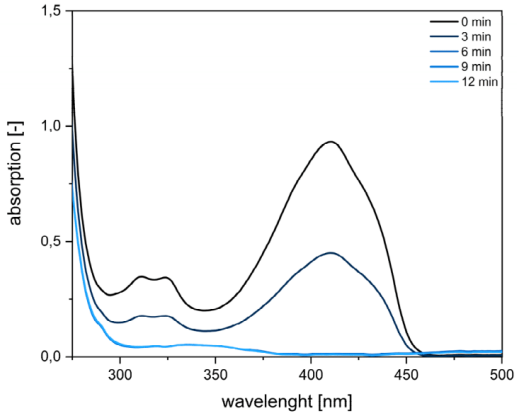

Figure S5. UV/Vis of the decrease in the absorption intensity of DBPF during the reaction with $^1O_2$ produced by **2.**

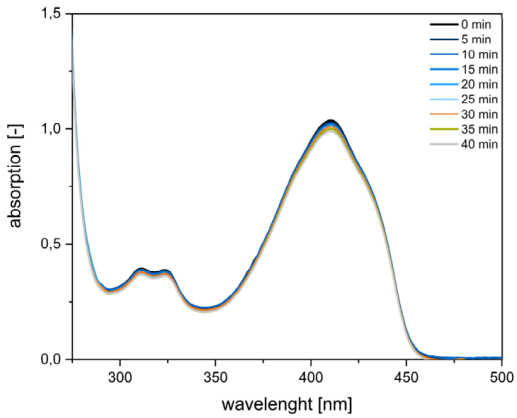

Figure S6. Control experiment of DBPF with **3** and without light irradiation over the duration of 40 minutes.

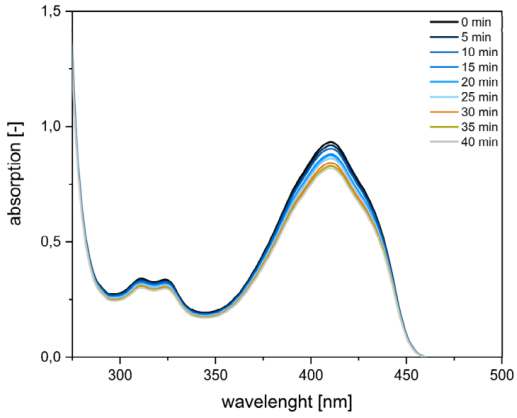

Figure S7. Control experiment of DBPF without **3** and with light irradiation over the duration of 40 minutes.

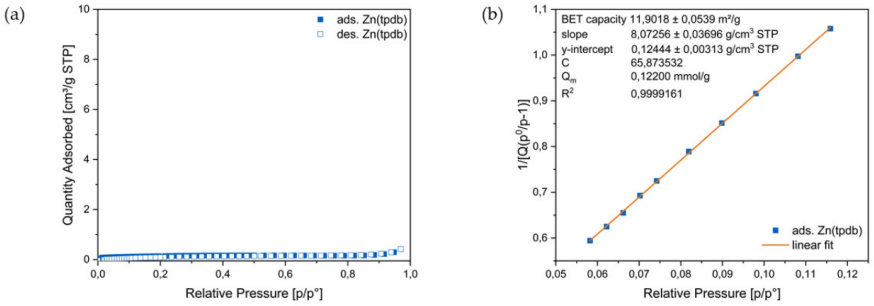

Figure S8: BET data of Zn(tpdb)(DMF)$_3$ showing the low surface area of it because of missing pores and the layer structure of the 2D coordination polymer. (a) Semi-log plot of the nitrogen isotherm at 77 K of Zn(tpdb). (b) BET plot with linear-fit control parameters and calculated monolayer capacity (Q_m).

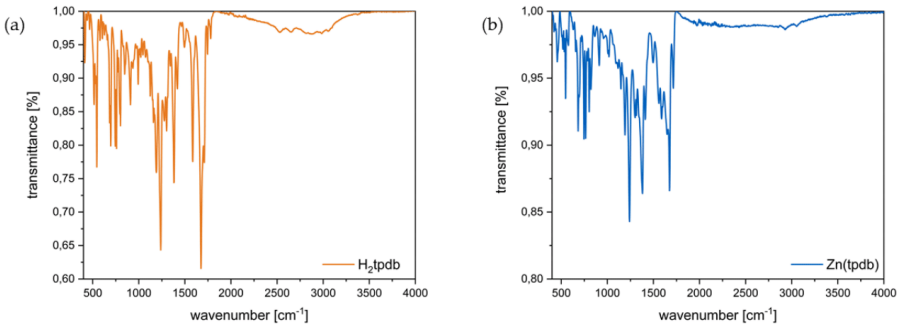

Figure S9: IR data of (a) linker **2** and (b) MOF **3**.

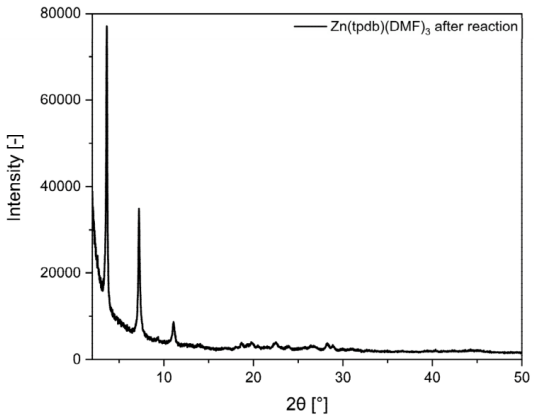

Figure S10: PXRD of **3** after $^1O_2$ evolution studies.

4. Single-Crystal X-Ray Diffraction Experiments

4.1 H_2tpdb (CCDC: Deposition Number 2153020)

Crystal data	
Chemical formula	$C_{38}H_{14}Cl_4N_2O_8 \cdot 2(C_4H_8O)$
M_r	912.52
Crystal system, space group	Monoclinic, *C*2/*c*
Temperature (K)	100
a, *b*, *c* (Å)	35.229 (4), 12.3677 (13), 21.757 (3)
β (°)	119.954 (6)
V (Å^3)	8213.3 (18)
Z	8
Radiation type	Mo *K*α
μ (mm^{-1})	0.35
Crystal size (mm)	0.23 × 0.09 × 0.06
Data collection	
Diffractometer	Bruker Photon CMOS
Absorption correction	Multi-scan *SADABS* 2016/2, Bruker, 2016
T_{min}, T_{max}	0.692, 0.745
No. of measured, independent and observed [$I > 2\sigma(I)$] reflections	150702, 8080, 7369
R_{int}	0.070
$(\sin \theta/\lambda)_{max}$ (Å^{-1})	0.617
Refinement	
$R[F^2 > 2\sigma(F^2)]$, $wR(F^2)$, *S*	0.078, 0.156, 1.22
No. of reflections	8080
No. of parameters	655

No. of restraints	121
H-atom treatment	H atoms treated by a mixture of independent and constrained refinement
	W = 1/[Σ²(*FO*²) + (0.0321*P*)² + 60.8212*P*] WHERE *P* = (*FO*² + 2*FC*²)/3
$\Delta\rho_{max}$, $\Delta\rho_{min}$ (e Å^{-3})	0.60, −0.77

Computer programs: *APEX* III Control Software (Bruker, 2016), *SAINT* (Bruker, 2017), SHELXT (Sheldrick, 2015), *SHELXL* (Sheldrick, 2017), SHELXLE (Huebschle, 2011), *PLATON* (Spek, 2011), and *enCIFer* (Allen, 2014).

4.2 Zntpdb(DMF)$_3$ (CCDC: Deposition Number 2153019)

Crystal data	
Chemical formula	$C_{85}H_{41}Cl_8N_7O_{19}Zn_2(C_3H_7NO)$
M_r	1965.81
Crystal system, space group	Monoclinic, *C*2/*c*
Temperature (K)	123
a, *b*, *c* (Å)	50.894 (3), 19.9711 (12), 16.310 (1)
β (°)	91.825 (2)
V (Å^3)	16569.2 (17)
Z	8
Radiation type	Mo *K*α
μ (mm^{-1})	0.92
Crystal size (mm)	0.28 × 0.10 × 0.05
Data collection	
Diffractometer	Bruker Photon CMOS
Absorption correction	Multi-scan *SADABS* 2016/2, Bruker, 2016
T_{min}, T_{max}	0.689, 0.736
No. of measured, independent and observed [$I > 2\sigma(I)$] reflections	204129, 16317, 11889
R_{int}	0.101

$(\sin \theta/\lambda)_{max}$ (Å^{-1})	0.617
Refinement	
$R[F^2 > 2\sigma(F^2)]$, $wR(F^2)$, S	0.080, 0.233, 1.04
No. of reflections	16317
No. of parameters	1143
No. of restraints	48
H-atom treatment	H-atom parameters constrained
	$W = 1/[\Sigma^2(FO^2) + (0.1242P)^2 + 156.7946P]$ WHERE $P = (FO^2 + 2FC^2)/3$
$\Delta\rho_{max}$, $\Delta\rho_{min}$ (e Å^{-3})	3.35, −1.81

Computer programs: *APEX* III Control Software (Bruker, 2016), *SAINT* (Bruker, 2017), SHELXT (Sheldrick, 2015), *SHELXL* (Sheldrick, 2017), SHELXLE (Huebschle, 2011), *PLATON* (Spek, 2011), and *enCIFer* (Allen, 2014).

5. References

[1] https://doi.org/10.1021/acs.langmuir.1c00122
[2] https://raw2aif.herokuapp.com/

6 Appendix

6.1 List of Figures

6.2 Reprint Permissions

SPRINGER NATURE LICENSE
TERMS AND CONDITIONS

Jul 09, 2022

This Agreement between Technical University Munich -- Sebastian Weishäupl ("You") and Springer Nature ("Springer Nature") consists of your license details and the terms and conditions provided by Springer Nature and Copyright Clearance Center.

License Number	5344880199927
License date	Jul 09, 2022
Licensed Content Publisher	Springer Nature
Licensed Content Publication	Nature
Licensed Content Title	Design and synthesis of an exceptionally stable and highly porous metal-organic framework
Licensed Content Author	Hailian Li et al
Licensed Content Date	Nov 18, 1999
Type of Use	Thesis/Dissertation
Requestor type	academic/university or research institute
Format	print and electronic
Portion	figures/tables/illustrations
Number of figures/tables/illustrations	1
Will you be translating?	no

Circulation/distribution	50000 or greater
Author of this Springer Nature content	no
Title	Chromophore-based Coordination Polymers (CPs) as Materials for Optical Applications
Institution name	Technical University of Munich
Expected presentation date	Sep 2022
Portions	Figure 1
Requestor Location	Technical University Munich Lichtenbergstr. 4 Garching, Bayern 85748 Germany Attn: Technical University Munich
Total	0.00 EUR

Terms and Conditions

Springer Nature Customer Service Centre GmbH
Terms and Conditions

This agreement sets out the terms and conditions of the licence (the **Licence**) between you and **Springer Nature Customer Service Centre GmbH** (the **Licensor**). By clicking 'accept' and completing the transaction for the material (**Licensed Material**), you also confirm your acceptance of these terms and conditions.

1. Grant of License

1. 1. The Licensor grants you a personal, non-exclusive, non-transferable, world-wide licence to reproduce the Licensed Material for the purpose specified in your order only. Licences are granted for the specific use requested in the order and for no other use, subject to the conditions below.

1. 2. The Licensor warrants that it has, to the best of its knowledge, the rights to license reuse of the Licensed Material. However, you should ensure that the material you are requesting is original to the Licensor and does not carry the copyright of another entity (as credited in the published version).

1. 3. If the credit line on any part of the material you have requested indicates that it was reprinted or adapted with permission from another source, then you should also

seek permission from that source to reuse the material.

2. Scope of Licence

2. 1. You may only use the Licensed Content in the manner and to the extent permitted by these Ts&Cs and any applicable laws.

2. 2. A separate licence may be required for any additional use of the Licensed Material, e.g. where a licence has been purchased for print only use, separate permission must be obtained for electronic re-use. Similarly, a licence is only valid in the language selected and does not apply for editions in other languages unless additional translation rights have been granted separately in the licence. Any content owned by third parties are expressly excluded from the licence.

2. 3. Similarly, rights for additional components such as custom editions and derivatives require additional permission and may be subject to an additional fee. Please apply to Journalpermissions@springernature.com/bookpermissions@springernature.com for these rights.

2. 4. Where permission has been granted **free of charge** for material in print, permission may also be granted for any electronic version of that work, provided that the material is incidental to your work as a whole and that the electronic version is essentially equivalent to, or substitutes for, the print version.

2. 5. An alternative scope of licence may apply to signatories of the STM Permissions Guidelines, as amended from time to time.

3. Duration of Licence

3. 1. A licence for is valid from the date of purchase ('Licence Date') at the end of the relevant period in the below table:

Scope of Licence	Duration of Licence
Post on a website	12 months
Presentations	12 months
Books and journals	Lifetime of the edition in the language purchased

4. Acknowledgement

4. 1. The Licensor's permission must be acknowledged next to the Licenced Material in print. In electronic form, this acknowledgement must be visible at the same time as the figures/tables/illustrations or abstract, and must be hyperlinked to the journal/book's homepage. Our required acknowledgement format is in the Appendix below.

5. Restrictions on use

5. 1. Use of the Licensed Material may be permitted for incidental promotional use and minor editing privileges e.g. minor adaptations of single figures, changes of format, colour and/or style where the adaptation is credited as set out in Appendix 1 below. Any other changes including but not limited to, cropping, adapting, omitting material that

affect the meaning, intention or moral rights of the author are strictly prohibited.

5. 2. You must not use any Licensed Material as part of any design or trademark.

5. 3. Licensed Material may be used in Open Access Publications (OAP) before publication by Springer Nature, but any Licensed Material must be removed from OAP sites prior to final publication.

6. Ownership of Rights

6. 1. Licensed Material remains the property of either Licensor or the relevant third party and any rights not explicitly granted herein are expressly reserved.

7. Warranty

IN NO EVENT SHALL LICENSOR BE LIABLE TO YOU OR ANY OTHER PARTY OR ANY OTHER PERSON OR FOR ANY SPECIAL, CONSEQUENTIAL, INCIDENTAL OR INDIRECT DAMAGES, HOWEVER CAUSED, ARISING OUT OF OR IN CONNECTION WITH THE DOWNLOADING, VIEWING OR USE OF THE MATERIALS REGARDLESS OF THE FORM OF ACTION, WHETHER FOR BREACH OF CONTRACT, BREACH OF WARRANTY, TORT, NEGLIGENCE, INFRINGEMENT OR OTHERWISE (INCLUDING, WITHOUT LIMITATION, DAMAGES BASED ON LOSS OF PROFITS, DATA, FILES, USE, BUSINESS OPPORTUNITY OR CLAIMS OF THIRD PARTIES), AND
WHETHER OR NOT THE PARTY HAS BEEN ADVISED OF THE POSSIBILITY OF SUCH DAMAGES. THIS LIMITATION SHALL APPLY NOTWITHSTANDING ANY FAILURE OF ESSENTIAL PURPOSE OF ANY LIMITED REMEDY PROVIDED HEREIN.

8. Limitations

8. 1. ***BOOKS ONLY:*** Where **'reuse in a dissertation/thesis'** has been selected the following terms apply: Print rights of the final author's accepted manuscript (for clarity, NOT the published version) for up to 100 copies, electronic rights for use only on a personal website or institutional repository as defined by the Sherpa guideline (www.sherpa.ac.uk/romeo/).

8. 2. For content reuse requests that qualify for permission under the STM Permissions Guidelines, which may be updated from time to time, the STM Permissions Guidelines supersede the terms and conditions contained in this licence.

9. Termination and Cancellation

9. 1. Licences will expire after the period shown in Clause 3 (above).

9. 2. Licensee reserves the right to terminate the Licence in the event that payment is not received in full or if there has been a breach of this agreement by you.

Appendix 1 — Acknowledgements:

For Journal Content:
Reprinted by permission from [**the Licensor**]: [**Journal Publisher** (e.g. Nature/Springer/Palgrave)] [**JOURNAL NAME**] [**REFERENCE CITATION** (Article name, Author(s) Name), [**COPYRIGHT**] (year of publication)

For **Advance Online Publication papers:**
Reprinted by permission from [**the Licensor**]: [**Journal Publisher** (e.g. Nature/Springer/Palgrave)] [**JOURNAL NAME**] [**REFERENCE CITATION** (Article name, Author(s) Name), [**COPYRIGHT**] (year of publication), advance online publication, day month year (doi: 10.1038/sj.[JOURNAL ACRONYM].)

For Adaptations/Translations:
Adapted/Translated by permission from [**the Licensor**]: [**Journal Publisher** (e.g. Nature/Springer/Palgrave)] [**JOURNAL NAME**] [**REFERENCE CITATION** (Article name, Author(s) Name), [**COPYRIGHT**] (year of publication)

Note: For any republication from the British Journal of Cancer, the following credit line style applies:

Reprinted/adapted/translated by permission from [**the Licensor**]: on behalf of Cancer Research UK: : [**Journal Publisher** (e.g. Nature/Springer/Palgrave)] [**JOURNAL NAME**] [**REFERENCE CITATION** (Article name, Author(s) Name), [**COPYRIGHT]** (year of publication)

For **Advance Online Publication** papers:
Reprinted by permission from The [**the Licensor**]: on behalf of Cancer Research UK: [**Journal Publisher** (e.g. Nature/Springer/Palgrave)] [**JOURNAL NAME**] [**REFERENCE CITATION** (Article name, Author(s) Name), [**COPYRIGHT**] (year of publication), advance online publication, day month year (doi: 10.1038/sj.[JOURNAL ACRONYM])

For Book content:
Reprinted/adapted by permission from [**the Licensor**]: [**Book Publisher** (e.g. Palgrave Macmillan, Springer etc) [**Book Title**] by [**Book author**(s)] [**COPYRIGHT**] (year of publication)

Other Conditions:

Version 1.3

Questions? customercare@copyright.com or +1-855-239-3415 (toll free in the US) or +1-978-646-2777.

JOHN WILEY AND SONS LICENSE
TERMS AND CONDITIONS

Jul 09, 2022

This Agreement between Technical University Munich -- Sebastian Weishäupl ("You") and John Wiley and Sons ("John Wiley and Sons") consists of your license details and the terms and conditions provided by John Wiley and Sons and Copyright Clearance Center.

License Number	5344880823430
License date	Jul 09, 2022
Licensed Content Publisher	John Wiley and Sons
Licensed Content Publication	Angewandte Chemie International Edition
Licensed Content Title	Multi-Photon Absorption in Metal–Organic Frameworks
Licensed Content Author	Roland A. Fischer, Karsten Reuter, Marek Samoć, et al
Licensed Content Date	Oct 24, 2017
Licensed Content Volume	56
Licensed Content Issue	46
Licensed Content Pages	6
Type of use	Dissertation/Thesis
Requestor type	University/Academic

Format	Print and electronic
Portion	Figure/table
Number of figures/tables	1
Will you be translating?	No
Title	Chromophore-based Coordination Polymers (CPs) as Materials for Optical Applications
Institution name	Technical University of Munich
Expected presentation date	Sep 2022
Portions	Figure 2+3
Requestor Location	Technical University Munich Lichtenbergstr. 4 Garching, Bayern 85748 Germany Attn: Technical University Munich
Publisher Tax ID	EU826007151
Total	0.00 EUR
Terms and Conditions	

TERMS AND CONDITIONS

This copyrighted material is owned by or exclusively licensed to John Wiley & Sons, Inc. or one of its group companies (each a"Wiley Company") or handled on behalf of a society with which a Wiley Company has exclusive publishing rights in relation to a particular work (collectively "WILEY"). By clicking "accept" in connection with completing this licensing transaction, you agree that the following terms and conditions apply to this transaction (along with the billing and payment terms and conditions established by the Copyright Clearance Center Inc., ("CCC's Billing and Payment terms and conditions"), at the time that you opened your RightsLink account (these are available at any time at http://myaccount.copyright.com).

Terms and Conditions

- The materials you have requested permission to reproduce or reuse (the "Wiley Materials") are protected by copyright.

- You are hereby granted a personal, non-exclusive, non-sub licensable (on a stand-alone basis), non-transferable, worldwide, limited license to reproduce the Wiley Materials for the purpose specified in the licensing process. This license, **and any CONTENT (PDF or image file) purchased as part of your order,** is for a one-time use only and limited to any maximum distribution number specified in the license. The first instance of republication or reuse granted by this license must be completed within two years of the date of the grant of this license (although copies prepared before the end date may be distributed thereafter). The Wiley Materials shall not be used in any other manner or for any other purpose, beyond what is granted in the license. Permission is granted subject to an appropriate acknowledgement given to the author, title of the material/book/journal and the publisher. You shall also duplicate the copyright notice that appears in the Wiley publication in your use of the Wiley Material. Permission is also granted on the understanding that nowhere in the text is a previously published source acknowledged for all or part of this Wiley Material. Any third party content is expressly excluded from this permission.

- With respect to the Wiley Materials, all rights are reserved. Except as expressly granted by the terms of the license, no part of the Wiley Materials may be copied, modified, adapted (except for minor reformatting required by the new Publication), translated, reproduced, transferred or distributed, in any form or by any means, and no derivative works may be made based on the Wiley Materials without the prior permission of the respective copyright owner.**For STM Signatory Publishers clearing permission under the terms of the STM Permissions Guidelines only, the terms of the license are extended to include subsequent editions and for editions in other languages, provided such editions are for the work as a whole in situ and does not involve the separate exploitation of the permitted figures or extracts,** You may not alter, remove or suppress in any manner any copyright, trademark or other notices displayed by the Wiley Materials. You may not license, rent, sell, loan, lease, pledge, offer as security, transfer or assign the Wiley Materials on a stand-alone basis, or any of the rights granted to you hereunder to any other person.

- The Wiley Materials and all of the intellectual property rights therein shall at all times remain the exclusive property of John Wiley & Sons Inc, the Wiley Companies, or their respective licensors, and your interest therein is only that of having possession of and the right to reproduce the Wiley Materials pursuant to Section 2 herein during the continuance of this Agreement. You agree that you own no right, title or interest in or to the Wiley Materials or any of the intellectual property rights therein. You shall have no rights hereunder other than the license as provided for above in Section 2. No right, license or interest to any trademark, trade name, service mark or other branding ("Marks") of WILEY or its licensors is granted hereunder, and you agree that you shall not assert any such right, license or interest with respect thereto

- NEITHER WILEY NOR ITS LICENSORS MAKES ANY WARRANTY OR REPRESENTATION OF ANY KIND TO YOU OR ANY THIRD PARTY, EXPRESS, IMPLIED OR STATUTORY, WITH RESPECT TO THE MATERIALS OR THE ACCURACY OF ANY INFORMATION CONTAINED IN THE MATERIALS, INCLUDING, WITHOUT LIMITATION, ANY IMPLIED WARRANTY OF MERCHANTABILITY, ACCURACY, SATISFACTORY QUALITY, FITNESS FOR A PARTICULAR PURPOSE, USABILITY, INTEGRATION OR NON-INFRINGEMENT AND ALL SUCH WARRANTIES ARE HEREBY EXCLUDED BY WILEY AND ITS LICENSORS AND WAIVED

BY YOU.

- WILEY shall have the right to terminate this Agreement immediately upon breach of this Agreement by you.
- You shall indemnify, defend and hold harmless WILEY, its Licensors and their respective directors, officers, agents and employees, from and against any actual or threatened claims, demands, causes of action or proceedings arising from any breach of this Agreement by you.
- IN NO EVENT SHALL WILEY OR ITS LICENSORS BE LIABLE TO YOU OR ANY OTHER PARTY OR ANY OTHER PERSON OR ENTITY FOR ANY SPECIAL, CONSEQUENTIAL, INCIDENTAL, INDIRECT, EXEMPLARY OR PUNITIVE DAMAGES, HOWEVER CAUSED, ARISING OUT OF OR IN CONNECTION WITH THE DOWNLOADING, PROVISIONING, VIEWING OR USE OF THE MATERIALS REGARDLESS OF THE FORM OF ACTION, WHETHER FOR BREACH OF CONTRACT, BREACH OF WARRANTY, TORT, NEGLIGENCE, INFRINGEMENT OR OTHERWISE (INCLUDING, WITHOUT LIMITATION, DAMAGES BASED ON LOSS OF PROFITS, DATA, FILES, USE, BUSINESS OPPORTUNITY OR CLAIMS OF THIRD PARTIES), AND WHETHER OR NOT THE PARTY HAS BEEN ADVISED OF THE POSSIBILITY OF SUCH DAMAGES. THIS LIMITATION SHALL APPLY NOTWITHSTANDING ANY FAILURE OF ESSENTIAL PURPOSE OF ANY LIMITED REMEDY PROVIDED HEREIN.
- Should any provision of this Agreement be held by a court of competent jurisdiction to be illegal, invalid, or unenforceable, that provision shall be deemed amended to achieve as nearly as possible the same economic effect as the original provision, and the legality, validity and enforceability of the remaining provisions of this Agreement shall not be affected or impaired thereby.
- The failure of either party to enforce any term or condition of this Agreement shall not constitute a waiver of either party's right to enforce each and every term and condition of this Agreement. No breach under this agreement shall be deemed waived or excused by either party unless such waiver or consent is in writing signed by the party granting such waiver or consent. The waiver by or consent of a party to a breach of any provision of this Agreement shall not operate or be construed as a waiver of or consent to any other or subsequent breach by such other party.
- This Agreement may not be assigned (including by operation of law or otherwise) by you without WILEY's prior written consent.
- Any fee required for this permission shall be non-refundable after thirty (30) days from receipt by the CCC.
- These terms and conditions together with CCC's Billing and Payment terms and conditions (which are incorporated herein) form the entire agreement between you and WILEY concerning this licensing transaction and (in the absence of fraud) supersedes all prior agreements and representations of the parties, oral or written. This Agreement may not be amended except in writing signed by both parties. This Agreement shall be binding upon and inure to the benefit of the parties' successors, legal representatives, and authorized assigns.
- In the event of any conflict between your obligations established by these terms and conditions and those established by CCC's Billing and Payment terms and conditions, these terms and conditions shall prevail.

- WILEY expressly reserves all rights not specifically granted in the combination of (i) the license details provided by you and accepted in the course of this licensing transaction, (ii) these terms and conditions and (iii) CCC's Billing and Payment terms and conditions.

- This Agreement will be void if the Type of Use, Format, Circulation, or Requestor Type was misrepresented during the licensing process.

- This Agreement shall be governed by and construed in accordance with the laws of the State of New York, USA, without regards to such state's conflict of law rules. Any legal action, suit or proceeding arising out of or relating to these Terms and Conditions or the breach thereof shall be instituted in a court of competent jurisdiction in New York County in the State of New York in the United States of America and each party hereby consents and submits to the personal jurisdiction of such court, waives any objection to venue in such court and consents to service of process by registered or certified mail, return receipt requested, at the last known address of such party.

WILEY OPEN ACCESS TERMS AND CONDITIONS

Wiley Publishes Open Access Articles in fully Open Access Journals and in Subscription journals offering Online Open. Although most of the fully Open Access journals publish open access articles under the terms of the Creative Commons Attribution (CC BY) License only, the subscription journals and a few of the Open Access Journals offer a choice of Creative Commons Licenses. The license type is clearly identified on the article.

The Creative Commons Attribution License

The Creative Commons Attribution License (CC-BY) allows users to copy, distribute and transmit an article, adapt the article and make commercial use of the article. The CC-BY license permits commercial and non-

Creative Commons Attribution Non-Commercial License

The Creative Commons Attribution Non-Commercial (CC-BY-NC)License permits use, distribution and reproduction in any medium, provided the original work is properly cited and is not used for commercial purposes.(see below)

Creative Commons Attribution-Non-Commercial-NoDerivs License

The Creative Commons Attribution Non-Commercial-NoDerivs License (CC-BY-NC-ND) permits use, distribution and reproduction in any medium, provided the original work is properly cited, is not used for commercial purposes and no modifications or adaptations are made. (see below)

Use by commercial "for-profit" organizations

Use of Wiley Open Access articles for commercial, promotional, or marketing purposes requires further explicit permission from Wiley and will be subject to a fee.

Further details can be found on Wiley Online Library
http://olabout.wiley.com/WileyCDA/Section/id-410895.html

Other Terms and Conditions:

v1.10 Last updated September 2015

Questions? customercare@copyright.com or +1-855-239-3415 (toll free in the US) or +1-978-646-2777.

Controlling Multiphoton Absorption Efficiency by Chromophore Packing in Metal–Organic Frameworks

Author: David C. Mayer, Aurora Manzi, Raghavender Medishetty, et al
Publication: Journal of the American Chemical Society
Publisher: American Chemical Society
Date: Jul 1, 2019

JOHN WILEY AND SONS LICENSE
TERMS AND CONDITIONS

Jul 09, 2022

This Agreement between Technical University Munich -- Sebastian Weishäupl ("You") and John Wiley and Sons ("John Wiley and Sons") consists of your license details and the terms and conditions provided by John Wiley and Sons and Copyright Clearance Center.

License Number	5344881033468
License date	Jul 09, 2022
Licensed Content Publisher	John Wiley and Sons
Licensed Content Publication	Angewandte Chemie International Edition
Licensed Content Title	Highly Efficient Multiphoton Absorption of Zinc-AIEgen Metal–Organic Frameworks
Licensed Content Author	Naifang Liu, Zhihui Chen, Wenxuan Fan, et al
Licensed Content Date	Feb 10, 2022
Licensed Content Volume	61
Licensed Content Issue	12
Licensed Content Pages	7
Type of use	Dissertation/Thesis
Requestor type	University/Academic

Format	Print and electronic
Portion	Figure/table
Number of figures/tables	1
Will you be translating?	No
Title	Chromophore-based Coordination Polymers (CPs) as Materials for Optical Applications
Institution name	Technical University of Munich
Expected presentation date	Sep 2022
Portions	Figure 1+3
Requestor Location	Technical University Munich Lichtenbergstr. 4 Garching, Bayern 85748 Germany Attn: Technical University Munich
Publisher Tax ID	EU826007151
Total	0.00 EUR
Terms and Conditions	

TERMS AND CONDITIONS

This copyrighted material is owned by or exclusively licensed to John Wiley & Sons, Inc. or one of its group companies (each a"Wiley Company") or handled on behalf of a society with which a Wiley Company has exclusive publishing rights in relation to a particular work (collectively "WILEY"). By clicking "accept" in connection with completing this licensing transaction, you agree that the following terms and conditions apply to this transaction (along with the billing and payment terms and conditions established by the Copyright Clearance Center Inc., ("CCC's Billing and Payment terms and conditions"), at the time that you opened your RightsLink account (these are available at any time at http://myaccount.copyright.com).

Terms and Conditions

- The materials you have requested permission to reproduce or reuse (the "Wiley Materials") are protected by copyright.

- You are hereby granted a personal, non-exclusive, non-sub licensable (on a stand-alone basis), non-transferable, worldwide, limited license to reproduce the Wiley Materials for the purpose specified in the licensing process. This license, **and any CONTENT (PDF or image file) purchased as part of your order,** is for a one-time use only and limited to any maximum distribution number specified in the license. The first instance of republication or reuse granted by this license must be completed within two years of the date of the grant of this license (although copies prepared before the end date may be distributed thereafter). The Wiley Materials shall not be used in any other manner or for any other purpose, beyond what is granted in the license. Permission is granted subject to an appropriate acknowledgement given to the author, title of the material/book/journal and the publisher. You shall also duplicate the copyright notice that appears in the Wiley publication in your use of the Wiley Material. Permission is also granted on the understanding that nowhere in the text is a previously published source acknowledged for all or part of this Wiley Material. Any third party content is expressly excluded from this permission.

- With respect to the Wiley Materials, all rights are reserved. Except as expressly granted by the terms of the license, no part of the Wiley Materials may be copied, modified, adapted (except for minor reformatting required by the new Publication), translated, reproduced, transferred or distributed, in any form or by any means, and no derivative works may be made based on the Wiley Materials without the prior permission of the respective copyright owner.**For STM Signatory Publishers clearing permission under the terms of the STM Permissions Guidelines only, the terms of the license are extended to include subsequent editions and for editions in other languages, provided such editions are for the work as a whole in situ and does not involve the separate exploitation of the permitted figures or extracts,** You may not alter, remove or suppress in any manner any copyright, trademark or other notices displayed by the Wiley Materials. You may not license, rent, sell, loan, lease, pledge, offer as security, transfer or assign the Wiley Materials on a stand-alone basis, or any of the rights granted to you hereunder to any other person.

- The Wiley Materials and all of the intellectual property rights therein shall at all times remain the exclusive property of John Wiley & Sons Inc, the Wiley Companies, or their respective licensors, and your interest therein is only that of having possession of and the right to reproduce the Wiley Materials pursuant to Section 2 herein during the continuance of this Agreement. You agree that you own no right, title or interest in or to the Wiley Materials or any of the intellectual property rights therein. You shall have no rights hereunder other than the license as provided for above in Section 2. No right, license or interest to any trademark, trade name, service mark or other branding ("Marks") of WILEY or its licensors is granted hereunder, and you agree that you shall not assert any such right, license or interest with respect thereto

- NEITHER WILEY NOR ITS LICENSORS MAKES ANY WARRANTY OR REPRESENTATION OF ANY KIND TO YOU OR ANY THIRD PARTY, EXPRESS, IMPLIED OR STATUTORY, WITH RESPECT TO THE MATERIALS OR THE ACCURACY OF ANY INFORMATION CONTAINED IN THE MATERIALS, INCLUDING, WITHOUT LIMITATION, ANY IMPLIED WARRANTY OF MERCHANTABILITY, ACCURACY, SATISFACTORY QUALITY, FITNESS FOR A PARTICULAR PURPOSE, USABILITY, INTEGRATION OR NON-INFRINGEMENT AND ALL SUCH WARRANTIES ARE HEREBY EXCLUDED BY WILEY AND ITS LICENSORS AND WAIVED

BY YOU.

- WILEY shall have the right to terminate this Agreement immediately upon breach of this Agreement by you.
- You shall indemnify, defend and hold harmless WILEY, its Licensors and their respective directors, officers, agents and employees, from and against any actual or threatened claims, demands, causes of action or proceedings arising from any breach of this Agreement by you.
- IN NO EVENT SHALL WILEY OR ITS LICENSORS BE LIABLE TO YOU OR ANY OTHER PARTY OR ANY OTHER PERSON OR ENTITY FOR ANY SPECIAL, CONSEQUENTIAL, INCIDENTAL, INDIRECT, EXEMPLARY OR PUNITIVE DAMAGES, HOWEVER CAUSED, ARISING OUT OF OR IN CONNECTION WITH THE DOWNLOADING, PROVISIONING, VIEWING OR USE OF THE MATERIALS REGARDLESS OF THE FORM OF ACTION, WHETHER FOR BREACH OF CONTRACT, BREACH OF WARRANTY, TORT, NEGLIGENCE, INFRINGEMENT OR OTHERWISE (INCLUDING, WITHOUT LIMITATION, DAMAGES BASED ON LOSS OF PROFITS, DATA, FILES, USE, BUSINESS OPPORTUNITY OR CLAIMS OF THIRD PARTIES), AND WHETHER OR NOT THE PARTY HAS BEEN ADVISED OF THE POSSIBILITY OF SUCH DAMAGES. THIS LIMITATION SHALL APPLY NOTWITHSTANDING ANY FAILURE OF ESSENTIAL PURPOSE OF ANY LIMITED REMEDY PROVIDED HEREIN.
- Should any provision of this Agreement be held by a court of competent jurisdiction to be illegal, invalid, or unenforceable, that provision shall be deemed amended to achieve as nearly as possible the same economic effect as the original provision, and the legality, validity and enforceability of the remaining provisions of this Agreement shall not be affected or impaired thereby.
- The failure of either party to enforce any term or condition of this Agreement shall not constitute a waiver of either party's right to enforce each and every term and condition of this Agreement. No breach under this agreement shall be deemed waived or excused by either party unless such waiver or consent is in writing signed by the party granting such waiver or consent. The waiver by or consent of a party to a breach of any provision of this Agreement shall not operate or be construed as a waiver of or consent to any other or subsequent breach by such other party.
- This Agreement may not be assigned (including by operation of law or otherwise) by you without WILEY's prior written consent.
- Any fee required for this permission shall be non-refundable after thirty (30) days from receipt by the CCC.
- These terms and conditions together with CCC's Billing and Payment terms and conditions (which are incorporated herein) form the entire agreement between you and WILEY concerning this licensing transaction and (in the absence of fraud) supersedes all prior agreements and representations of the parties, oral or written. This Agreement may not be amended except in writing signed by both parties. This Agreement shall be binding upon and inure to the benefit of the parties' successors, legal representatives, and authorized assigns.
- In the event of any conflict between your obligations established by these terms and conditions and those established by CCC's Billing and Payment terms and conditions, these terms and conditions shall prevail.

- WILEY expressly reserves all rights not specifically granted in the combination of (i) the license details provided by you and accepted in the course of this licensing transaction, (ii) these terms and conditions and (iii) CCC's Billing and Payment terms and conditions.

- This Agreement will be void if the Type of Use, Format, Circulation, or Requestor Type was misrepresented during the licensing process.

- This Agreement shall be governed by and construed in accordance with the laws of the State of New York, USA, without regards to such state's conflict of law rules. Any legal action, suit or proceeding arising out of or relating to these Terms and Conditions or the breach thereof shall be instituted in a court of competent jurisdiction in New York County in the State of New York in the United States of America and each party hereby consents and submits to the personal jurisdiction of such court, waives any objection to venue in such court and consents to service of process by registered or certified mail, return receipt requested, at the last known address of such party.

WILEY OPEN ACCESS TERMS AND CONDITIONS

Wiley Publishes Open Access Articles in fully Open Access Journals and in Subscription journals offering Online Open. Although most of the fully Open Access journals publish open access articles under the terms of the Creative Commons Attribution (CC BY) License only, the subscription journals and a few of the Open Access Journals offer a choice of Creative Commons Licenses. The license type is clearly identified on the article.

The Creative Commons Attribution License

The Creative Commons Attribution License (CC-BY) allows users to copy, distribute and transmit an article, adapt the article and make commercial use of the article. The CC-BY license permits commercial and non-

Creative Commons Attribution Non-Commercial License

The Creative Commons Attribution Non-Commercial (CC-BY-NC)License permits use, distribution and reproduction in any medium, provided the original work is properly cited and is not used for commercial purposes.(see below)

Creative Commons Attribution-Non-Commercial-NoDerivs License

The Creative Commons Attribution Non-Commercial-NoDerivs License (CC-BY-NC-ND) permits use, distribution and reproduction in any medium, provided the original work is properly cited, is not used for commercial purposes and no modifications or adaptations are made. (see below)

Use by commercial "for-profit" organizations

Use of Wiley Open Access articles for commercial, promotional, or marketing purposes requires further explicit permission from Wiley and will be subject to a fee.

Further details can be found on Wiley Online Library
http://olabout.wiley.com/WileyCDA/Section/id-410895.html

Other Terms and Conditions:

v1.10 Last updated September 2015

Questions? customercare@copyright.com or +1-855-239-3415 (toll free in the US) or +1-978-646-2777.

Keywords: Calvin–Benson cycle, CO_2 fixation, thioredoxin, glutaredoxin, glutathionylation, nitrosylation, photosynthesis, redox regulation

Citation: Michelet L, Zaffagnini M, Morisse S, Sparla F, Pérez-Pérez ME, Francia F, Danon A, Marchand CH, Fermani S, Trost P, and Lemaire SD (2013) Redox regulation of the Calvin–Benson cycle: something old, something new. *Front. Plant Sci.* **4**:470. doi: 10.3389/fpls.2013.00470

Received: 18 September 2013; **Accepted:** 30 October 2013;
Published online: 25 November 2013.

Edited by:
Nicolas Rouhier (http://www.frontiersin.org/people/u/62631), Université de Lorraine, France

Reviewed by:
Renate Scheibe (http://www.frontiersin.org/people/u/54527), University of Osnabrueck, Germany
David B. Knaff (http://www.frontiersin.org/people/u/113252), Texas Tech University, USA

***Correspondence:** Paolo Trost, Laboratory of Plant Redox Biology, Department of Pharmacy and Biotechnology (FaBiT), University of Bologna, Via Irnerio 42, 40126 Bologna, Italy e-mail: paolo.trost@unibo.it;
Stéphane D. Lemaire, Laboratoire de Biologie Moléculaire et Cellulaire des Eucaryotes, FRE3354 Centre National de la Recherche Scientifique, Institut de Biologie Physico-Chimique, Université Pierre et Marie Curie, 13 rue Pierre et Marie Curie, 75005 Paris, France e-mail: stephane.lemaire@ibpc.fr

JOHN WILEY AND SONS LICENSE
TERMS AND CONDITIONS

Jul 09, 2022

This Agreement between Technical University Munich -- Sebastian Weishäupl ("You") and John Wiley and Sons ("John Wiley and Sons") consists of your license details and the terms and conditions provided by John Wiley and Sons and Copyright Clearance Center.

License Number	5344890433754
License date	Jul 09, 2022
Licensed Content Publisher	John Wiley and Sons
Licensed Content Publication	Chemistry - A European Journal
Licensed Content Title	Metal–Organic Frameworks as a Versatile Tool To Study and Model Energy Transfer Processes
Licensed Content Author	Natalia B. Shustova, Derek E. Williams
Licensed Content Date	Aug 27, 2015
Licensed Content Volume	21
Licensed Content Issue	44
Licensed Content Pages	6
Type of use	Dissertation/Thesis
Requestor type	University/Academic

Format	Print and electronic
Portion	Figure/table
Number of figures/tables	2
Will you be translating?	No
Title	Chromophore-based Coordination Polymers (CPs) as Materials for Optical Applications
Institution name	Technical University of Munich
Expected presentation date	Sep 2022
Portions	Figure 1+3
Requestor Location	Technical University Munich Lichtenbergstr. 4 Garching, Bayern 85748 Germany Attn: Technical University Munich
Publisher Tax ID	EU826007151
Total	0.00 EUR

Terms and Conditions

TERMS AND CONDITIONS

This copyrighted material is owned by or exclusively licensed to John Wiley & Sons, Inc. or one of its group companies (each a"Wiley Company") or handled on behalf of a society with which a Wiley Company has exclusive publishing rights in relation to a particular work (collectively "WILEY"). By clicking "accept" in connection with completing this licensing transaction, you agree that the following terms and conditions apply to this transaction (along with the billing and payment terms and conditions established by the Copyright Clearance Center Inc., ("CCC's Billing and Payment terms and conditions"), at the time that

you opened your RightsLink account (these are available at any time at http://myaccount.copyright.com).

Terms and Conditions

- The materials you have requested permission to reproduce or reuse (the "Wiley Materials") are protected by copyright.

- You are hereby granted a personal, non-exclusive, non-sub licensable (on a stand-alone basis), non-transferable, worldwide, limited license to reproduce the Wiley Materials for the purpose specified in the licensing process. This license, **and any CONTENT (PDF or image file) purchased as part of your order,** is for a one-time use only and limited to any maximum distribution number specified in the license. The first instance of republication or reuse granted by this license must be completed within two years of the date of the grant of this license (although copies prepared before the end date may be distributed thereafter). The Wiley Materials shall not be used in any other manner or for any other purpose, beyond what is granted in the license. Permission is granted subject to an appropriate acknowledgement given to the author, title of the material/book/journal and the publisher. You shall also duplicate the copyright notice that appears in the Wiley publication in your use of the Wiley Material. Permission is also granted on the understanding that nowhere in the text is a previously published source acknowledged for all or part of this Wiley Material. Any third party content is expressly excluded from this permission.

- With respect to the Wiley Materials, all rights are reserved. Except as expressly granted by the terms of the license, no part of the Wiley Materials may be copied, modified, adapted (except for minor reformatting required by the new Publication), translated, reproduced, transferred or distributed, in any form or by any means, and no derivative works may be made based on the Wiley Materials without the prior permission of the respective copyright owner.**For STM Signatory Publishers clearing permission under the terms of the STM Permissions Guidelines only, the terms of the license are extended to include subsequent editions and for editions in other languages, provided such editions are for the work as a whole in situ and does not involve the separate exploitation of the permitted figures or extracts,** You may not alter, remove or suppress in any manner any copyright, trademark or other notices displayed by the Wiley Materials. You may not license, rent, sell, loan, lease, pledge, offer as security, transfer or assign the Wiley Materials on a stand-alone basis, or any of the rights granted to you hereunder to any other person.

- The Wiley Materials and all of the intellectual property rights therein shall at all times remain the exclusive property of John Wiley & Sons Inc, the Wiley Companies, or their respective licensors, and your interest therein is only that of having possession of and the right to reproduce the Wiley Materials pursuant to Section 2 herein during the continuance of this Agreement. You agree that you own no right, title or interest in or to the Wiley Materials or any of the intellectual property rights therein. You shall have no rights hereunder other than the license as provided for above in Section 2. No right, license or interest to any trademark, trade name, service mark or other branding ("Marks") of WILEY or its licensors is granted hereunder, and you agree that you shall not assert any such right, license or interest with respect thereto

- NEITHER WILEY NOR ITS LICENSORS MAKES ANY WARRANTY OR REPRESENTATION OF ANY KIND TO YOU OR ANY THIRD PARTY, EXPRESS, IMPLIED OR STATUTORY, WITH RESPECT TO THE MATERIALS OR THE ACCURACY OF ANY INFORMATION CONTAINED IN THE MATERIALS, INCLUDING, WITHOUT LIMITATION, ANY IMPLIED WARRANTY OF MERCHANTABILITY, ACCURACY, SATISFACTORY QUALITY, FITNESS FOR A PARTICULAR PURPOSE, USABILITY,

INTEGRATION OR NON-INFRINGEMENT AND ALL SUCH WARRANTIES ARE HEREBY EXCLUDED BY WILEY AND ITS LICENSORS AND WAIVED BY YOU.

- WILEY shall have the right to terminate this Agreement immediately upon breach of this Agreement by you.
- You shall indemnify, defend and hold harmless WILEY, its Licensors and their respective directors, officers, agents and employees, from and against any actual or threatened claims, demands, causes of action or proceedings arising from any breach of this Agreement by you.
- IN NO EVENT SHALL WILEY OR ITS LICENSORS BE LIABLE TO YOU OR ANY OTHER PARTY OR ANY OTHER PERSON OR ENTITY FOR ANY SPECIAL, CONSEQUENTIAL, INCIDENTAL, INDIRECT, EXEMPLARY OR PUNITIVE DAMAGES, HOWEVER CAUSED, ARISING OUT OF OR IN CONNECTION WITH THE DOWNLOADING, PROVISIONING, VIEWING OR USE OF THE MATERIALS REGARDLESS OF THE FORM OF ACTION, WHETHER FOR BREACH OF CONTRACT, BREACH OF WARRANTY, TORT, NEGLIGENCE, INFRINGEMENT OR OTHERWISE (INCLUDING, WITHOUT LIMITATION, DAMAGES BASED ON LOSS OF PROFITS, DATA, FILES, USE, BUSINESS OPPORTUNITY OR CLAIMS OF THIRD PARTIES), AND WHETHER OR NOT THE PARTY HAS BEEN ADVISED OF THE POSSIBILITY OF SUCH DAMAGES. THIS LIMITATION SHALL APPLY NOTWITHSTANDING ANY FAILURE OF ESSENTIAL PURPOSE OF ANY LIMITED REMEDY PROVIDED HEREIN.
- Should any provision of this Agreement be held by a court of competent jurisdiction to be illegal, invalid, or unenforceable, that provision shall be deemed amended to achieve as nearly as possible the same economic effect as the original provision, and the legality, validity and enforceability of the remaining provisions of this Agreement shall not be affected or impaired thereby.
- The failure of either party to enforce any term or condition of this Agreement shall not constitute a waiver of either party's right to enforce each and every term and condition of this Agreement. No breach under this agreement shall be deemed waived or excused by either party unless such waiver or consent is in writing signed by the party granting such waiver or consent. The waiver by or consent of a party to a breach of any provision of this Agreement shall not operate or be construed as a waiver of or consent to any other or subsequent breach by such other party.
- This Agreement may not be assigned (including by operation of law or otherwise) by you without WILEY's prior written consent.
- Any fee required for this permission shall be non-refundable after thirty (30) days from receipt by the CCC.
- These terms and conditions together with CCC's Billing and Payment terms and conditions (which are incorporated herein) form the entire agreement between you and WILEY concerning this licensing transaction and (in the absence of fraud) supersedes all prior agreements and representations of the parties, oral or written. This Agreement may not be amended except in writing signed by both parties. This Agreement shall be binding upon and inure to the benefit of the parties' successors, legal representatives, and authorized assigns.
- In the event of any conflict between your obligations established by these terms and conditions and those established by CCC's Billing and Payment terms and conditions,

these terms and conditions shall prevail.

- WILEY expressly reserves all rights not specifically granted in the combination of (i) the license details provided by you and accepted in the course of this licensing transaction, (ii) these terms and conditions and (iii) CCC's Billing and Payment terms and conditions.
- This Agreement will be void if the Type of Use, Format, Circulation, or Requestor Type was misrepresented during the licensing process.
- This Agreement shall be governed by and construed in accordance with the laws of the State of New York, USA, without regards to such state's conflict of law rules. Any legal action, suit or proceeding arising out of or relating to these Terms and Conditions or the breach thereof shall be instituted in a court of competent jurisdiction in New York County in the State of New York in the United States of America and each party hereby consents and submits to the personal jurisdiction of such court, waives any objection to venue in such court and consents to service of process by registered or certified mail, return receipt requested, at the last known address of such party.

WILEY OPEN ACCESS TERMS AND CONDITIONS

Wiley Publishes Open Access Articles in fully Open Access Journals and in Subscription journals offering Online Open. Although most of the fully Open Access journals publish open access articles under the terms of the Creative Commons Attribution (CC BY) License only, the subscription journals and a few of the Open Access Journals offer a choice of Creative Commons Licenses. The license type is clearly identified on the article.

The Creative Commons Attribution License

The Creative Commons Attribution License (CC-BY) allows users to copy, distribute and transmit an article, adapt the article and make commercial use of the article. The CC-BY license permits commercial and non-

Creative Commons Attribution Non-Commercial License

The Creative Commons Attribution Non-Commercial (CC-BY-NC)License permits use, distribution and reproduction in any medium, provided the original work is properly cited and is not used for commercial purposes.(see below)

Creative Commons Attribution-Non-Commercial-NoDerivs License

The Creative Commons Attribution Non-Commercial-NoDerivs License (CC-BY-NC-ND) permits use, distribution and reproduction in any medium, provided the original work is properly cited, is not used for commercial purposes and no modifications or adaptations are made. (see below)

Use by commercial "for-profit" organizations

Use of Wiley Open Access articles for commercial, promotional, or marketing purposes requires further explicit permission from Wiley and will be subject to a fee.

Further details can be found on Wiley Online Library
http://olabout.wiley.com/WileyCDA/Section/id-410895.html

Other Terms and Conditions:

v1.10 Last updated September 2015

Questions? customercare@copyright.com or +1-855-239-3415 (toll free in the US) or +1-978-646-2777.

Rylene and Rylene Diimides: Comparison of Theoretical and Experimental Results and Prediction for High-Rylene Derivatives

Author: Xiaohong Zhao, Yushuai Xiong, Jie Ma, et al
Publication: The Journal of Physical Chemistry A
Publisher: American Chemical Society
Date: Sep 1, 2016

SPRINGER NATURE

A Potassium Metal-Organic Framework based on Perylene-3,4,9,10-tetracarboxylate as Sensing Layer for Humidity Actuators

Author: José Manuel Seco et al

Publication: Scientific Reports

Publisher: Springer Nature

Date: Sep 26, 2018

SPRINGER NATURE

Stable radical anions generated from a porous perylenediimide metal-organic framework for boosting near-infrared photothermal conversion

Author: Baozhong Lü et al

Publication: Nature Communications

Publisher: Springer Nature

Date: Feb 15, 2019

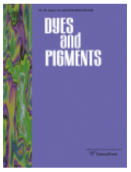

A nitrophenyl-carbazole based push-pull linker as a building block for non-linear optical active coordination polymers: A structural and photophysical study

Author:
Sebastian J. Weishäupl,David C. Mayer,Erling Thyrhaug,Jürgen Hauer,Alexander Pöthig,Roland A. Fischer

Publication: Dyes and Pigments
Publisher: Elsevier
Date: February 2021

Coordination Polymers Based on Carbazole-Derived Chromophore Linkers for Optimized Multiphoton Absorption: A Structural and Photophysical Study

Author: Sebastian J. Weishäupl, Yang Cui, Simon N. Deger, et al
Publication: Chemistry of Materials
Publisher: American Chemical Society
Date: Aug 1, 2022

Open Access Article

A Perylenediimide-Based Zinc-Coordination Polymer for Photosensitized Singlet-Oxygen Generation

by
Simon N. Deger (https://sciprofiles.com/profile/author/eWNFWHJmSTZERDVkSXg2ZDhqZEpZUjMrNEFpTmtLeFhJc1F0UEg
† (mailto:please_login),
Sebastian J. Weishäupl (https://sciprofiles.com/profile/author/ZlBvSzhzVG05dTc3Q0hXcTMyZEpmSHBkc0xuNHgwTVdKcW
† (mailto:please_login),

***Energies* (/journal/energies)**, EISSN 1996-1073, Published by MDPI **Disclaimer**

RSS (/rss/journal/energies) **Content Alert (/journal/energies/toc-alert)**

6.3 Complete List of Publications

6.3.1 Thesis based Publications

[1] **Weishäupl, S. J.**, Mayer, D. C., Thyrhaug, E.; Hauer, J., Pöthig, A., Fischer, R. A., A nitrophenyl-carbazole based push-pull linker as a building block for non-linear optical active coordination polymers: A structural and photophysical study. *Dyes and Pigments* **2021,** *186*, 109012.

[2] **Weishäupl, S. J.**†, Mayer, D. C.†, Cui, Y., Kumar, P., Oberhofer, H., Fischer, R. A., Hauer, J., Pöthig, A., Recent advances of multiphoton absorption in metal–organic frameworks. *Journal of Materials Chemistry C* **2022,** *10* (18), 6912-6934.

[3] Deger, S. N.†, **Weishäupl, S. J.**†, Pöthig, A., Fischer, R. A., A Perylenediimide-Based Zinc-Coordination Polymer for Photosensitized Singlet-Oxygen Generation. *Energies* **2022,** *15* (7), 2437.

[4] **S. J. Weishäupl**†, Y. Cui†, S. Deger, H. Syed, A. Pöthig, A. Ovsianikov, J. Hauer and R. A. Fischer, *Chemistry of Materials*, **2022**. *Submitted, under revision.*

6.3.2 Other Publications

[1] S. Guan, D. C. Mayer, C. Jandl, **S. J. Weishäupl**, A. Casini, A. Pöthig*, Investigation of Solvatomorphism and Its Photophysical Implications for Archetypal Trinuclear Au_3(1-Methylimidazolate)$_3$. *Molecules* **2021**, 26(15):4404.

6.3.3 Conference Contributions

[1] 31. Deutsche Zeolith Tagung, Dresden, Germany, March 2019, poster presentation: *Metal-organic Frameworks (MOFs) as materials for optical applications.*

[2] Tools for Chemical Bonding, Bremen, Germany, July 2019, poster presentation: *Metal-organic Frameworks (MOFs) as inorganic/organic hybrid materials for optical applications*.

[3] E-conversion conference, Venice, Italy, September 2019, poster presentation: *Metal-organic Frameworks (MOFs) as prospective hybrid materials in optical applications.*

[4] EuroMOF 2019, Paris, France, October 2019, poster presentation: *Metal-Organic frameworks as materials for nonlinear optical properties.*

7 References

1. Hecht, E., *Optics, EBook, Global Edition*. Pearson Education, Limited: Harlow, UNITED KINGDOM, 2016.

2. Sutherland, R. L., *Handbook of nonlinear optics*. CRC press: 2003.

3. Locharoenrat, K., *Linear and nonlinear optics: materials, properties, and applications*. Jenny Stanford Publishing: 2021.

4. Lehn, J.-M., *Supramolecular chemistry*. Vch: 1995.

5. James, S. L., Metal-organic frameworks. *Chemical Society Reviews* **2003,** *32* (5), 276-288.

6. Morsali, A.; Hashemi, L., Chapter Two - Nanoscale coordination polymers: Preparation, function and application. In *Advances in Inorganic Chemistry*, Ruiz-Molina, D.; van Eldik, R., Eds. Academic Press: 2020; Vol. 76, pp 33-72.

7. Kitagawa, S.; Noro, S., Coordination Polymers: Infinite Systems. In *Comprehensive Coordination Chemistry II*, 2004; Vol. 7, pp 231-261.

8. Robin, A. Y.; Fromm, K. M., Coordination polymer networks with O- and N-donors: What they are, why and how they are made. *Coordination Chemistry Reviews* **2006,** *250* (15), 2127-2157.

9. Valkunas, L., Abramavicius, D. and Mančal, T., Quantum States of Molecules and Aggregates. In *Molecular Excitation Dynamics and Relaxation*, 2013; pp 101-132.

10. Li, C., *Nonlinear optics*. Springer: 2017.

11. Boyd, R. W., 1.1 Introduction to Nonlinear Optics. In *Nonlinear Optics (3rd Edition)*, Elsevier.

12. Franken, P. A.; Hill, A. E.; Peters, C. W.; Weinreich, G., Generation of Optical Harmonics. *Physical Review Letters* **1961,** *7* (4), 118-119.

13. Maiman, T. H., Stimulated Optical Radiation in Ruby. *Nature* **1960,** *187* (4736), 493-494.

14. Munn, R. W.; Ironside, C., *Principles and applications of nonlinear optical materials*. Springer: 1993.

15. Li, R.; Wang, X.; Zhou, Y.; Zong, H.; Chen, M.; Sun, M., Advances in nonlinear optical microscopy for biophotonics. *Journal of Nanophotonics* **2018,** *12* (3), 033007.

16. Kumar, V.; Coluccelli, N.; Polli, D., Chapter 5 - Coherent Optical Spectroscopy/Microscopy and Applications. In *Molecular and Laser Spectroscopy*, Gupta, V. P., Ed. Elsevier: 2018; pp 87-115.

17. Erbe, A.; Nayak, S.; Chen, Y. H.; Niu, F.; Pander, M.; Tecklenburg, S.; Toparli, C., How to Probe Structure, Kinetics, and Dynamics at Complex Interfaces In Situ and Operando by Optical Spectroscopy. In *Encyclopedia of Interfacial Chemistry*, Wandelt, K., Ed. Elsevier: Oxford, 2018; pp 199-219.

18. Kaiser, W.; Garrett, C. G. B., Two-Photon Excitation in CaF2:Eu2+. *Physical Review Letters* **1961,** *7* (6), 229-231.

19. Shen, Y.-R., Principles of nonlinear optics. **1984**.

20. Boyd, R. W., *Nonlinear optics*. Academic press: 2020.

21. He, G. S.; Tan, L.-S.; Zheng, Q.; Prasad, P. N., Multiphoton Absorbing Materials: Molecular Designs, Characterizations, and Applications. *Chemical Reviews* **2008,** *108* (4), 1245-1330.

22. He, G. S. A. L., Song H, *Physics of Nonlinear Optics*. 2000.

23. Steiger, W.; Gruber, P.; Theiner, D.; Dobos, A.; Lunzer, M.; Van Hoorick, J.; Van Vlierberghe, S.; Liska, R.; Ovsianikov, A., Fully automated z-scan setup based on a tunable fs-oscillator. *Opt. Mater. Express* **2019,** *9* (9), 3567-3581.

24. Kuehne, A. J. C.; Gather, M. C., Organic Lasers: Recent Developments on Materials, Device Geometries, and Fabrication Techniques. *Chemical Reviews* **2016,** *116* (21), 12823-12864.

25. Medishetty, R.; Zaręba, J. K.; Mayer, D.; Samoć, M.; Fischer, R. A., Nonlinear optical properties, upconversion and lasing in metal–organic frameworks. *Chemical Society Reviews* **2017,** *46* (16), 4976-5004.

26. Weishäupl, S. J.; Mayer, D. C.; Cui, Y.; Kumar, P.; Oberhofer, H.; Fischer, R. A.; Hauer, J.; Pöthig, A., Recent advances of multiphoton absorption in metal–organic frameworks. *Journal of Materials Chemistry C* **2022,** *10* (18), 6912-6934.

27. Li, H.; Eddaoudi, M.; O'Keeffe, M.; Yaghi, O. M., Design and synthesis of an exceptionally stable and highly porous metal-organic framework. *Nature* **1999,** *402* (6759), 276-279.

28. Kuppler, R. J.; Timmons, D. J.; Fang, Q.-R.; Li, J.-R.; Makal, T. A.; Young, M. D.; Yuan, D.; Zhao, D.; Zhuang, W.; Zhou, H.-C., Potential applications of metal-organic frameworks. *Coordination Chemistry Reviews* **2009,** *253* (23), 3042-3066.

29. Li, H.; Li, L.; Lin, R.-B.; Zhou, W.; Zhang, Z.; Xiang, S.; Chen, B., Porous metal-organic frameworks for gas storage and separation: Status and challenges. *EnergyChem* **2019,** *1* (1), 100006.

30. Pascanu, V.; González Miera, G.; Inge, A. K.; Martín-Matute, B., Metal–Organic Frameworks as Catalysts for Organic Synthesis: A Critical Perspective. *Journal of the American Chemical Society* **2019,** *141* (18), 7223-7234.

31. Horcajada, P.; Gref, R.; Baati, T.; Allan, P. K.; Maurin, G.; Couvreur, P.; Férey, G.; Morris, R. E.; Serre, C., Metal–Organic Frameworks in Biomedicine. *Chemical Reviews* **2012,** *112* (2), 1232-1268.

32. Anik, Ü.; Timur, S.; Dursun, Z., Metal organic frameworks in electrochemical and optical sensing platforms: a review. *Microchimica Acta* **2019,** *186* (3), 196.

33. Zaręba, J. K.; Nyk, M.; Samoć, M., Nonlinear Optical Properties of Emerging Nano- and Microcrystalline Materials. *Advanced Optical Materials* **2021,** *9* (23), 2100216.

34. Fang, X.; Zong, B.; Mao, S., Metal–Organic Framework-Based Sensors for Environmental Contaminant Sensing. *Nano-Micro Letters* **2018,** *10* (4), 64.

35. Kreno, L. E.; Leong, K.; Farha, O. K.; Allendorf, M.; Van Duyne, R. P.; Hupp, J. T., Metal–Organic Framework Materials as Chemical Sensors. *Chemical Reviews* **2012,** *112* (2), 1105-1125.

36. Li, H.; Wang, K.; Sun, Y.; Lollar, C. T.; Li, J.; Zhou, H.-C., Recent advances in gas storage and separation using metal–organic frameworks. *Materials Today* **2018,** *21* (2), 108-121.

37. Alhumaimess, M. S., Metal–organic frameworks and their catalytic applications. *Journal of Saudi Chemical Society* **2020,** *24* (6), 461-473.

38. Yang, D.; Gates, B. C., Catalysis by Metal Organic Frameworks: Perspective and Suggestions for Future Research. *ACS Catalysis* **2019,** *9* (3), 1779-1798.

39. Karimi, M.; Mehrabadi, Z.; Farsadrooh, M.; Bafkary, R.; Derikvandi, H.; Hayati, P.; Mohammadi, K., Chapter 4 - Metal–organic framework. In *Interface Science and Technology*, Ghaedi, M., Ed. Elsevier: 2021; Vol. 33, pp 279-387.

40. Batten, S. R.; Champness, N. R.; Chen, X.-M.; Garcia-Martinez, J.; Kitagawa, S.; Öhrström, L.; O'Keeffe, M.; Suh, M. P.; Reedijk, J., Terminology of metal–organic frameworks and coordination polymers (IUPAC Recommendations 2013). *Pure and Applied Chemistry* **2013,** *85* (8), 1715-1724.

41. Batten, S. R.; Champness, N. R.; Chen, X.-M.; Garcia-Martinez, J.; Kitagawa, S.; Öhrström, L.; O'Keeffe, M.; Suh, M. P.; Reedijk, J., Coordination polymers, metal–organic frameworks and the need for terminology guidelines. *CrystEngComm* **2012,** *14* (9), 3001-3004.

42. Horike, S.; Shimomura, S.; Kitagawa, S., Soft porous crystals. *Nature Chemistry* **2009,** *1* (9), 695-704.

43. Reticular Chemistry—Construction, Properties, and Precision Reactions of Frameworks. *Journal of the American Chemical Society* **2016,** *138* (48), 15507-15509.

44. Yaghi, O. M., Reticular Chemistry—Construction, Properties, and Precision Reactions of Frameworks. *Journal of the American Chemical Society* **2016,** *138* (48), 15507-15509.

45. Jiang, H.; Alezi, D.; Eddaoudi, M., A reticular chemistry guide for the design of periodic solids. *Nature Reviews Materials* **2021,** *6* (6), 466-487.

46. Li, M.; Li, D.; O'Keeffe, M.; Yaghi, O. M., Topological Analysis of Metal–Organic Frameworks with Polytopic Linkers and/or Multiple Building Units and the Minimal Transitivity Principle. *Chemical Reviews* **2014,** *114* (2), 1343-1370.

47. Eddaoudi, M.; Kim, J.; Rosi, N.; Vodak, D.; Wachter, J.; O'Keeffe, M.; Yaghi, O. M., Systematic Design of Pore Size and Functionality in Isoreticular MOFs and Their Application in Methane Storage. *Science* **2002,** *295* (5554), 469-472.

48. Cao, C.; Bao, S.-J.; Tang, X.-Y.; Xu, Z.-M.; Ni, C.-Y.; Lang, J.-P., Heterobimetallic Cluster-Based Coordination Polymers: Assembly, Structures and Third-Order Nonlinear Optical Properties. *Chemistry – An Asian Journal* **2021,** *16* (18), 2674-2680.

49. Gupta, M.; Kottilil, D.; Tomar, K.; Lu, S.; Vijayan, C.; Ji, W.; Bharadwaj, P. K., Two-Photon Absorption and Fluorescence in Micrometer-Sized Single Crystals of a Rhodamine B Coordinated Metal–Organic Framework. *ACS Applied Nano Materials* **2018,** *1* (10), 5408-5413.

50. Mayer, D. C.; Manzi, A.; Medishetty, R.; Winkler, B.; Schneider, C.; Kieslich, G.; Pöthig, A.; Feldmann, J.; Fischer, R. A., Controlling Multiphoton Absorption Efficiency by Chromophore Packing in Metal–Organic Frameworks. *Journal of the American Chemical Society* **2019,** *141* (29), 11594-11602.

51. Jagatap, B. N.; Meath, W. J., Contributions of permanent dipole moments to molecular multiphoton excitation cross sections. *J. Opt. Soc. Am. B* **2002,** *19* (11), 2673-2681.

52. Sajan, D.; Vijayan, N.; Safakath, K.; Philip, R.; Karabacak, M., Multi-photon absorption effect and intra-molecular charge transfer of donor-π-acceptor chromophore ethyl p-amino benzoate. *Spectrochimica Acta Part A: Molecular and Biomolecular Spectroscopy* **2013,** *108*, 197-210.

53. W. Spangler, C., Recent development in the design of organic materials for optical power limiting. *Journal of Materials Chemistry* **1999,** *9* (9), 2013-2020.

54. Albota, M.; Beljonne, D.; Brédas, J.-L.; Ehrlich, J. E.; Fu, J.-Y.; Heikal, A. A.; Hess, S. E.; Kogej, T.; Levin, M. D.; Marder, S. R.; McCord-Maughon, D.; Perry, J. W.; Röckel, H.; Rumi, M.; Subramaniam, G.; Webb, W. W.; Wu, X.-L.; Xu, C., Design of Organic Molecules with Large Two-Photon Absorption Cross Sections. *Science* **1998,** *281* (5383), 1653-1656.

55. Marder, S. R.; Torruellas, W. E.; Blanchard-Desce, M.; Ricci, V.; Stegeman, G. I.; Gilmour, S.; Brédas, J.-L.; Li, J.; Bublitz, G. U.; Boxer, S. G., Large Molecular Third-Order Optical Nonlinearities in Polarized Carotenoids. *Science* **1997,** *276* (5316), 1233-1236.

56. Norman, P.; Luo, Y.; Ågren, H., Large two-photon absorption cross sections in two-dimensional, charge-transfer, cumulene-containing aromatic molecules. *The Journal of Chemical Physics* **1999,** *111* (17), 7758-7765.

57. Reinhardt, B. A.; Brott, L. L.; Clarson, S. J.; Dillard, A. G.; Bhatt, J. C.; Kannan, R.; Yuan, L.; He, G. S.; Prasad, P. N., Highly Active Two-Photon Dyes: Design, Synthesis, and Characterization toward Application. *Chem. Mater.* **1998,** *10* (7), 1863-1874.

58. Medishetty, R.; Zareba, J. K.; Mayer, D.; Samoc, M.; Fischer, R. A., Nonlinear optical properties, upconversion and lasing in metal-organic frameworks. *Chem. Soc. Rev.* **2017,** *46* (16), 4976-5004.

59. Jiang, Y.; Wang, Y.; Hua, J.; Tang, J.; Li, B.; Qian, S.; Tian, H., Multibranched triarylamine end-capped triazines with aggregation-induced emission and large two-photon absorption cross-sections. *Chem. Commun.* **2010,** *46* (26), 4689-4691.

60. Hu, Z.; Huang, G.; Lustig, W. P.; Wang, F.; Wang, H.; Teat, S. J.; Banerjee, D.; Zhang, D.; Li, J., Achieving exceptionally high luminescence quantum efficiency by immobilizing an AIE molecular chromophore into a metal–organic framework. *Chemical Communications* **2015,** *51* (15), 3045-3048.

61. Quah, H. S.; Chen, W.; Schreyer, M. K.; Yang, H.; Wong, M. W.; Ji, W.; Vittal, J. J., Multiphoton harvesting metal–organic frameworks. *Nature Communications* **2015,** *6* (1), 7954.

62. Quah, H. S.; Nalla, V.; Zheng, K.; Lee, C. A.; Liu, X.; Vittal, J. J., Tuning Two-Photon Absorption Cross Section in Metal Organic Frameworks. *Chemistry of Materials* **2017,** *29* (17), 7424-7430.

63. Medishetty, R.; Nemec, L.; Nalla, V.; Henke, S.; Samoć, M.; Reuter, K.; Fischer, R. A., Multi-Photon Absorption in Metal–Organic Frameworks. *Angewandte Chemie International Edition* **2017,** *56* (46), 14743-14748.

64. Liu, N.; Chen, Z.; Fan, W.; Su, J.; Lin, T.; Xiao, S.; Meng, J.; He, J.; Vittal, J. J.; Jiang, J., Highly Efficient Multiphoton Absorption of Zinc-AIEgen Metal–Organic Frameworks. *Angewandte Chemie International Edition* **2022,** *34* (12), e202115205.

65. Barnett, T. P.; Pierce, D. W.; Schnur, R., Detection of Anthropogenic Climate Change in the World's Oceans. *Science* **2001,** *292* (5515), 270-274.

66. Janna Olmos, J. D.; Kargul, J., A quest for the artificial leaf. *The International Journal of Biochemistry & Cell Biology* **2015,** *66*, 37-44.

67. Michl, J., Towards an artificial leaf? *Nat. Chem.* **2011,** *3* (4), 268-269.

68. Nocera, D. G., The Artificial Leaf. *Accounts Chem. Res.* **2012,** *45* (5), 767-776.

69. Michelet, L.; Zaffagnini, M.; Morisse, S.; Sparla, F.; Pérez-Pérez, M. E.; Francia, F.; Danon, A.; Marchand, C.; Fermani, S.; Trost, P.; Lemaire, S., Redox regulation of the Calvin–Benson cycle: something old, something new. *Frontiers in Plant Science* **2013,** *4* (470).

70. Grätzel, M., The Artificial Leaf, Molecular Photovoltaics Achieve Efficient Generation of Electricity from Sunlight. *Comments on Inorganic Chemistry* **1991,** *12* (2-3), 93-111.

71. Williams, D. E.; Shustova, N. B., Metal–Organic Frameworks as a Versatile Tool To Study and Model Energy Transfer Processes. *Chemistry – A European Journal* **2015,** *21* (44), 15474-15479.

72. Zhu, J.; Shaikh, S.; Mayhall, N.; Morris, A., Energy Transfer in Metal-Organic Frameworks. 2018; pp 581-654.

73. Kent, C. A.; Mehl, B. P.; Ma, L.; Papanikolas, J. M.; Meyer, T. J.; Lin, W., Energy Transfer Dynamics in Metal−Organic Frameworks. *Journal of the American Chemical Society* **2010,** *132* (37), 12767-12769.

74. Wang, J.-X.; Yin, J.; Shekhah, O.; Bakr, O. M.; Eddaoudi, M.; Mohammed, O. F., Energy Transfer in Metal–Organic Frameworks for Fluorescence Sensing. *ACS Applied Materials & Interfaces* **2022,** *14* (8), 9970-9986.

75. Sun, L.; Xing, H.; Liang, Z.; Yu, J.; Xu, R., A 4 + 4 strategy for synthesis of zeolitic metal–organic frameworks: an indium-MOF with SOD topology as a light-harvesting antenna. *Chemical Communications* **2013,** *49* (95), 11155-11157.

76. Kent, C. A.; Liu, D.; Ito, A.; Zhang, T.; Brennaman, M. K.; Meyer, T. J.; Lin, W., Rapid energy transfer in non-porous metal–organic frameworks with caged Ru(bpy)32+ chromophores: oxygen trapping and luminescence quenching. *Journal of Materials Chemistry A* **2013,** *1* (47), 14982-14989.

77. Kent, C. A.; Liu, D.; Meyer, T. J.; Lin, W., Amplified Luminescence Quenching of Phosphorescent Metal–Organic Frameworks. *Journal of the American Chemical Society* **2012,** *134* (9), 3991-3994.

78. An, J.; Shade, C. M.; Chengelis-Czegan, D. A.; Petoud, S.; Rosi, N. L., Zinc-Adeninate Metal−Organic Framework for Aqueous Encapsulation and Sensitization of Near-infrared and Visible Emitting Lanthanide Cations. *Journal of the American Chemical Society* **2011,** *133* (5), 1220-1223.

79. Zheng, Y.; Liu, K.; Sun, X.; Guan, R.; Su, H.; You, H.; Qi, C., A series of nano/micro-sized metal–organic frameworks with tunable photoluminescence properties. *CrystEngComm* **2015,** *17* (11), 2321-2326.

80. Feijó de Melo, E.; Santana, N. d. C.; Bezerra Alves, K. G.; de Sá, G. F.; Pinto de Melo, C.; Rodrigues, M. O.; Júnior, S. A., LnMOF@PVA nanofiber: energy transfer and multicolor light-emitting devices. *Journal of Materials Chemistry C* **2013,** *1* (45), 7574-7581.

81. Son, H.-J.; Jin, S.; Patwardhan, S.; Wezenberg, S. J.; Jeong, N. C.; So, M.; Wilmer, C. E.; Sarjeant, A. A.; Schatz, G. C.; Snurr, R. Q.; Farha, O. K.; Wiederrecht, G. P.; Hupp, J. T., Light-Harvesting and Ultrafast Energy Migration in Porphyrin-Based Metal–Organic Frameworks. *Journal of the American Chemical Society* **2013,** *135* (2), 862-869.

82. So, M. C.; Wiederrecht, G. P.; Mondloch, J. E.; Hupp, J. T.; Farha, O. K., Metal–organic framework materials for light-harvesting and energy transfer. *Chemical Communications* **2015,** *51* (17), 3501-3510.

83. Zhang, T.; Lin, W., Metal–organic frameworks for artificial photosynthesis and photocatalysis. *Chemical Society Reviews* **2014,** *43* (16), 5982-5993.

84. Basham, J. I.; Mor, G. K.; Grimes, C. A., Förster Resonance Energy Transfer in Dye-Sensitized Solar Cells. *ACS Nano* **2010,** *4* (3), 1253-1258.

85. Jang, S.; Newton, M. D.; Silbey, R. J., Multichromophoric F\"orster Resonance Energy Transfer. *Physical Review Letters* **2004,** *92* (21), 218301.

86. Stryer, L., Fluorescence Energy Transfer as a Spectroscopic Ruler. *Annual Review of Biochemistry* **1978,** *47* (1), 819-846.

87. Loura, L. M. S., Simple estimation of Förster Resonance Energy Transfer (FRET) orientation factor distribution in membranes. *Int J Mol Sci* **2012,** *13* (11), 15252-15270.

88. Laible, P. D.; Knox, R. S.; Owens, T. G., Detailed Balance in Förster−Dexter Excitation Transfer and Its Application to Photosynthesis. *The Journal of Physical Chemistry B* **1998,** *102* (9), 1641-1648.

89. Kasha, M., Energy Transfer Mechanisms and the Molecular Exciton Model for Molecular Aggregates. *Radiation Research* **1963,** *20* (1), 55-70.

90. Davydov, A. S., THE THEORY OF MOLECULAR EXCITONS. *Soviet Physics Uspekhi* **1964,** *7* (2), 145-178.

91. Hestand, N. J.; Spano, F. C., Expanded Theory of H- and J-Molecular Aggregates: The Effects of Vibronic Coupling and Intermolecular Charge Transfer. *Chemical Reviews* **2018,** *118* (15), 7069-7163.

92. Kasha, M.; Rawls, H. R.; El-Bayoumi, M. A., The exciton model in molecular spectroscopy. *Pure and Applied Chemistry* **1965,** *11* (3-4), 371-392.

93. Würthner, F., Perylene bisimide dyes as versatile building blocks for functional supramolecular architectures. *Chemical Communications* **2004,** (14), 1564-1579.

94. Zhao, X.; Xiong, Y.; Ma, J.; Yuan, Z., Rylene and Rylene Diimides: Comparison of Theoretical and Experimental Results and Prediction for High-Rylene Derivatives. *The Journal of Physical Chemistry A* **2016,** *120* (38), 7554-7560.

95. Zhao, F.-J.; Zhang, G.; Ju, Z.; Tan, Y.-X.; Yuan, D., The Combination of Charge and Energy Transfer Processes in MOFs for Efficient Photocatalytic Oxidative Coupling of Amines. *Inorganic Chemistry* **2020,** *59* (5), 3297-3303.

96. Troeger, A.; Ledendecker, M.; Margraf, J. T.; Sgobba, V.; Guldi, D. M.; Vieweg, B. F.; Spiecker, E.; Suraru, S.-L.; Würthner, F., p-Doped Multiwall Carbon Nanotube/Perylene

Diimide Derivative Photoelectrochemical Cells for Photocurrent Generation. *Advanced Energy Materials* **2012,** *2* (5), 536-540.

97. Weissman, H.; Shirman, E.; Ben-Moshe, T.; Cohen, R.; Leitus, G.; Shimon, L. J. W.; Rybtchinski, B., Palladium Complexes of Perylene Diimides: Strong Fluorescence Despite Direct Attachment of Late Transition Metals to Organic Dyes. *Inorganic Chemistry* **2007,** *46* (12), 4790-4792.

98. Dinçalp, H.; Kızılok, Ş.; İçli, S., Fluorescent macromolecular perylene diimides containing pyrene or indole units in bay positions. *Dyes and Pigments* **2010,** *86*, 32-41.

99. Würthner, F.; Saha-Möller, C. R.; Fimmel, B.; Ogi, S.; Leowanawat, P.; Schmidt, D., Perylene Bisimide Dye Assemblies as Archetype Functional Supramolecular Materials. *Chemical Reviews* **2016,** *116* (3), 962-1052.

100. Zeng, L.; Liu, T.; He, C.; Shi, D.; Zhang, F.; Duan, C., Organized Aggregation Makes Insoluble Perylene Diimide Efficient for the Reduction of Aryl Halides via Consecutive Visible Light-Induced Electron-Transfer Processes. *Journal of the American Chemical Society* **2016,** *138* (12), 3958-3961.

101. Seco, J. M.; San Sebastián, E.; Cepeda, J.; Biel, B.; Salinas-Castillo, A.; Fernández, B.; Morales, D. P.; Bobinger, M.; Gómez-Ruiz, S.; Loghin, F. C.; Rivadeneyra, A.; Rodríguez-Diéguez, A., A Potassium Metal-Organic Framework based on Perylene-3,4,9,10-tetracarboxylate as Sensing Layer for Humidity Actuators. *Scientific Reports* **2018,** *8* (1), 14414.

102. Lü, B.; Chen, Y.; Li, P.; Wang, B.; Müllen, K.; Yin, M., Stable radical anions generated from a porous perylenediimide metal-organic framework for boosting near-infrared photothermal conversion. *Nature Communications* **2019,** *10* (1), 767.

103. Weishäupl, S. J.; Mayer, D. C.; Thyrhaug, E.; Hauer, J.; Pöthig, A.; Fischer, R. A., A nitrophenyl-carbazole based push-pull linker as a building block for non-linear optical active coordination polymers: A structural and photophysical study. *Dyes and Pigments* **2021,** *186*, 109012.

104. Weishäupl, S. J.; Cui, Y.; Deger, S. N.; Syed, H.; Ovsianikov, A.; Hauer, J.; Pöthig, A.; Fischer, R. A., Coordination Polymers Based on Carbazole-Derived Chromophore Linkers for Optimized Multiphoton Absorption: A Structural and Photophysical Study. *Chemistry of Materials* **2022**.

105. Deger, S. N.; Weishäupl, S. J.; Pöthig, A.; Fischer, R. A., A Perylenediimide-Based Zinc-Coordination Polymer for Photosensitized Singlet-Oxygen Generation. *Energies* **2022,** *15* (7), 2437.

106. Liu, N.; Chen, Z.; Fan, W.; Su, J.; Lin, T.; Xiao, S.; Meng, J.; He, J.; Vittal, J. J.; Jiang, J., Highly Efficient Multiphoton Absorption of Zinc-AIEgen Metal–Organic Frameworks. *Angewandte Chemie International Edition* **2022,** *61* (12), e202115205.

8 Eidesstaatliche Erklärung

Ich, Sebastian Josef Weishäupl, erkläre an Eides statt, dass ich die bei der promotionsführenden Einrichtung "Lehrstuhl für Anorganische und Metallorganische Chemie"

der TUM zur Promotionsprüfung vorgelegte Arbeit mit dem Titel:

Chromophore based Coordination Polymers (CPs) as Materials for Optical Applications.

unter der Anleitung und Betreuung durch: Prof. Dr. Dr. h.c. Roland A. Fischer

ohne sonstige Hilfe erstellt und bei der Abfassung nur die gemäß § 7 Abs. 6 und 7 angegebenen Hilfsmittel benutzt habe.

☐ Ich habe keine Organisation eingeschaltet, die gegen Entgelt Betreuer*innen für die Anfertigung von Dissertationen sucht, oder die mir obliegenden Pflichten hinsichtlich der Prüfungsleistungen für mich ganz oder teilweise erledigt.

☐ Ich habe die Dissertation in dieser oder ähnlicher Form in keinem anderen Prüfungsverfahren als Prüfungsleistung vorgelegt.

☐ Teile der Dissertation wurden in _____ veröffentlicht.

☐ Ich habe den angestrebten Doktorgrad noch nicht erworben und bin nicht in einem früheren Promotionsverfahren für den angestrebten Doktorgrad endgültig gescheitert.

☐ Ich habe bereits am _____ bei der promotionsführenden Einrichtung _____ der Hochschule _____ unter Vorlage einer Dissertation mit dem Thema _____

die Zulassung zur Promotion beantragt mit dem Ergebnis:

_____

☐ Ich habe keine Kenntnis über ein strafrechtliches Ermittlungsverfahren in Bezug auf wissenschaftsbezogene Straftaten gegen mich oder eine rechtskräftige strafrechtliche Verurteilung mit Wissenschaftsbezug.

Die öffentlich zugängliche Promotionsordnung sowie die Richtlinien zur Sicherung guter wissenschaftlicher Praxis und für den Umgang mit wissenschaftlichem Fehlverhalten der TUM sind mir bekannt, insbesondere habe ich die Bedeutung von § 27 PromO (Nichtigkeit der Promotion) und § 28 PromO (Entzug des Doktorgrades) zur Kenntnis genommen. Ich bin mir der Konsequenzen einer falschen Eidesstattlichen Erklärung bewusst.

Mit der Aufnahme meiner personenbezogenen Daten in die Alumni-Datei bei der TUM bin ich

☐ einverstanden, ☐ nicht einverstanden.

Ort, Datum, Unterschrift